Graduate School ETD Form 9
(01/07)

PURDUE UNIVERSITY
GRADUATE SCHOOL
Thesis Acceptance

This is to certify that the thesis prepared

By Liangzhu Wang

Entitled Coupling of Multizone and CFD Programs for Building Airflow and Contaminant Transport Simulations

Complies with University regulations and meets the standards of the Graduate School for originality and quality

For the degree of Doctor of Philosophy

Final examining committee members

Qingyan Chen , Chair

James E. Braun

Albert J. Heber

Jayathi Y. Murthy

Approved by Major Professor(s): Qingyan Chen

Approved by Head of Graduate Program: Anil K. Bajaj

Date of Graduate Program Head's Approval: February 28, 2007

COUPLING OF MULTIZONE AND CFD PROGRAMS FOR BUILDING AIRFLOW AND CONTAMINANT TRANSPORT SIMULATIONS

A Dissertation

Submitted to the Faculty

of

Purdue University

by

Liangzhu Wang

In Partial Fulfillment of the

Requirements for the Degree

of

Doctor of Philosophy

May 2007

Purdue University

West Lafayette, Indiana

To my mother and father, Juncai Li and Tingtang Wang, who devotes their whole lives to raising and educating my two sisters and me; to the memory of my step-grandmother and my grandfather, Qingmei Ji and Wenyi Wang, who reminds me to be always strong and optimistic; to my beloved wife, Jinxia Liu, who always stands by my side throughout the ups and downs of those past years.

ACKNOWLEDGMENTS

My thanks and appreciation first goes to Dr. Qingyan (Yan) Chen for his perseverance with me as my advisor to complete this research and write the dissertation, and for his thoroughness and promptness in guiding my work in progress. Without his on-going encouragement, it would have been impossible to complete the project and to maintain the standard of scholarship that the project required. I am also grateful to him for the opportunity to work under his supervision at Purdue University, which was one of the most important and formative experiences in my life.

I would like to express my gratitude to the members of my dissertation committee, Dr. Andrew Persily from U.S. National Institute of Standards and Technology, Dr. James Braun, Dr. Albert Heber, and Dr. Jayathi Murthy from Purdue University, who have generously given their time and expertise to better my work. My thanks also go to George Walton, Stuart Dols, and Steven Emmerich at U.S. National Institute of Standards and Technology for their encouragement and valuable contributions to the research. I also owe thanks to Dr. Patricia Davies, the director of Ray W. Herrick Laboratories, who shared with me the wisdom of life and encouraged me throughout my studies.

I must acknowledge as well my many friends and colleagues, especially Zhipeng Zhong, Jinsong Zhang, Zhiqiang (John) Zhai and Jennifer Gosselin, for their friendship and knowledge. I also appreciate the great help from all the technicians and secretaries at Ray W. Herrick Laboratories. Finally, my special thanks go to the kindly sponsorships from Indoor Air Quality and Ventilation Group of U.S. National Institute of Standards and Technology under the grant of 70NANB5H1051, and the contracts of SB1341-04-Q-0771 and RFQ-03-Q-9537.

TABLE OF CONTENTS

Page

Page

Page

LIST OF TABLES

Table Page

Table Page

LIST OF FIGURES

Figure Page

Figure Page

Figure Page

Figure Page

Appendix Figure

Figure Page

NOMENCLATURE

a	coefficient of an unknown variable
A	area of an opening; cross-sectional area of a room
Ar	the Archimedes number
b	source term in a mass continuity equation
b'	source term in the linear form of mass continuity equation for a zone in a multizone program
$\mathbf{B}$	vector of source terms in an assembled momentum conservation equation
$\mathbf{B_c}$	vector of source term in an assembled species conservation equation
$\mathbf{B_e}$	vector of source terms in an assembled energy conservation equation
$\mathbf{B_1}$	vector of the source terms in the assembled total matrix equation for Method 1
c	index of CFD zones
C	nonlinear flow coefficient; ratio of inflow opening area to the cross-sectional area of a room; contaminant concentration
$\overline{C}$	average contaminant concentration

$\mathbf{C}$	coefficient matrix in an assembled total matrix equation
$\mathbf{C_c}$	coefficient matrix in an assembled species conservation equation
$\mathbf{C_1}$	coefficient matrix in the assembled total matrix equation for Method 1
$\mathbf{C_m}$	coefficient matrix in an assembled momentum conservation equation
$\mathbf{C_e}$	coefficient matrix in an assembled energy conservation equation
C	system equations for a CFD program
C_L	linear flow coefficient
C_p	heat capacity at constant pressure
d	difference between the local pressure of a flow path and the pressure of the zone, to which the path connects
F	air mass flow rate; volumetric airflow rate
F	vector of unknown flow rates through interface paths and cells
f	airflow rate through the face of a CFD cell, perpendicular to the flow direction
g	acceleration of gravity
Gr	the Grashof number
h	height
H	reference height

i	index of the zones for a multizone program; input parameter for *C*
ic	index of the flow paths linking zone i and zone c
ij	index of the flow paths linking zone i and zone j
j	index of the zones for a multizone program
L	characteristic length
m	index of non-uniformity of contaminant
M	system equations for a multizone program
M	vector of species concentration of an assembled species conservation equation
n	flow exponent
N	total number of sample cells/points
p	pressure at a grid point
P	pressure of a zone; index of grid points or cells
P	vector of unknown pressures of multizone and CFD cells
P_d	downwind total pressure of an airflow path
P_H	undisturbed wind pressure at the reference height H
P_S	pressure difference due to density and elevation differences

P_u upwind total pressure of an airflow path

P_W pressure difference due to wind; wind pressure

Q heat input in w

Q vector of heat inputs in an assembled energy conservation equation

r input parameter for ***M***

Re the Reynolds number

S source term

S vector of source terms in an assembled species conservation equation

St the Stanton number

T temperature

T vector of temperatures in an assembled energy conservation equation

U wind velocity; velocity in X direction

U vector of airflow velocity through an opening

U_H wind velocity at the reference height H

V velocity; volume; velocity in Y direction

V velocity vector

$\bar{V}$ average wind velocity

W width; velocity in Z direction

a exponent for wind velocity profile

b Volumetric thermal expansion coefficient

d atmospheric boundary layer thickness

θ azimuth direction

r air density

t dimensionless temperature gradient

υ air kinematic viscosity

Δ difference

f general variable

Γ diffusion coefficient for *f*

Subscripts

av average

b bottom

exp	experiment
i	index of the zones of a multizone program; index of CFD cell
ic	index of the flow paths linking zone i and zone c
ij	index of the flow paths linking zone i and zone j
in	inflow
j	index of the zones of a multizone program; coordinate direction
k	index of coupling iterations
met	meteorological
nb	neighboring
P	index of grid points or cells
r	room
s	building surface
t	top
w	wind

ABSTRACT

Wang, Liangzhu. Ph. D., Purdue University, May, 2007. Coupling of Multizone and CFD Programs for Building Airflow and Contaminant Transport Simulations. Major Professor: Dr. Qingyan (Yan) Chen, School of Mechanical Engineering.

Building ventilation designs and Indoor Air Quality (IAQ) analyses are important to provide a safe, healthy, and comfortable indoor environment, and to improve the energy savings and substantiality of buildings. However, current design tools have their own merits and drawbacks. Multizone programs can achieve a fast computing speed, but they are still limited to the predictions of the average characteristics of airflows and contaminant distributions due to the various assumptions that revolve around them. CFD programs can provide more accurate results, yet they demand higher computing costs. An integrated program of multizone-CFD methods can combine the merits of both programs while eliminating their drawbacks. This thesis thus investigates the fundamentals, strategies, implementations, validations, and applications of coupling a multizone program, CONTAM, with a CFD program, CFD0-C, for building airflow and contaminant transport simulations.

This research first identifies the situations, where the major assumptions of multizone models become problematic: non-uniform distributions of wind pressures, momentum effects, temperatures, and contaminant concentrations. Two coupling strategies have been developed to improve CONTAM assumptions. For non-uniform wind pressure distributions on a building surface, this study develops an indirect coupling strategy, which exchanges wind pressures indirectly between CONTAM and CFD0-C. For the cases with non-uniform distributions of momentum effects, temperatures, and

contaminant concentrations, a direct coupling scheme is employed to exchange iteratively information between CONTAM and CFD0-C. Theoretical analyses then prove that the direct coupling scheme has a solution, which is a unique one. This study also finds that for the direct coupling, the most stable method is to exchange pressure boundary conditions between the multizone and CFD programs.

This research conducted experiments in a test chamber to validate the coupled CONTAM-CFD0 program. This study shows that the calculations of the coupled program are reasonably accurate, while preserving acceptable computing costs. The performances of the coupled program are also demonstrated by several case studies, illustrating how the coupled CONTAM-CFD0 program can effectively improve CONTAM simulations. Finally, dimensional analyses are conducted to provide suggestions on when multizone assumptions become problematic and thus CFD methods are needed.

CHAPTER 1. INTRODUCTION

1.1. General Statement of the Problem

People in developed countries spend about 90% of their lifetime indoors (U. S. EPA, 1995). With properly controlled air temperature, humidity, and velocity, people feel comfortable and are productive in an indoor environment. An uncomfortable indoor environment and poor indoor air quality (IAQ) can lead to low productivity at work, resulting in significant economic loss (Raw et al., 1990; Mendell, 1993; Wolkoff, 1995). Conservatively estimated, the loss of productivity due to impoverished IAQ can be up to 6% (Dorgan et al., 1998). In US commercial buildings, the corresponding economic losses could be about $20 to $160 billion per year (Fisk, 2000).

Issues related to indoor environments do not only involve comfort, but also encompass people's health. Long periods of exposure to poor IAQ can cause various health problems. If building occupants repeatedly report a complex range of vague and subjective health complaints, they are experiencing what is called “Sick Building Syndrome” (SBS). Serious SBS can lead to morbidity, disability, disease, and even death in extreme cases (Ren, 2002). The current increase of indoor pollutants is resulting in more frequent cases of SBS. In developing countries, more than 2,000,000 people, mainly women and children, die yearly because of the deadly mixture of pollutants resulting from the burning of biomass, especially when cooking indoors (Sundell, 2004). In developed countries, more and more synthetic building materials are being used in building insulations, internal furnishings, and craft materials. Many sources of contaminants, such as volatile organic compounds (VOCs), are being introduced into indoor working and living environments. Some VOCs can cause eye, nose, and throat irritation, as well as damage to the liver, kidney, and the central nervous system. Studies

have found that the VOC levels are 2 to 5 times higher indoors than outdoors. Especially after the immediate use of materials containing VOCs, such as those used during paint stripping, for example, the VOC levels can be 1,000 times higher than outdoor levels (U. S. EPA, 1995). Buildings have become sources of contamination and are often more polluted than their surroundings (Spengler and Chen, 2000).

Moreover, highly populated buildings can become dangerous if the building ventilation system performs poorly during emergencies. Between November 2002 and June 2003, the severe acute respiratory syndrome (SARS) epidemic caused unprecedented international panic. SARS is primarily transmitted by bio-aerosol droplets or direct personal contact. Originating in China, SARS spread to the rest of the world when an infected medical doctor stayed in a hotel at Hong Kong. The medical doctor was later treated in a hospital, where the ventilation and air-conditioning system were later found to be highly possible causes of a large SARS outbreak (Li et al., 2005b). The most serious reported community SARS outbreak worldwide was at the Amoy Gardens of Hong Kong, with a total of 329 infected cases and 42 deaths. Li et al. (2005a) found that natural ventilation might have played an important role in circulating the SARS virus at the Amoy Gardens. Such an incident showed the importance of proper ventilation designs in high-rise residential buildings.

Some other types of emergencies also show the importance of building ventilation designs and IAQ analysis. The September 11, 2001 terrorist attacks on New York City and Washington D.C. and the following anthrax dispersion by mail have spawned concerns about various possible forms of terrorism, including airborne/aerosolized chemical and biological warfare agent (CBWA) attacks. The events have confirmed that the attacks are no longer a hypothesis but a reality. Most CBWAs are highly poisonous. A small amount of CBWA can seriously affect one’s health or even threaten lives. For instance, one may suffer a mild injury, a serious injury, and death, respectively, while inhaling as little as 0.9, 10, and 15 milligrams of the lethal nerve agent VX gas, according to the US Army Chemical Biological Defense Command (Zhai et al., 2003). Once the

terrorists and rogue nations own weapons such as CBWA, they could deliver small packages to an embassy, military facility, or a building with a high civilian population density (Arvelo et al., 2002). Another type of potential warfare agents is radiological materials, which may cause less instant damage but more serious long-term effects than CBWAs. In 1995, a TV reporter was directed by Chechnya rebels to a park in central Moscow, where she found a package with a small amount of explosives and something else: Cesium-137, a radioactive isotope. This was the debut of what has become a household word: a dirty bomb. The explosives in a dirty bomb are not the true threat, but Cesium-137, which is very dispersible, like talc powder, is very dangerous. With typical air speed, it could travel six miles, if unobstructed, in half an hour. The resultant radioactive contamination will be deposited on building walls, plants, and soils. Unless it is cleaned up, this radioactivity, with the potential of damaging human DNA, will stay in place for decades (Higginson, 2003).

The concept of a building design that is immune toward these potential chemical, biological, and radiological warfare agent (CBRWA) attacks has gained wide attention in recent years. To design an immune building, it is very important to understand the transport physics of CBRWAs, especially their transport phenomena with air movement. Thus, an appropriate design of building ventilation system does not only mean supplying air with a suitable temperature and velocity to achieve a comfortable and healthy indoor environment. The ventilation system must be designed in such a way that during emergencies, enough clean (or fresh) air is distributed in a properly controlled manner to dilute or remove various types of hazardous pollutants in a timely and effective fashion.

The planned amount of clean air, however, hinges on other factors, including, for example, energy and sustainability concerns. Buildings consume a lot of energy. In Western Europe, 52% of energy is delivered to maintain acceptable climate conditions within buildings (Clarke and Maver, 1991). In the US, buildings account for one-third of all used energy and two-thirds of all electricity consumption (U.S. EIA, 1995). Recently, the shortage in crude oil caused an increase in the price of gas, which caused people to

worry about a recurrence of the 1970's energy crisis. Building ventilation designs thus have to consider sustainability. One of the popular strategies is to use natural ventilation, which can provide occupants with good IAQ and less energy costs than conventional mechanical ventilation (Allard and Inard, 1992; Etheridge and Sandberg, 1996). However, the design of natural ventilation cannot be successful without a proper design tool. In conclusion, building ventilation designs and IAQ analyses should consider the relationship between various aspects, including the safety, health, and comfort of people, and the energy consumption and sustainability of buildings. Sophisticated design tools are therefore required.

1.2. Current Design Tools for Building Ventilation and IAQ Analyses

The traditional method to design building ventilation systems is the paper-and-pencil method, which is based on design handbooks and engineering experiences. With the invention of computers, computer programs can now carry out the tedious manual calculations. In the last three decades, many computer design models and tools have been developed. According to underlying design regimes and calculation methods, one can classify the design tools as "individual building ventilation and IAQ analysis tools" and "integrated building ventilation and IAQ analysis tools."

1.2.1. Individual Building Ventilation and IAQ Analysis Tools

Although all building ventilation and IAQ analysis tools are designed for predictions of airflow distribution and contaminant transport, they serve different purposes when used individually. Some tools focus on the average characteristics of infiltration airflows, contaminant distribution, and lower computational costs, such as multizone airflow network (multizone) models. These models often employ many assumptions in order to achieve fast computing speed. Some other tools use much less assumptions and are able to obtain detailed spatial values of airflow and contaminant concentrations. Nevertheless, these tools demand more computing time than multizone models, e.g. computational fluid dynamics (CFD) models. A third type of model is the zonal model, which is a simplified

form of CFD models. Zonal models normally demand less computational time than CFD models while providing more detailed results than multizone models. Zonal models, however, have their own drawbacks. The merits and drawbacks of these models are compared in detail in the following section.

Multizone airflow network models

Multizone airflow network models have been used as a research and design tool for over twenty years (Emmerich, 2001). A 1992 survey reported that nearly fifty multizone models are available (Feustel and Dieris, 1992). They are widely used in such areas as air distribution analysis, smoke controls, and building pressurization tests, etc. The simulated building types include residential buildings (Persily, 1998; Emmerich et al., 2002), commercial buildings (Salemi et al., 1996), and industrial buildings (Li et al., 2000).

Multizone models calculate the airflow and contaminant transport between the rooms of a building and between the building and the outdoors. The rooms of a building are typically represented as zones, with homogeneous air properties and contaminant concentrations. Airflows pass through the paths interconnecting the various zones, and they have user-defined leakage characteristics (Musser, 2001). The airflow rates through paths and the average contaminant concentrations are calculated based on the mass balance. Since multizone models solve only mass and contaminant balance equations for each room, the computational time is much less than that required by other models, such as a computational fluid dynamics (CFD) program.

To achieve a fast computing speed, multizone models use a number of assumptions, which can lead to some problems. The key assumptions of the multizone network models are (Persily, 2003):

- Uniform pressure, temperature and species concentration in each zone
- Quiescent or still air in zones; airflow through zones does not impact zone pressure
- Kinetic energy and momentum not accounted for by flow path models

- Instantaneous contaminant transport along each flow path, e.g. no delays in ductwork

Note that multizone models in fact assume that pressure is hydrostatically distributed in each zone. Here by meaning uniform pressure, we refer to the total pressure of each zone without the hydrostatic part, which is consistent with the custom of CFD methods. These assumptions may compromise the accuracy of the results obtained. In addition, multizone models cannot provide the spatial parameters of airflow and the transport of contaminant. To reduce the assumptions used, and to obtain more detailed indoor airflow information, some other models should be used, such as the zonal airflow models.

Zonal airflow models

The development of zonal models aims to obtain approximate but faster simulation methods than the CFD ones to predict a building's airflow and the transport of contaminant (Mora et al., 2003). The first zonal model was proposed by Lebrun (1970), who divided a single zone into sub-zones based on the characteristics of the main driving flows. Instead of a uniform temperature, a rough estimate of thermal stratification was calculated for the zone. Since Lebrun's pioneering work, various zonal models (Inard, 1988; Li et al., 1998b; Haghighat et al., 2001) have been developed for different applications, e.g. flows with plumes, jets, and boundary layers etc. Grelat (1987), Bouia and Dalicieux (1991), and Wurtz (1995) generalized the zonal models by developing a so-called pressure zonal model, in which a room is divided into sub-zones with non-uniform pressures. The pressures are then solved by imposing mass balances to each sub-zone.

Zonal models introduce more dynamics into the prediction of mean flows, compared to multizone airflow network models. By using a mesh to divide the room air into control volumes, zonal models provide more information than multizone models and require less computing power than the CFD models (Zhai, 2003). However, current zonal models also have many limitations. One of the problems is the method of dividing a room into sub-zones, namely the zoning method. Most zoning methods use regular hexahedrons, in

which air properties and contaminant concentrations are assumed homogeneous. Airflow patterns and contaminant concentration distributions often have to be known before a room can be correctly divided into sub-zones. Presently, zonal models only provide airflow patterns for some typical indoor airflow problems; thus, their applications are limited. Furthermore, Griffith (2002) found that many zonal models are not numerically stable. Even if zonal models are numerically stable, the pressure variable solved in zonal models is really an internal variable used to balance the flow equations, and has no physical significance (Musy, 1999).

Computational fluid dynamics (CFD) models

Over the past half century, computational fluid dynamics (CFD) has become an important methodology for attacking the complex problems in fluid mechanics and heat transfer (Tannehill et al., 1997). CFD techniques have achieved encouraging results for diverse indoor environmental and HVAC studies (Emmerich, 1997; Ladeinde and Nearon, 1997; Nielsen, 1998; Spengler and Chen, 2000). Compared to multizone and zonal airflow models, CFD is the most sophisticated method. It calculates the detailed spatial distribution of air velocity, temperature, and contaminant concentrations by solving the Navier-Stokes and species-conservation equations. CFD can be further divided into direct numerical simulation (DNS), large eddy simulation (LES), and the Reynolds averaged Navier-Stokes equations with turbulence models (RANS).

Direct numerical simulation is to compute the turbulent flow and the contaminant dispersion by solving the highly reliable Navier-Stokes equations without approximations. Very fine grid resolution is required to capture the smallest eddies in the turbulent flow at very small time steps, even for a flow at steady state. It would take years of computing time for DNS to predict contaminant dispersion in buildings.

Large eddy simulation (Deardorff, 1970) separates turbulent motion into large eddies and small eddies. The large eddies corresponding to the three-dimensional time-dependent equations can be directly simulated, while small eddies are modeled. It has been

successfully applied to study airflow in a single space (Emmerich and McGrattan, 1998; Jiang and Chen, 2001; Jiang, 2002). Although large eddy simulation requires a much smaller computer capacity and is much faster than direct numerical simulation, large eddy simulation, for predicting the airflow and contaminant dispersion in a building, demands a large computer memory capacity (10^{10}-byte memory) and a long computing time (weeks), which is not practical.

The Reynolds Averaged Navier-Stokes (RANS) equations with turbulence models solve the statistically averaged Navier-Stokes equations by using turbulence transport models to simplify the calculation of the turbulence effect. The use of turbulence models leads to some errors, but can significantly reduce the need for computer memory and speed. The RANS modeling provides detailed information on airflow and contaminant concentration distributions. The method has been successfully applied to a building's indoor airflow, as well as to thermal comfort and indoor air quality analysis, as reviewed by Emmerich (1997), Ladeinde and Nearon (1997), and Nielsen (1998). The RANS modeling can be easily used to study the airflow and contaminant dispersion in a room.

Table 1.1 Comparison of computational costs among different CFD methods (Jiang, 2002).

CFD methods	Grid		Computational time	
	Building	Airplane	Building	Airplane
RANS	10^5	10^7	2 hours	200 hours
LES	10^6	10^8	100 hours	1 year
DNS	10^{11}	10^{16}	10^5 years	10^{12} years

Table 1.1 compares grid resolutions and computational costs when the three CFD methods are used in the airflow simulations of buildings and airplanes. The RANS method requires the fewest number of grids and is the fastest CFD method. It is very difficult to apply LES and DNS to real design practices due to their enormous computational costs. Currently, RANS is the most commonly used CFD method in building ventilation design and IAQ analysis.

However, CFD methods have their own drawbacks when compared to multizone and zonal models. Although the RANS method is the fastest CFD method, it still requires much more computational cost than multizone and zonal models. Although two hours seem acceptable for a building with 10^5 grids in Table 1.1 when simulated by RANS, multizone models only need several seconds for the same problem. The difference in computational costs between CFD and multizone models will be even more significant for transient simulations over a long period of time. Thus, the CFD method is seldom used for a whole-year building simulation. Presently, CFD models also face some challenges in building ventilation design and IAQ analysis. It is hard for CFD methods to simulate air infiltrations or exfiltrations, especially when the locations of building cracks, through which filtrations occur, cannot be identified. For simulations of buoyancy-driven flows with pressure boundary conditions, under-relaxation factors must be carefully selected for convergence. Sometimes, multiple runs are required to test different CFD parameters for convergence. CFD methods, therefore, normally need more expertise and experience than other methods for a successful simulation.

Above all, when multizone, zonal, and CFD methods are used individually, they have different merits and drawbacks, as summarized and compared in Table 1.2. The multizone model is the fastest method with many assumptions, whereas the CFD is the most accurate, with the most computational costs. Zonal methods stand between these two models in terms of accuracy and computational time. For simulation capacities, each method has its own merits when applied to different problems. Multizone models can provide average characteristics of airflow and contaminant transport, while CFD and zonal methods can calculate the spatial distributions of these parameters. Therefore, an integration of multizone, zonal, and CFD methods is supposed to combine the merits and avoid the drawbacks of each of these methods.

Table 1.2 Comparison of simulation characteristics among multizone, zonal, and CFD RANS models. (√=Good, √√=Better, √√√=Best).

Items	Multizone	Zonal	CFD
Simulation assumptions			
Perfect mixing in each room	√		
Quiescent or still air in each room	√		
Neglect of air resistance in each room	√		
Neglect of inflow momentum effect, if any	√		
Instantaneous contaminant transport inside a room	√		
Airflow driven only by pressure difference	√	√	
Hydrostatic distribution of pressure inside a room	√		
Simulation potentials			
Ductwork design	√		
Building energy calculation		√	√√
Distribution of airflow and contaminant concentration		√	√√
Wind pressure profile around buildings			√
Popularity in whole building simulation	√√√	√	√√
Popularity in yearly dynamic simulation	√√√	√	√√
Modeling capacity of orifice type openings	√√√	√√	√
Modeling capacity of large openings	√	√√	√√√
Modeling of large spaces	√	√√	√√√
Integration capacity with building controls	√		
Modeling of building infiltrations	√√√	√√	√
Evaluation of ventilation efficiency		√	√√
Evaluation of personal exposure inside a room		√	√√
Miscellaneous items			
Simulation accuracy	√	√√	√√√
Computational speed	√√√	√√	√
Numerical convergence and stability	√√√	√	√√
Adaptability	√√√	√	√√
Less simulation skills required	√√√	√√	√

1.2.2. Integrated Building Ventilation and IAQ Analysis Tools

Most of the current integrated tools are coupled multizone and zonal models, or coupled multizone and CFD models. Although some studies (Peng and Paassen, 1995; Kato et al., 1998) extracted CFD information for their simulations by zonal models, their studies did not integrate zonal and CFD methods. In fact, as a simplified form of CFD, zonal models

do not need to be integrated with CFD models. By using coupled multizone and zonal models, or multizone and CFD models, one of the major motivations is to remedy the well-mixing assumption of multizone models.

Since zonal models can provide non-uniform distributions of pressures and airflow patterns, they are useful in improving the accuracy of multizone model simulations. Stewart and Ren (2003) nested zonal models within a multizone model – COMIS (Feustel, 1999) and developed a new program called CoWZ, for "COMIS with sub-zones." Although CoWZ was able to improve the accuracy of contaminant distributions calculated by COMIS, the zonal models of CoWZ can only be applied to single rooms with a limited set of driving forces (Ren, 2002). Based on a more robust simulation environment of zonal models – SPARK, Buhl et al. (1993) and Mora (2003) also tried to couple zonal and multizone models. However, the limitations of zonal models themselves prevented the application of a coupled multizone-zonal model. Musy (1999) pointed out that the pressure variable solved in zonal models is really an internal variable used to balance the flow equations, which should not be confused with the pressure variable solved in multizone models. So Mora et al. (2003) concluded that when zonal models are coupled with multizone models, the pressure predictions by zonal models should be ignored, and only the airflows should be used at the interfaces shared by the two models. Mora et al. therefore suggested that Computational Fluid Dynamics (CFD) should be an alternative to zonal models for coupling with multizone models in building air distribution simulations.

Although the idea of the coupling of multizone and CFD models in building airflow simulations was proposed fairly early (Schaelin et al., 1994), literature reviews show that not many coupling studies have been conducted. Schaelin et al. proposed a method called "method of detailed flow path values," in which the well mixing assumptions of multizone models were remedied, providing detailed pressures, velocities, and contaminant concentrations of flow paths from the CFD. This study, however, only implemented the coupling of contaminant concentrations and did not actually perform the

coupling in airflow simulations. The coupling procedure was also an external or "manual" iteration.

Moreover, Clarke et al. (1995a), and Negrao (1998) implemented an automatic airflow coupling inside ESP-r (Clarke, 1985) with the CFD. However, in their studies, different coupling methods resulted in dramatically different results for the same airflow problem, which indicated multiple solutions of airflow coupling. Bartak et al. (2002) recently refined the CFD module of ESP-r and adopted a "conflation controller" (Beausoleil-Morrison, 2002) to improve the simulation capacities of the CFD module of ESP-r. In the airflow coupling, however, their evaluation of possible coupling methods was incomplete. The conflation controller by default only transfers the CFD-calculated airflows to the multizone model. They did not explain why the CFD-calculated pressures should be ignored. Musser (2001), Srinivas (2001), and Yuan and Srebric (2002) compared results from multizone and CFD programs for contaminant transport simulations. However, all of them avoided the problem of coupled airflow simulations by using predefined airflow rates in contaminant transport simulations. Recently, Jayaraman et al. (2004) tried to develop an algorithm for coupled multizone and CFD programs for airflow simulations, demonstrating the algorithm on a two-dimensional building with a large space. Their preliminary study showed that coupling CFD with a multizone model could result in more realistic predictions of airflow and contaminant transport in buildings with large spaces. The details of their algorithm, however, were not provided in the literature.

Among the past coupling endeavors in building ventilation simulations, the coupling of multizone and CFD models is considered the most sophisticated (Musser, 2001). As reviewed above, current design tools of coupled multizone and CFD programs still have many limitations. Several issues remain unsolved, e.g. the development of an appropriate coupling algorithm and a stable coupling method, and the study of the solution characteristics, validations, and applications of such a coupled program to real problems. This thesis aims to tackle these challenges to develop a new design tool by coupling a multizone and a CFD program.

1.3. Research Objectives and Thesis Outline

Previous sections of this chapter show that building ventilation design and IAQ analysis are essential for providing people with a safe, healthy, and comfortable indoor environment. Current design tools, e.g. multizone, zonal, and CFD models, have their own merits and drawbacks when used individually. Integrated tools can combine the merits of the individual tools and avoid their drawbacks. By comparing current integrated models in previous studies, we find that the coupled multizone and zonal models have many limitations due to the restrictions of current zonal models. The coupled program of multizone and CFD models is promising, although many questions remain unsolved.

With the aim to develop a new design tool integrating multizone and CFD programs, this thesis tries to

- evaluate the assumptions of multizone models and identify the major limitations, pointing to the areas in which the multizone assumptions are inappropriate, thus verifying the need for CFD models;

- develop coupling strategies to remedy the multizone assumptions in these situations, and implement the coupling algorithms in a coupled program of multizone and CFD models;

- analyze the solution existence and uniqueness of the coupled program, and evaluate the numerical performance of the coupling methods for the implementation of the coupling algorithms;

- verify the CFD model and validate the coupled program through experimental data for the situations in which the multizone assumptions are inappropriate;

- apply the coupled program to realistic cases of building ventilation and IAQ analysis; and

- investigate under what conditions the multizone assumptions become inappropriate and provide suggestions for selection of CFD zones for a coupled multizone-CFD simulation.

This thesis is organized as follows:

- CHAPTER 2 first selects CONTAM (Walton and Dols, 2003), a multizone program, and CFD0-C, a CFD program, for the current study. The chapter then evaluates the major assumptions of CONTAM, which could become problematic in both outdoor and indoor airflow situations. The situations include the description of wind pressures around buildings, buoyancy-driven flows with temperature gradient, wind-driven flows with momentum effect, and indoor airflows with contaminant concentration gradient. To remedy the CONTAM assumptions, the current study discusses the concepts of two coupling strategies: the indirect coupling for outdoor airflow simulations, and the direct coupling for indoor airflow and contaminant transport simulations.

- CHAPTER 3 develops the coupling schemes to carry out the indirect and the direct coupling strategies. The indirect coupling employs two coupling schemes, the Wind Pressure and Contaminant (WPC) link, and the Wind Pressure Profile (WPP) link, to predict the non-uniform distribution of wind pressures for CONTAM. To remedy the assumptions associated with indoor airflow and contaminant transport simulations, the direct coupling provides coupling algorithms for three types of CONTAM simulations: steady airflow and steady contaminant transport, steady airflow and transient contaminant transport, and transient airflow and transient contaminant transport. This chapter then conducts theoretical analyses on the solutions and the coupling methods of the direct coupling algorithms. The analyses involve the existence and uniqueness of a coupled airflow simulation, and the numerical convergences and stabilities of different coupling methods. With the aim to find the most stable coupling method, this chapter then verifies the theoretical study by two

numerical experiments: one is the pressure-gradient flows in an office suite, and the other is cross ventilation in a four-zone building model.

- CHAPTER 4 verifies the capabilities of CFD0-C by comparing the numerical results with the published data for indoor and outdoor airflows. Indoor airflows include airflow through a 90-degree planar branch, natural ventilation in a stairwell, displacement ventilation, and cross ventilation in a 4-zone building model. Outdoor airflow verification includes external airflow around a building model and wind pressure and airflow distribution of a low-rise house with a slope roof. To validate the coupled program of CONTAM and CFD0-C, experimental measurements are conducted in a chamber facility for three cases: non-uniform distributions of momentum effects, contaminant concentrations, and temperatures.

- CHAPTER 5 demonstrates the indirect coupling in a simulation of outdoor airflows around a cubic building. The direct coupling algorithms are applied to simulations of natural ventilation in a three-story building with a large atrium. The simulations include three direct coupling algorithms: steady airflow and steady contaminant transport, steady airflow and transient contaminant transport, and transient airflow and transient contaminant transport.

- CHAPTER 6 conducts dimensionless analyses on the conditions, under which the multizone assumptions of uniform air momentum effect, air temperature, and contaminant concentration become inappropriate. Based on these conditions, this thesis develops a judging procedure for selection of CFD zone in a coupled CONTAM-CFD0 simulation.

- CHAPTER 7 summarizes the conclusions from the current investigation, identifies remaining challenges and points out recommendations for future work.

CHAPTER 2. MAJOR LIMITATIONS OF MULTIZONE MODELS AND REMEDY STRATEGIES ATTAINED BY COUPLING MULTIZONE AND CFD PROGRAMS

2.1. Major Assumptions of Multizone Models

One of the major motivations informing the development of an integrated multizone-CFD program is to remedy the limitations characterizing current multizone models. The major limitations of current multizone network models are associated with many of their assumptions. Due to these assumptions, multizone programs should be used only to predict building infiltrations/exfiltrations and the average values of contaminant concentrations. For other situations, where the assumptions become inappropriate, multizone programs may provide inaccurate results.

For example, multizone network models are based on the assumption that each room of a building is a zone with a uniform temperature and pressure. They also neglect the airflow momentum preserved inside a zone. These assumptions may compromise the accuracy of the results obtained for the simulations. Previous studies have noticed the problems inherent in multizone assumptions. Murakami et al. (1991) found that current multizone network models fail to account for the preservation of the kinetic energy of the airflow. Schaelin et al. (1994) thought that the local variables near the flow paths within each zone, e.g. air velocity and temperature, could have a strong influence on multizone model predictions. Later, Upham (1997) pointed out that, for non-uniform distributions of contaminant concentrations, the results of using a multizone contaminant dispersion model are questionable. Clarke (2001) also noted that current buildings' airflow modeling-by-network approach has significant limitations: because momentum effects are neglected, intra-room airflow and temperature distribution cannot be correctly determined. Recently, Gao and Chen (2003) found that multizone models produce

incorrect results if the preserved momentum within a zone is neglected. Yuan (2002) further showed, through his on-site experiments of a zone with a contaminant source, the shortcomings of the well-mixing assumption of contaminants in multizone models.

Such previous studies and the analysis of Persily (2003) summarize the major assumptions and limitations linked to multizone models as:

1. wind pressures on a building's surface are uniform by default;
2. room pressures, temperatures, and concentration of species are uniform in each zone;
3. the transport of contaminants along each flow path or within a room is instantaneous;
4. momentum and kinetic energy are not accounted for by flow path models;
5. air is quiescent or still in each zone, so the airflow through zones does not impact zone pressures.

Assumption 1 could cause problems when the wind pressures vary dramtically with the different locations on a building’s surface. Assumptions 2 and 3 are also called the well-mixing assumption, which could be problematic for simulations with poorly mixed air parameters and contaminant concentrations. Some common examples are buoyancy-driven airflows with temperature gradients, and the transport of contaminant with poorly mixed contaminant concentrations. For airflows with strong inflow momentum effects, which could influence pressure and airflow distributions inside a zone, Assumptions 4 and 5 will become inapplicable.

The above assumptions can be summed up as uniform distributions of wind pressures, temperatures, momentum effects, and contaminant concentrations, respectively. These assumptions can become critical for the following problems:

1. Description of wind pressures around buildings
2. Buoyancy-driven airflows with temperature gradient
3. Indoor airflows with strong momentum effect
4. Indoor airflows with contaminant concentration gradients

Cases 1-3 are closely related to natural ventilation designs, and Cases 3 and 4 to ventilation designs during emergencies, e.g. the emergency ventilation design that dilutes polluted air during a CBRWA attack.

On the other hand, nearly fifty multizone models have been developed during the past twenty years (Feustel and Dieris, 1992). It is hard to evaluate every multizone program for the above cases. This chapter therefore focuses on CONTAM (Walton and Dols, 2003), a public-domain multizone program from the National Institute of Standard and Technology (NIST), USA. The discussions in this chapter, however, are not limited to CONTAM since most multizone programs use similar assumptions.

CFD0-C, a three-dimensional CFD code, is selected as the CFD program to be coupled with CONTAM. Srebric et al. (1999) developed CFD0, which is also called CFD0-F, since it was written in FORTRAN. With many new capabilities, the CFD0-C is upgraded from CFD0-F through the conversion of FORTRAN to C. The conversion makes the coupling much easier because CONTAM is written in C. CFD0 utilizes SIMPLE algorithm and the solver of line-by-line TDMA (Patankar, 1980). Turbulence is accounted for by the indoor zero-equation eddy-viscosity model (Chen and Xu, 1998).

2.1.1. Description of Wind Pressures around Buildings

For buildings with natural ventilation, wind pressure is the most important driving force for airflow through the building envelope. The wind pressure is a function of wind speed, wind direction, building configuration, and local terrain effects (ASHRAE, 2005). In versions prior to CONTAM 2.1, users can account for the effects of wind pressure by three options. One can choose to ignore the effects of wind, define wind pressure to be constant, or implement variable wind pressures for each envelope penetration. CONTAM provides a general approach for handling the variable effects of wind on the building envelope. This approach requires users to provide CONTAM with a local wind pressure coefficient, C_p, for the building surface (Walton and Dols, 2003). A wind pressure profile

is required, which contains surface-averaged pressure coefficients for each building surface.

In fact, air movement around buildings is a three-dimensional turbulent flow. A more accurate approach than surface-averaged pressure coefficient is to account for variations in wind pressure coefficients by location over a building surface. Swami and Chandra (1988) presented a correlation of wind pressure coefficients for high-rise buildings, where the value of C_p was determined for a specific point on the building façade instead of being averaged over the entire façade. Since it may only apply to high-rise buildings and cannot represent average ones, the correlation has not been incorporated into CONTAM. The most reliable means of determining C_p for a specific building are through on-site measurements or wind tunnel studies (Persily and Ivy, 2001). However, the measurements can be expensive, and are often associated with technical difficulties. Hence, the CFD simulation of turbulent flows around buildings seems a better option to obtain wind pressures.

Gao (2002) has used a single-story apartment, as shown in Fig. 2.1, to demonstrate that CFD can supply specific wind pressure for each opening on a building envelope. Table 2.1 shows the wind pressures for different windows of the building when the wind speed is 3 m/s at 10m above the ground. Without reliable information, the CONTAM user might specify the same wind pressure coefficients for windows 2, 3, and 5, and for windows 7 and 8. Because the relative wind direction, as well as the difference of the wall azimuth angle and the wind azimuth angle is the same for windows 2, 3, and 5, the calculated pressure would be the same. As shown in Table 2.1, the wind pressures calculated by a CFD program vary a lot at different locations on the same building surface. Uniform wind pressure coefficients may cause significant errors for windows 2, 3, and 5. The same conclusion could be applied for windows 7 and 8.

Gao's study reveals that CFD can be used to provide non-uniform wind-pressure distributions on building surfaces. CHAPTER 3 of this thesis will develop a coupling

method, applying it to CONTAM and CFD0-C, in which CFD0-C calculates non-uniform distributions of wind pressures to improve the calculations of natural ventilation in CONTAM.

Table 2.1 Pressure distribution at the window opening.

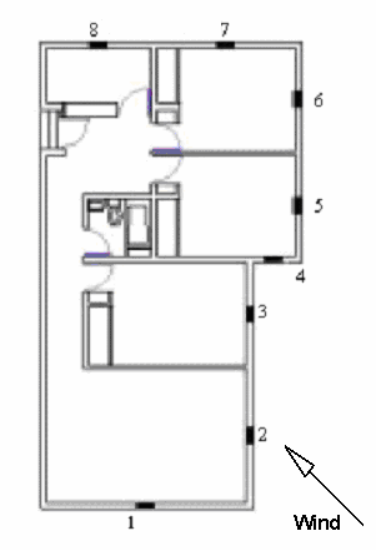

Window #	Pressure from CFD (Pa)
1	7.43
2	7.055
3	7.215
4	7.215
5	3.769
6	1.983
7	0.008
8	-6.5

Fig. 2.1 Plan view of a single-level apartment.

2.1.2. Buoyancy-driven Airflows with Temperature Gradients

Besides the effects of wind pressures, buoyancy-driven airflows are also common in natural ventilation. In simulations of buoyancy-driven flows, zone temperature is a crucial factor. Since the current version of CONTAM does not include the calculation of energy conservation, a uniform temperature must be manually specified for each zone. An improper setting of the zone temperature may result in inaccurate or even wrong results. The temperature can also stratify along the height of a zone and the assumption of a uniform temperature does not hold.

To illustrate the importance of temperature and temperature gradient in CONTAM calculations, this investigation uses a case studied by Zohrabian et al. (1990). They conducted a series of measurements of buoyancy-driven airflows between the two

compartments of a stairwell, as shown in Fig. 2.2. The study focused on the dependence of the buoyancy-induced flows on parameters such as heating, outside temperature, and heat losses through walls and inlet/outlet openings.

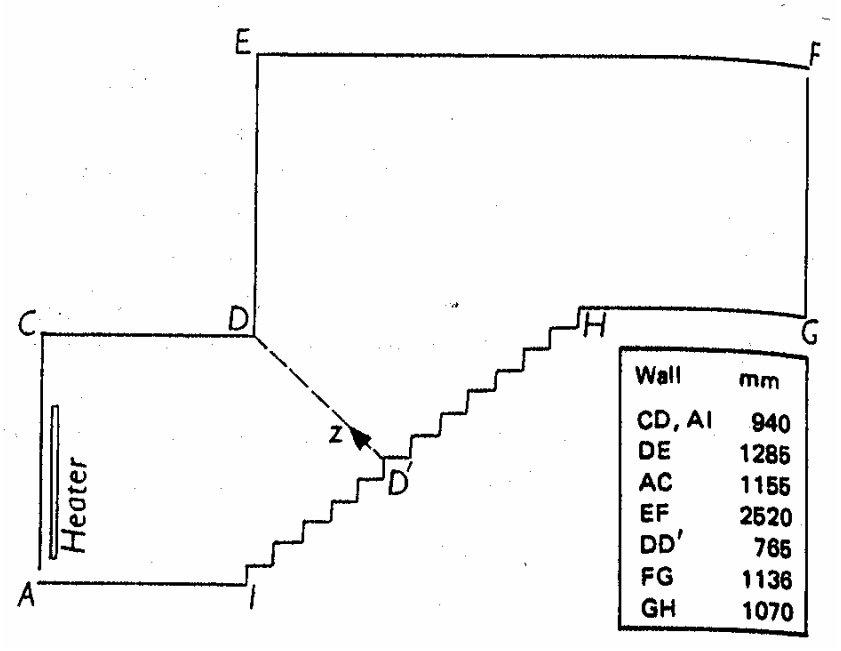

Fig. 2.2 Schematic diagram of the half-scale stairwell model.

The stairwell had two small openings at A and F. The throat area was indicated by DD´ and the sidewall was defined by ACDEFGHIA (Zohrabian et al., 1990).

The current study models the stairwell in CONTAM as a single zone by using the measured results, as shown in Table 2.2. Temperatures from the experiment are averaged as inputs for the CONTAM simulation. By using average zone temperatures, CONTAM cannot consider the temperature gradient, which is important to obtain correct airflow results for buoyancy-driven flows. Table 2.2 illustrates that in the current case, the measured vertical temperature gradient can be 7°C for 300 W and 17°C for 900 W. As a result, the calculated airflow rates by CONTAM are quite different from the measured ones.

Table 2.2 Measured results and their comparison with calculated airflow rates by CONTAM.

Q (power of the heater) (W)	Measured vertical temperature gradient (°C)	Measured average temperature (°C)	CONTAM mass flow rate$\times 10^3$ (kg/s)	Experiment mass flow rate$\times 10^3$ (kg/s)
300	7	29.6	2.850	4.484
900	17	40.4	4.485	7.223

The above analysis shows that the temperature and temperature gradient are very important parameters for buoyancy-driven flows. CONTAM users could obtain the temperature and temperature gradient by carrying out certain experiments, but such a process may not be easy. Even if the temperature gradient obtained from experiments is available, it cannot be used by CONTAM due to the well-mixing assumption. Thus, obtaining zone temperatures when experimental data is unavailable and assessing the temperature gradient in buoyancy-driven flows are two of the major problems facing CONTAM.

2.1.3. Indoor Airflows with Strong Momentum Effects

CONTAM assumes that the air in a zone is quiescent or still, and the airflow through a zone does not have an impact on zone pressure. The assumption is valid for the cases, in which air velocity through openings is low enough to be immediately dissipated or distributed after entering the zone. This is commonly true in the case of infiltration through small openings.

However, a strong momentum effect may be preserved, contributing to spatial variations in zone pressure, such as airflows provided by large openings in the case of a building's natural ventilation. Murakami et al. (1991) used a multizone network model to study cross ventilations with an open window. The airflow preserved a large part of its mean kinetic energy when it remained inside the room. They found that current multizone network models could not account for the preservation of the airflow's kinetic energy. So

the models tended to overestimate the pressure loss and underestimate the total pressure. Since natural ventilation design has become a new trend, it is important that CONTAM should be able to address such a flow.

In order to further illustrate the problem concerning the neglect of the momentum effect in multizone models, the present study selects a case from Hayes et al. (1989), and Kelka and Choudhury (2000). They studied a 90-degree planar branch case, as shown in Fig. 2.3. It should be noted that this study selects the 90-degree planar branch since it can be regarded as flow through corridors. The connection of two corridors is very similar to the planar branch so we can study how flow is distributed in two corridors. Table 2.3 further lists different fractional flow rates in the main branch, Φ, versus different Reynolds numbers. Since CONTAM neglects the momentum and the kinetic energy of airflow within the zone, the flow through the main branch will be the same as that through the side branch, so Φ will be always 0.5. As shown in Table 2.3, when the momentum is insignificant (or the Reynolds number is very small), Φ is approaching 0.5. As the Reynolds number increases, CONTAM would not produce acceptable results.

The momentum effect becomes significant for airflow distributions in cases of natural ventilation or emergency ventilation, e.g. during a fire. The above case shows that since CONTAM neglects the preserved momentum effect inside a zone, it will provide inaccurate results for the study of airflow distributions.

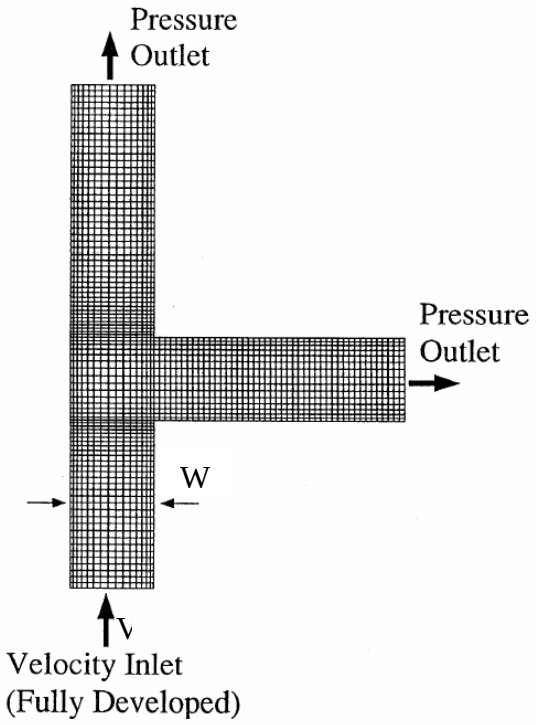

Fig. 2.3 Geometry and grid of 90-degree planar branch (Kelka and Choudhury, 2000).

Table 2.3 Fractional flow rate in main branch as a function of Reynolds number (Kelka and Choudhury, 2000).

Re (Reynolds number)	Φ (Fractional flow rate in main branch)
10	0.522
100	0.725
200	0.830
300	0.883
400	0.911

2.1.4. Indoor Airflows with Contaminant Concentration Gradients

CONTAM also assumes the existence of species concentrations in each zone to be uniform at all time steps. Within each time step, the contaminant is distributed throughout a zone with zero time delay. When the time scale for a zone is small compared to the total transport time concerned, e.g. in a whole building, this assumption may be acceptable. Otherwise, we must account for the time delay, which may be a crucial factor in some cases, e.g. when we need to compute the time required for a sensor to produce a control signal.

Schaelin et al. (1994) noticed the possible errors caused by the assumption of uniform contaminant concentration. They illustrated a zone with three openings and a contaminant source in the zone, as in Fig. 2.4. The contaminant concentration distribution, indicated by the contour lines in Fig. 2.4, was not uniform in the zone. Table 2.4 shows that the contaminant concentration at the three openings could be very different, depending on the

airflow pattern and the position of the contaminant sources. CONTAM, however, would treat the contaminant transported to the neighbor zone with the same concentration for all the openings.

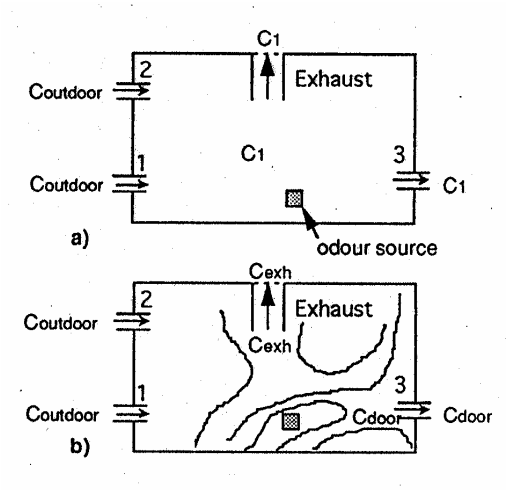

Fig. 2.4 (a) Contaminant values in a multizone model. (b) Contaminant values in CFD (Schaelin et al., 1994).

Table 2.4 Concentration values at different locations for different models (Schaelin et al., 1994).

The case with wind	Mean contaminant (ppm)	C_{door} (ppm)	C_{exh} (ppm)
a) Multizone only (perfect mixing)	0.15	0.15	0.15
b) Detailed flow path value method	0.12	0.09	0.185

The transport of contaminant from one zone to a neighboring space depends on the local concentrations at the flow paths. These local concentrations are influenced by the positions of heat and contaminant sources and of the resultant airflow pattern. Schaelin et al. applied CFD to calculate the airflow pattern and non-uniform contaminant concentration in the zone. Then they extracted local concentrations from the CFD results as inputs for the multizone program. The procedure was called a "ping-pong" technique, which was a one-iteration coupling between the CFD and the multizone model. Their test cases showed that the calculated concentrations from this technique differ by a factor of up to 2.5 from the pure multizone approach. Their results from the coupled simulation look more reasonable than those obtained from only multizone simulation.

Recently, Yuan (2003) tried to consider the non-uniform contaminant concentration in CONTAM by using CFD results. He also validated the results with on-site experimental

data and found that the CONTAM results could be improved. Although his approach was a manual coupling procedure, it is a good starting point for further studies. Inspired by such research, this study develops several strategies to integrate CONTAM with a CFD program, CFD0-C as discussed in the following sections.

2.2. Remedy Strategies by Coupling CONTAM and CFD0-C

The above analysis shows some major limitations of multizone programs:

- the assumption of uniform wind pressures around buildings could result in an inaccurate description of wind pressures on a building surface;
- the assumption of uniform temperature distribution could not consider the temperature gradient in buoyancy-driven flows;
- the assumption of neglecting inflow momentum fails to consider the momentum effect on airflow distributions;
- the assumption of uniform contaminant concentration could cause inaccurate predictions when a contaminant is poorly mixed inside a zone.

Depending on whether the above problems are airflow simulations around or in buildings, the current study develops different remedy strategies for the coupled CONTAM-CFD0 program.

Indirect/Virtual coupling for outdoor airflow simulations

To remedy the assumption of uniform wind pressures on a building surface, an indirect (or virtual) coupling strategy should be used. The strategy uses CFD0-C to simulate the wind flow around a building, which can be illustrated by a three-story building in Fig. 2.5. The building will be simulated as a solid block without internal zones, by the CFD0-C. Then the CFD0-C calculates the wind pressures at different locations of the building as denoted by arrows in Fig. 2.5. CONTAM afterwards simulates airflows for all the internal zones by obtaining the calculated wind pressure information from the CFD0-C.

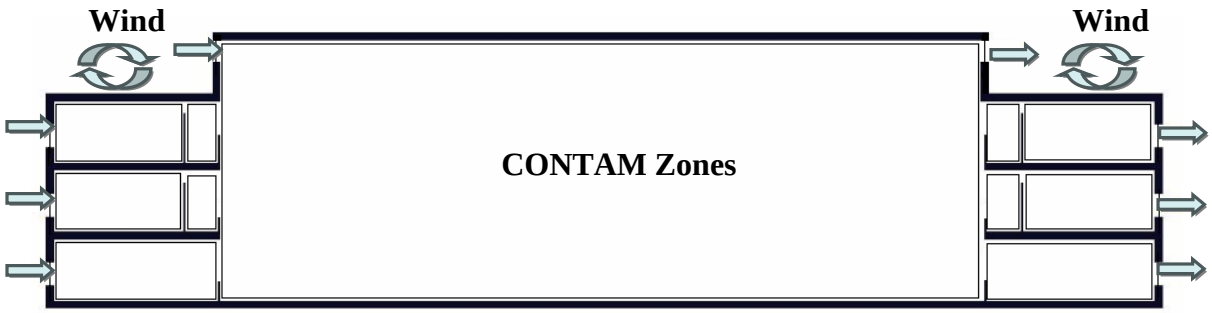

Fig. 2.5 A conceptual illustration of the indirect coupling of CONTAM and CFD0-C for outdoor airflow simulations in a three-story building with a large atrium.

Since the building is simulated in CFD0-C as a solid block, which is a common technique in CFD simulations (Jiang, 2002), no information is needed from the internal CONTAM zones. The information is exchanged between CFD0-C and CONTAM only once, through wind pressures. Thus, the above procedure is described as an indirect or virtual coupling, compared to the direct/dynamic coupling, which will be discussed next.

Direct/Dynamic coupling for indoor airflow and the transport of contaminant simulations

For indoor airflow and contaminant transport simulations, CONTAM uses the assumptions of the uniform distribution of momentum effect, temperature, or contaminant concentration. A direct/dynamic coupling strategy is developed to remedy the assumptions. The strategy will divide a building's rooms into two types of zones. For zones where these assumptions are inappropriate, CFD0-C will be used and CONTAM is applied to the rest of the zones. Fig. 2.6 illustrates the direct coupling concept in the same building, as in the previous section. CFD0-C is used for the atrium, which is so large that air and contaminant properties apparently cannot be distributed uniformly. The rest zones are much smaller than the atrium and CONTAM can be used by rule of thumb.

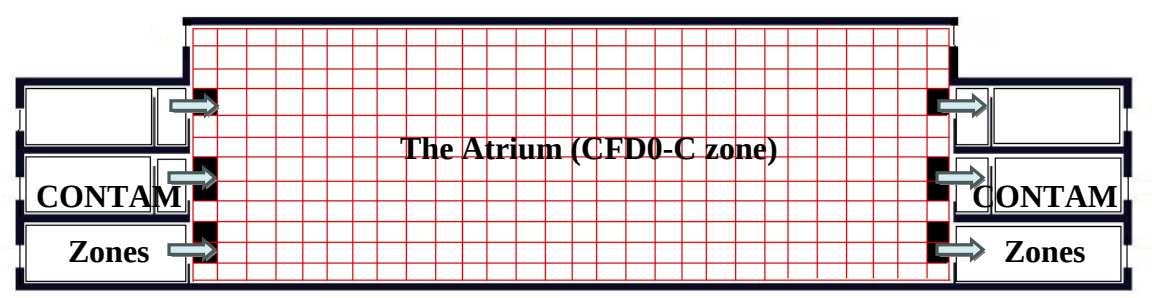

Fig. 2.6 A conceptual illustration of the direct coupling of CONTAM and CFD0-C for indoor airflow and contaminant transport simulations in a three-story building with a large atrium.

The zones of CFD and CONTAM are connected by the airflow paths at their interfaces (hereafter, interface paths as designated by arrows in Fig. 2.6). Specifically, the solid cells in the CFD zone connect the atrium directly to the CONTAM zones. Due to these physical connections, the information of airflow and contaminant transport needs to be exchanged between the two programs. Compared to the indirect coupling, the direct coupling is an iterative procedure since CONTAM and CFD0-C often cannot reach convergence with only a one-time information exchange. Therefore, the direct coupling is also called the dynamic coupling of CONTAM and CFD0-C.

Moreover, the direct coupling is also more complex than the indirect coupling. Given that the information is exchanged iteratively between CONTAM and CFD0-C, the coupling procedure might not reach stable solutions. Although stable solutions exist, another question is whether the solution is unique. In addition, the above analysis only conceptually illustrates the strategies of coupling CONTAM and CFD0-C. To integrate these two programs, each of which has its own program and data structure, appropriate coupling schemes also need to be developed. CHAPTER 3 will provide answers to these questions.

2.3. Summary

This chapter studies the situations, in which the major multizone assumptions could become problematic. When wind pressures vary with the locations of openings on a building surface, the assumption of uniform wind pressures of CONTAM is inappropriate. For indoor airflow simulations, the CONTAM assumptions could cause problems with non-uniform distributions of momentum effect and temperature gradient, as well as contaminant concentration.

This chapter proposes the concept of an indirect coupling strategy for the problem associated with non-uniform wind pressure distribution and a direct coupling strategy for the remaining situations, as summed up in Fig. 2.7.

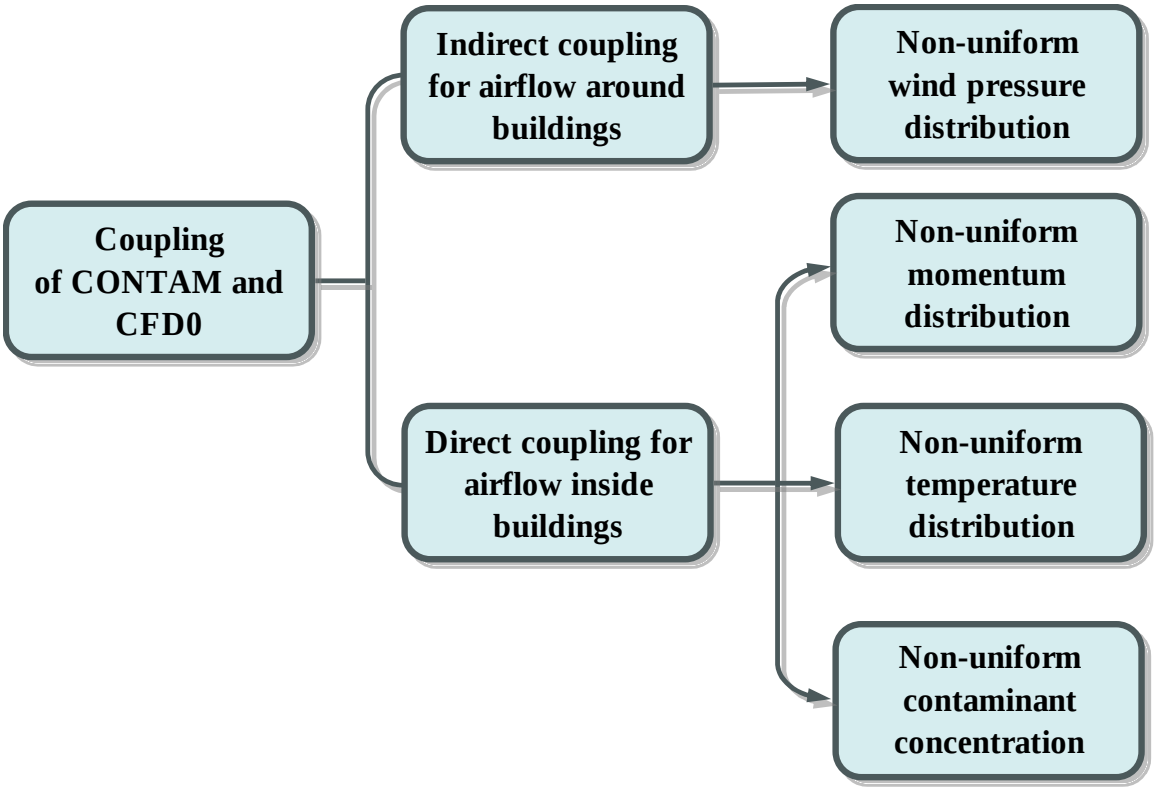

Fig. 2.7 Coupling strategies for coupled simulations of non-uniform distributions of wind pressure, momentum, temperature, and contaminant concentration.

Fig. 2.7, however, only proposes the concepts about how to couple CONTAM and CFD0-C. CHAPTER 3 will develop the coupling schemes to implement the coupling strategies. More studies will also be conducted on the solution characteristics for coupled indoor airflow simulations.

CHAPTER 3. COUPLING CONTAM AND CFD0 FOR AIRFLOW AND CONTAMINANT TRANSPORT AROUND AND IN BUILDINGS

The coupling of CONTAM and CFD0-C is meant to integrate these two individual programs in a single coupled program. However, the program and data structures of CONTAM and CFD0-C are quite different from each other, as shown in Fig. A.6 and Fig. B.1 in the Appendices. The integration of the two programs should keep the programs' integrity and at the same time cause minimal modifications in each program. To be specific, the coupled program should be developed with knowledge of

- what information needs to be exchanged between the two programs;
- how the exchanged information should be formatted in one program to be directly accepted by the other;
- where, when and how the information should be exchanged in both programs.

To answer the above questions, this thesis thus develops different coupling schemes for the indirect and the direct coupling, as discussed next.

3.1. Indirect/Virtual Coupling of CONTAM and CFD0-C for the Non-uniform Distribution of Wind Pressure around Buildings

The indirect coupling strategy only uses one-step, sequential runs of CFD0-C and CONTAM. First, the CFD0-C calculates the distribution of wind pressures or wind pressure coefficients on building surfaces, which are stored in a file. CONTAM then extracts these data from this file for simulations of indoor airflow and contaminant transport. Since wind pressure or wind pressure coefficient is exchanged between the CONTAM and the CFD0-C only once through the file, this process is an indirect or virtual coupling of the two programs. The indirect coupling is realized through two

methods: a Wind Pressure and Contaminant (WPC) link, which provides wind pressures, and a Wind Pressure Profile link, which calculates wind pressure coefficients for CONTAM simulations.

3.1.1. Indirect Coupling of CONTAM and CFD0-C by the Wind Pressure and Contaminant (WPC) Link

To implement the indirect coupling, a coupling scheme specifying wind pressures in CONTAM is developed, as shown in Fig. 3.1. The scheme uses a Wind Pressure and Contaminant file (WPC file) to provide wind pressure data for each path on the building envelope, which are required by CONTAM. Note that CONTAMX in Fig. 3.1 is the solver and CONTAMW is the Graphic User Interface (GUI) of CONTAM. To create the WPC file, the CFD0-C first generates an intermediate file, External Wind pressure and a Contaminant (EWC) file, as well as a CFD0-formatted file with three-dimensional wind pressures. Due to the format differences of EWC and WPC files, a format-converting program, WPC translator, converts the EWC file into a WPC file by reading a Path Location Data (PLD) file, which provides path location information. The advantage of this method is that when the path location changes, wind pressure can be obtained easily without running CFD0-C again.

On the other hand, wind pressure distribution also depends on terrain characteristics at a building site, wind direction and velocity. The WPC link needs to recalculate wind pressures when the wind direction and velocity vary or the building location is changed. The resultant computing time will be enormous especially under a transient weather condition. The WPC link can be improved by a method as discussed next.

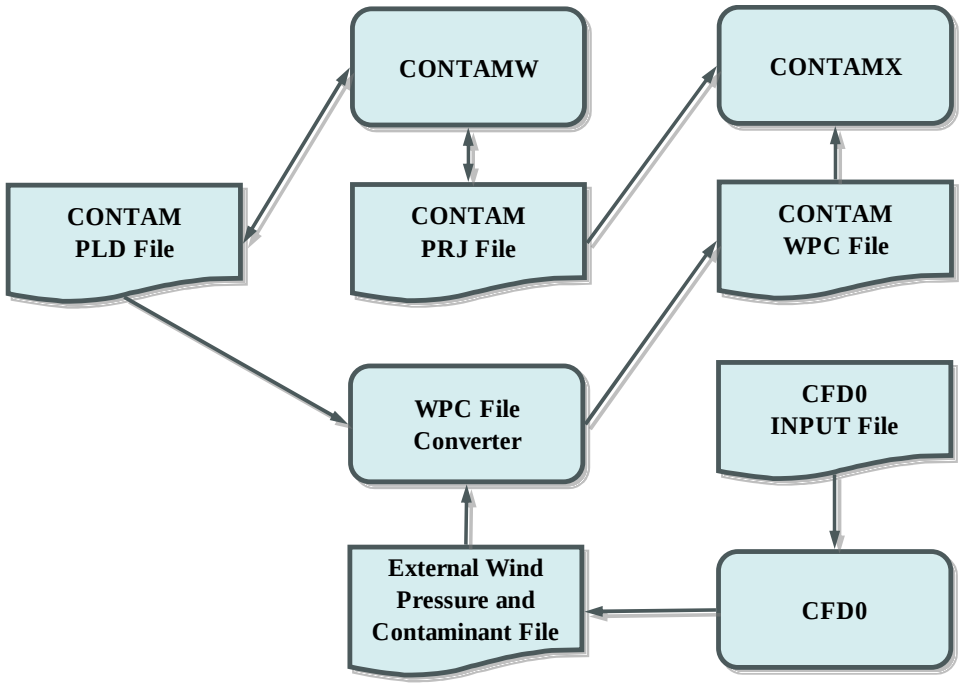

Fig. 3.1 The schematic of the indirect coupling attained by using the WPC link (Walton and Dols, 2003).

3.1.2. Indirect Coupling of CONTAM and CFD0-C by the Wind Pressure Profile (WPP) Link

For the calculation of wind pressures under variable wind velocity and direction, one of the methods to reduce the computing cost of the WPC link is to use wind pressure coefficients.

$$C_P = \frac{P_W - P_H}{\frac{1}{2}\rho U_H^2} \tag{3.1}$$

where C_P is the wind pressure coefficient, P_W is the wind pressure at the building surface, P_H is the undisturbed wind pressure at the reference height H, and U_H is the wind velocity at the reference height H.

Eq. (3.1) shows that wind pressure coefficients are dimensionless and independent of wind velocity. Hence, wind pressures for a certain wind velocity can be obtained from previously calculated wind pressure coefficients without running CFD simulation again. The value of the wind pressure coefficient, C_P, however, does depend on local terrain features (ASHRAE, 2005), which can be considered by the adjustment of wind velocity profile, U_H, through the following equation.

$$U_H = U_{met}\left(\frac{\delta_{met}}{H_{met}}\right)^{\alpha_{met}}\left(\frac{H}{\delta}\right)^{\alpha} \tag{3.2}$$

where U_{met} is the wind velocity at the height of H_{met}, δ_{met} is the atmospheric boundary layer thickness, α_{met} is the exponent, and H_{met} is the reference height at the meteorological station; δ, H, and α are the corresponding values for the local terrain. These terrain features can be determined from Table 3.1.

Table 3.1 Atmospheric boundary layer parameters (ASHRAE, 2005).

Terrain Category	α (Exponent)	δ (m, Layer Thickness)
Large city centers	0.33	460
Urban and suburban areas	0.22	370
Open terrain with scattered obstructions	0.14	270
Flat, unobstructed areas	0.10	210

The method of using wind pressures coefficients for the indirect coupling is called a Wind Pressure Profile (WPP) link, which includes two steps as illustrated by Fig. 3.2. In the first step, CFD0-C calculates a database of wind pressure coefficients, the WPP file, with specified terrain features by users. A format-converting program, the WPP converter, will then extract the wind pressure coefficients from the WPP file and create a CONTAM library file of C_P values at each path of a building for variable wind directions. In Step 2, CONTAM will convert wind pressure coefficients to wind pressures, P_W,

through Eq. (3.1). Since the WPP link employs wind pressure coefficients instead of wind pressures, it can reuse the calculated wind pressure data and reduce computational cost.

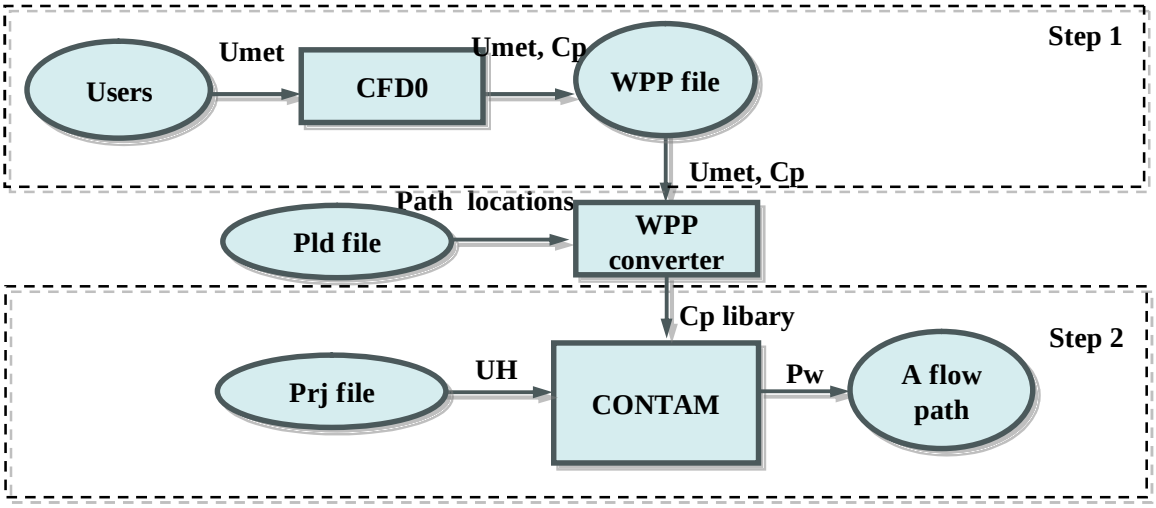

Fig. 3.2 The schematic of the indirect coupling attained by using the WPP link.

The indirect coupling attained by using a WPC link and a WPP link is indeed a sequential run of CFD0-C and CONTAM. The wind pressures or wind pressure coefficients are exchanged only once between the two programs through the CONTAM WPC/WPP file. The procedure is straightforward and thus can be easily controlled. Nevertheless, this is not the case for the direct coupling.

3.2. Direct Coupling of CONTAM AND CFD0-C for Non-uniform Distributions of Momentum, Temperature, and Contaminant Concentrations in Buildings

3.2.1. Direct Coupling Controller and Coupling Data Interface

Compared to the one-step, sequential procedure of the indirect coupling, the direct coupling needs to exchange information iteratively until both CONTAM and CFD0-C reach convergence. Thus, the direct coupling is a multi-step, iterative procedure. “What”

are exchanged between the CONTAM and the CFD0-C can be airflow rates and pressures for airflow simulations, as well as contaminant concentrations for contaminant transport simulations. In order to manage the exchanged information easily, the direct coupling stores the exchanged information in the data interface of a computer's memory, as shown in Fig. 3.3. A coupling controller controls the locations, "where" the information should be exchanged, and the running sequences of the two programs. Appendix B.3 provides the locations in the CONTAM code, where the information is exchanged. It also shows that by using the coupling controller and the data interface, the resultant modifications in CONTAM and CFD0-C are minimal.

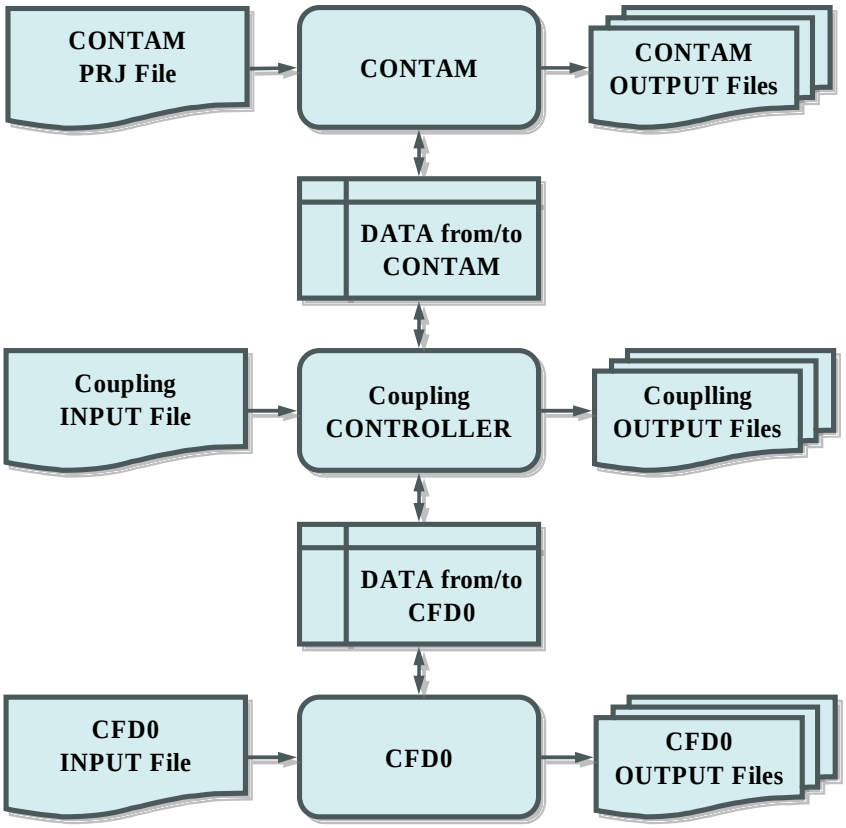

Fig. 3.3 The schematic of the direct coupling attained by using the coupling controller and the coupling data interface.

3.2.2. Direct Coupling Algorithms for Different Simulation Types

In addition to deciding "where" the information is exchanged, the coupling controller in Fig. 3.3 also determines "when" the information is exchanged by following certain coupling algorithms, and "how" to exchange the information by using certain coupling methods.

This study develops the coupling algorithms within the framework of different CONTAM solution methods. CONTAM has five solution methods for different combinations of airflow and contaminant transport simulations, as shown in Table 3.2 (Walton and Dols, 2003). Since cyclic simulations are special cases of transient simulation, the current study only needs to develop coupling schemes for Types 1-3. The scheme for Type 2 can be used for Type 4, and Type 3 for Type 5.

Table 3.2 Simulation types for airflow and contaminant simulations in CONTAM.

Simulation Type	Airflow Simulation	Contaminant Simulation
Type 1	Steady State	Steady State
Type 2	Steady State	Transient
Type 3	Transient	Transient
Type 4	Steady State	Cyclic
Type 5	Transient	Cyclic

This investigation has proposed three coupling algorithms for the coupled airflow and contaminant simulations. As shown in Fig. 3.4, the coupled program first reads a CONTAM project file to provide all the information for CONTAM and a coupling definition file for the coupling. The zones, where CFD0-C is applied to, are then "de-coupled" from the airflow network of CONTAM.

For steady-state airflow and contaminant transport (Type 1), the scheme will use previously calculated airflow data if it is available. The coupled program will import the airflow data from CFD0 and provide them directly to CONTAM. CONTAM will then calculate the transport of contaminants for a whole building and the results are used as

boundary conditions for CFD zones. CFD0 will calculate contaminant distributions for the CFD zones and send back the contaminant data as corrected sources or sinks for the CONTAM zones. Without previously calculated airflow data, the coupled program needs to obtain airflow field. CONTAM will first calculate the pressures and airflow rates. Then the CFD0 will be called to calculate the airflow for the CFD zones. Iterations with CONTAM are necessary until convergence. With the converged airflow data, the contaminant distribution can be calculated in the same way stated above.

For steady-state airflow and unsteady contaminant transport (Type 2), the calculation of airflow is the same as that for Type 1, which is framed by the dash line on the left of Fig. 3.4. A transient coupling is then performed for contaminant transport. At each time step, a similar procedure to that of Type 1 can be applied. The coupling simulation continues until the maximum time specified for contaminant transport is reached.

For transient airflow and transient contaminant transport (Type 3), similar procedures of coupling for airflow and contaminant simulations of Type 1 can be used for each time step, as shown in Fig. 3.4.

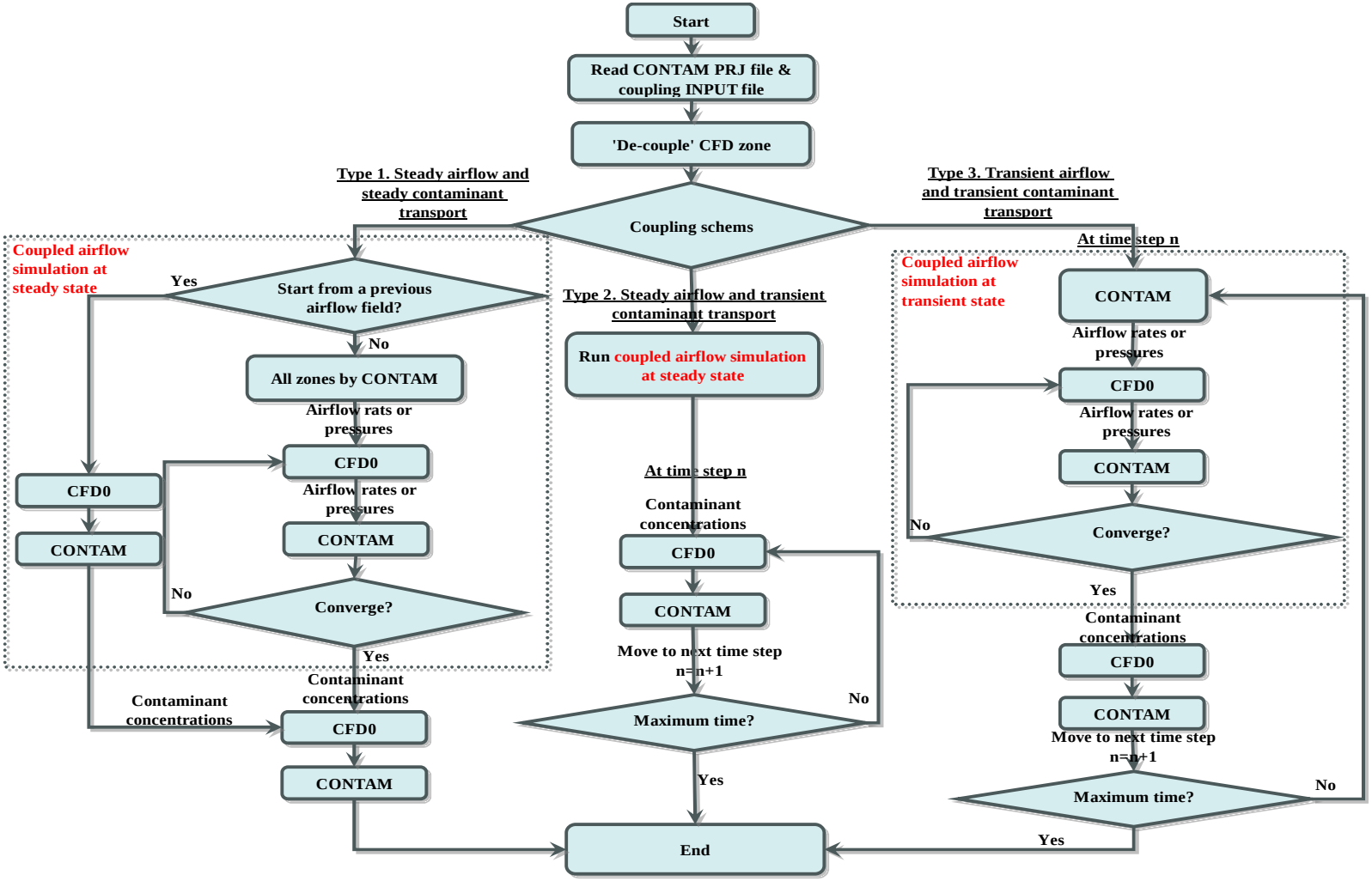

Fig. 3.4 Three coupling schemes for the coupled CONTAM and CFD0-C simulations.

After deciding on the "what, where, and when" of the exchange of information in direct coupling, the coupling controller needs to follow certain coupling methods to determine "how" to exchange the information. Some previous studies (Negrao, 1998; Bartak et al., 2002; Beausoleil-Morrison, 2002) developed several coupling methods. However, they found convergence and stability problems with some of the methods. In some cases, multiple coupling solutions could happen as well. Thus, it is necessary in this study to conduct theoretical analysis to answer the following questions:

- Are there solutions to direct coupling?
- If the solutions exist, is the solution unique?
- If the solution is unique, which coupling method is the best, namely, which is the most stable method to obtain a unique solution?
- If the solution is not unique, what reasons cause multiple solutions?

3.2.3. Coupling Solution Existence and Uniqueness

CONTAM and CFD0-C solve different sets of conservation equations. CONTAM only solves air mass and contaminant conservation equations, while CFD0-C solves the Reynolds Averaged Navier-Stokes equations. When the two programs are coupled, it is not known for certain whether there are solutions and if the solution is unique without relying on theoretical analysis. Unfortunately, not much work has been done on theoretical investigations, although previous studies (Schaelin et al., 1994; Negrao, 1998; Musser, 2001; Jayaraman et al., 2004) show promising numerical results. On the other hand, in the coupled building energy and CFD simulations, Clarke et al. (1995b) proved the existence of a coupling solution by analyzing a super-matrix of the coupling. Zhai and Chen (2003) investigated the uniqueness of the solution by performing parametric analysis for both energy simulation and CFD models. Inspired by their studies, this chapter uses an analogue methodology to investigate whether a coupled multizone and CFD program can have a solution for an airflow problem, and if the solution is unique.

Basic equations and coupling principles

In order to analyze if a coupled multizone and CFD simulation has a solution and if the solution is unique, the analysis should start with the fundamentals of direct coupling. The idea behind multizone-CFD coupling is to apply a multizone program to most zones of a building while applying a CFD program to the zones, where the multizone assumptions are not appropriate. Fig. 3.5 illustrates the coupling schematic for natural ventilation in a portion of the three-story building illustrated in Fig. 2.6. The atrium is so large that the well-mixing assumption is inappropriate and zone c is thus chosen as the CFD zone, while the remaining zones are modeled with the multizone program. Although the zones modeled with the multizone program are connected to zone c by paths at their interfaces, the equations solved by the multizone and the CFD programs are quite different from each other.

If path ij connects zone i and zone j and F_{ij} is defined as the airflow rate through path ij, F_{ij} is normally calculated in a multizone program by a power-law function of the pressure drop across path ij,

$$F_{ij} = C_{ij} \mid \Delta P_{ij} \mid^{n_{ij}} = C_{ij} \mid P_i - P_j + P_{S,ij} + P_{W,ij} \mid^{n_{ij}} \tag{3.3}$$

where F_{ij} is the airflow rate, C_{ij} is the flow coefficient, ΔP_{ij} is the pressure difference, $P_{S,ij}$ is the pressure difference due to desity and elevation difference, $P_{W,ij}$ is the pressure difference due to wind through path ij; P_i and P_j is the total pressure of zone i and j, respectively.

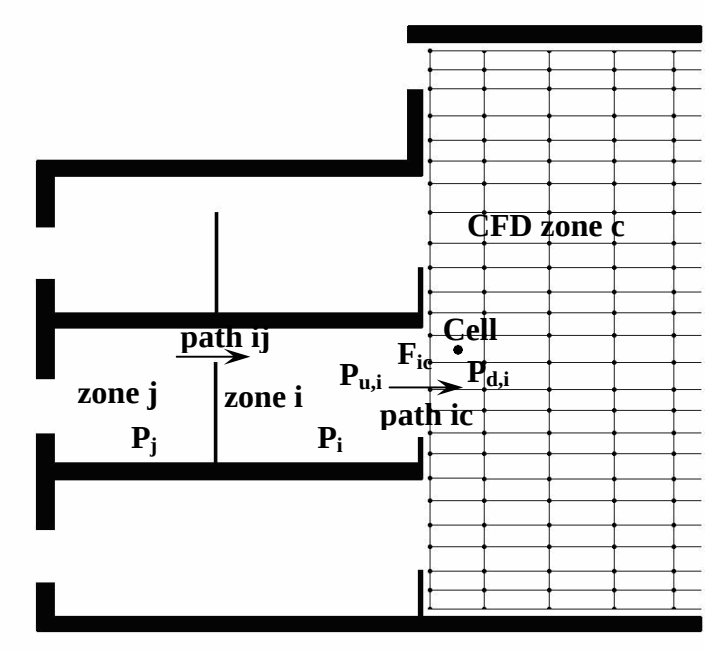

Fig. 3.5 Coupling schematic in a portion of a three-story building with an atrium.

Suppose path ic connects zone i for the multizone program and zone c for the CFD program, and the flow rate through path ic is F_{ic}, a mass continuity equation under a steady state condition can be obtained for zone i by the multizone program

$$\sum_j F_{ij} - F_{ic} = b_i \tag{3.4}$$

where F_{ic} is the airflow rate through path ic and b_i is the mass source term of zone i.

In the CFD program, a set of partial differential governing equations for mass, momentum, and energy conservation are solved. The equation can be written for steady state flow in a general form

$$\nabla(r\mathbf{V}f) - \Gamma_f \nabla^2 f = S_f \tag{3.5}$$

where f can be 1 for mass continuity, U_j for air velocity component in the j direction (j=x, y, z), and T for temperature. With the SIMPLER algorithm (Patankar, 1980) the mass continuity equation actually becomes a pressure equation. If path ic has n discrete grid points and we focus only on the grid point P (or cell P), the pressure equation for point P can be written in the following linear form

$$\sum a_{nb} p_{nb} - a_P p_P + f_P = b_P \tag{3.6}$$

where a_{nb} and p_{nb} is the coefficient and pressure of the neighboring grid point, respecively; a_p is the coefficient, p_p is the pressure, f_p is the net airflow rate through the face of a CFD cell, and b_p is the mass source term at the grid point p in CFD.

A linear form can also be obtained for non-linear Eq. (3.4) in a multizone program

$$\sum_j C_{L,ij}(P_j - P_i) - F_{ic} = b_i' \tag{3.7}$$

where $b_i' = b_i - \sum_j C_{L,ij}(P_{S,ij} + P_{W,ij})$, by defining a linear flow coefficient

$$C_{L,ij} = \frac{F_{ij}}{\Delta P_{ij}} \tag{3.8}$$

Eqs. (3.6) and (3.7) show mathematically that F_{ic} and f_P are the only linkages between the multizone and the CFD equations. It is thus important to know how they are calculated in both programs and how they are related to each other.

A CFD program calculates

$$f_P = C_P(P_{u,ic} - p_P)^{n_P} = C_{L,P}(P_{u,ic} - p_P) \tag{3.9}$$

where $P_{u,ic}= P_i + d_{ic}$, which is the upwind total pressure of path ic if the airflow is from zone i to zone c; C_p, n_p and $C_{L,p}$ is nonlinear flow coefficient, exponent, and linear flow coefficient of the grid point p, respectively . In a multizone program

$$F_{ic} = C_{ic}(P_{u,ic} - P_{d,ic})^{n_{ic}} = C_{L,ic}(P_{u,ic} - P_{d,ic}) \tag{3.10}$$

where C_{ic} is the flow coefficient, n_{ic} is the exponent, $C_{L,ic}$ is the linear flow coefficient, and $P_{d,ic}$ is the average downwind total pressure for path ic. Eq. (3.10) is actually the integral form of Eq. (3.9) and it comes

$$F_{ic} = \sum_{P=1}^{n} f_P \tag{3.11}$$

where n is the total number grid points in CFD for path ic.

An assembled total matrix equation can then be obtained by applying Eqs. (3.6) and (3.7) to all the zones in Fig. 3.5.

$$\mathbf{CP} + \mathbf{F} = \mathbf{B} \tag{3.12}$$

where **C** is the flow coefficient maxtrix, **P** is the unknown pressure vector of zones and cells, **F** is the vector of unknown flow rates at the interface paths and cells, and **B** is the vector of source terms. To ensure that Eq. (3.12) is closed, two coupling principles must be followed.

- Eq. (3.11) should be used as the convergence criterion of the coupled simulation.
- The relationship of the flow rate and the pressure drop in Eq. (3.9) must be the known condition for each grid point of path ic.

To implement Eq. (3.9) in the coupling program as the convergence criterion, a relative residue is defined by:

$$\frac{\sum_{k=1}^{m}(|F_{ic}-\sum_{P=1}^{n}f_P|)_k}{F_{inf\,low}} \le \varepsilon \qquad (3.13)$$

where k and m are the index and the total number of the interface paths, respectively, F_{inflow} is the total inflow to the CFD zone, and ε is 1% in current study.

With the above two principles and Eq. (3.12), we can examine important parameters linking the multizone and the CFD equations in the coupling.

Parameter analysis

In the coupling, the important parameters are $P_{u,ic}$, $P_{d,ic}$ and F_{ic} for both multizone and CFD programs. In order to conduct theoretical analysis on these parameters, this investigation uses the following simplifications:

- Flow coefficients $C_{L,P}$, $C_{L,ij}$, and $C_{L,ic}$; the source terms, b_i, $b_i^{'}$, d_{ic}, b_P, and B; and the coefficients, a_P and a_{nb} are constant from one coupling iteration to the next (one coupling iteration includes one call of multizone and one call of CFD).
- In the CFD calculation, the flow coefficients, $C_{L,P}$ and a_P, and the pressures, p_P and p_{nb}, are uniform at path ic.
- The derivatives of $P_{d,ic}$ and F_{ic} over $P_{u,ic}$ are existent and bounded.

Although both problems formulated by multizone and CFD simulations are nonlinear, it is appropriate to assume mathematically the flow coefficients of the multizone method, $C_{L,ij}$ and $C_{L,ic}$ as defined by Eq. (3.8), to be constant. This assumption is valid as long as the change of pressure difference, ΔP, is small from one multizone call to the next during coupled iterations. If we focus on the vicinity of ΔP, the flow coefficients can shift slowly with ΔP so it can be considered constant. In CFD, the coefficients, $C_{L,P}$, a_P and a_{nb}, can also be assumed to be constant as long as the boundary conditions do not change significantly from one CFD call to the next. Technically, this can be realized in the coupling program by under-relaxing the flow coefficients in both the multizone and

CFD methods. Users can check how the flow coeffients are under-relaxed from the output file for a coupled simulation as discussed in Appendix B.2. On the other hand, for nonlinear problems, it is hard or sometimes impossible to conduct theoretical studies such as solution uniqueness and stability analysis. Thus, such simplifications are necessary for the nonlinear problem.

From the above simplifications, we can obtain the following relationships for a multizone program by using Eqs. (3.7) and (3.10)

$$P_{d,ic} = \frac{C_{L,ic} + C_{L,ij}}{C_{L,ic}} P_{u,ic} - \frac{C_{L,ij} P_j - C_{L,ij} d_{ic} - b_i'}{C_{L,ic}} \tag{3.14}$$

$$F_{ic} = -C_{L,ij} P_{u,ic} + C_{L,ij} P_j - C_{L,ij} d_{ic} - b_i' \tag{3.15}$$

By using Eqs. (3.6), (3.9), (3.10) and (3.11) for a CFD program we have

$$P_{d,ic} = \frac{C_{L,P}}{a_P + C_{L,P}} P_{u,ic} + \frac{\sum a_{nb} p_{nb} - b_P}{a_P + C_{L,P}} \tag{3.16}$$

$$F_{ic} = \frac{a_P C_{L,ic}}{a_P + C_{L,P}} P_{u,ic} - \frac{C_{L,ic} (\sum a_{nb} p_{nb} - b_P)}{a_P + C_{L,P}} \tag{3.17}$$

These equations reveal the mathematical relationships of $P_{u,ic}$, $P_{d,ic}$, and F_{ic}, which are exchanged between the two programs iteratively through boundary conditions. The existence and uniqueness of the solution to this iterative procedure can be investigated by studying the derivatives of these equations for a coupled simulation.

Solution existence and uniqueness

Zhai (2003) successfully coupled a program for building energy simulation with a CFD program. This investigation uses a similar approach to their study to prove the existence

and uniqueness of a solution for a coupled multizone and CFD program. The basic idea is to analogize pressure in coupled airflow simulations and air temperature in coupled energy simulations.

Applying the derivatives over $P_{u,ic}$ for both sides of Eqs. (3.14) - (3.17), we have

$$\frac{\partial P_{d,ic}}{\partial P_{u,ic}} = \begin{cases} \dfrac{C_{L,ic} + C_{L,ij}}{C_{L,ic}} - \dfrac{C_{L,ij}}{C_{L,ic}} \dfrac{\partial P_j}{\partial P_i} \text{(multizone)} \\ \dfrac{C_{L,P}}{a_P + C_{L,P}} + \dfrac{\sum a_{nb} \dfrac{\partial p_{nb}}{\partial P_{u,ic}}}{a_P + C_{L,P}} \text{(CFD)} \end{cases} \tag{3.18}$$

$$\frac{\partial F_{ic}}{\partial P_{u,ic}} = \begin{cases} -C_{L,ij} + C_{L,ij} \dfrac{\partial P_j}{\partial P_i} \text{(multizone)} \\ \dfrac{a_P C_{L,ic}}{a_P + C_{L,P}} - \dfrac{\sum a_{nb} \dfrac{\partial p_{nb}}{\partial P_{u,ic}}}{(a_P + C_{L,P})/C_{L,ic}} \text{(CFD)} \end{cases} \tag{3.19}$$

One of the conditions of unique solution to a steady-state airflow simulation in a multizone program is that increase of pressure in one zone should increase or maintain the net outflow to the neighboring zones (Lorenzetti, 2002). This implies that in Fig. 3.5, the increase of P_i should increase or maintain P_j

$$\frac{\partial P_j}{\partial P_i} \geq 0 \tag{3.20}$$

In a CFD program, the increase of $P_{u,ic}$ will increase or maintain the pressures of the nodes next to it and the flow rate through Path ic

$$\frac{\partial p_{nb}}{\partial P_{u,ic}} \geq 0 \tag{3.21a}$$

$$\frac{\partial F_{ic}}{\partial P_{u,ic}} \geq 0 \tag{3.21b}$$

Furthermore, P_j and $P_{u,ic}$ are calculated by multizone programs and their changes from one coupling iteration to the next can attribute to the change of the boundary pressure, $P_{d,ic}$ from CFD programs. So

$$\frac{\partial P_j}{\partial P_i} = \frac{\partial P_j}{\partial P_{u,ic}} = \frac{\partial P_j / \partial P_{d,ic}}{\partial P_{u,ic} / \partial P_{d,ic}} \tag{3.22}$$

Applying the condition of unique solution in a multizone program to Path ic of Fig. 3.5, we obtain

$$\frac{\partial F_{ic}}{\partial P_{d,ic}} \leq 0 \tag{3.23}$$

$$\frac{\partial P_{u,ic}}{\partial P_{d,ic}} \geq 0 \tag{3.24}$$

If applying the derivative over $P_{d,ic}$ for both sides of Eq. (3.10) and also considering Eq. (3.23), we then get

$$\frac{\partial P_{u,ic}}{\partial P_{d,ic}} \leq 1 \tag{3.25}$$

We then apply Eqs. (3.23) – (3.25) for Path ij in Fig. 3.5

$$\frac{\partial P_j}{\partial P_i} = \frac{\partial P_j}{\partial P_{u,ic}} \le 1 \tag{3.26}$$

Combining Eqs. (3.20) and (3.26), one can obtain for multizone programs

$$0 \le \frac{\partial P_j}{\partial P_i} \le 1 \tag{3.27}$$

Applying inequalities (3.21) and (3.23) to Eqs. (3.18) and (3.19), we finally have

$$\frac{\partial P_{d,ic}}{\partial P_{u,ic}} = \begin{Bmatrix} (1, \dfrac{C_{L,ic} + C_{L,ij}}{C_{L,ic}}](\text{multizone}) \\ [\dfrac{C_{L,P}}{a_P + C_{L,P}}, 1)(\text{CFD}) \end{Bmatrix} \tag{3.28}$$

$$\frac{\partial F_{ic}}{\partial P_{u,ic}} = \begin{Bmatrix} [-C_{L,ij}, 0)(\text{multizone}) \\ (0, \dfrac{a_P C_{L,ic}}{a_P + C_{L,P}}](\text{CFD}) \end{Bmatrix} \tag{3.29}$$

Note that Eqs. (3.28) and (3.29) exclude the situation when $\partial P_{d,ic} / \partial P_{u,ic} = 1$ and $\partial F_{ic} / \partial P_{u,ic} = 0$, which indicates that F_{ic} is constant/known so the coupled simulation is not needed for Path ic. Eqs. (3.28) and (3.29) illustrate how $P_{d,ic}$ and F_{ic} change with $P_{u,ic}$ in multizone and CFD programs. The parenthesis indicates an open side of an interval and the bracket means closed side, e.g., in Eq. (3.28), for multizone method $1 < (\partial P_{d,ic} / \partial P_{u,ic}) \le (C_{L,ic} + C_{L,ij}) / C_{L,ic}$. The solution existence and uniqueness of a coupled simulation can then be studied through Eqs. (3.28) and (3.29).

The $P_{d,ic}$ - $P_{u,ic}$ relations are plotted in Fig. 3.6. If there is a solution for the coupled multizone and CFD program, the two curves will intersect, as shown in Fig. 3.6. Eq.

(3.28) shows that the derivative of $P_{d,ic}$ over $P_{u,ic}$ for multizone calculation is always greater than unity, while that of CFD is less than unity, as shown in Fig. 3.6(a). Therefore, both curves can at least intersect at one point, which indicates that at least one coupling solution exists.

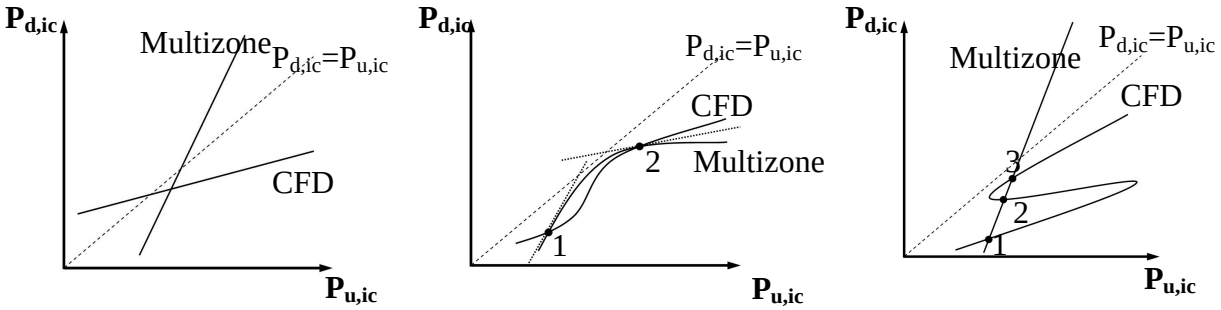

(a) Analysis of solution existence (b) Scenario of two solutions (c) Scenario of three solutions

Fig. 3.6 Solution existence and uniqueness analysis of the curves of $P_{d,ic}$-$P_{u,ic}$.

The method of reduction to absurdity is used to investigate the uniqueness of the coupling solution. For the $P_{d,ic}$ - $P_{u,ic}$ relations, Fig. 3.6(b) and Fig. 3.6(c) show two possible scenarios of multiple solutions. Suppose we already find a solution at Point 1 through the above analysis of solution existence. We can then assume that the $P_{d,ic}$ - $P_{u,ic}$ curves may intersect at other points. In the first scenario, as indicated by Point 2 in Fig. 3.6(b), the slope of CFD curve at Point 2 is less than unity, which satisfies Eq. (3.28). The slope of the multizone curve at Point 2, however, does not satisfy Eq. (3.28), so the first scenario is impossible and Point 2 cannot be a coupled solution. The second scenario shown in Fig. 3.6(c) is also impossible because one specific pressure boundary condition, $P_{u,ic}$ in CFD, can have only one corresponding $P_{d,ic}$ for a given situation (including given numerical models and techniques). Therefore, Points 2 and 3 cannot be coupled solutions and Point 1 is the only solution for multizone and CFD coupling. Please note that this conclusion is based on the assumption that both the CFD and multizone methods can have a unique solution.

The analysis here only discusses the situation in which the airflow of path ic is from zone i to zone c, as shown in Fig. 3.5. It is easy to apply a similar analysis to prove the existence and uniqueness of a solution when the airflow of path ic is from zone c to zone i. In conclusion, there is thus one and only one solution for multizone and CFD coupling. The question now is how to obtain this unique solution.

3.2.4. Different Coupling Methods

The unique solution of airflow coupling can only be obtained by applying appropriate coupling methods, which determine how the boundary conditions are exchanged between multizone and CFD models. Negrao (1995) claimed that the pressure boundary condition was applicable to the cases, where the inlet momentum changes the flow locally but does not substantially affect the airflow pattern of the CFD zone. The velocity boundary condition should be used for inlet openings, where the momentum magnitude can significantly modify the zone airflow pattern and must be known in advance. Unfortunately, we could not find the details.

This study investigates the coupling methods by studying the basic governing equations of airflow coupling. As shown in Fig. 3.5, when the airflow of path ic is from zone i to zone c, the upwind total pressure, $P_{u,ic}$, the downwind total pressure, $P_{d,ic}$, and the airflow rate, F_{ic}, are the boundary conditions to be exchanged between the two programs. Three coupling methods are possible according to permutation and combination:

- Method 1: multizone gives $P_{u,ic}$ to CFD and CFD returns $P_{d,ic}$ to multizone;
- Method 2: multizone gives $P_{u,ic}$ to CFD and CFD returns F_{ic} to multizone; and
- Method 3: multizone gives F_{ic} to CFD and CFD returns $P_{d,ic}$ to multizone.

We find that the above three coupling methods will result in different assembled matrix equations. When pressure and airflow rate boundary conditions are used together, such as in Methods 2 and 3, the assembled matrix equation is in the form of Eq. (3.12). However, when only pressure boundary conditions are employed (Method 1), Eq. (3.12) becomes

$$\mathbf{C_1 P = B_1} \tag{3.30}$$

where $\mathbf{C_1}$ is the flow coefficient maxtrix for Method 1 and $\mathbf{B_1}$ is the vector of the source terms for Method 1.

Different assembled matrix equations will not have the same numerical characteristics. The numerical performance of one matrix equation could be better than the other matrix equation.

3.2.5. Selection of the Best Coupling Method by the Scarborough Criterion

Scarborough (1966) established a convergent criterion for a Gauss-Seidel solution for a set of linear equations. The criterion is often used to evaluate CFD equations. In this study, multizone and CFD programs provide complementary boundary conditions and the coupled program tries to obtain a Gauss-Seidel solution of the assembled matrix equation. Thus, the Scarborough criterion could be used.

For the Gauss-Seidel solution of a linear system like Eq. (3.31), a sufficient convergence condition, the Scarborough criterion, is to satisfy inequality (3.32):

$$a_{f,P} f_P = \sum a_{f,nb} f_{nb} + b_f \tag{3.31}$$

$$\frac{\sum |a_{f,nb}|}{|a_{f,P}|} \begin{cases} \leq 1 & \text{For all equations} \quad (3.32a) \\ < 1 & \text{For at least one equation} \quad (3.32b) \end{cases}$$

The Scarborough criterion concludes that Eq. (3.31) has a convergent solution if the matrix is "diagonally dominant."

In a coupled simulation, inequality (3.32b) can always be satisfied so long as at least one zone connects directly to another with a constant pressure in Eq. (3.12) or (3.30). The multizone calculation itself actually requires that at least one zone with unknown pressure be connected to another with constant pressure. Otherwise, the airflow system in a multizone program will be singular and can have no unique solutions (Lorenzetti, 2002). The zone with constant pressure can be the ambient with zero pressure or a zone with constant pressure specified. Inequality (3.32b) is therefore satisfied automatically in a coupled simulation.

Among the three methods, only Method 1 satisfies inequality (3.32a) since it solves Eq. (3.30), which is a combination of Eqs. (3.7) and (3.10) and where each independent off-diagonal pressure will introduce its coefficient to that of the diagonal pressure of the matrix. Methods 2 and 3 solve the matrices in the form of Eq. (3.12) and **F** is an independent vector. The coefficients of **F** do not contribute to those of the diagonal pressure in the matrix. The condition of "diagonal dominance" may not always be satisfied for Eq. (3.12). Method 1 therefore is the only one that satisfies the Scarborough criterion and is guaranteed to have a convergent solution.

Since the Scarborough criterion is only a sufficient condition and the other two methods may still produce a convergent solution, it may be not convincing enough to conclude that Method 1 is the best method. A stability analysis should be performed to provide an in-depth investigation of the numerical performance of the coupling methods.

3.2.6. Selection of the Best Coupling Method by Numerical Stability Analysis

In order to investigate further the stability of the three coupling methods, we have examined the iterative procedure when exchanging boundary conditions between the multizone and CFD programs in a coupled simulation. Fig. 3.7 shows that, during a coupled solving procedure, the output of one program becomes the input of the other. When both inputs and outputs stabilize (their values do not change), the solution of the coupling is considered convergent. This iterative coupling procedure can be regarded as a

closed-loop system. If r is the input parameter of a multizone program from CFD and r_k is its value at the coupling iteration k, we can define the difference of r at this iteration as $\Delta r_k = | r_{k+1} - r_k |$.

Fig. 3.7 illustrates that the system equation for a multizone program is *M*, and its solution at iteration k, i_k, can be calculate as $i_k = M\{r_k\}$. Similarly, we have $r_{k+1} = C\{i_k\}$ for the CFD program.

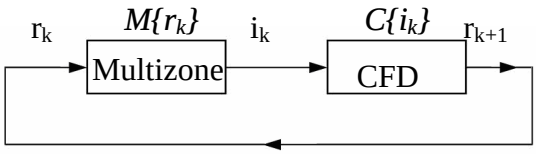

Fig. 3.7 Schematic of the coupling procedure at the coupling iteration k.

If Δr_k can be expressed by the partial derivatives of *M* and *C*, we have

$$\Delta r_k = \left| \frac{\partial M}{\partial r} \times \frac{\partial C}{\partial i} \right| \times \Delta r_{k-1} = \left| \frac{\partial M}{\partial r} \times \frac{\partial C}{\partial i} \right|^k \times \Delta r_0 \tag{3.33}$$

where Δr_k is the difference of the input for multizone method between the coupling iteration k+1 and k, *M* is the system equations for a multizone program, *C* is the system equations for a CFD program, i is the input for a CFD program, r is the input for a multizone program, and Δr_0 is the initial value of Δr.

Then when k is sufficiently large, the coupled simulation will be stable and convergent only if

$$\left| \frac{\partial M}{\partial r} \times \frac{\partial C}{\partial i} \right| \le 1 \tag{3.34}$$

Here, we call the term $|\frac{\partial M}{\partial \mathrm{r}} \times \frac{\partial C}{\partial \mathrm{i}}|$ the fluctuation term. The derivatives of M and C are shown in Eqs. (3.18) and (3.19). Table 3.3 compares the fluctuation terms among the three coupling methods. The last column provides the stability criteria for a coupled solution.

Table 3.3 Stability conditions for the three coupling methods.

Method	i	r	$\lvert\frac{\partial M}{\partial \mathrm{r}} \times \frac{\partial C}{\partial \mathrm{i}}\rvert$	Stability Criteria
1	$P_{u,ic}$	$P_{d,ic}$	$[\frac{C_{L,ic}}{C_{L,ic}+C_{L,ij}} \times \frac{C_{L,P}}{a_P+C_{L,P}}, 1)$	unconditionally stable for all $C_{L,ic}$, $C_{L,ij}$, $C_{L,P}$, and a_P
2	$P_{u,ic}$	F_{ic}	$(0, \frac{a_P C_{L,ic}}{C_{L,ij}(a_P+C_{L,P})}]$	$\frac{C_{L,ij}}{C_{L,ic}}(1+\frac{C_{L,P}}{a_P}) = \begin{cases} <1, \text{conditionally stable} \\ \geq 1, \text{stable} \end{cases}$
3	F_{ic}	$P_{d,ic}$	$(0, \frac{C_{L,ij}C_{L,P}}{a_P(C_{L,ij}+C_{L,ic})}]$	$\frac{a_P}{C_{L,P}}(1+\frac{C_{L,ic}}{C_{L,ij}}) = \begin{cases} <1, \text{conditionally stable} \\ \geq 1, \text{stable} \end{cases}$

The stability criterion for Method 1 is satisfied unconditionally because $C_{L,ic}$, $C_{L,ij}$, $C_{L,P}$ and a_p are all positive and the derivatives of M and C are always less than one. Together with the convergence analysis, one can conclude that Method 1 can lead to convergent and stable solutions. In addition, it is also indicated that the greater $C_{L,ij}$ and a_p are, the faster the coupled program reaches a convergent solution.

The criteria for Methods 2 and 3 shows that the two methods are conditionally stable. With Method 2, the greater $C_{L,ij}$ and the smaller $C_{L,ic}$ are, the more stable the coupling. However, Method 3 requires a smaller $C_{L,ij}$ to reach a better stability in the coupled solution. Thus, Method 1 seems the best. This can be further proved by numerical experiments.

3.2.7. Numerical Experiments

The numerical experiment is designed with the following considerations:

- The assumptions of multizone models is inappropriate for at least one zone, so that the airflow coupling with the CFD program for the zone is necessary;
- The numerical experiments should be able to illustrate how non-uniform distributions of airflow variables, especially pressures, and airflow patterns affect building airflow distributions;
- The numerical experiments should be as simple as possible so that it is easy to apply the theoretical analysis.

Based on these considerations, this study investigates two types of flows: pressure gradient flows in an office suite and cross ventilation in a four-zone building model. In both cases, multizone network models cannot provide reasonable predictions of air distributions and therefore the coupled program is employed to improve the calculations.

Pressure gradient flows in an office suite

The first case concerns isothermal pressure gradient flows at a steady state in an office suite with four offices and a long hallway, as shown in Fig. 3.8. For the sake of simplicity, this investigation offers a two-dimensional portrayal of the office suite in an X-Y plane.

The hallway, 3 m (X) × 10 m (Y), is selected as the CFD zone. The open area of Doors 1 and 2 is 0.5 m^2 each, and that of Doors 3 through 6 is 1 m^2 each. When windows a, b, c and d are closed, the crack area is estimated to be 0.0002 m^2 each. Other possible leakages in the office suite, e.g. cracks at wall joints, are neglected in the current simulation. When they are opened, the cross-sectional area is 1 m^2 each. The flow is assumed to be isothermal so that the pressure difference due to density difference is zero for every flow path and the wind pressure is the only driving force. At door 1, the wind pressure is assumed to be constant, at 1 Pa, and those of other doors are 0 Pa. This investigation studies two scenarios:

- Scenario A: windows a, b, c and d are closed so that the airflow rates and thus the pressure drops through doors 3, 4, 5 and 6 are close to zero;
- Scenario B: windows a, b, c and d are open so that the airflow rates and thus the pressure drops of doors 3, 4, 5 and 6 are non-zero.

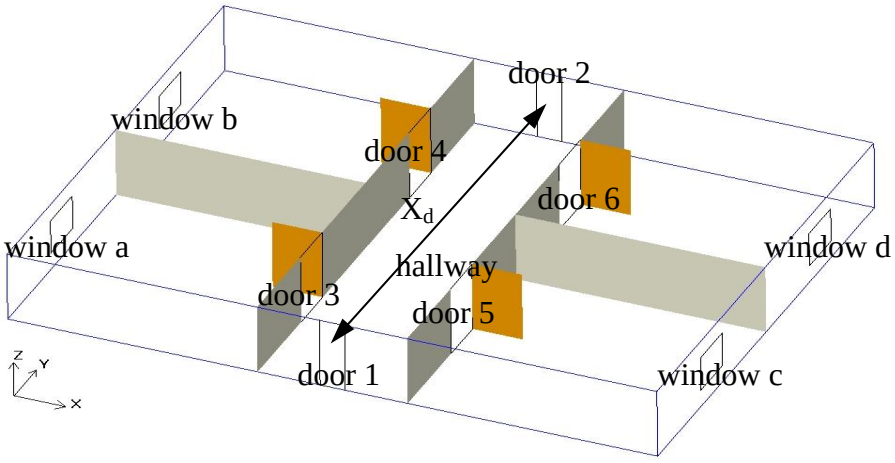

Fig. 3.8 The layout of an office suite with four offices and one hallway.

For the two-dimensional CFD calculations, the convergence criterion is that the normalized residuals are less than 0.01 for all the variables solved and the grid of 21×42 (X×Y) is used for the hallway. For multizone calculations, the non-linear equation solver of the simple trust region is used and the flow model of the orifice equation is applied to all flow paths of the multizone method. The total computing time of the coupled simulation of method 1 is 125s for Scenario A, and 53s for Scenario B on a Pentium 4 2.0 GHz PC. The total computing time can be divided into three parts: multizone calls (multizone internal iterations), the iterative exchange of boundary conditions between multizone and CFD (external iterations), and CFD calls (CFD internal iterations). CFD internal iterations take most of the total computing time. At the early stage of the coupled simulation, each CFD call needs more than 1000 internal iterations to obtain an intermittent-converged CFD solution. At a later stage, when the coupled simulation tends

to converge, one internal iteration of CFD is sufficient for CFD convergence. Therefore, the exchange of boundary conditions between multizone and CFD programs gets more frequent when the coupled simulation is closer to the coupling convergence.

Fig. 3.9 shows the changes of airflow rates with coupling iterations by the three coupling methods in these two scenarios. Fig. 3.9(a) is for door 1 in Scenario A, and Fig. 3.9(b) is for door 3 in Scenario B. Fig. 3.9(a) shows that with Methods 1 and 3, the coupled simulation converges after about 15 iterations. This means that the exchange of boundary conditions between multizone and CFD programs occurs for 15 times before the coupling convergence, as evaluated by Eq. (3.11). The calculated airflow rates are 0.367 kg/s with Method 1 and 0.372 kg/s with Method 3. The two numbers are close so they support the theory of the uniqueness of the solution. The small difference may be due to their different ways in applying boundary conditions in CFD calculations. In Method 1, a uniform boundary pressure is employed, while Method 3 assumes a uniform distribution of velocity for each path. Method 2 diverges after the first several iterations in Scenario A, even if very high under-relaxations are used. The calculated airflow rates by Method 2 are too unrealistic, so the results of Method 2 are not plotted in Fig. 3.9. On the other hand, since door 1 is connected to the ambient with a known pressure, its airflow rate can be calculated directly from the local pressures of CFD calculation at each iteration. Therefore, for Method 3, only the convergence history of CFD0 (Method-3-CFD0) is shown because it is the same as that of CONTAM.

Compared with Scenario A, the three coupling methods behave differently for Scenario B, as shown in Fig. 3.9(b), which shows the flow rates through door 3 during coupling. For Scenario B, Methods 1 and 2 can give a convergent solution and calculate the same flow rate through door 3. Method 3 diverges quickly and fails to produce reasonable airflow rates during the iteration.

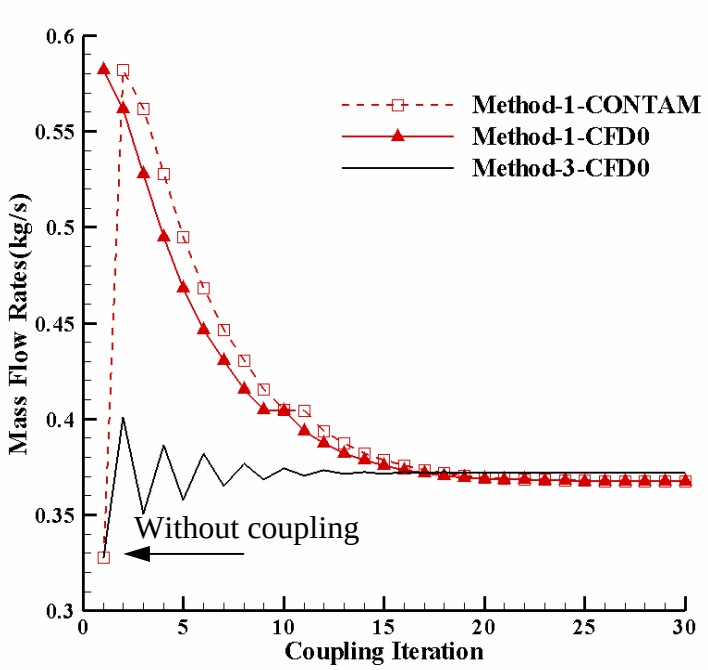

(a)

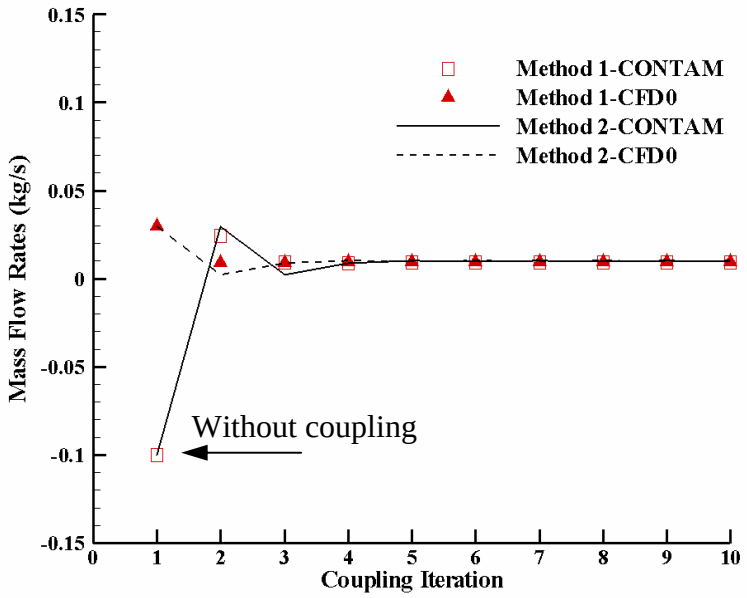

(b)

Fig. 3.9 Airflow rates calculated with different coupling methods (a) airflow rate through door 1 in Scenario A by Methods 1 and 3; (b) airflow rate through door 3 in Scenario B by Methods 1 and 2.

The distinct numerical performances of the three coupling methods can be explained by studying their stability performance based on the stability criteria in Table 3.3. By calculating the coefficients, $C_{L,ic}$, $C_{L,P}$, $C_{L,ij}$ and a_P, for Scenarios A and B, one can obtain the fluctuation terms $|\frac{\partial M}{\partial \mathrm{r}} \times \frac{\partial C}{\partial \mathrm{i}}|$ for all coupling methods, as shown in Table 3.4. The stability criteria require that the fluctuation terms must be smaller than 1.0, so Method 1 is unconditionally stable for Scenarios A and B. Furthermore, the smaller the fluctuation term is, the faster the coupled simulation reaches convergence. This can be easily seen in Fig. 3.9, in which it took Method 1 four iterations in Scenario B to reach convergence, as opposed to 15 iterations in Scenario A. Furthermore, Table 3.4 illustrates that the fluctuation terms of Method 2 in Scenario B and Method 3 in Scenario A are much smaller than 1.0, which guarantee converged solutions. The instabilities of Method 2 in Scenario A and Method 3 in Scenario B can also be explained by their high fluctuation terms, as shown in Table 3.4. The fluctuation term can be greater than 1.0 during coupling iterations, which finally leads to divergences.

Table 3.4 The fluctuation terms of different coupling methods for Scenarios A and B for the pressure gradient flows in an office suite.

	$\lvert\frac{\partial \boldsymbol{M}}{\partial \mathbf{r}} \times \frac{\partial \boldsymbol{C}}{\partial \mathbf{i}}\rvert$	
	Scenario A	Scenario B
Method 1	[0.5, 1)	[0.002,1)
Method 2	(0, 1879.7]	(0, 0.003]
Method 3	(0, 0.002]	(0, 41.5]

Fig. 3.9 also compares the calculated airflow rates with and without coupling (the results of the iterations versus those at Iteration 1). If a positive value means an inflow for the hallway, the relative differences can be 11% for door 1 in Scenario A. Fig. 3.10 provides comparisons with more detail. For Scenario A, as shown in Fig. 3.10(a), since windows a, b, c and d are closed, the flow rates of doors 3 through 6 are close to zero with coupling. The largest difference without and with coupling is around 30%. When windows a, b, c and d are open in Scenario B, the flow directions through doors 3 and 5 even change from

outflows to inflows with coupling, as shown in Fig. 3.10(b). As a result, the airflow rates of other doors change dramatically in Scenario B.

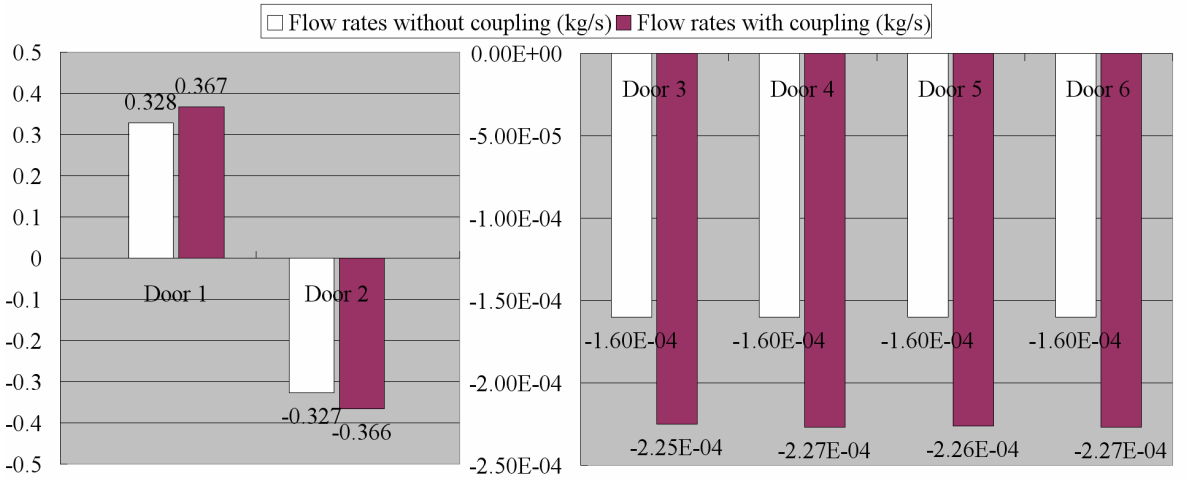

(a)

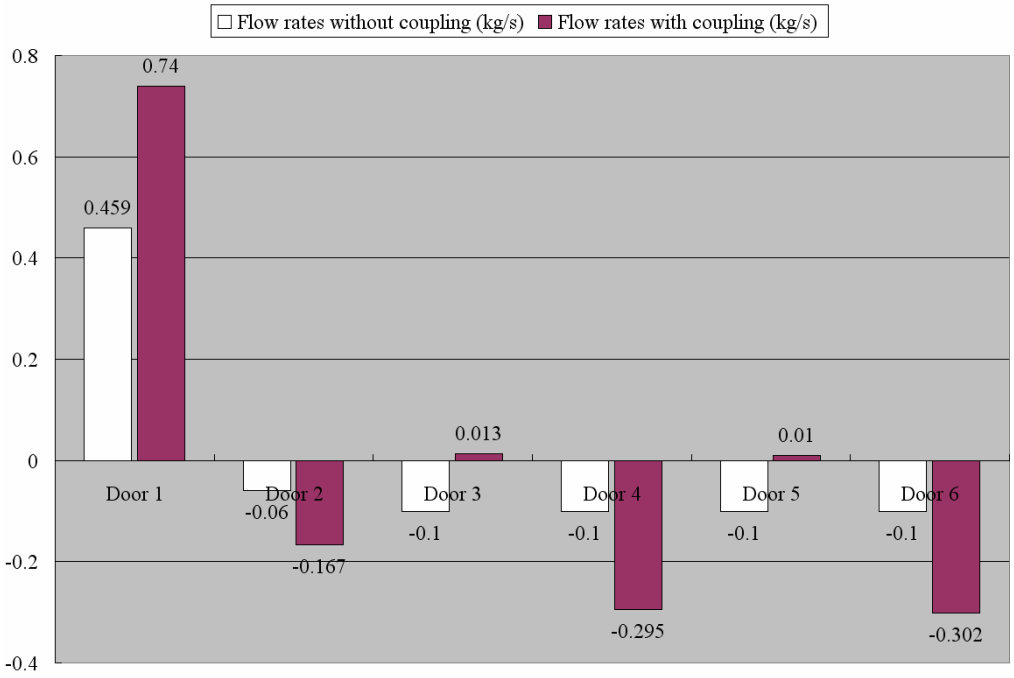

(b)

Fig. 3.10 Comparisons of calculated airflow rates through different openings in an office suite with and without coupling (a) Scenario A and (b) Scenario B.

The dramatic changes of airflow rates with coupling in Scenario B provide clear evidence that, when the homogeneous assumption of multizone models are inappropriate, the airflow pattern plays an important role in building air distributions. Fig. 3.11 shows the airflow patterns in the hallway, calculated by CFD. For Scenario A, shown in Fig. 3.11(a), a recirculation area forms at each side of door 1, whereas it is not big enough to affect doors 3 and 5. Moreover, the local pressures at doors 3 through 6 are almost the same so that the calculated airflow rates are close to each other.

However, when windows a, b, c, and d are open in Scenario B, Fig. 3.11(b) shows that the airflow pattern changes dramatically. Compared with Scenario A, the airflow through door 1 has less flow resistance, and the flow momentum is preserved after entering the hallway. The recirculation areas therefore extend far enough to affect the local flow near doors 3 and 5. Instead of outflows calculated by CONTAM, air is induced through doors 3 and 5 into the hallway. Fig. 3.11(b) also illustrates that the pressure distribution in Scenario B is non-uniform, which explains why the airflow rates of doors 4 and 6 change more with coupling than those in Scenario A.

Fig. 3.10 and Fig. 3.11 show that CFD solutions were a little asymmetrical, e.g. for door 3 and door 5 in Fig. 3.10(b), the flow rates were 0.013 and 0.01 respectively. One explanation is that the CFD convergence criterion in this case is that the CFD residual is less than 1%. The residual of CFD simulation can be roughly calculated as [(0.302-0.295) + (0.013-0.01)]/ (0.763) ~ 0.01 (0.763 is the total inflow rate). So the small difference of flow rates is caused by simulation residuals. On the other hand, perfect symmetry normally is not easy to be achieved in CFD simulations (Chen and Jiang, 1992).

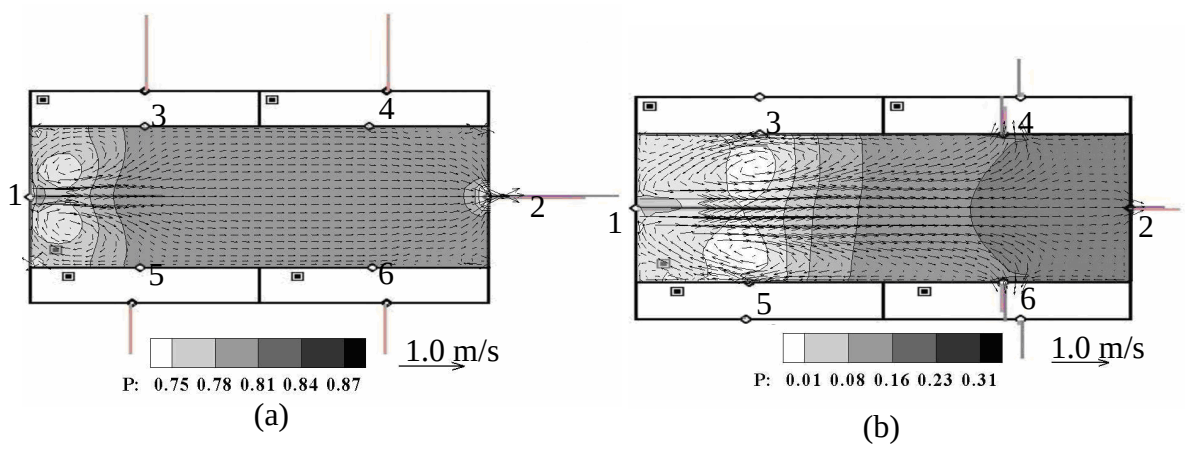

Fig. 3.11 Airflow patterns and pressure distributions with coupling in the office suite (a) Scenario A with closed windows a, b, c, and d; (b) Scenario B with open windows a, b, c, and d.

The numerical experiment for the pressure gradient flows in the office suite demonstrates that the coupled solution exists and is unique. Method 1 is indeed the best coupling method. Furthermore, the coupled program can improve the accuracy of the multizone models by considering the airflow patterns and non-uniform pressures inside the CFD zones.

Cross ventilation in a four-zone building model

For the sake of simplicity, the numerical experiment for the office suite is conducted two-dimensionally. Negrao (1995) found that the airflow coupling of multizone and CFD models may not work for three-dimensional cases. In order to test further the coupled program, a more complex three-dimensional problem, with cross ventilation in a four-zone building model, is studied.

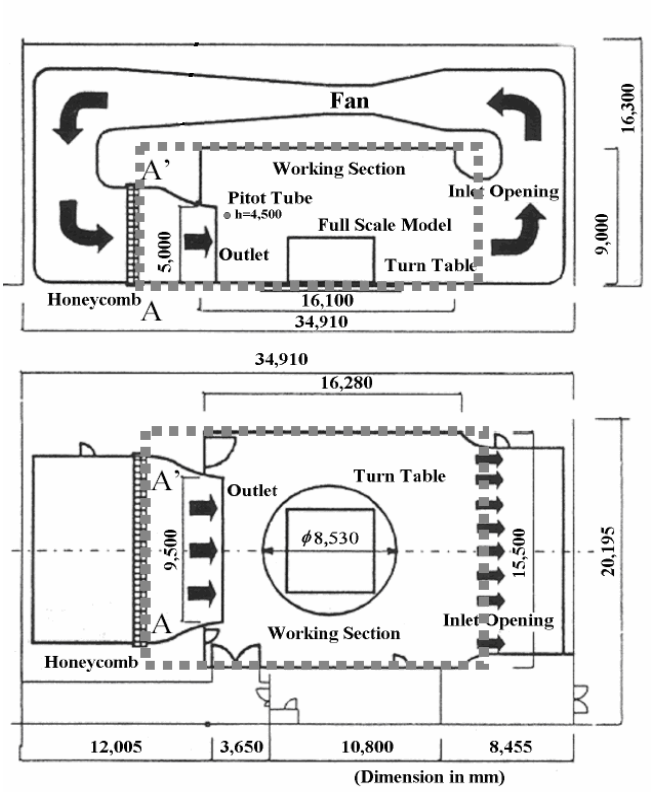

(a)

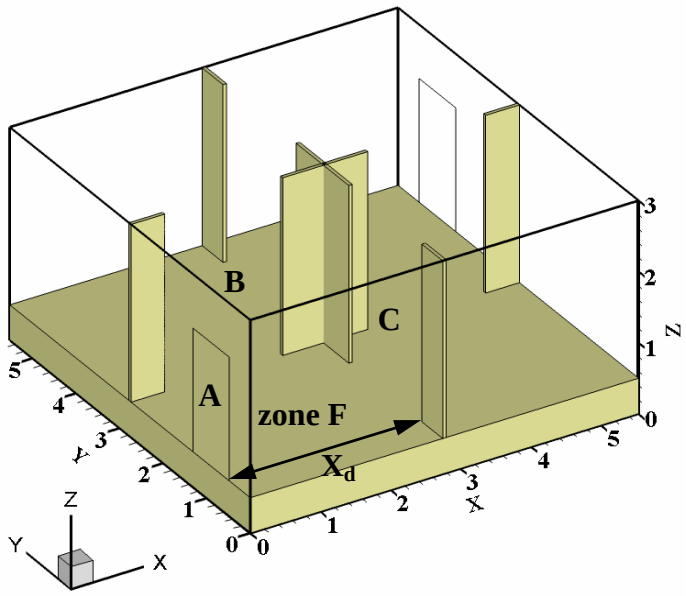

(b)

Fig. 3.12 The 4-zone building model (a) section (top) and plane (bottom) of the wind tunnel laboratory (Sawachi et al., 2003); (b) the three-dimensional view of the building model.

Sawachi et al. (2003) used a full-scale building model in a wind tunnel to measure the discharge coefficients at the building openings under different wind directions. Fig. 3.12(a) shows the wind tunnel sketch. The test model placed in the wind tunnel was a full-scale building model that was 5.53 m (X) × 5.53 m (Y) ×3.0 m (Z), and was divided into four sub-zones with the same size. The full-scale building model could be turned around to study the impact of different wind directions. This study only uses the case where the wind was perpendicular to the opening in the building model. Fig. 3.12(b) illustrates the three-dimensional view of the 4-zone building model. With a strong momentum, the wind flows into zone F through path A, the size of which is 0.86m (W)× 1.74m (H), and is distributed among the other three sub-zones through internal paths B and C, the size of which is 1.68m (W)× 2.5m (H) each. Zone F is therefore subject to the momentum effect of the incoming wind, and the coupled simulation selected zone F as the CFD zone.

The same convergence criterion as the previous case is used for the three-dimensional CFD runs, and the grid in this case is 19×19×24 (X×Y×Z). The total computing time of the coupled simulation of Method 1 is 184 s on a Pentium 4 2.0 GHz PC, which is more than that of the previous case because of the increased grid numbers in the CFD simulation.

Fig. 3.13(a) illustrates the experimental airflow pattern for the building model. It shows that, due to the preserved momentum of the incoming wind, the air in zone F mostly flowed from opening A through path C. Opening B has little flow. Obviously, the momentum effect was very significant for this case. Fig. 3.13(b) shows the calculated airflow pattern with coupling by Method 1, which is similar to that used in the experiment except that the calculated recirculation area is smaller. The difference is mainly caused by specifying the uniform distribution of velocities in opening A, which is not uniform in the experiment. On the other hand, since the coupled simulation applied the CFD simulation only to zone F, its prediction is a combination of the results of

multizone and CFD simulations. Therefore, the calculated airflow pattern may be different from the experiment.

Although the coupled simulation may not be as accurate as the application of CFD to all zones, it is still able to provide more reasonable airflow predictions than that provided by multizone models alone. When the flow rate through path A is 2.386 kg/s, CONTAM alone would calculate the same flow rate for paths B and C at 1.193 kg/s due to neglecting the preserved momentum inside zone F. However, the coupled program calculates the flow rate of 0.746 kg/s for path B and 1.640 kg/s for path C. The difference is around 60% between the solutions by CONTAM alone and by the coupled program. This is because the coupled program can capture the strong momentum at path A when applying CFD for zone F.

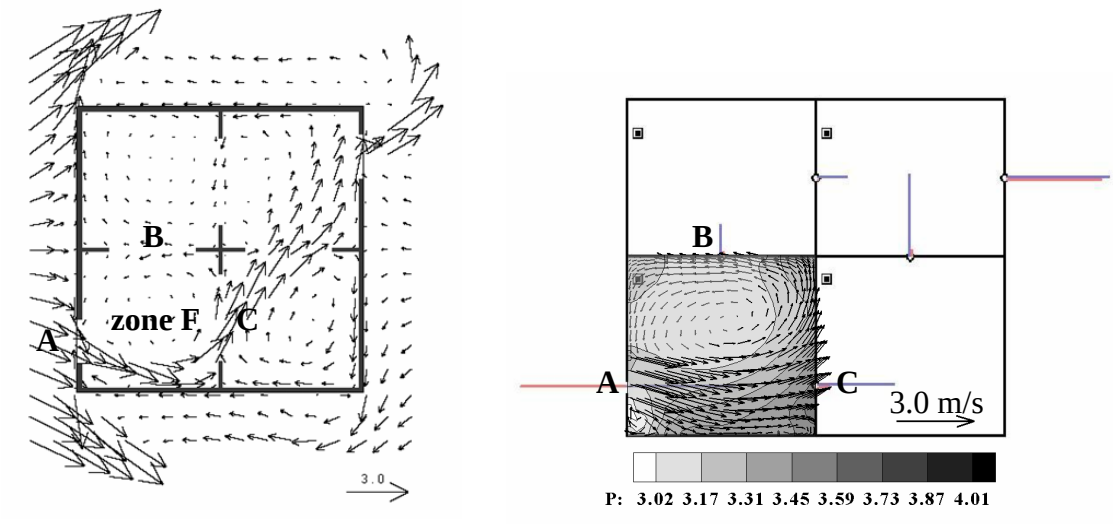

(a) (b)

Fig. 3.13 The coupled simulation in a four-zone house model with cross ventilation (a) the measured velocity field of the four-zone house model; (b) the velocity and pressure fields by the coupled simulations.

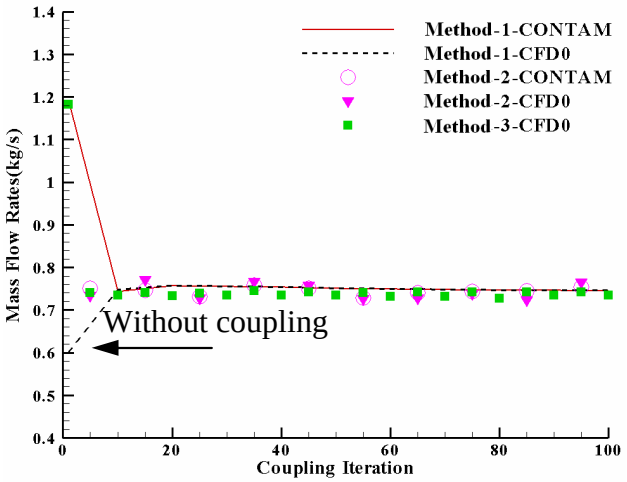

Fig. 3.14 Airflow rate through path B during the iteration with the three coupling methods in a four-zone building model with cross ventilation.

The above analysis uses the results obtained from Method 1 with and without coupling. By using Methods 2 and 3, we can also achieve converged solutions for this case. Fig. 3.14 shows the airflow rates of path B during the coupled solution with the three methods. All the three methods have led to the same flow rate at path B, which again supports the theory of unique solution. Compared with Method 1, the coupling by Methods 2 and 3, however, fluctuates during iterations, as shown in Fig. 3.14. This further proves the conditional stability of the two methods. Due to the nonlinearity of the problem, the linear flow coefficients, $C_{L,ij}$ and $C_{L,ic}$, can change during the iterative coupling. Although the overall trend of the coupling is convergent, the stability criteria in Table 3.3 may not always be satisfied at some iteration, which as a result causes the fluctuations.

This investigation is for large openings, where CFD plays an important role and can improve the results. If cracks become very important, multizone models alone can handle it, where no coupling between the CFD and the multizone is required. This study does not address the coupling of CFD with multizone methods in the event that cracks exist.

3.3. Summary

This chapter develops the indirect coupling scheme for airflow simulations around buildings and the direct coupling for airflow and contaminant transport simulations in buildings. The coupling schemes decide "what" information, and "how", "where", and "when" the information should be exchanged between CONTAM and CFD0-C.

The indirect coupling scheme uses the WPC link and the WPP link to provide calculated wind pressures and wind pressure coefficients, respectively, by CFD0-C for CONTAM. Since only one-time interaction of CONTAM and CFD0-C is involved, it is not a direct coupling but a virtual coupling procedure.

The direct coupling scheme is used to solve the coupled simulations in buildings. This scheme will exchange airflow rates or pressures between CONTAM and CFD0-C, iteratively. To determine "where" and "when" the information should be exchanged, a direct coupling controller and three different coupling algorithms are developed, respectively. Three coupling methods are then proposed to decide "how" the direct coupling exchanges the information between a multizone network model and a CFD program (Fig. 3.5):

- Multizone gives $P_{u,ic}$ to CFD and CFD returns $P_{d,ic}$ to multizone;
- Multizone gives $P_{u,ic}$ to CFD and CFD returns F_{ic} to multizone;
- Multizone gives F_{ic} to CFD and CFD returns $P_{d,ic}$ to multizone.

Through theoretical analyses, this chapter has proven that the coupled program has a solution and the solution is unique, based on the three coupling methods.

This investigation also uses the Scarborough criterion to evaluate the convergent performances and to analyze the stability of the three coupling methods during their iterative coupling processes. Method 1, which exchanges pressure boundary conditions between multizone and CFD programs, is unconditionally stable, while Methods 2 and 3 are conditionally stable. Two numerical experiments are conducted to demonstrate the

theory: one is pressure gradient flow in an office suite, and the other is cross ventilation in a four-zone building model. Numerical results show that the coupling solution is indeed unique and Method 1 is the most stable method. Thus, the theory analysis is correct and valid.

CHAPTER 4. VALIDATIONS

CONTAM could provide inaccurate results in the simulations with non-uniform momentum effect, temperature, and contaminant concentration. Before improving CONTAM by CFD0-C, it is necessary to check whether CFD0-C itself can perform better than CONTAM in the simulations, where CONTAM assumptions fail. Therefore, the validation of CFD0-C is needed. On the other hand, many uncertainties can be involved when the two programs are integrated, although the individual program has already been validated. It is important to compare the numerical solutions with the experimental data and to reveal the advantages of the coupled CONTAM and the CFD0-C program over the individual CONTAM and CFD0-C program. Hence, this chapter first verifies CFD0-C through the data obtained from the literature, and then validates the coupled CONTAM and the CFD0-C program through the measured data from a series of chamber experiments.

4.1. Part I – Validation of CFD0-C

The validation of CFD0-C is necessary because it is converted and upgraded from the FORTRAN version of CFD0, CFD0-F. Before validating the coupled program of CONTAM and CFD0-C, it is necessary to verify the conversion. The verification of the CFD0-C program is carried out by comparing the simulation results with published data. This study selects the following cases based on the facts that:

1. a 90-degree planar branch case tests the CFD0-C's capability of using pressure boundary conditions, which is required by the coupling Method 1;
2. a case of the buoyancy-driven airflows in a stairwell validates CFD0-C in the prediction of the buoyancy-driven flow with a non-uniform distribution of temperature;

3. a 4-zone case of cross ventilation examines the capability of CFD0-C to simulate airflows with a non-uniform distribution of the momentum effect;
4. a case of displacement ventilation reveals the ability of CFD0-C to predict airflows with a non-uniform distribution of temperatures and contaminant concentrations; and
5. an external airflow around a building model in a wind tunnel validates the prediction of non-uniform wind pressures on a cubic house by CFD0-C.

4.1.1. Flow through a 90-degree Planar Branch

CHAPTER 3 has revealed that the best coupling method is Method 1, in which pressure boundary conditions are exchanged between the CONTAM and the CFD0-C. However, to describe pressure as a boundary condition is a new capability of CFD0-C. This section thus validates the ability of CFD0-C to handle pressure boundary conditions through a classic case, the airflow through a 90-degree planar branch. The case has been used to validate CFD simulations with pressure boundary conditions in several previous studies (Hayes et al., 1989; Kelka and Choudhury, 2000; Zhai et al., 2004). Although the 90-degree planar branch is not a building, it is quite similar to a corridor. The current study therefore chooses it as a validation case.

Fig. 4.1 illustrates the geometry of the branch. The flow domain is divided into 30×58 grids by the CFD0-C. Uniform velocity is specified for the inlet, and zero pressure for the two outlets. As shown in Fig. 4.1, when the Reynolds number is small, e.g. Re=10, the air stream almost bifurcates equally between the two outlets. As the Reynolds number increases to 400, recirculation is observed at the elbow of the branch. The outflow to the straight or main branch is greater than the side branch. This is because the higher the Reynolds number is, the stronger the momentum effect.

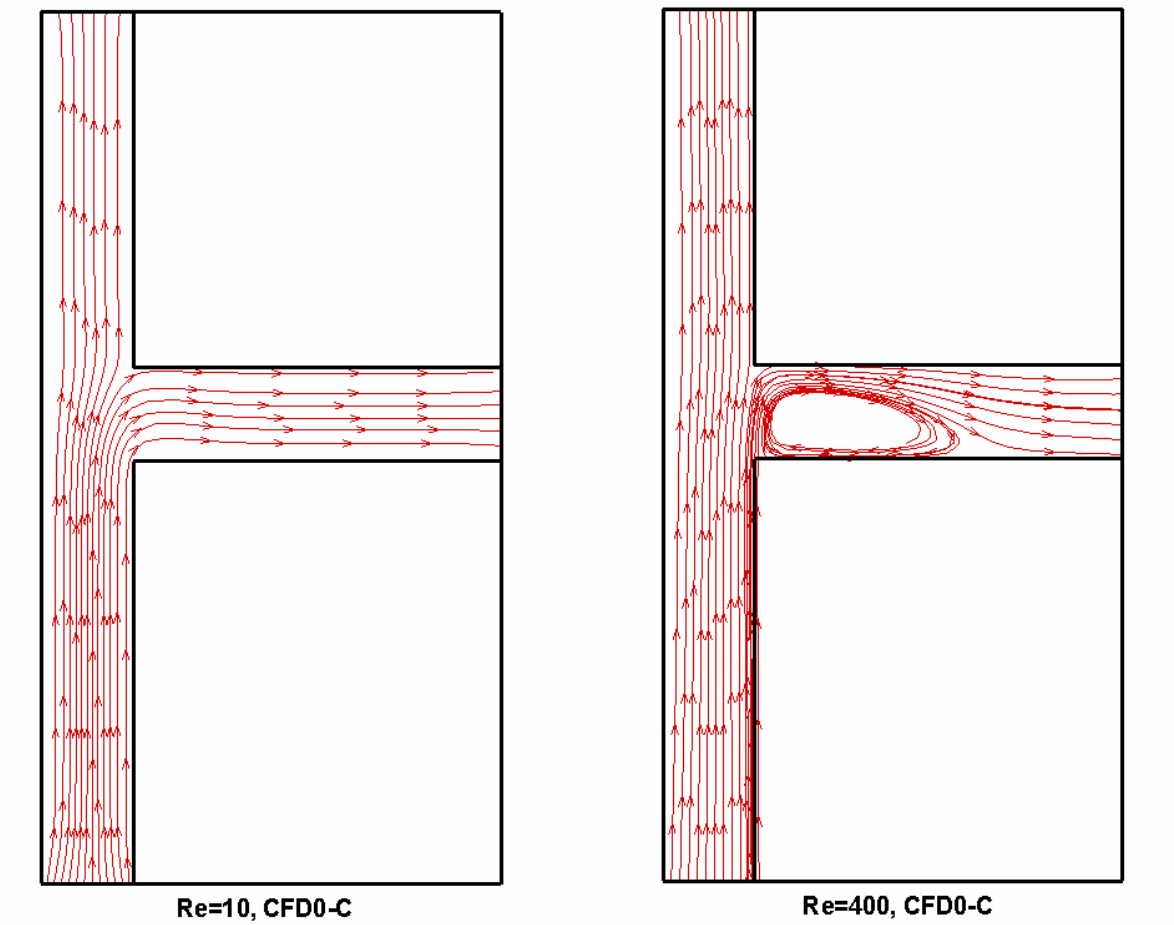

Fig. 4.1 Streamline lines in the 90-degree planar branch: (a) Re=10, (b) Re = 400.

Hayes et al. (1989), Kelka and Choudhury (2000), and Zhai et al. (2004) have simulated the 90-degree planar branch using different CFD codes. Fig. 4.2 compares the results obtained by the CFD0-C with the three studies. The fractional flow rates of the main branch calculated by the CFD0-C are close to those obtained by the published results. Both the CFD0-C and MIT-CFD (Zhai, 2003) use the zero-equation turbulence model (Chen and Xu, 1998), which is different from the κ-ε model used by Hayes and Kelkar. MIT-CFD and CFD0-C use different implementation approaches for pressure boundary conditions: CFD0-C uses the method of Patankar (1980), and MIT-CFD uses the method of Versteeg and Malalasekera (1995). All of these factors could contribute to the differences in simulation results. However, the differences are insignificant. Therefore, this case verifies that pressure boundary condition in CFD0-C is implemented correctly.

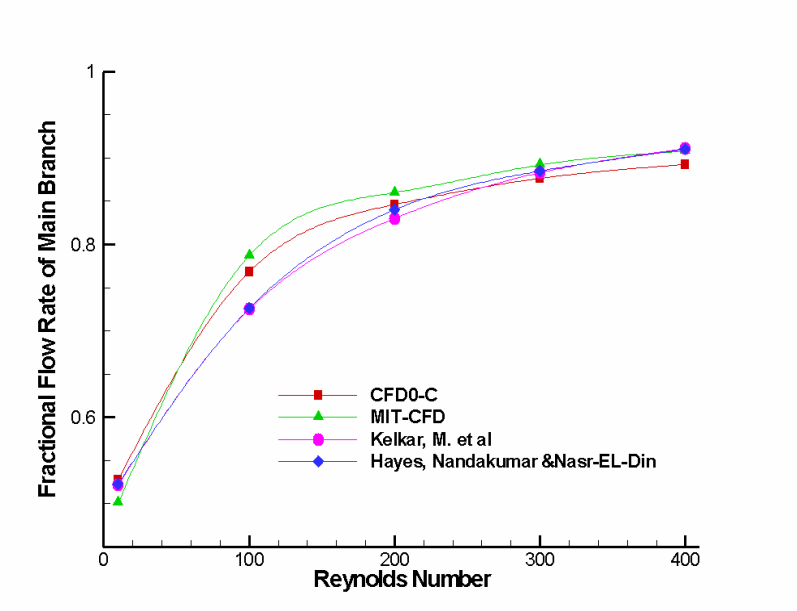

Fig. 4.2 Fractional flow rates in main branch as a function of the Reynolds number.

4.1.2. Buoyancy-driven Airflows in a Stairwell

For buoyancy-driven airflows, temperature variations play an important role in ventilation rates. This is because the directional buoyancy force has a large influence on the flow patterns within the space and on the nature of the exchange with the outside (Linden, 1999). In CHAPTER 2, we compare the results of CONTAM with experimental data in the buoyancy-driven flow in a stairwell. The CONTAM results are quite different from those obtained by the experiment due to the well-mixing assumption of uniform temperatures. Before improving the CONTAM results by coupling it with CFD0-C, it is necessary to validate the ability of CFD0-C to model buoyancy-driven flows.

Fig. 2.2 in CHAPTER 2 shows the geometry of the stairwell model. Thirteen steps form the stairway and the width of the stairwell is 0.608 m. The circulation of air is maintained by a continuous supply of heat to the lower compartment. There are two small openings measuring 0.01 m×0.608 m, one in the lower and one in the upper compartment. The heater, a 1 kW Dimplex oil-filled electric radiator with 0.570 m×0.659 m dimensions (both sides are exposed to air), is placed in the corner of the lower compartment.

In CFD0-C simulation, a fine grid number of 95×28×81 is used. Special attention is paid to the specification of boundary conditions. Zero pressure is applied at the two openings. The overall heat flux data is available and it may be specified as boundary conditions at the walls of the stairwell. Since this study does not calculate heat conduction in the walls, it needs to specify the convective heat fluxes instead of the overall heat fluxes. The convective heat fluxes are calculated based on the overall heat balance in the walls:

$$q_c = q - q_r \tag{4.1}$$

where q_c, q_r, and q denote the convective, radiative, and total heat fluxes, respectively. It is assumed that the surfaces of the stairwell are opaque and gray bodies. This investigation further assumes that the medium (air) do not participate in radiative heat transfers (Mokhtarzadeh-Dehghan et al., 1994).

Table 4.1 shows the measured air temperatures and temperature gradients for different input powers from the heater. With the increase in power, the differences in the temperature inside and outside the stairwell, and the vertical temperature gradient, increase dramatically. The vertical temperature gradient is 3.5 °C for 100 W and can reach 17 °C for 900 W. CONTAM cannot consider such high temperature gradients, as revealed in Fig. 4.3.

Table 4.1 Measured air parameters of the buoyancy-driven flow in a stairwell.

Q (power of the heater) (W)	Ambient temperature T_{amb} (°C)	Average inside temperature T_{ins} (°C)	Temperature differences $\Delta T=T_{amb}-T_{ins}$ (°C)	Vertical temperature gradient (°C)
100	21.8	25.8	4	3.5
300	23.7	29.6	5.9	7
600	24.9	37.9	13	11
900	24.9	40.4	15.5	17

As we can see, the mass flow rates computed by CONTAM are all less than the measured results. When the temperature gradient is low, e.g. 3.5 °C for 100 W, the difference between CONTAM and the experimental results is not significant. With the increase of the temperature gradient, such a difference increases considerably. The huge discrepancy is found in the case of 900 W with the maximum temperature gradient. Therefore, the temperature gradient is important for buoyancy-driven flows, whereas CONTAM may provide inaccurate results due to its well-mixing assumption.

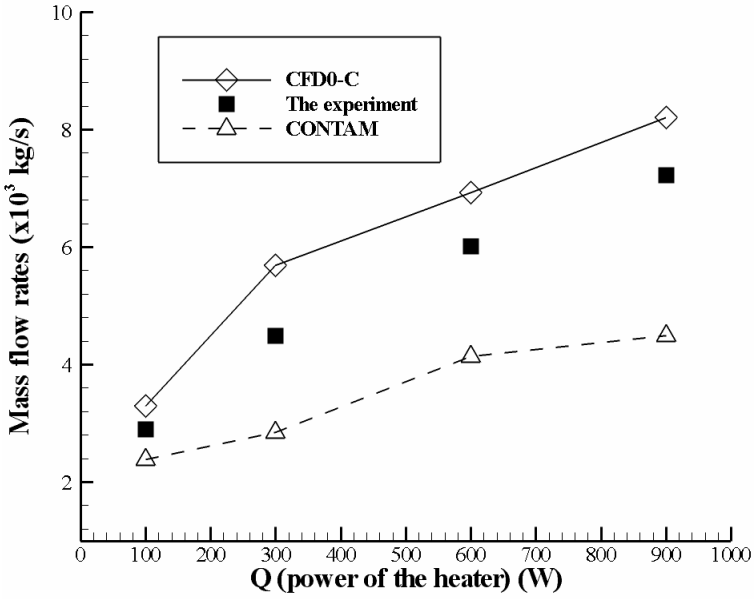

Fig. 4.3 Comparison of mass flow rates of CFD0-C, Experiment and CONTAM for the buoyancy-driven flow in a stairwell.

CFD0-C can consider a non-uniform distribution of temperatures with reasonable accuracy, as shown in Fig. 4.3. The calculated results obtained from the CFD0-C are close to the experiment, although the CFD0-C tends to overestimate the airflow rates. One reason for this overestimation is the method used in calculating the convective heat flux. Based on the results, it seems that the method might have overestimated the convective heat fluxes. Another possible reason is the reliability of the experimental data,

which did not ascertain how the heat fluxes of walls are measured. It would be better if wall temperatures were available for the CFD0-C computations.

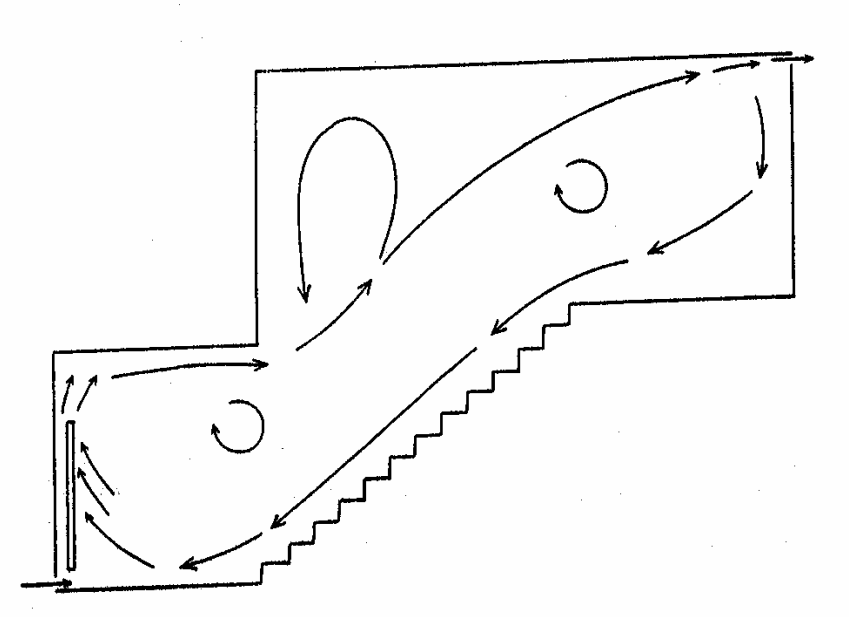

Fig. 4.4 The flow pattern in the experiment.

Fig. 4.4 shows the measured airflow pattern. The air rises along the heater due to buoyancy and two large vortices are formed in the upper compartment. The relatively cold air moves from the upper to the lower compartment along the stairs and then is reheated by the heater. The flow patterns computed by the CFD0-C are close to the measured one, as shown in Fig. 4.5.

The study of the buoyancy-driven flows in a stairwell reveals that CFD0-C can predict airflow rates and temperature gradients with reasonable accuracy. The current study thus can use CFD0-C for the problems with a non-uniform distribution of temperature.

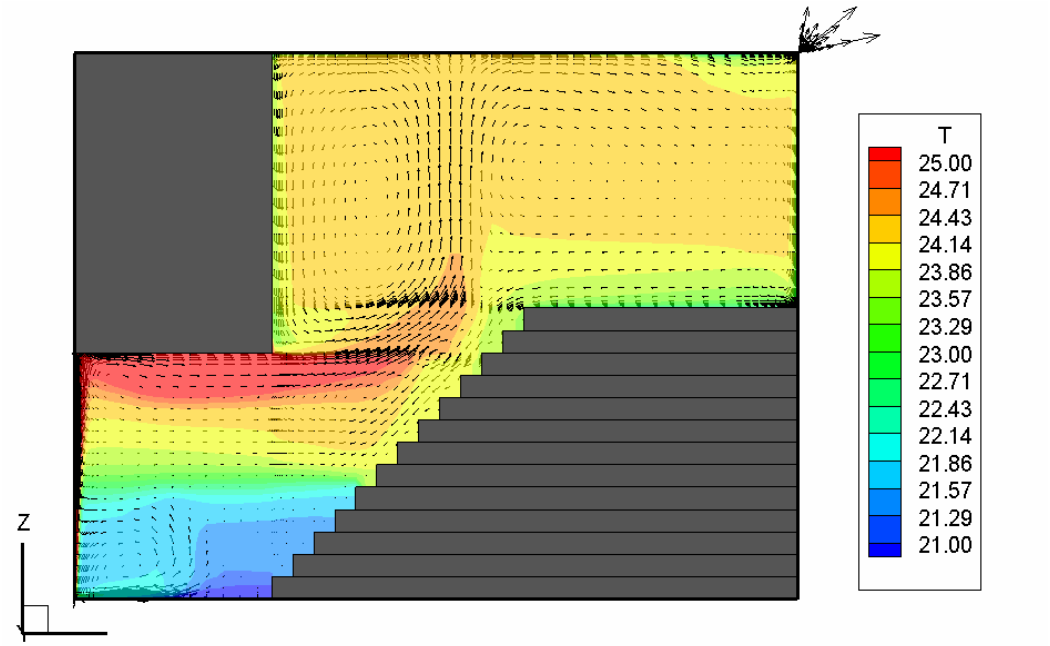

Fig. 4.5 The flow patterns by the numerical simulation by CFD0-C for the input power of 300 W.

4.1.3. Displacement Ventilation

In the previous two cases, we try to validate CFD0-C by comparing it with published results. Due to limited experimental data, we do not compare spatial distributions of air velocities and contaminant concentrations. More validations are required to check the reliability of CFD0-C to calculate spatial air and contaminant parameters. Hence, we selected the displacement ventilation case from the studies of Srebric et al. (1999) for further validation.

Fig. 4.6 shows the displacement ventilation case. Conditioned air with the temperature of 17 °C is supplied from a 0.53 m × 1.1 m air diffuser at the low air velocity of 0.086 m/s. The return is located at the ceiling through which the warm room air is released. The supply air spreads over the floor and then rises as it is heated by the heat sources in the occupied zone. Heat sources (e.g. persons or computers) in the occupied zone create upward convective flows in the form of thermal plumes. These plumes remove heat and contaminants that are less dense than the air from the surrounding occupied zone.

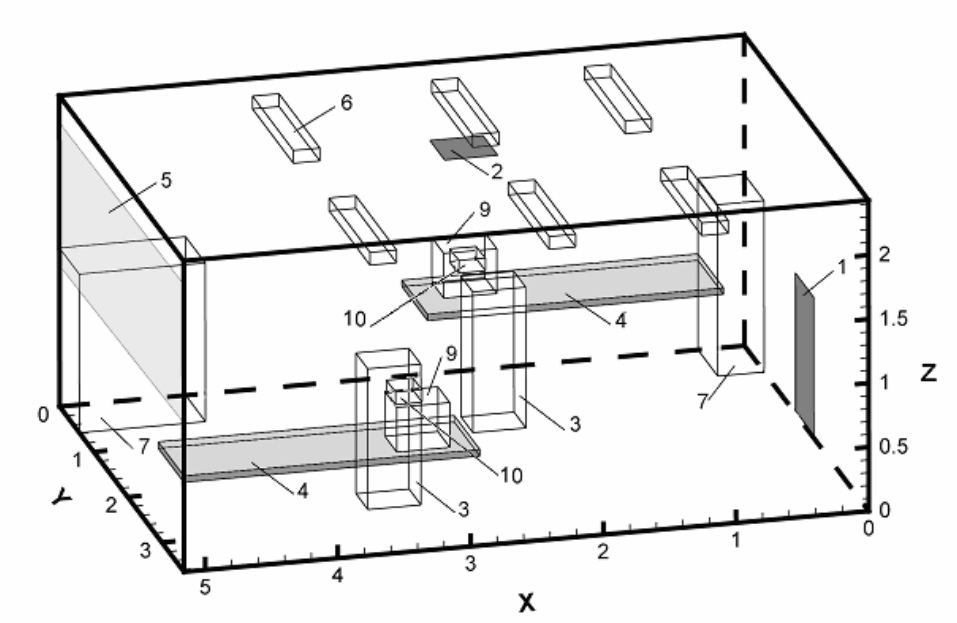

Fig. 4.6 The layout of the displacement ventilation simulated and tested in the chamber (inlet -1, outlet -2, person -3, table -4, window -5, fluorescent lamps -6, cabinet -7, computer -9, tracer gas sources -10).

Fig. 4.7(a) and Fig. 4.7(b) show the calculated air velocity plotted in two sections in the room. Fig. 4.7(d) illustrates the airflow distribution by smoke visualization. The computed results are in good agreement with the flow pattern observed, e.g. the recirculation in the lower part of the room is well captured. Fig. 4.7(b) also shows the upward plumes due to the buoyancy generated from the heat sources (the hot window, two computers, and two persons). A remarkable stratification of temperature can be observed in Fig. 4.7(c). The cold air at about 17 °C moves slowly along the floor, is heated by the heat sources, and finally leaves the room through the ceiling outlet with a temperature around 26.7 °C.

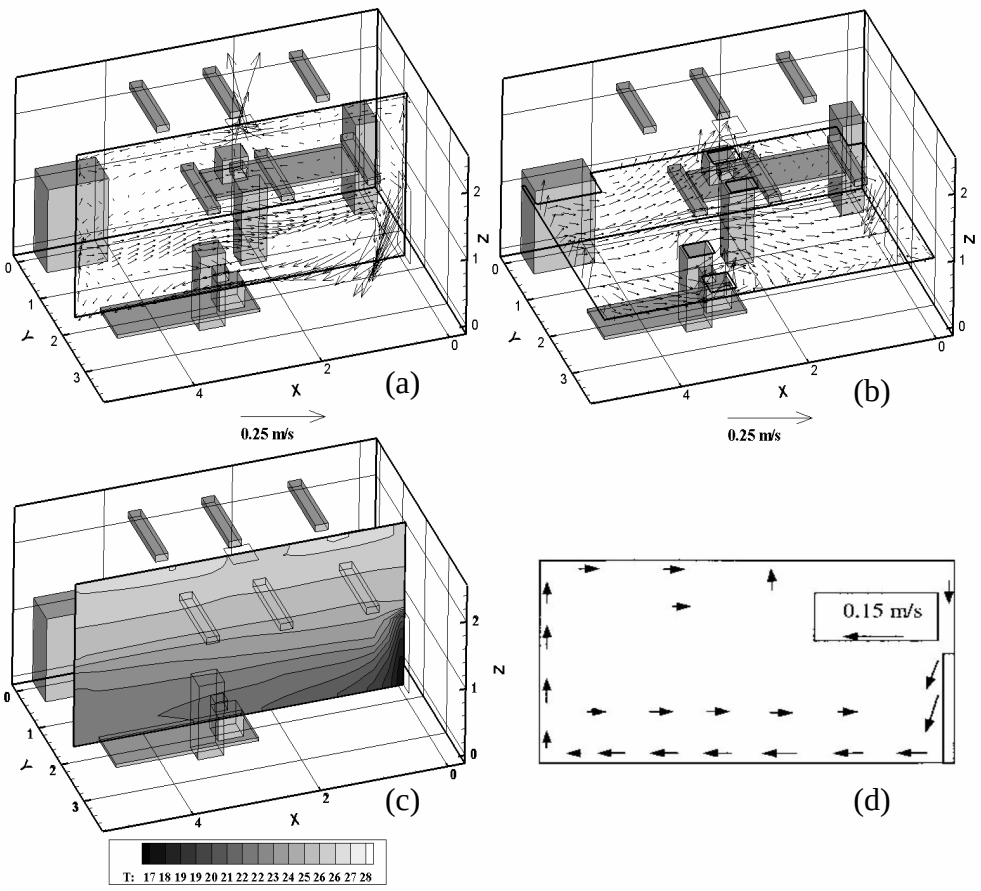

Fig. 4.7 The air distribution for the displacement ventilation case. (a) computed velocity in a middle section, (b) computed velocity in a horizontal section, (c) computed temperature in a middle section, and (d) airflow pattern observed by smoke visualization in a middle section.

Fig. 4.8, Fig. 4.9, and Fig. 4.10, respectively, show the comparison of measured and calculated velocity, temperature, and concentration of tracer-gas (SF_6). The right bottom figure shows the floor plan of the room, where the measurements were carried out at nine positions. Fig. 4.10 also illustrates the positions of the tracer-gas sources, e.g. S1 and S2. The computed results are compared with the experimental data in different vertical sections in the room. Although some discrepancies are observed, e.g. temperatures near the ceiling in Fig. 4.9, the computed velocity and temperature distributions generally agree very well with the measured results. The comparison for concentration, however, is

not as good as that for velocity and temperature. As shown in Fig. 4.10, both the concentration near the ceiling and the floor do not agree well with the experimental data, especially near the tracer-gas sources. The same problem has been found in similar studies. The most plausible reason is that the flow is not very stable and it is difficult to measure the time-averaged concentration. For each point, the concentration measurement took 30 seconds. It took six minutes to measure 12 points of the tracer-gas concentration.

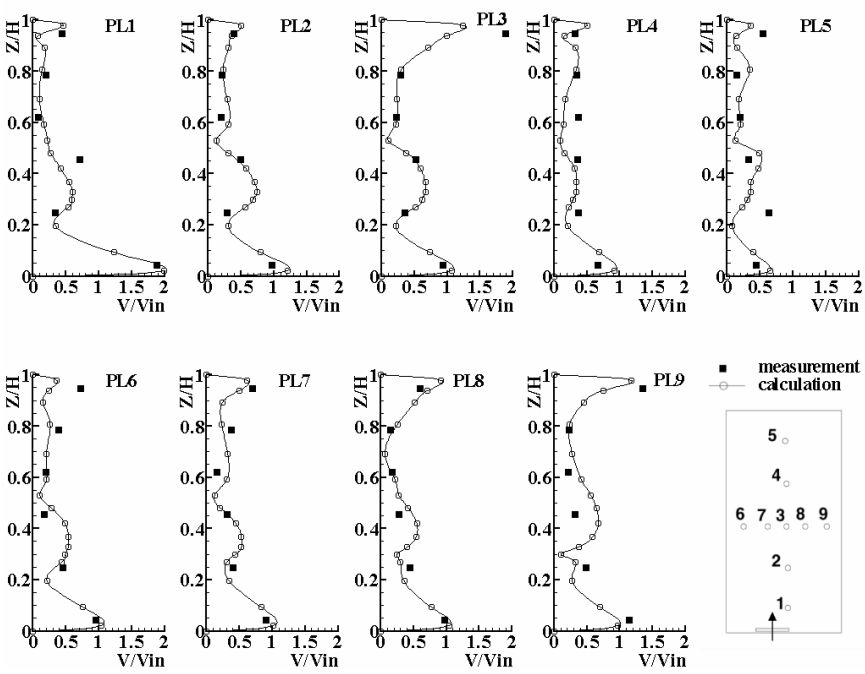

Fig. 4.8 The comparison of the velocity profiles at nine positions in the room between the calculated and measured data for the displacement ventilation case. Z = height, H = total room height, V = velocity, Vin = inlet velocity, H = 2.43 m, Vin = 0.086 m/s.

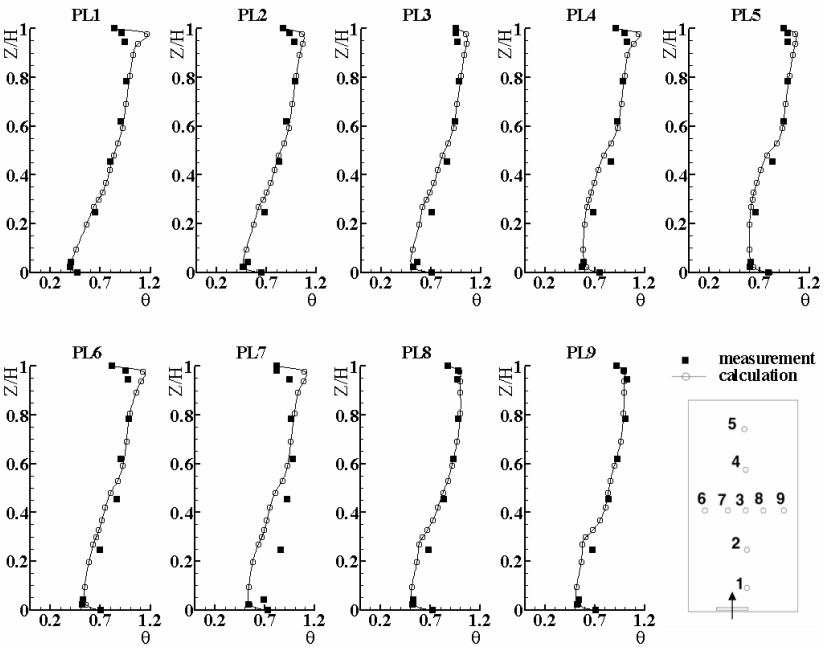

Fig. 4.9 The comparison of the temperature profiles at nine positions in the room between the calculated and measured data for the displacement ventilation case. Z = height, H = total room height, θ = (T-Tin/Tout-Tin), H = 2.43 m, Tin = 17.0 ^{o}C, Tout = 26.7 ^{o}C.

Nevertheless, the CFD0-C results are close to the experimental data, and the accuracy is acceptable. If a RMS value of the divergence of the calculated data from the measured results is calculated, it is 9.6% for air velocity, 3.2% for air temperature, and 13% for SF_6 concentration. The RMS difference of SF_6 concentration is higher than that of air velocity and temperature due to the above reasons. The CFD case and grid quality are also relevant to the accuracy of the simulation. As noted in Fig. 4.10, the source of tracer gas is originally modeled as a cube, the side of which is 20 cm. Later it is found that a cube with the side of 10 cm is more appropriate. Fine grids also improve the results. On the other hand, it seems more suitable to model the transfer-gas source as “Fluid” blockage, which allows air to flow through, than “Solid” blockage. Generally, the results of the CFD0-C are acceptable.

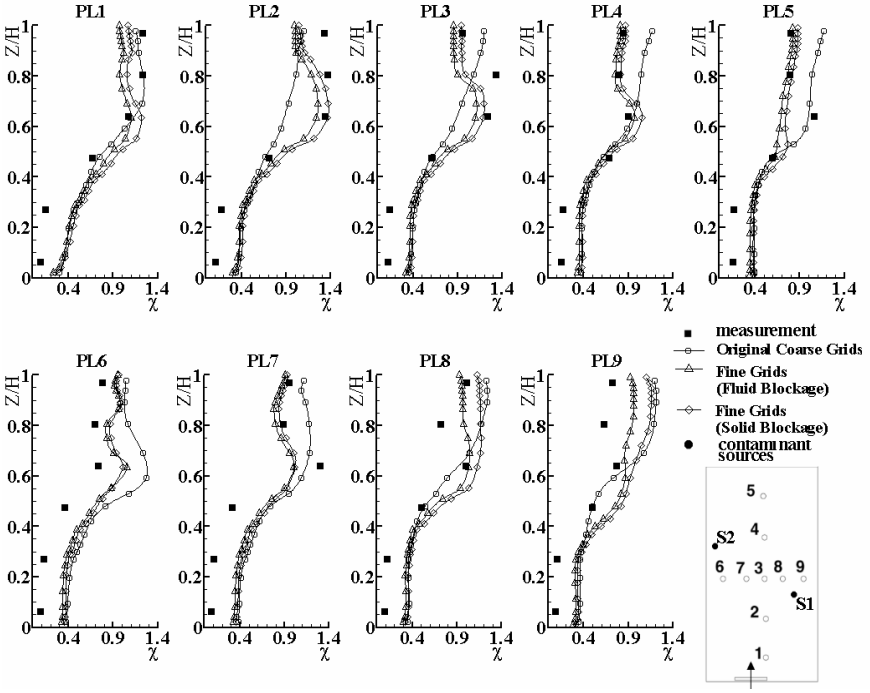

Fig. 4.10 The comparison of the contaminant profiles (ppm) at nine positions in the room between the calculated and measured data for the displacement ventilation case. Z = height, H = total room height, χ = (C-Cin/Cout-Cin), H = 2.43m, Cin = 0.0, Cout = 0.421.

4.1.4. Cross Ventilation in a 4-zone Building Model

In addition to buoyancy-driven airflows, natural ventilation driven by wind is also very common. Cross ventilation is one of the popular ways to deal with hot indoor environment in summer and shoulder seasons. A strong momentum effect is often observed in airflows with cross ventilation. In order to validate CFD0-C in solving airflows with strong momentum effect, the current study selects a case of cross ventilation in a 4-zone building model.

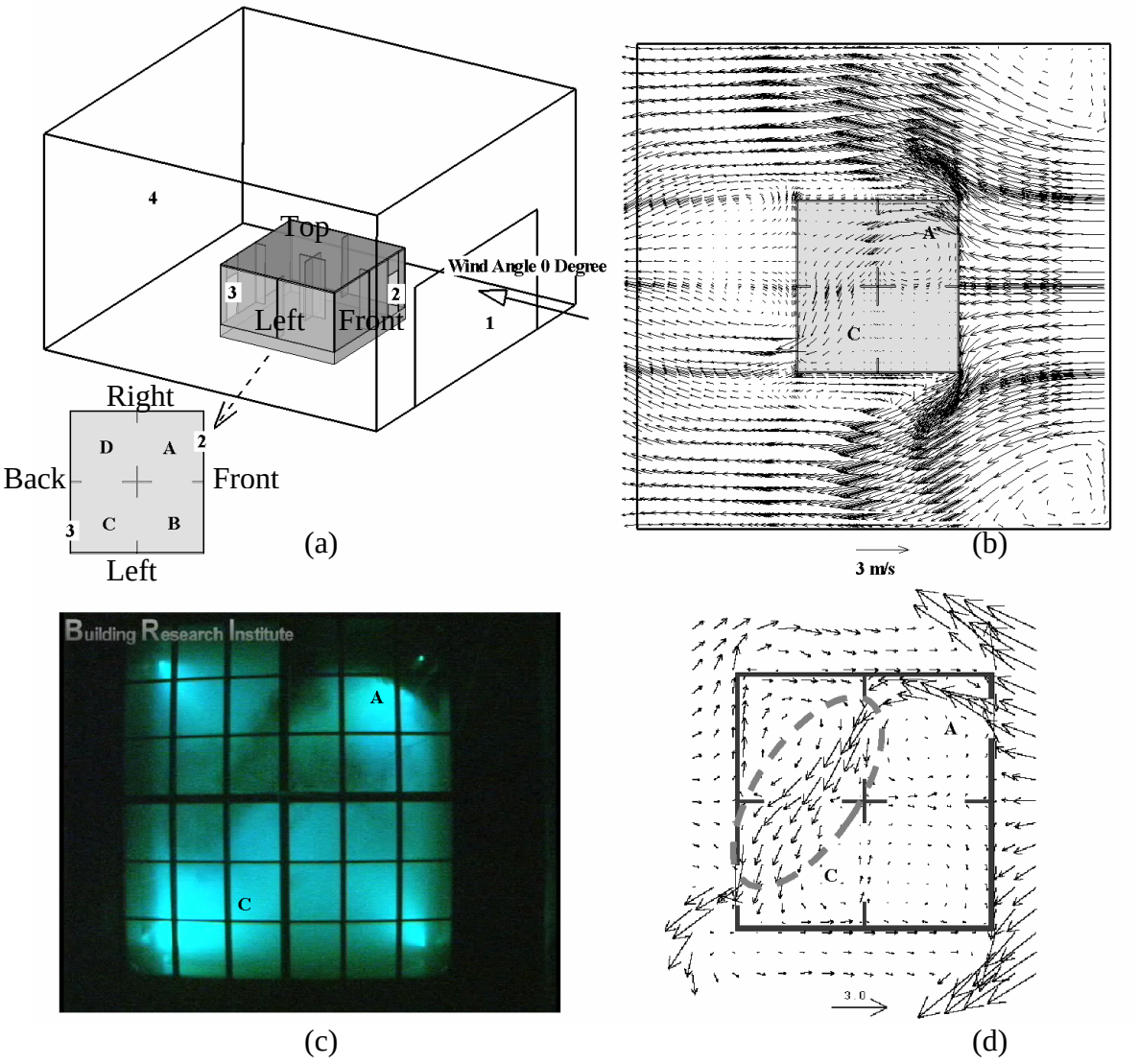

Fig. 4.11 Comparison of calculated and measured flow field with the wind coming perpendicular to the opening (a) The CFD0-C model, (b) CFD0-C flow field, (c) flow visualization in the test model, and (d) measured airflow field.

Sawachi et al. (2003) designed a full-scale wind tunnel to measure the variable discharge coefficients of openings due to different wind directions. Fig. 3.12 in CHAPTER 2 shows the wind tunnel sketch. The test model placed in the wind tunnel is a full-scale room, 5.53 m (L) × 5.53 m (B) ×3.0 m (H), divided into 4 sub-zones with the same size. Pressures and velocities are measured at many points around and inside the test model by differential pressure transducers and ultra-sonic three-dimensional anemometers. Laser

light sheet and smoke generation are used to visualize the flow fields, as illustrated in Fig. 4.11(c) for the case in which the wind is perpendicular to the opening (zero degree).

In this study, the flow boundary condition of the "air inlet 1" in Fig. 4.11(a) is specified with the uniform velocity of 3 m/s, and a zero pressure boundary is used for the outlet 4. The air flowing through opening A is at an angle due to a strong momentum effect, as shown in the measured flow field (Fig. 4.11(d)). Most of the flow goes into sub-zone D. The momentum of the air is still preserved even when leaving sub-zone C. Recirculation is observed in each of the sub-zones, some of which have caused two-way flows, such as across the two openings of sub-zone B. As shown in Fig. 4.11(b), the flow field calculated by CFD0-C is quite close to that measured. The recirculation in the left upper corner of sub-zone D, however, is not as obvious as the measured one. Reasons for the discrepancies could be insufficient grid resolution in that area and the isotropic assumption of turbulence in the turbulence model.

When the wind angle is zero degree, the measured ventilation rate by Sawachi of this 4-zone house was 8.2×10^3 m^3/h. By integration over door 2 in Fig. 4.11(a), the CFD0-C-calculated ventilation rate is about 7.158×10^3 m^3/h and the relative difference is 12.7%. Nishizawa et al. (2003) simulated the same case by a k-e model with a commercial CFD code, STREAM, and the ventilation rate they obtained was around 9.1×10^3 m^3/h. Their relative difference was about 11.0%. Inadequate geometry data may be one reason for the high relative difference.

4.1.5. External Airflow around a Building Model in a Wind Tunnel

The previous sections have validated CFD0-C for indoor airflow and contaminant transport simulations, which are characterized by low air velocities and turbulence effects. Compared to indoor airflows, atmospheric airflows around buildings involve higher air speed, more turbulence separation, reattachment, and vortices (Cochran, 2000). Literature review shows that not many validation studies have been conducted for such outdoor simulations with the CFD zero-equation turbulence model. Therefore, it is

necessary to examine the performance of CFD0-C for atmospheric airflows around buildings.

This thesis chose the same building model of Sawachi et al. (2003), who also measured external wind pressure distribution except that doors 2 and 3 in Fig. 4.11 were completely closed to obtain a solid building block. Sawachi et al. also measured the wind velocities at opening 1 as shown in Fig. 4.12, which was not the normal power-law/logarithm distribution. To consider the non-uniform distribution of wind velocities, opening 1 was modeled by eight vertically-arranged openings, each of which has uniform velocity specified in CFD0-C. A minimum grid spacing of 300mm as suggested by Cochran (2000), which is a similar size to the separation vortex, was used for the building block and a total grid number of 57×63×42 (X×Y×Z) was created for the wind tunnel.

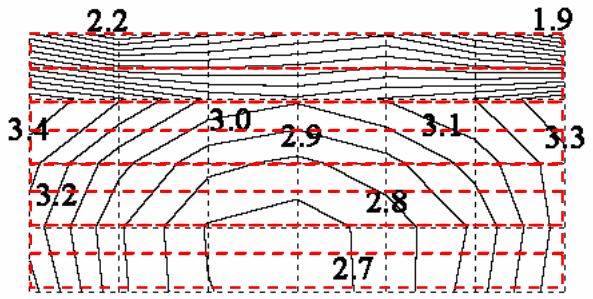

Fig. 4.12 Measured wind velocity distribution (m/s) at the wind supply opening 1.

CFD0-C illustrated variable performances for different building surfaces when simulating wind pressure distributions. Fig. 4.13 shows that for the front surface, which is under least flow separation, the predicted C_p values had a maximum of 20% difference from the measured data. However, the maximum difference could be 80% for the rest surfaces, which had strong turbulence separation and recirculation flows. Therefore, CFD0-C performs better for the surface with less turbulence separation and recirculation. In fact, the Reynolds Averaged Navier-Stokes (RANS) equations were found incapable to resolve the turbulence vortices and the curvature-sensitive separation flow features in

wind flow around buildings (Cochran 2000). Better results could be obtained by Large Eddy Simulations (LES), which however cause more computing time than RANS models. For engineering applications, the calculated wind pressure coefficients by CFD0-C may be enough to remedy the assumption of uniform wind pressures of CONTAM as illustrated by a demonstration case in CHAPTER 5.1.2.

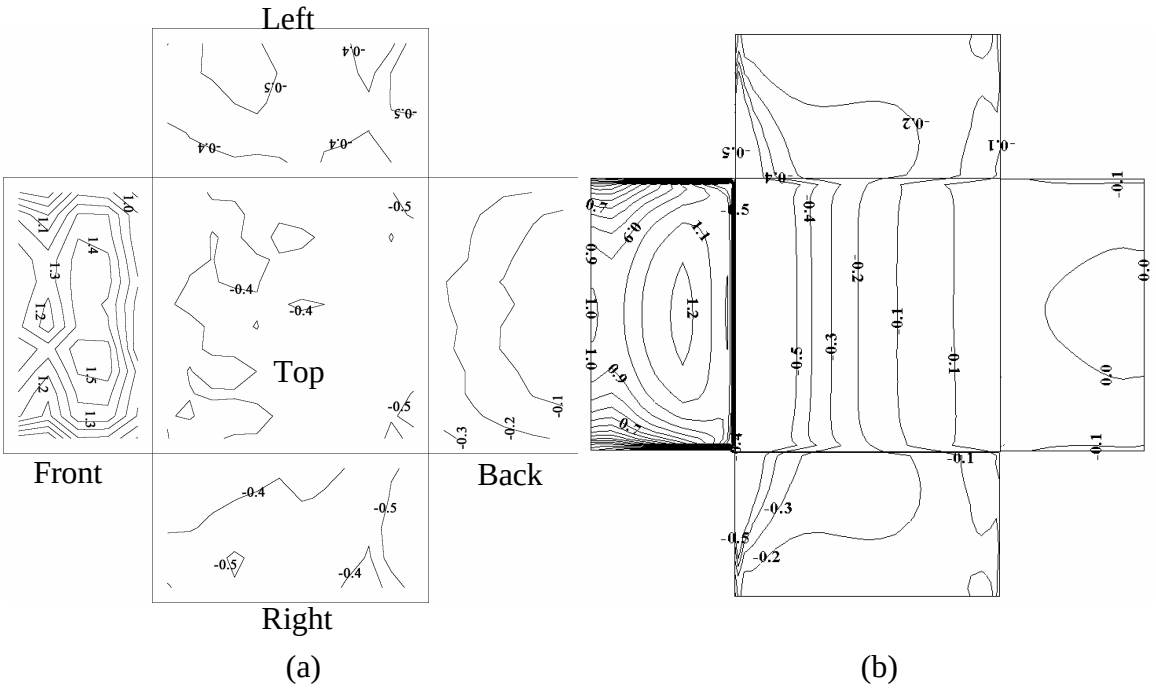

Fig. 4.13 Comparison of (a) measured wind pressure coefficients with (b) calculated wind pressure coefficients by CFD0-C when wind direction is zero degree.

Note that to calculate C_p the reference wind velocity, U_H in Eq. (3.1), was measured when there was no building model inside the wind tunnel, which was lower than the actual velocity for the wind tunnel with the building model. As a result, the maximum wind pressure coefficient became more than "1.0" in this case (Nishizawa et al., 2003).

4.2. Part II – Validations of Coupled Program

Even if CFD0-C and CONTAM may have been already validated individually, it cannot be guaranteed that the coupled CONTAM-CFD0 program will provide acceptable results. Since the coupled program only applies CFD0-C to some zones of a building, it will not be a surprise if the calculated results are not as accurate as those obtained by using CFD0-C for the whole building. However, the results from a coupled simulation should at least be better than CONTAM. Otherwise, there is no need to use the coupled program. It is therefore necessary to validate the coupled program to check how accurate the results are, when compared to a whole building simulation by only using CFD0, checking as well how well it can improve CONTAM calculations.

4.2.1. Experimental Design

In order to validate the coupled program and to show that the coupled program is superior to a multizone program, the experiment should be designed to study the situations where the CONTAM assumptions fail. As discussed previously, the situations include

1. non-uniform air momentum distributions ;
2. non-uniform contaminant concentration distributions; and/or
3. non-uniform air temperature distributions.

In this investigation, three experimental cases are designed for each of the above situation. The experiment uses an environmental chamber facility in the Ray W. Herrick Laboratories at Purdue University (Fig. 4.14(a)). The current study partitioned the facility further into four zones by a foam board, as shown in Fig. 4.14(b). All the cracks are sealed by duct tape to avoid filtrations.

This investigation measures the wall temperatures, spatial distributions of air velocities and temperatures, contaminant concentrations simulated by sulfur hexafluoride (SF_6), and airflow rates through the openings between the zones. Air velocities and temperatures are measured at 63 locations with omni-directional hot-sphere anemometers, as shown in Fig. 4.15(a). Eighteen thermal couples are embedded in the walls for wall temperature

measurements, supplemented with an infrared thermometer. Spatial SF_6 concentration is measured at 45 locations by a tracer gas analyzer.

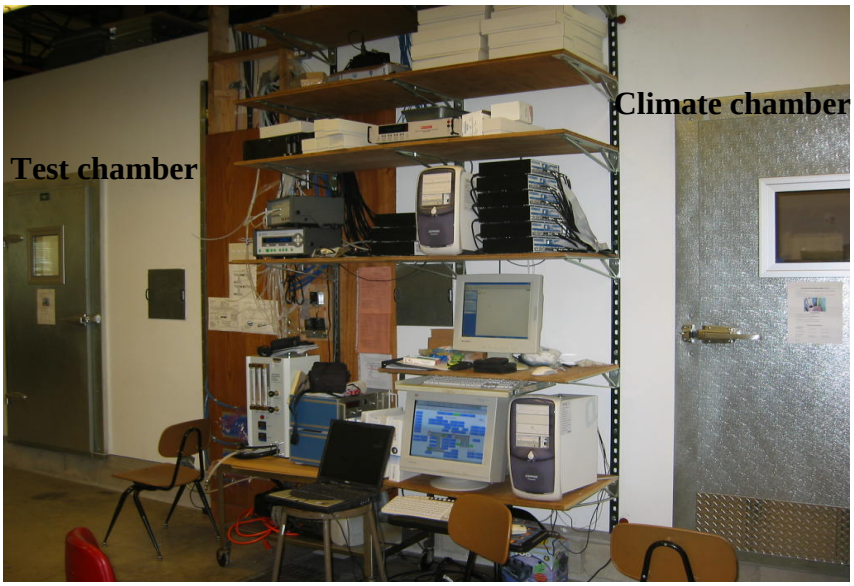

(a) External view of the environmental chamber

(b) Internal view of the environment chamber partitions inside the test chamber with the partition door removed for each zone

Fig. 4.14 The environment chamber of Ray W. Herrick Laboratories.

(a) Sensor location (b) Flow rate measurements

Fig. 4.15 Example of the sensors used for air velocity, air temperature, and flow rate measurements and their locations.

Fig. 4.15(b) shows three tracer-gas sampling tubes in an opening simulated by a window, used to measure the airflow rate through the window. The measurements were based on the steady-state tracer gas method. The equilibrium flow rate through an opening was calculated by:

$$Q = \frac{\dot{m}}{\overline{C}} \tag{4.2}$$

where, Q = flow rate through an opening,

$\dot{m}$ = tracer-gas source (SF_6) flow rate,

$\overline{C} = (\sum_i C_i A_i)/A$, the average SF_6 concentration through the opening.

4.2.2. Non-Uniform Momentum Distributions

This section will first present the experimental conditions for airflow and contaminant transport in the four-zone chamber facility with non-uniform momentum distribution in a zone. The numerical results of CONTAM, CFD0, and the coupled simulations are then compared with the measurement data.

We used mechanical ventilation through an air supply to create a strong non-uniform momentum effect in zone 1, as shown in Fig. 4.16. Zone 1 has two openings, one on the opposite side of the supply and the other far from the supply. Multizone models could not consider the non-uniform momentum effect in zone 1 created by the air supply. As a result, the airflow rate through the two openings, calculated by multizone models, would be the same. In reality, we know that opening 1 would have a higher flow rate caused by the momentum effect from the air supply than opening 2, as the zone geometry in the downstream was almost symmetrical.

The supply opening size was 0.3 m × 0.2 m, with an effective area ratio of 0.77. The airflow rates used in the experiment were 0.034, 0.053, 0.105, 0.14, and 0.215 m^3/s. The size of the openings 1 and 2 was 0.40 m × 0.20 m each and the other openings in zones 2 and 3 (windows 1 and 2) were 0.65 m × 0.20 m.

The case is simulated by three methods:

- CONTAM simulations
- Coupled CONTAM and CFD0 simulations in which 67 × 25 × 35 grids were used in zone 1 for CFD0
- CFD0 simulations of all four zones with 67 × 71 × 35 grids

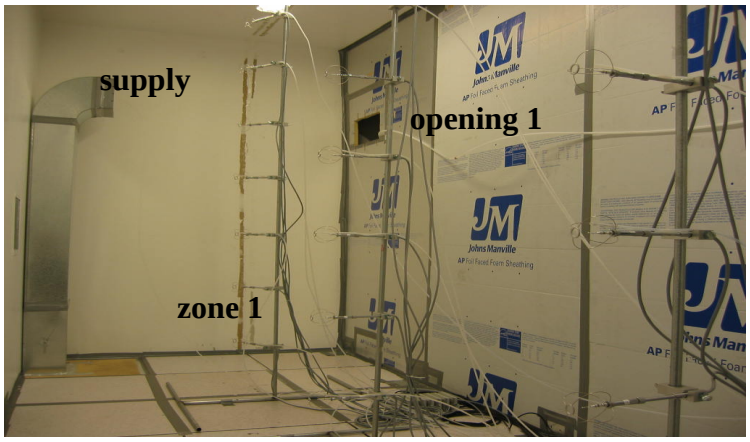

(a) Physical conditions for zone 1

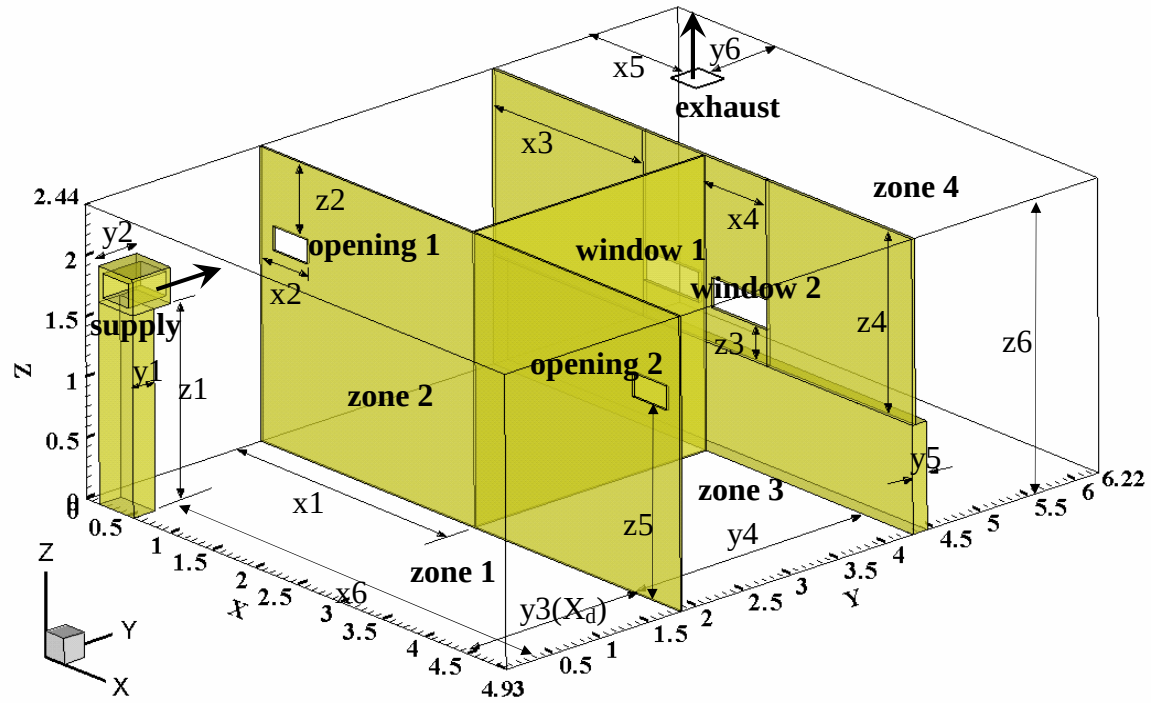

	1	2	3	4	5	6
x(m)	2.49	0.55	1.76	0.73	1.07	4.43
y(m)	0.20	0.40	1.83	2.44	0.18	0.75
z(m)	1.72	0.62	0.35	1.50	1.62	2.44

(b) The geometric conditions of the four-zone chamber

Fig. 4.16 The scheme of the four-zone chamber used to study non-uniform momentum distribution in zone 1.

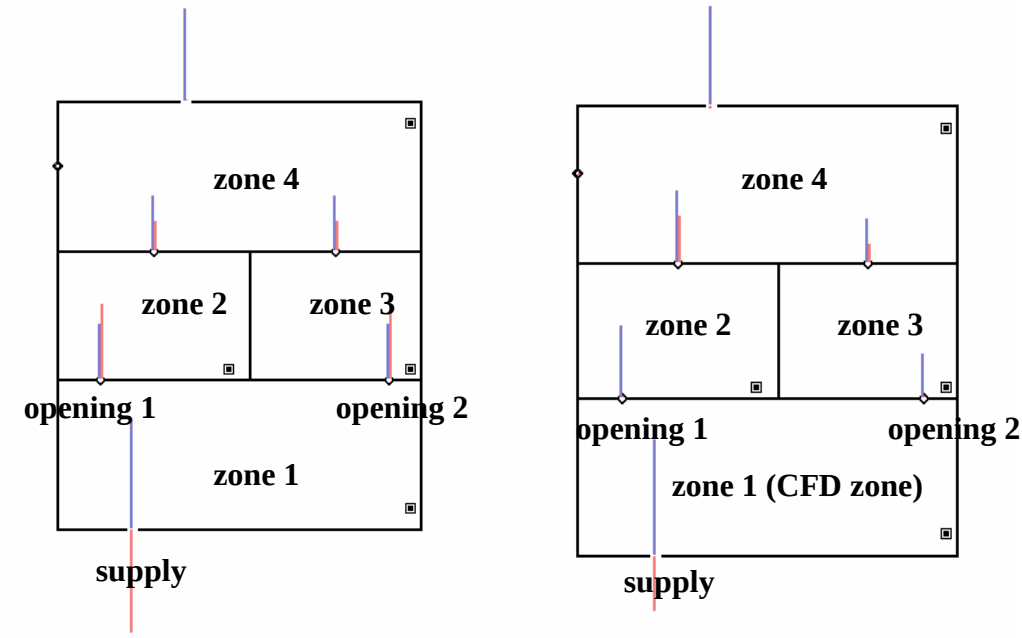

(a) (b)

Fig. 4.17 Airflow and pressure distributions in the four-zone chamber facility (a) calculated by CONTAM and (b) calculated by the coupled CONTAM and CFD0 program.

Fig. 4.17 compares the airflow results of the CONTAM simulation with those of the coupled simulation for the case with 0.105 m^3/s of air supply. The blue lines stand for airflow rates and the red lines for pressure differences across the airflow paths. A multizone model, such as CONTAM, could not consider the non-uniform momentum effect in zone 1 created by the supply air. As a result, the airflow rate through the two openings calculated by CONTAM would be the same, as shown in Fig. 4.17. In reality, opening 1 would have a higher flow rate than opening 2 caused by the momentum effect from the air supply, as the zone geometry in the downstream was almost symmetrical. Thus, the multizone model fails to calculate accurately airflow distribution for this case with non-uniform momentum flow.

The measured airflow rates in Fig. 4.18 further verify that the airflows measured through openings 1 and 2 were not equal, although the geometry is symmetrical. The higher the

momentum (airflow rate) from the supply is, the higher the ratio of the flow through opening 1 over opening 2 will be.

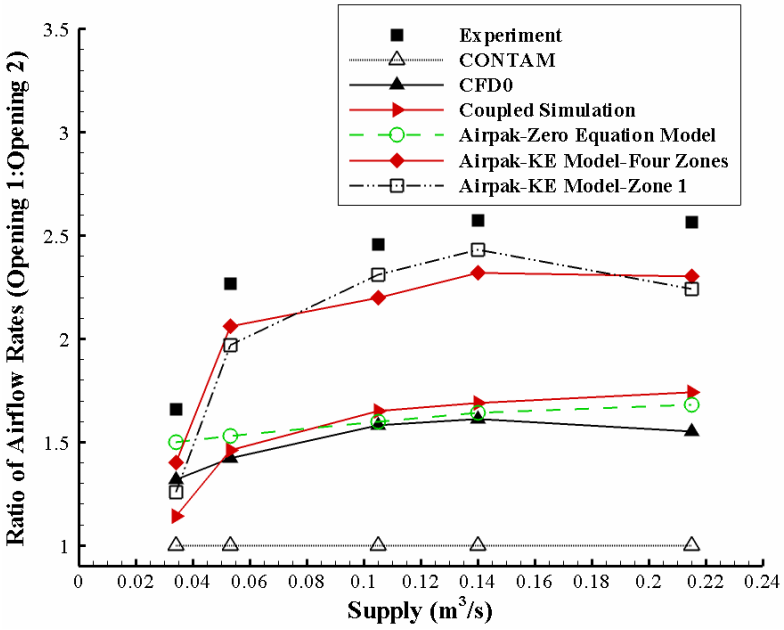

Fig. 4.18 Comparison of measured airflow rates with different simulated results.

When the coupled CONTAM-CFD0 program was used, where CFD0 was applied to zone 1 and CONTAM for the rest zones, Fig. 4.19 shows that the pressure near opening 1 was much greater than that near opening 2. Because of the non-uniform distribution of pressure in zone 1, the flow rate through opening 1 was greater than that through opening 2. However, the discrepancies between the calculated results and the measured data were very significant as shown in Fig. 4.18. These results were consistent with different airflow rate and were unexpected.

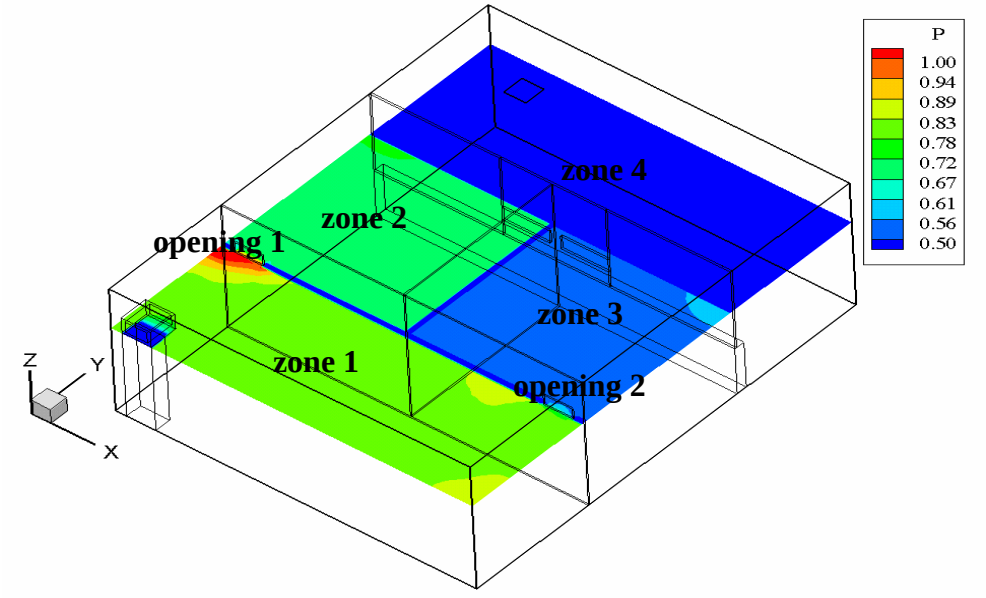

Fig. 4.19 The pressure distribution at 1.66 m from the floor in the four-zone chamber calculated by CFD0.

By applying CFD0 to all the four zones, the calculated airflow ratios did not improve further, compared with those obtained with the coupled CONTAM-CFD0 program. Then, a commercial CFD program, Airpak (Fluent, 2002), was applied to all the four zones by using the same zero-equation turbulence model as that used in CFD0. The results obtained by Airpak were almost identical to those by CFD0. Clearly, for this particular case, the zero-equation model was unable to predict accurately the airflow in the four-zone facility, although the reason was not clear.

If we replaced the zero-equation model by the standard k-ε model in Airpak and simulated all the four zones, the computed ratios of airflow rates of opening 1 over opening 2 were very close to the experimental data as also shown in Fig. 4.18. This further verified that the turbulence model played a very important role in this case. Finally, this investigation applied Airpak with the standard k-ε model to zone 1 and CONTAM to the other three zones. The computed results were in reasonable agreement with the experimental data and those obtained by using Airpak with the standard k-ε

model to all the zones. This validates that a coupled multizone and CFD program with the standard k-ε model can be used for the prediction of airflow in zones with non-uniform momentum distributions.

For this case, the computation time is about 490 minutes for the simulation with CFD0 for all the four zones and 185 minutes for the coupled CONTAM-CFD0 simulation for zone 1. The coupled simulation used less computing time than the CFD0 simulation since it applied CFD0 to zone 1 only. Although the computing cost was much greater than CONTAM, which only takes a few seconds, the coupled simulation provided more accurate results than CONTAM. The simulations with the standard k-ε turbulence model required more computing time than those with the zero-equation model. An Airpak simulation with the same grid number as CFD0 for the four zones by the standard k-ε model costs 620 minutes, which doubled the simulation time with the zero-equation model in Airpak.

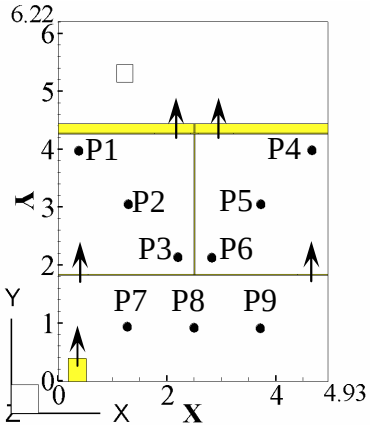

Fig. 4.20 The plan view of the four-zone facility with the nine measuring poles.

In addition to flow rates, our experiment also measured the air velocity and temperature in sixty-three locations in the chamber facility. The sixty-three locations were in nine poles, and each pole has seven points from the floor to the ceiling. Fig. 4.20 shows the positions of the nine measuring poles that were in Zones 1, 2, and 3. Fig. 4.21 compares

the air velocities calculated by CFD0, the coupled CONTAM-CFD0, and the Airpak simulation of the four zones by the standard k-ε model for selected positions with the experimental data. Since the coupled CONTAM-CFD0 simulation applied CFD0 only to zone 1, the comparison can only be made for P7, P8, and P9. The Airpak simulation with the standard k-ε model provided the best results while the CFD0 results had some discrepancies from the experimental data. The discrepancies could be attributed to the turbulence model, as discussed previously. The calculated air velocities by the coupled program generally agree well with those by the CFD0, although similar degree of discrepancies was found. Even if the coupled simulation only applied CFD0 to one zone, the coupled CONTAM-CFD0 performed as well as CFD0 for all the zones.

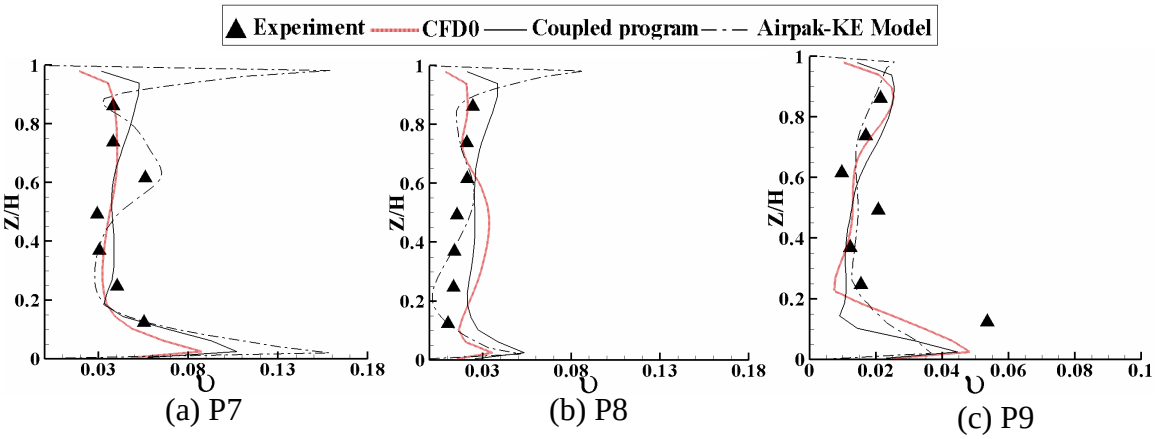

Fig. 4.21 Comparison of air velocities at P7, P8, and P9 in zone 1 with non-uniform momentum distribution (H=2.44m; $\upsilon=U/U_{in}$, non-dimensional velocity when U_{in}=2.281 m/s is the supply air velocity and the supply rate is 0.105 m^3/s.

The results from this case imply that

- CONTAM could not consider a zone with a strong non-uniform momentum flow
- The coupled CONTAM-CFD0 program performs better than the CONTAM
- The coupled CONTAM-CFD0 program, where CFD0 was used for zone 1, is as good as CFD0 for all the zones, but with a major reduction in computing time
- The CFD0 with the zero-equation model is as good as Airpak with the same model

- The Airpak with a standard k-ε turbulence model gives better results, but also the longest computing time
- The zero-equation model could not correctly simulate the airflow for zone 1 in this case.

4.2.3. Non-Uniform Contaminant Concentration Distributions

CONTAM assumed the instantaneous mixing of a contaminant in a zone. Such an assumption is acceptable if the zone is small and the mixing is intensive. In many cases, the mixing is not perfect. By applying CFD to such a zone, the non-uniform mixing can be considered so that the simulated results can be greatly improved.

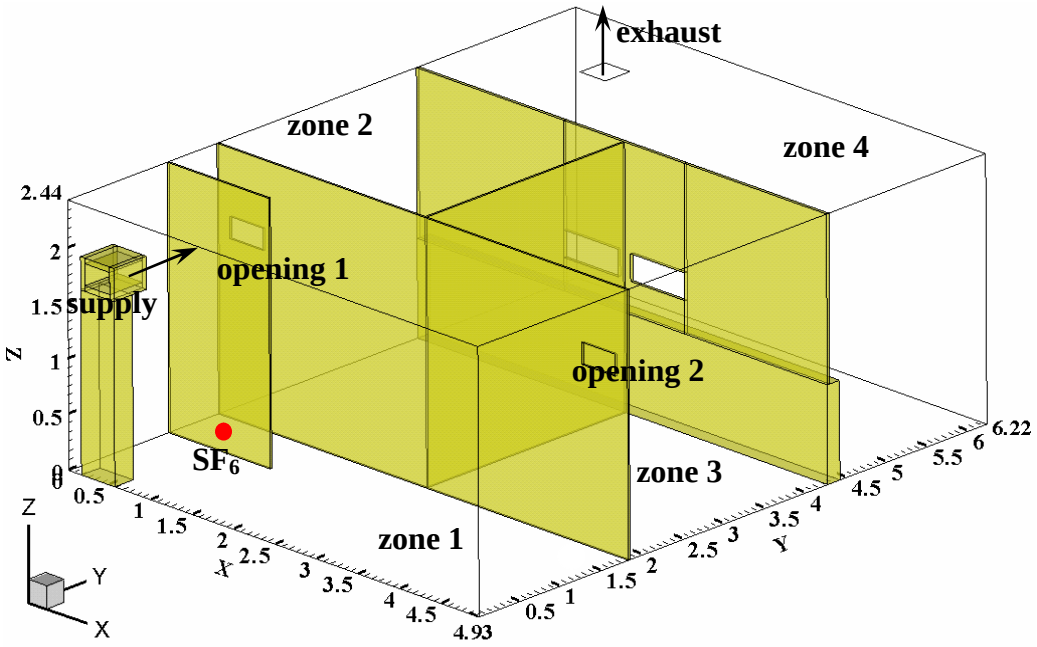

Source Location	x (m)	y (m)	z (m)
SF_6	0.36	1.53	0

Fig. 4.22 The chamber schematic used for contaminant transport study and the contaminant source locations.

This investigation has designed a case to study non-perfect contaminant mixing. The case was the same as Fig. 4.16 in previous section, except for adding a partition wall in front of the air supply in zone 1 to create non-uniform contaminant distributions, as shown in Fig. 4.22. This study created a non-uniform SF_6 distribution in zone 1 by placing a contaminant source, which was simulated by SF_6, behind the partition.

It was possible to improve CONTAM results by separating the area behind the partition wall as another zone. However, the airflow between the new zone and the rest of zone 1 could be multi-directional through the large opening. That creates a very challenging problem for CFD0. On the other hand, our aim is to demonstrate how CFD0 could be used to improve the airflow modeling not to demonstrate how we could do better by using CONTAM alone.

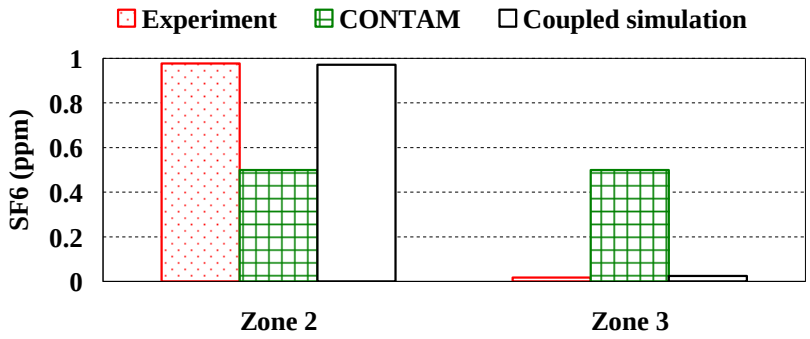

Fig. 4.23 Comparison of measured and simulated SF_6 concentrations (ppm) in zones 2 and 3.

Thus, if a CONTAM simulation is applied for the whole space of zone 1, it could not predict the non-uniform distribution of SF_6 in zone 1. CONTAM also interprets the flow and geometrical conditions to be symmetrical, because it could not take the partition wall into account. As a result, CONTAM would predict the same SF_6 concentration in zone 2 and zone 3, as shown in Fig. 4.23. Without concerning about airflow models, the coupled CONTAM and CFD0 simulation, in which the CFD0 was applied to zone 1, could consider the non-uniform SF_6 concentration in zone 1. Clearly, the zone next to the SF_6

source had a high SF_6 concentration than the other zone, although the geometry is symmetrical. The SF_6 concentration in zone 2 was 0.977 ppm, which was obtained by averaging the SF_6 concentration over the 15 locations along Poles 1-3. The average SF_6 concentrations were 0.022 ppm for zone 1 and 0.018 ppm for zone 3. Most of the SF_6 was transported to zone 2 so the average concentration in zone 1 was low.

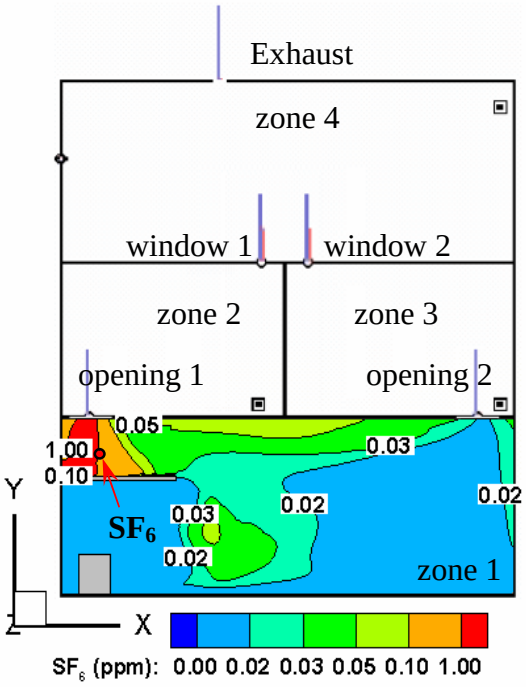

Fig. 4.24 SF_6 concentration distribution at openings 1 and 2 height in the four-zone chamber facility calculated by the coupled CONTAM and CFD0 program.

The huge difference in SF_6 concentrations between zones 2 and 3 was caused by the non-uniform SF_6 distribution in zone 1, as illustrated in Fig. 4.24. When SF_6 is placed behind the partition, the partition wall confined the SF_6 in a corner. As a result, the SF_6 concentration near opening 1 was about 50 times higher than that near opening 2. The coupled program can correctly calculate the SF_6 concentrations by predicting the detailed SF_6 distribution in zone 1.

Fig. 4.24 also shows the airflow distributions from the coupled simulation. The blue lines stand for airflow rates and the red lines for pressure differences across the airflow paths. The partition board in front of the supply blocked the inflow so that air was almost equally distributed between openings 1 and 2. Table 4.2 illustrates that the calculated airflow rates through openings 1 and 2 were close to the measured data.

Table 4.2 Comparison of airflow rates through openings O1 and O2 by the measurement and by the coupled simulation (m^3/s).

	Experiment	Coupled simulation
opening 1	0.049	0.048
opening 2	0.050	0.051

Fig. 4.25 compares the SF_6 concentrations in zone 1 obtained with different methods. The SF_6 concentrations were measured at 45 locations at the same nine poles as in the previous case. When applying CFD0 to the entire flow domain (all the four zones), the CFD0 results were reasonably close to the experimental data, although some fluctuations of experimental data existed. Since it took 30 s to measure the SF_6 concentration in one location, the data obtained between the two measurements that were two minutes apart may not be the same for the same location. The solid triangles show the mean SF_6 concentration measured and the horizontal bars show the fluctuation. Our experience also shows that it is very difficult to obtain good agreement between CFD simulations and experimental measurements for tracer-gas concentration. The coupled CONTAM and CFD0 simulation predicted higher SF_6 concentrations for Poles 7-9. This is probably caused by the inaccurate flow rate provided by CONTAM in other zones for the CFD0 as boundary conditions.

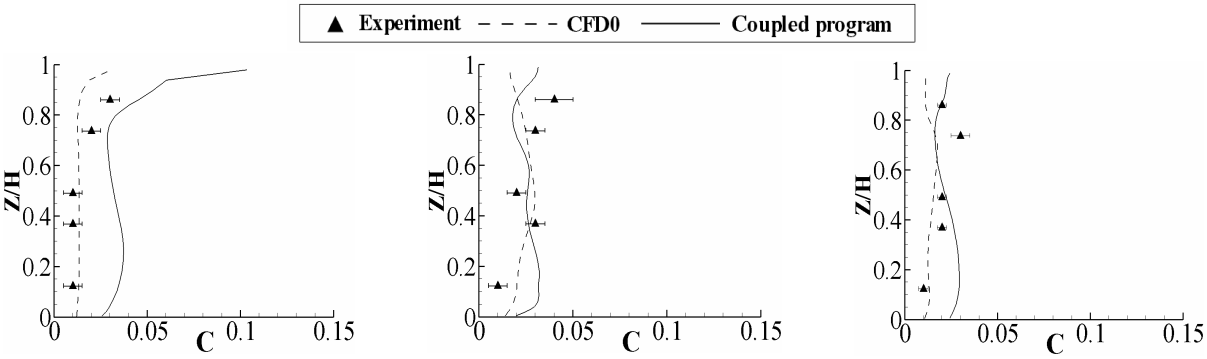

(a) P7 (b) P8 (b) P9

Fig. 4.25 Comparison of measured and computed SF_6 concentrations (ppm) at P7, P8, and P9 in Zone 1 for the non-uniform contaminant distribution case.

4.2.4. Non-Uniform Temperature Distributions

A multizone model, such as CONTAM, could consider the impact of temperature on the airflow between zones. However, the model assumes that the temperature is uniformly distributed in each zone. Therefore, the impact caused by the temperature gradient is normally not accounted for. Hence, this investigation designed another case with a high temperature gradient to examine the impact of the temperature gradient on the airflow rate calculated by CONTAM.

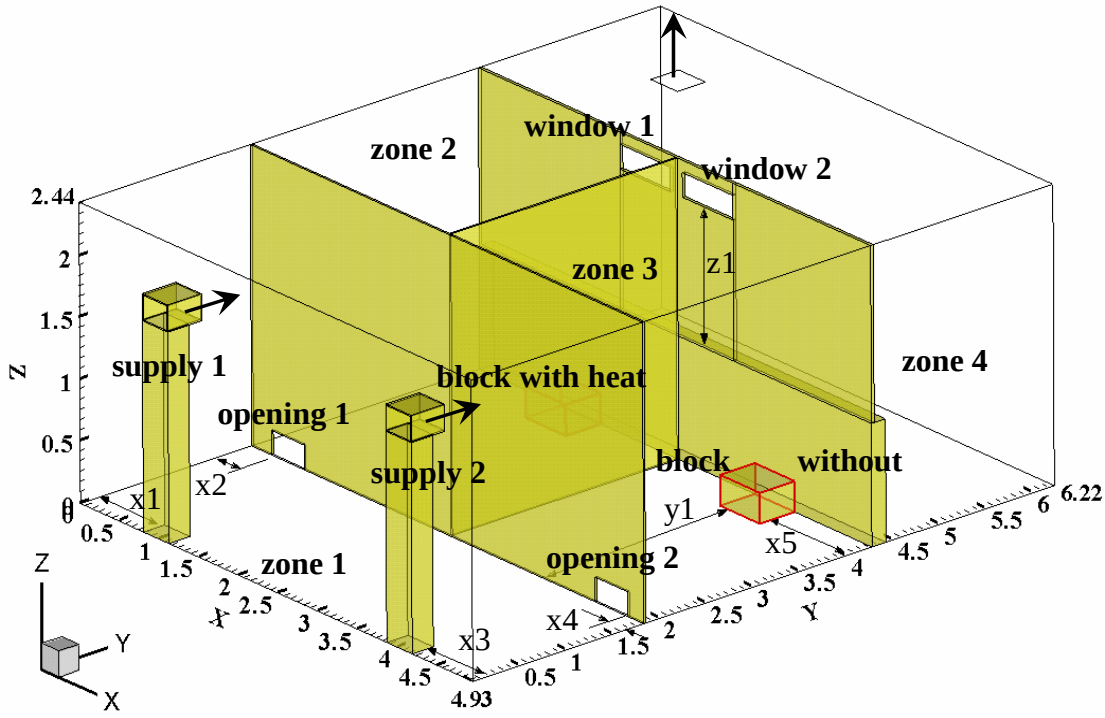

x1	x2	x3	x4	x5	y1	z1
0.81	0.26	0.76	0.21	0.97	2.04	1.2

Fig. 4.26 Schematic of the case used to study non-uniform temperature distribution.

Fig. 4.26 shows the schematic of the case design. Another supply was added in zone 1 to create a symmetrical flow-supply condition. However, as shown in Table 4.3, the flow rate and the supply of air temperature were not exactly symmetrical in the experiment. A heated box was placed in zone 2 and a non-heated box of the same size was symmetrically placed in zone 3. Because the heat from the box was highly concentrated, it generated a large temperature gradient in zone 2. This experiment also placed openings 1 and 2 in the lower part of the partition. Because zone 2 was of a higher temperature than zone 3 due to the heat source, the stack effect created a higher flow into zone 2 than zone 3.

Table 4.3 Actual flow conditions from the two air supplies.

Heat source	Air supply 1		Air supply 2	
	Flow rates (m^3/s)	Temperature (°C)	Flow rates (m^3/s)	Temperature (°C)
0 W	0.0477	18.5	0.0543	18.5
288 W	0.0510	18.9	0.0467	18.7
859 W	0.0514	18.5	0.0533	18.3

CONTAM, the coupled CONTAM-CFD0, and CFD0 were used to simulate the case. Fig. 4.27 shows the airflow and pressure distributions obtained by CONTAM (Fig. 4.27(a)) and by the coupled CONTAM-CFD0 (Fig. 4.27(b)). In the coupled simulation, CFD0 was only applied to zone 2. There are differences in the results but they are not evident.

Although not shown in this chapter, the detailed comparison of air velocity and temperature in the sixty-three locations in the room for this case is very similar to the other two cases.

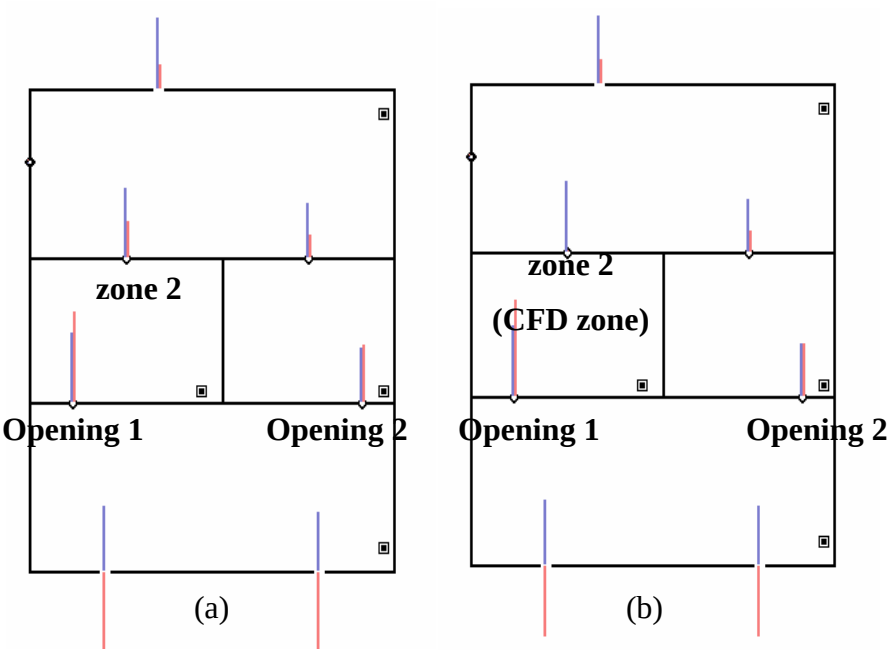

Fig. 4.27 Comparison of airflow and pressure distributions for the case with non-uniform temperature distribution by (a) CONTAM and by (b) the coupled CONTAM and CFD0.

Fig. 4.28 shows that the measured airflow ratios through opening 1 over opening 2 increased with the stack effects in zone 2, which were caused by increasing the surface temperatures of the heated box. As shown in Fig. 4.28, CONTAM generally under-predicted the airflow ratios by 10%, although it could consider the stack effects caused by the temperature difference of zones 2 and 3. The reason was that CONTAM neglected the temperature gradients inside zone 2. To consider the temperature gradients, this study applied CFD to zone 2 and CONTAM to the other zones in the coupled CONTAM-CFD0 simulations. The measured surface temperatures of the heated box were used as boundary conditions in the coupled simulations so that the temperature gradients could be correctly considered. Fig. 4.28 illustrates that the calculated airflow ratios by the coupled program were very close to the measured data except for the box surface temperature of 30°C. This study then used CFD0 to simulate all the four zones and found that the results of CFD0 were close to those of the coupled simulations for all the three cases. When the surface temperature was 30 °C, therefore, the discrepancy between the measured and calculated results could be attributed to the experimental errors.

On the other hand, the assumption of uniform temperature in each zone seems to be tolerable in this case. The difference of 10% of CONTAM simulations from the experimental data was within the normal acceptable range of 20% for multizone simulations (Emmerich, 2001). Of course, the experiments provided CONTAM simulations a good estimation of air temperature for each zone. Otherwise, the difference of 10% may be difficult to obtain.

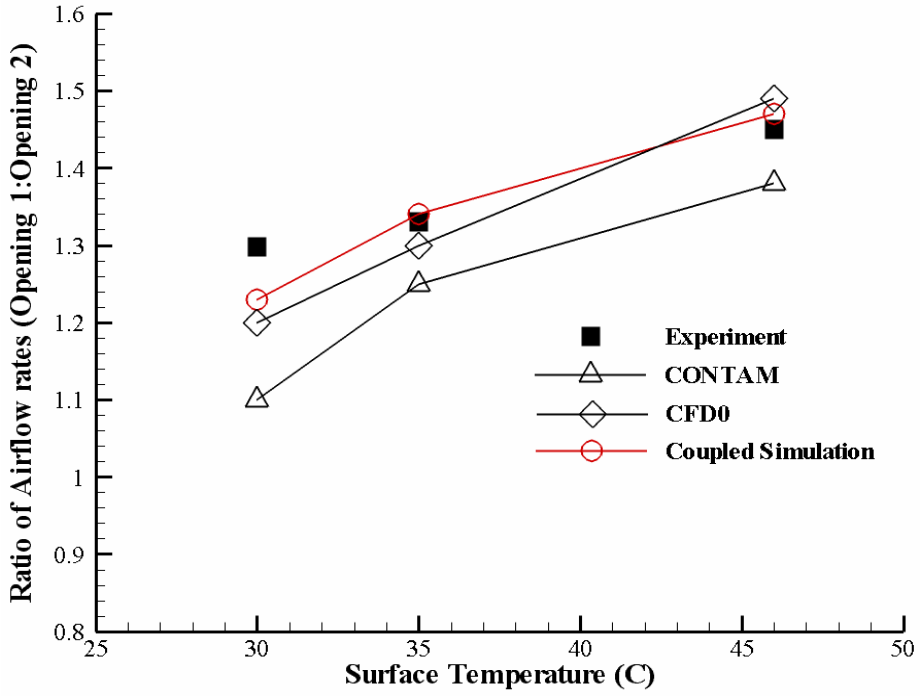

Fig. 4.28 Comparison of airflow rates for the case with different methods.

The moderate temperature gradients in this case explained why the assumption of uniform temperature was not crucial. Fig. 4.29 illustrates the temperature distribution of Poles 1-3 of zone 2 when the surface temperature of the heated box was 35 °C. The measured temperature gradient of the bulk air in zone 2 was as high as 3.7 °C, although the temperature gradient near the heated box could be higher. The temperature gradient could reach to 5.5 °C when the surface temperature of the heated box was 46 °C. Li et al. (1998a) also found that when the temperature gradient was moderate, there was reasonable agreement between the ventilation flow rates predicted by multizone and CFD approaches. However, when the temperature gradient was more than 10 °C, the calculated ventilation rates by multizone methods can differ from the measured data by more than 30% (Kotani et al., 2003).

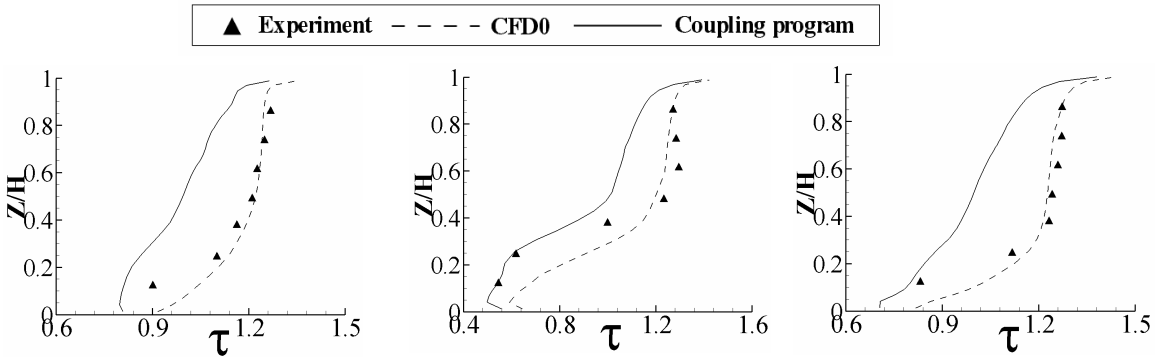

(a) P1 (b) P2 (c) P3

Fig. 4.29 Comparison of the air temperatures at the three poles in zone 2 for the non-uniform temperature distribution when the surface temperature of the heated box was 35 °C (H=2.44m; $\tau = (T-T_{in})/(T_{out}-T_{in})$ is non-dimensional temperature where T_{in}=18.2 °C was the supply air temperature and T_{out}=24.3 °C was the exhaust air temperature).

Fig. 4.29 also compares the calculated temperature distributions of poles 1-3 with the measured data. Since the coupled simulation only applied CFD to zone 2, the calculated temperatures were quite different from the measured data, although the pattern of the temperature differences was similar to the data. The results could be improved if CFD0 was applied to all the four zones as also shown in Fig. 4.29. However, the computing time of the CFD0 simulation for all four zones was one-order magnitude greater than the coupled program. When the accuracy of the spatial temperatures was not a primary concern, the coupled program provides acceptable results.

Note that, for the purpose of experimental validation of the coupled CONTAM-CFD0 program, the chamber experiments in this section used extreme cases of non-uniform air momentum effects and contaminant concentrations. For common cases, CHAPTER 6 developed guidelines when and what case such coupling is needed.

4.3. Summary

By comparing the numerical results with the experimental data, this chapter conducts extensive verifications and validations of the CFD0-C and the coupled program of CONTAM and CFD0-C. For most of the cases, it shows the calculated results are reasonably close to those of the experiments.

The CFD0-C is verified by comparing its results with published data. It shows that CFD0-C performs reasonably well in solving the following problems: airflow with strong momentum effect and prescribed pressure boundary conditions, buoyancy-driven flows with temperature gradients, displacement ventilation with temperature and contaminant concentration gradients, and external airflow around a building model in a wind tunnel. Therefore, the upgrade of CFD0-C from CFD0-F is successful.

To validate the coupled CONTAM and CFD0 program, a series of experiments were conducted in a chamber facility for airflows with non-uniform distributions of momentum, temperature, and contaminant concentrations. Although some discrepancies exist, the calculated results by the coupled program generally agree well with the experimental data. The coupled program thus can be used to improve CONTAM while costing less computational time than the simulation that only uses CFD0-C in the whole flow domain.

Since the verifications and validations are only for steady-state problems and real design problems are often at a transient state, it is necessary to apply the coupled program to simulations with a transient airflow and a contaminant transport. CHAPTER 5 will demonstrate the coupled program through several realistic cases.

CHAPTER 5. APPLICATIONS

To use the coupled CONTAM and CFD0-C program as a design tool, it is important to apply the coupled program to realistic cases. Therefore, for coupled outdoor airflow simulations, this study demonstrates the WPC link to simulate the ambient airflow around a cubic building and the WPP link for the airflow around a low-rise house with a sloping roof. For building indoor airflows, although the numerical experiments in CHAPTER 3 and the validation studies in CHAPTER 4 demonstrate the capabilities of the coupled program, the studies are limited to steady-state analysis. It is also essential to apply the coupled program to transient simulations, since most of the real cases are at transient state. For that reason, this chapter selects a realistic case, natural ventilation in a three-story building with a large atrium, to demonstrate how the coupling algorithms can be employed to improve CONTAM results.

5.1. Demonstration of the Indirect Coupling for Outdoor Airflow Simulations

5.1.1. Demonstration of the Indirect Coupling by the Wind Pressure and the Contaminant (WPC) Link

Fig. 3.1 in CHAPTER 2 illustrates that the indirect coupling needs a WPC translator for the WPC link of CONTAM and CFD0-C. At present, a WPC translator has been developed to find wind pressure data obtained from CFD0-C for specific openings in CONTAM simulation. Two simulations are performed to demonstrate how the translator converts the EWC files to WPC files, and how CONTAM uses the WPC files to calculate airflow in a building. A building with a cubic shape is selected because CONTAM developers use it as a typical case to demonstrate the WPC link. In order to show the

impact of wind direction on wind pressure distribution, two types of wind direction are simulated. The first case involves wind blowing perpendicularly at a building wall, and in the other case, the wind blowing at an angle.

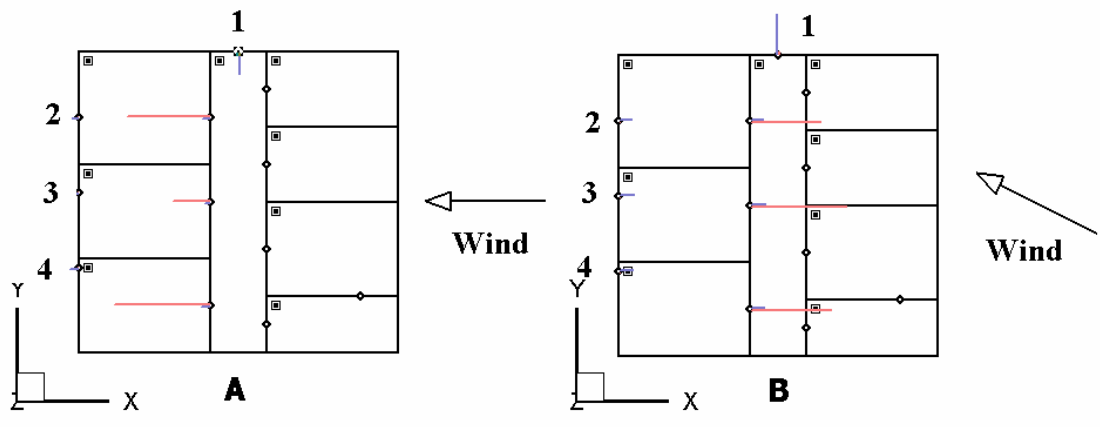

Fig. 5.1 Building plane view and CONTAM results using the WPC File.

The building is located in a place with 6 m/s wind velocity coming from the direction of a positive X-axis, as shown in Fig. 5.1. The building has four closed doors on its envelope, as labeled in the figure. Table 5.1 shows the door locations with the reference points of (0, 0, 0) in the lower-left corner of this building.

Fig. 5.2 shows the pressure contours and the velocity field computed by CFD0-C, viewed from two different angles. Fig. 5.2A and Fig. 5.2B are for the case with the perpendicular wind and Fig. 5.2C and Fig. 5.2D are for the wind blowing at an angle. The small white box is the building simulated and the large one is the CFD computational domain. The zero reference pressure is at the line of ‘x=0, z=0’.

Table 5.1 Opening locations, the relative wind pressures computed by CFD0-C, and airflow rates computed by CONTAM under the wind speed of 6 m/s.

Openings	1	2	3	4
Locations x, y, z (m)	5.0, 10.0, 1.0	0.0, 7.5, 1.0	0.0, 5.0, 1.0	0.0, 2.5, 1.0
Wind pressure for perpendicular wind (Pa)	-17.71	-21.17	-19.31	-21.65
Wind pressure for wind at an angle (Pa)	-33.97	-27.3	-24.96	-26.29
Air exchange rate for perpendicular wind (ACH)	0.0229	0.0059	0.0034	0.0062
Air exchange rate for wind at an angle (ACH)	0.0432	0.0087	0.0106	0.0095

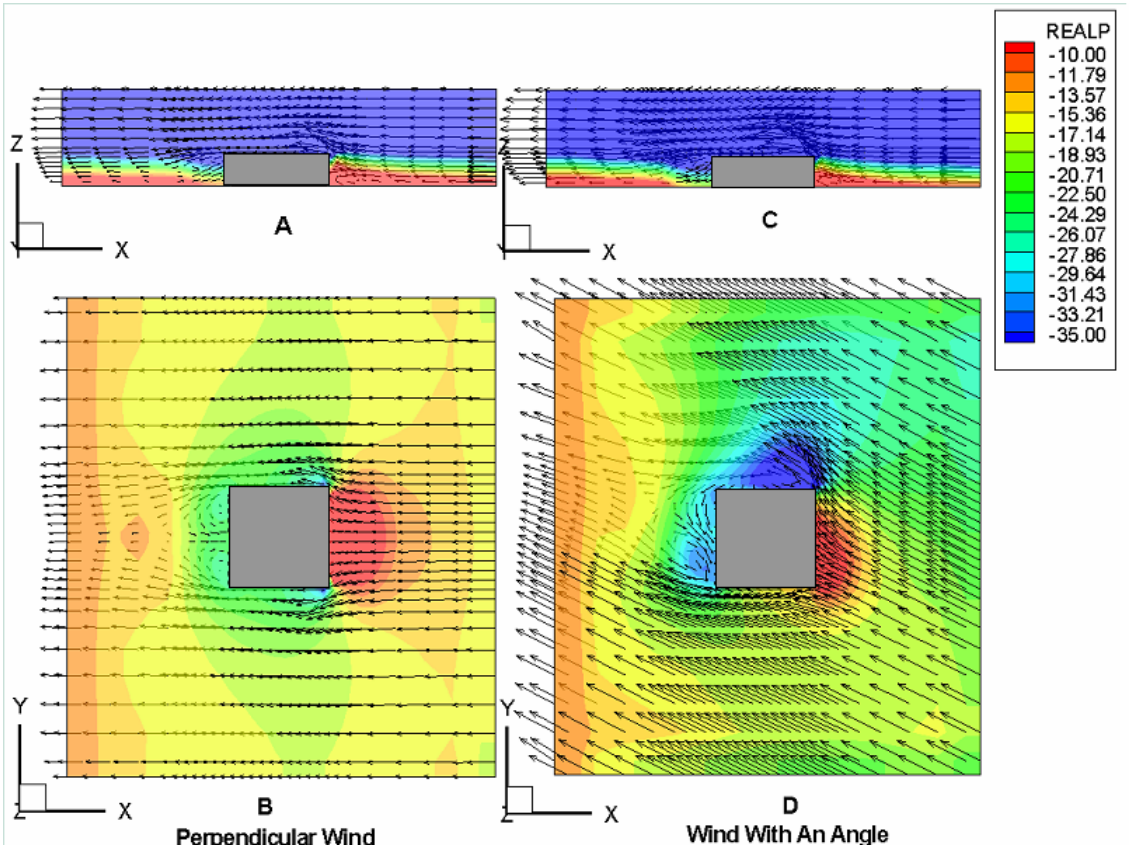

Fig. 5.2 Pressure contours (Pa) and velocity fields around a building, as computed by CFD0.

Fig. 5.2A and Fig. 5.2C show a strong recirculation behind the building, but CFD0-C fails to calculate the recirculation on the roof. This is a well-known problem for CFD programs using the Reynolds Averaged Navier-Stokes (RANS) equations and the turbulence models. Fig. 5.2B shows no recirculation on the sidewalls of the building. Please note that the wind for these two cases is specified as a constant distribution instead of a parabolic distribution, and thus the velocity at the 'sky' (the top of the CFD domain) becomes smaller. The contours of Fig. 5.2B also indicate that wind pressure on paths 2, 3, and 4 are smaller than that on path 1, so there is inflow through path 1 (as shown in Fig. 5.1A).

These three-dimensional pressures shown in Fig. 5.2 are saved in EWC files. The WPC translator is used to read the PLD file that provides flow-path locations, and then link to the EWC file. The WPC translator searches for the needed pressure data in the EWC files and then creates the WPC files.

Finally, CONTAM reads the WPC files for wind pressure data. Fig. 5.1 graphically shows the pressures and flow rates computed by CONTAM with the WPC file. Fig. 5.1A is for the case featuring the wind blowing perpendicularly at the wall, and Fig. 5.1B is for the case with the wind hitting the wall at an angle. The blue lines show the direction and scale of the airflow rate through the doors, and the red lines show the pressure drops. Since the wind pressure at door 1 is greater than the rest, and all the doors are located at the same height, the flow at door 1 is inwards. Table 5.1 shows the wind pressure computed by CFD0-C. Although wind speed is high (6 m/s), the airflow rate is small since all the doors are closed and this building is quite tight.

The case in which the wind hits the wall at an angle uses the same building geometry and opening locations as the case in which the wind is perpendicular to the wall. However, wind velocity is 6 m/s in the x component and 3 m/s in the y component. Table 5.1, Fig. 5.1, and Fig. 5.2 compare the results for this case with those of the previous one.

Without the WPC link, CONTAM would calculate the same airflow rates through the openings 2-4 due to the assumption of uniform wind pressures on a building surface. Nevertheless, this study shows that the wind direction dramatically changes the pressure distribution on the building envelope in Fig. 5.2D, even though the wind angle change is less than 30^{o}. These changes also alter the airflows inside the building. Table 5.1 shows that the calculated airflow rates of openings 2-4 by the WPC link are different from each other. It is more reasonable because Fig. 5.2 reveals that wind pressures should be non-uniform on a building surface. Therefore, wind pressure data is crucial for CONTAM simulations. The above two test cases demonstrate that the WPC translator was able to transfer the pressure distribution computed by CFD0-C for CONTAM use.

5.1.2. Demonstration of the Indirect Coupling by the Wind Pressure Profile (WPP) Link

Instead of calculating wind pressures as in the WPC link, the WPP link provides wind pressure coefficients for CONTAM so that CFD0-calculated airflow data can be reused if the wind velocity and/or building site change. To demonstrate the WPP link, this thesis selected another case to investigate the distributions of wind pressures and air infiltrations under different wind directions for a common low-rise house.

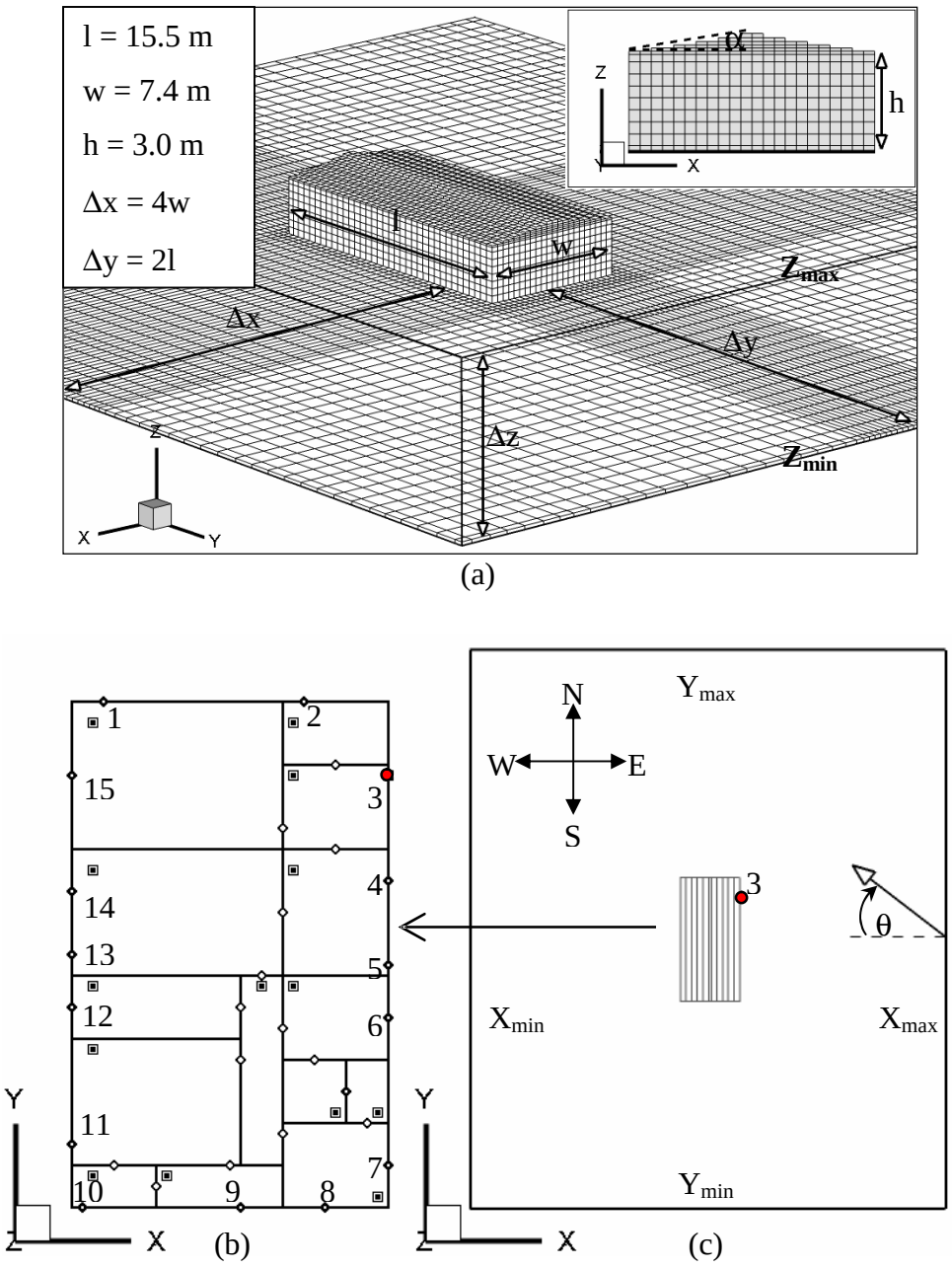

Fig. 5.3 (a) CFD0-C mesh, (b) the internal zone configuration of the low-rise house with a sloping roof, and (c) plane view of the CFD0-C domain.

Holmes (1986; 1994) measured wind pressure distribution on a low-rise house model for various wind directions in an open circuit, boundary-layer wind tunnel. Fig. 5.3(a) shows the house model after being scaled up to a full-sized house in CFD0-C simulation. To

simulate atmospheric conditions around the house appropriately, this study carefully selected the size of the whole CFD domain through test runs so that the impacts of the domain size on the airflow pattern and the total grid number were minimal. The size of the flow domain was 15.5 m $\times$ 7.4 m $\times$ 3.0 m (l $\times$ w $\times$ h) and the total grid number was 74 $\times$ 87 $\times$ 24 (X $\times$ Y $\times$ Z), as shown in Fig. 5.3(a). Slippery flow boundary conditions were applied for the Z_{min} and Z_{max} planes while a wind velocity profile was prescribed for "inflows" and a "free outflow" boundary condition for "outflows". Table 5.2 shows the boundary conditions for the four open planes, X_{min}, X_{max}, Y_{min}, and Y_{max}, when the wind direction is "θ" to the X_{max} plane, as shown in Fig. 5.3(c).

Table 5.2 Prescription of boundary conditions when the wind direction is "θ" from the X_{max} plane for airflows around a low-rise house.

Flow planes	Boundary conditions
X_{max} and Y_{min}	$U = -\bar{V}\cos\theta$; $V = \bar{V}\sin\theta$
X_{min} and Y_{max}	Free outflows

The wind velocity, $\bar{V}$, was defined by Eq. (5.1) and prescribed by a power-law profile in Fig. 5.4, which was for the urban and suburban area (ASHRAE, 2005), and is similar to that in the Holmes' experiment.

$$\bar{V} = \sqrt{U^2 + V^2 + W^2} \tag{5.1}$$

where $\bar{V}$ is the average wind velocity, U, V, and W is the wind veloicity in the X, Y, and Z direction, respectively.

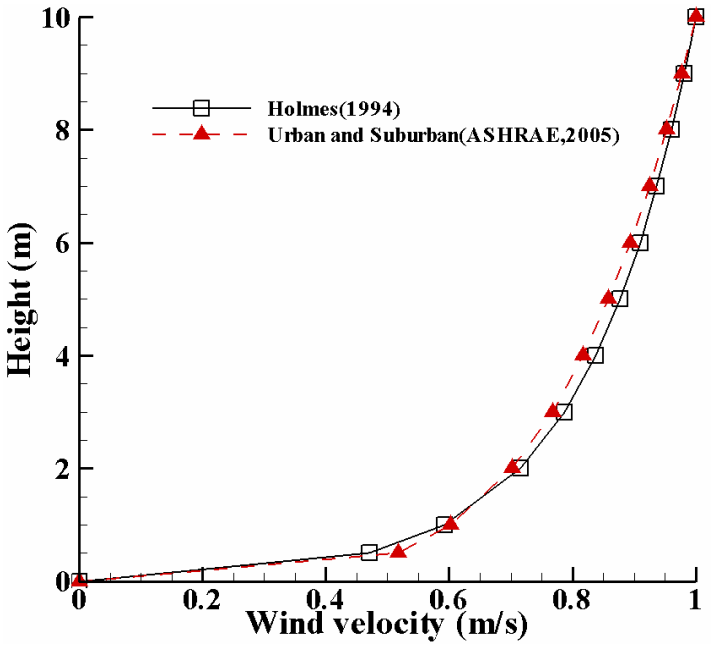

Fig. 5.4 The profile of mean wind velocity $\bar{V}$ for inflows.

The simulations were performed for the relative wind direction, θ, between 0° and 360° with a step of 30°. As illustrated in Fig. 5.3(b), the relative wind direction to a building surface is the clockwise angle from the building surface azimuth direction to the wind azimuth direction (Walton and Dols, 2003),

$$\theta = \theta_w - \theta_s \tag{5.2}$$

where, θ_w is the wind azimuth direction, e.g. N = 0° and E = 90° etc.; θ_s is the building surface azimuth direction.

Wind pressure coefficients at building surface change dramatically with wind directions. Fig. 5.5 shows that the surface-averaged wind pressure coefficient (Swami and Chandra, 1987) varies between "-0.6" and "0.6" depending on wind directions. The wind pressure coefficient also depends on the path location at the building surface. Fig. 5.5 illustrates the local wind pressure coefficient measured by Holmes (1986; 1994) and calculated

values by the WPP link at Path 3, as shown in Fig. 5.3. Apparently, the surface-averaged value cannot consider the dependence of wind pressure on the path location since the C_p values are symmetric around "θ=180°", which in fact could only happen for the middle point at a surface. If compared to the local wind pressure at Path 3, the average wind pressure also overestimated C_p between 0° and 90° while underestimating it from 270° to 360°.

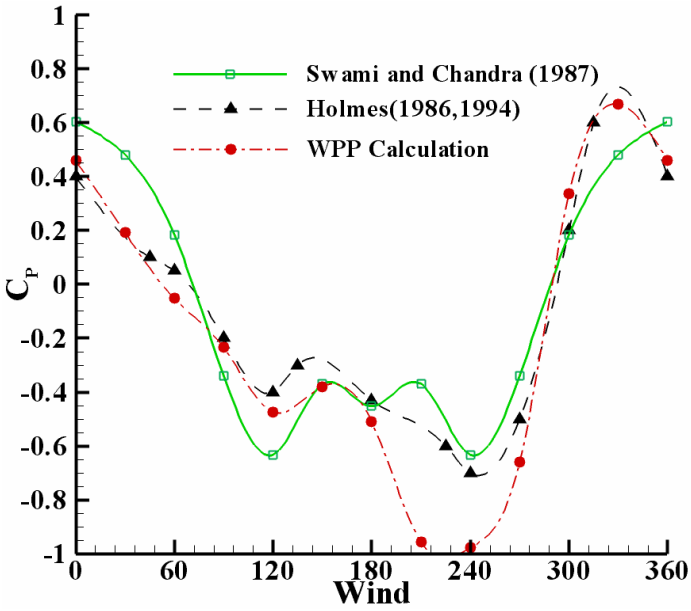

Fig. 5.5 Comparison of calculated wind pressure coefficient by the WPP link with measured data at Path 3 of the house for the relative wind direction to the surface with Path 3 (θ =0° ~ 360°).

The calculated C_p at Path 3 by the WPP Link generally agreed with the measured data except for the wind direction, from 180° to 270°. Due to the same reason as in the previous section, the discrepancy was caused by the inability of CFD0 to predict wind pressures correctly in the regions with strong turbulence separations and recirculation flows near Path 3. As a result, the WPP Link does not significantly improve the calculation of non-uniform distribution of wind pressure coefficients. The relative

discrepancy of the WPP-calculated C_p was only 40% while the surface-averaged value was 50% from the measured local value at Path 3.

Although the WPP link did not notably improve the calculation of wind pressure coefficients, it still considers the non-uniform distribution of wind pressures so that infiltrations can still be calculated more accurately than without it. To verify this effect, this study simulated the infiltrations through the low-rise house with fourteen zones and fifteen envelope paths, as shown in Fig. 5.3(b). The configuration of the zones was based on the manufacture house in Figure 14 of Chapter 34 in the ASHRAE Handbook (2005), except that the house was naturally ventilated. The leakages of airflow paths were adopted from Table 2 in the same chapter of ASHRAE Handbook.

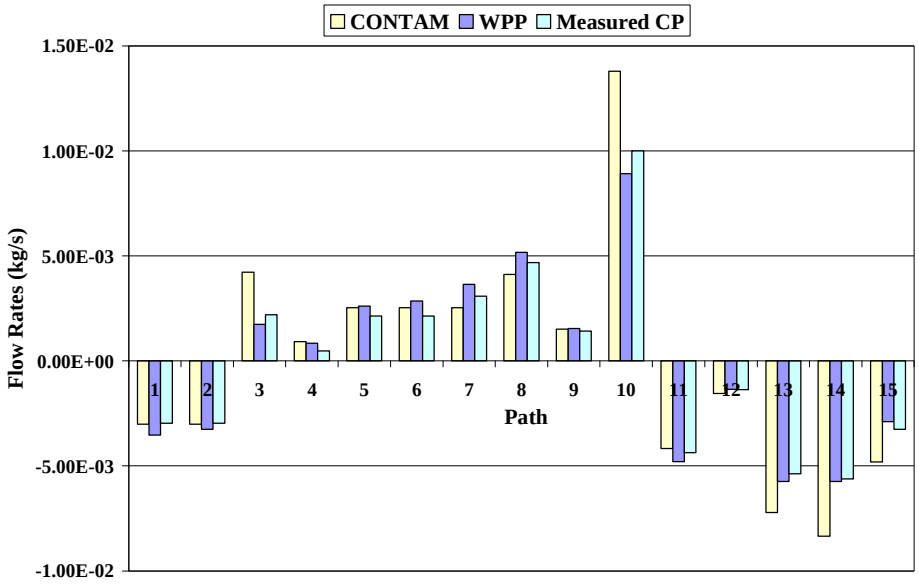

Fig. 5.6 Comparison of calculated infiltration rates by CONTAM, the WPP Link, and using measured non-uniform wind pressure coefficients when $\theta = 60°$.

Fig. 5.6 illustrates the calculated infiltration values, of which the inflows are positive while the outflows are of negative values, by using three different prescription methods of C_p for $\theta = 60°$:

- Method 1: CONTAM method, which uses the surface-averaged wind pressure coefficient as provided by Swami (1987);
- Method 2: WPP method, which uses the calculated local wind pressure coefficient by the WPP link;
- Method 3: Measured C_p method, which uses the measured local wind pressure coefficients from Holmes (1986; 1994).

Compared to the most accurate method, Method 3, the WPP link generally predicted better results than CONTAM. The average relative difference of calculated infiltrations is 17% for the WPP link and 30% for CONTAM, compared to those obtained by Method 3. For wind directions other than $\theta = 60°$, similar results were obtained. Therefore, the WPP link could improve CONTAM calculations by considering the non-uniform distribution of wind pressures.

5.2. Demonstration of the Direct Coupling for Indoor Airflow and Contaminant Transport Simulations

5.2.1. Simulation of Steady Airflow and Steady Contaminant Transport

To demonstrate the direct coupling for the simulation of steady airflow and steady contaminant transport, the first case uses a three-story building with a large atrium in the center and with natural ventilation. We use natural ventilation because the supply airflow rates in natural ventilation are not pre-defined, so it is more challenging to simulate such a case. Fig. 5.7 shows the three-dimensional views and the plan view of the building. The room dimensions are:

- Rooms 1-8: 12 m×6 m×2.7 m
- Rooms 9-12: 6 m×9 m×2.7 m
- Rooms 13-14: 6 m×5 m×2.7 m
- The atrium: 48 m ×11 m×10.8 m

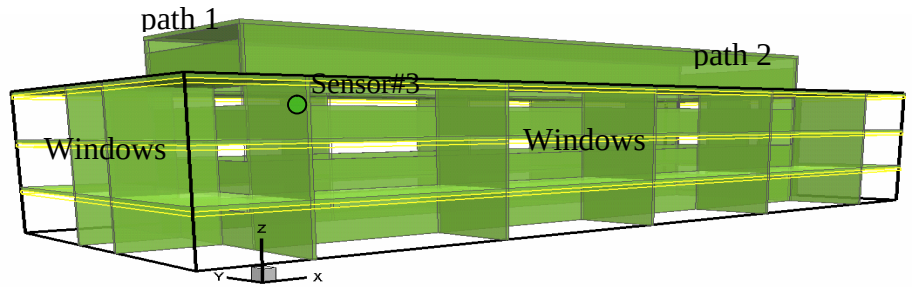

(a)

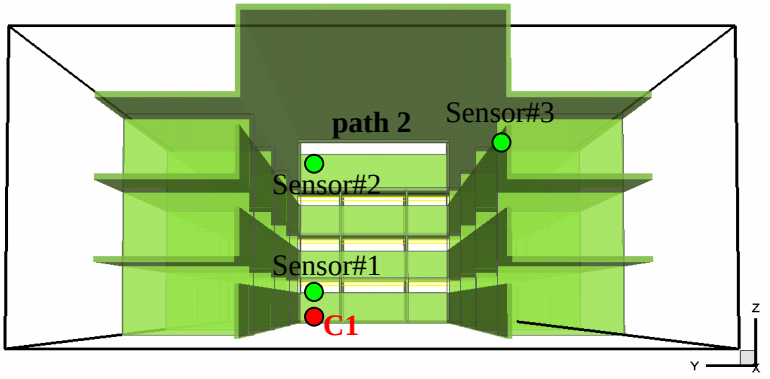

(b)

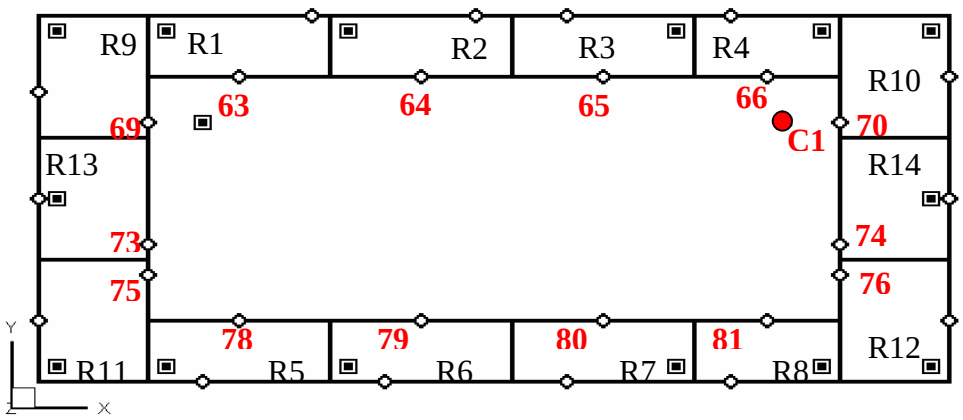

(c)

Fig. 5.7 Views of the three-story building. (a) Three-dimensional outside view with the external walls removed; (b) Three-dimensional internal view; and (c) Plan view in CONTAM with the contaminant of C1.

The floor plane is the same for the three stories, except for the atrium. All flow paths of the building are open windows with a height of 0.9 m and the width of the room. The west (-X) and the east (+X) windows on the top of the atrium are also open. The cooling load is set to 40 W/m^2 from the occupied zone (0 – 1.8 m above the floors) in the rooms and the atrium. The heat gain/loss from the building envelope is neglected.

The mean wind speed was assumed to be at a constant of 10 km/hour from the west, the mean outdoor air temperature to be 15 ^oC, and the mean relative humidity to be 70%.

This study also assumes that an imaginary contaminant (hereafter C1) is released in the northeast corner of the atrium on the ground floor, at a constant rate of 1.0×10^{-5} kg/s. Since the C1 concentration will be non-uniform for such a large space, the perfect mixing assumption would not work well so the case is selected as a demonstration case for the coupled CONTAM and the CFD0-C simulation. This study therefore selects the central atrium as the CFD zone and applies CONTAM to the rest of the zones.

The central atrium is divided into a total grid of 104×27×40 (X×Y×Z) for the CFD simulation. For the CONTAM simulation, the orifice equation (Walton and Dols 2003) is applied to the airflow paths of all the CONTAM zones. The temperatures of the CONTAM zones are determined by the iterative calculation of energy conservation for each zone.

The convergence criterion is 0.1% for CFD0 calculation and 1% for the coupled simulation. Twenty-five coupling iterations are required for convergence, and the total computing time is about 72 minutes on a Pentium 4 2.0 GHz PC.

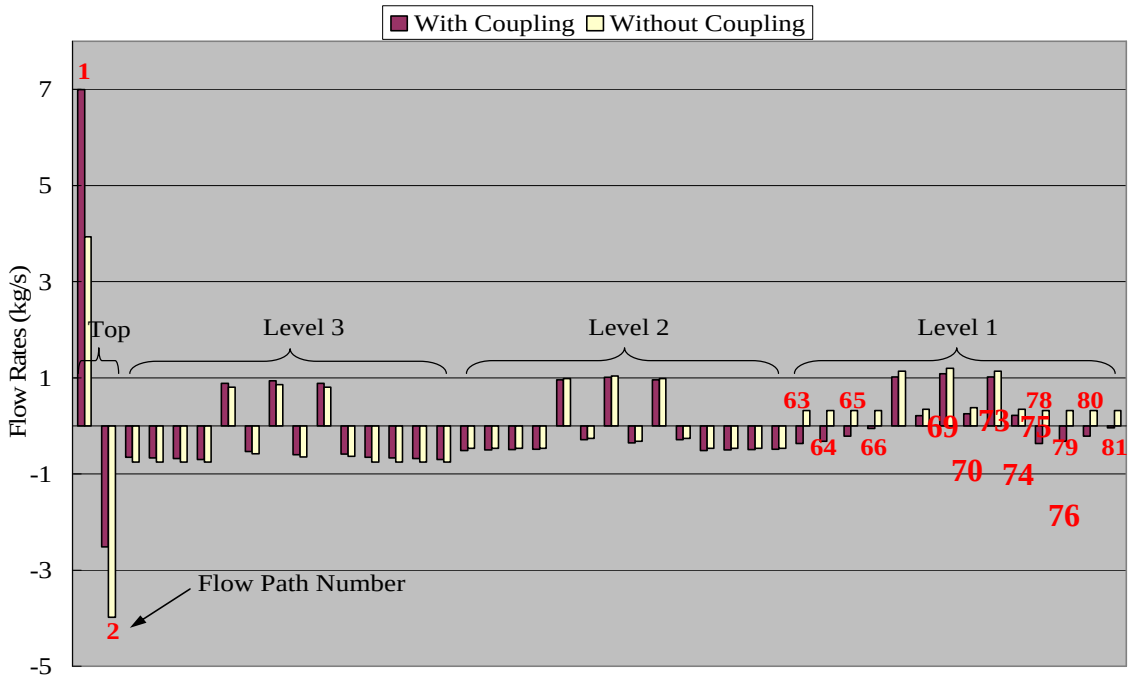

Fig. 5.8 Comparison of airflow rates with and without coupling.

Fig. 5.8 compares the airflow rates with CONTAM only and with the coupled program for the 44 airflow paths (each floor had 14 paths and there were two paths at the top) of the three-story atrium. Except for the paths at Levels 2 and 3, the flow rates of some paths at Level 1 and the two paths at the atrium top (red numbers in Fig. 5.8) had changed significantly with the coupled program. If a positive value was for the inflow to the atrium and a negative one for the outflow, the inflow through path 1 (Fig. 5.7(a)) increases from 4.1 kg/s without coupling to 7.0 kg/s with coupling. The flow directions through Paths 63 through 66 and 78 through 81 change from inflow to outflow if simulated by the coupled program.

Such changes of airflows with coupling could be explained by the temperature and pressure gradients inside the atrium. Fig. 5.9 illustrates the airflow and temperature distributions at section Y=5.5m in the atrium (CONTAM zones are also shown for comparison). Due to the buoyancy effect, the west wind with the temperature of 15 ^{o}C travels downwards after entering the atrium through path 1. The cold air then flows along

the atrium floor and rises at the right end of the atrium so that a huge recirculation zone is formed. The temperature gradients are about 4 K in the horizontal direction and 3 K in the vertical direction. So the assumption of uniform temperature may not hold in this case and the flow rates through paths 1 and 2 change with the coupling.

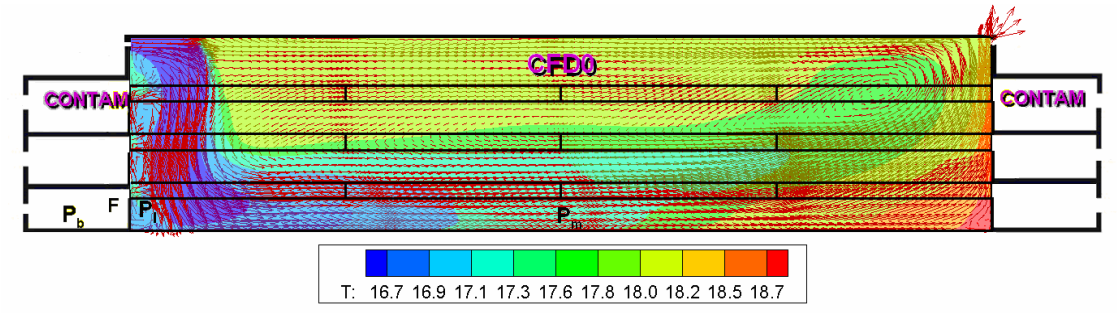

Fig. 5.9 Velocity fields and temperature contour at the section of Y=5.5m.

The changes in airflow distribution with coupling, especially the change of flow directions, will greatly affect the contaminant transport. Fig. 5.10 illustrates the results of C1 concentrations with coupling at the four planes of the atrium. The positions of the planes are shown in Fig. 5.11. Without coupling, all the neighboring zones of the atrium in Fig. 5.10(a) have zero C1 concentrations because the atrium only has inflows from all the neighboring zones. With coupling, the flows at Paths 63 through 66 and 78 through 81 become outflows for the atrium, so the C1 concentrations were non-zero for the neighboring zone 1 through 8. The closer the neighboring zone is to the source, the higher the C1 concentration of the neighboring zone.

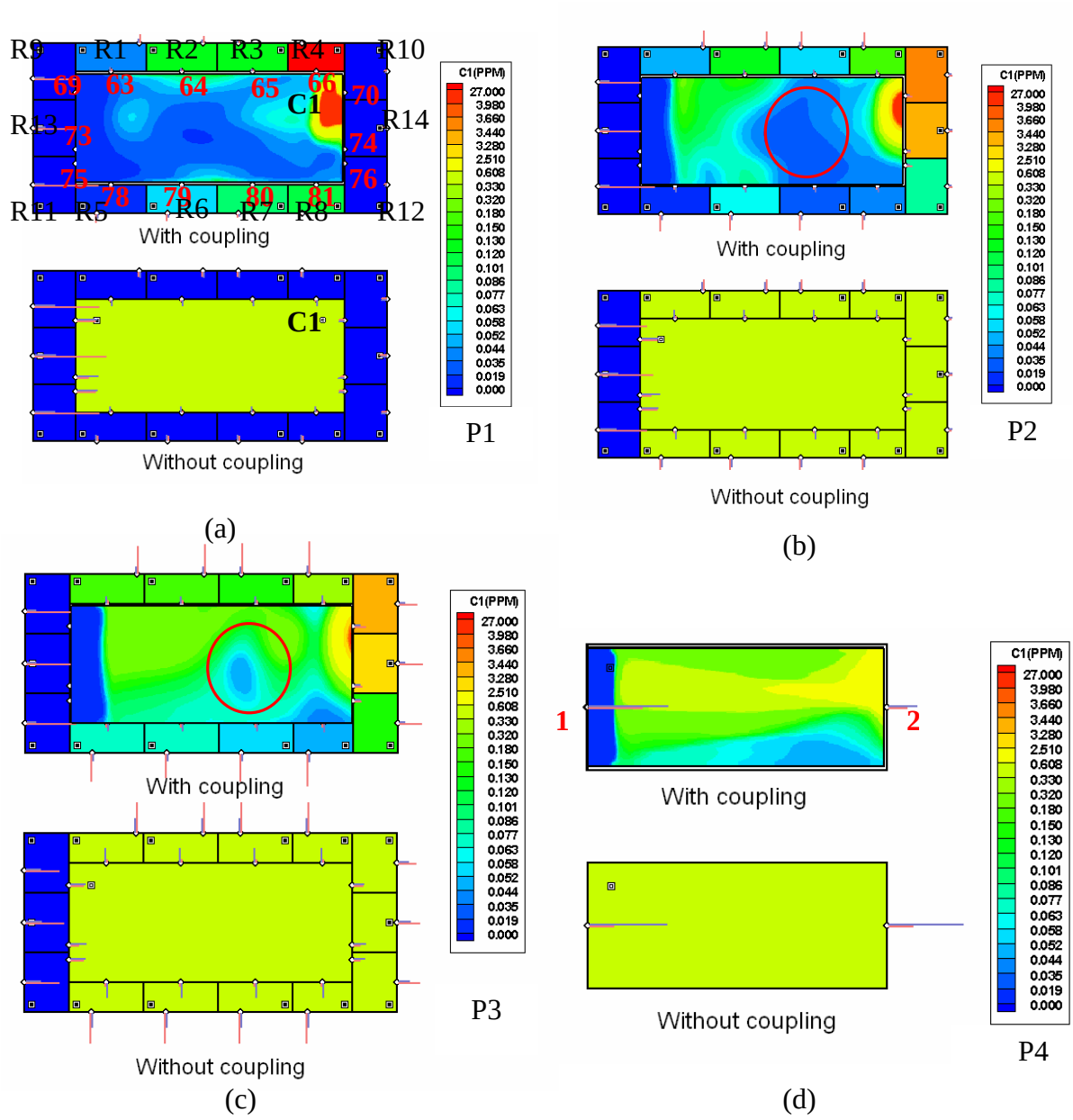

Fig. 5.10 Comparison of C1 concentrations with and without coupling at (a) Plane 1 (P1); (b) Plane 2 (P2); (C) Plane 3 (P3); and (d) Plane 4 (P4).

Besides airflow directions, airflow patterns also play an important role for contaminant transport. Although the directions of airflows in Fig. 5.10(b) and Fig. 5.10(c) do not change with coupling, the airflow pattern inside the atrium makes the C1 concentration highly poor-mixed. The coupled simulation is thus required to calculate C1

concentrations more accurately than CONTAM alone. The airflow pattern can also cause a discontinuous distribution of concentrations inside the atrium. The C1 concentration marked by the red circle in Fig. 5.10(c) is lower than the surroundings, which could be explained by the airflow pattern in Fig. 5.11. At the circled region in Fig. 5.10(c), the fresh air moves upwards so the concentration inside this region at P3 is lower than the surroundings. The same reason can be applied to the circled region in Fig. 5.10(b). The impact of airflow patterns on the distribution of C1 concentration can further be observed for the P4 plane in Fig. 5.10(d). The fresh air moves downwards after entering the atrium for about five meters and the air flows leftward at the right side of the atrium top (Fig. 5.9). Therefore, the C1 concentration at the right of the atrium top is higher than that at the left.

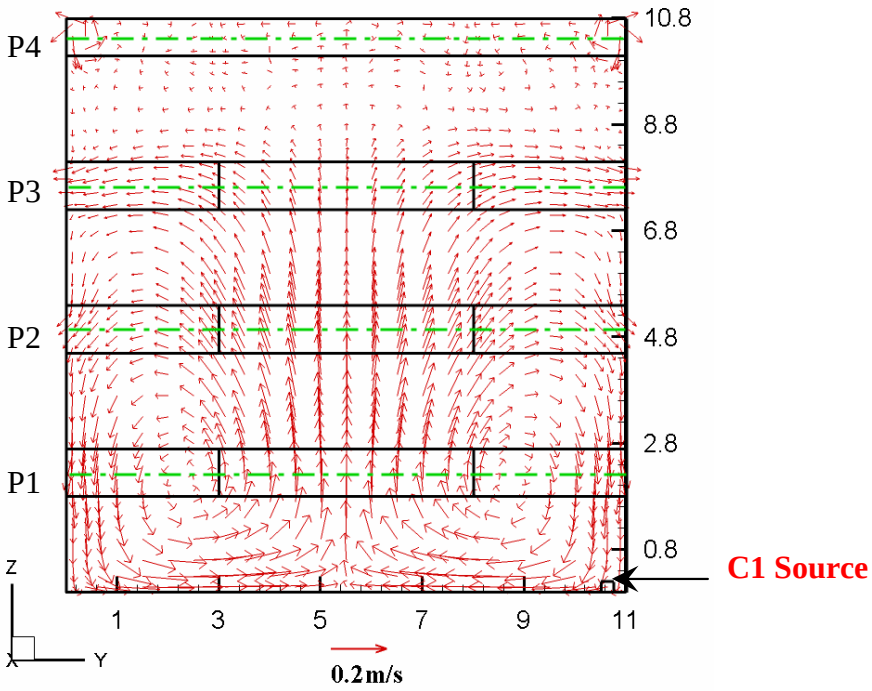

Fig. 5.11 Velocity distribution at the cross section of X=30m.

The above analysis illustrates that the coupled simulation of a steady airflow and the steady contaminant transport can provide distributions of temperature, pressure,

contaminant concentration and airflow patterns for the CFD zones. As a result, the well-mixing assumption of CONTAM is remedied and the dispersion of airborne contaminants in a building can be well predicted.

5.2.2. Simulation of Steady Airflow and Transient Contaminant Transport

For the steady airflow and the transient transport of contaminants, multizone models assume that the contaminant transport along each flow path is instantaneous. This assumption becomes problematic when the transport of the contaminants from the source zone to the neighboring zones is not instant. For example, in the naturally ventilated three-story building of Fig. 5.7, the atrium is so large that the transport time from the C1 source to the neighboring zones can be long. To calculate the transport time, the CFD simulation should be applied to the atrium. This study simulates the contaminant transport for 30 minutes with a time step of ten seconds, which is small enough to account for the transport time of C1 within the atrium.

Fig. 5.12 compares the C1 concentrations with and without coupling for selected zones on the first floor. Without coupling, the neighboring zones on the first floor, zone 1 through 8 in Fig. 5.12(a) (except zone 4, which is shown in Fig. 5.12(b) for a better comparison) has zero concentration all the time since the atrium only has inflows from the neighboring zones. With coupling, the C1 concentrations of zone 1 through 8 become non-zero due to the reversed airflow directions of Paths 63 through 66, and 78 through 81, as shown in Fig. 5.8.

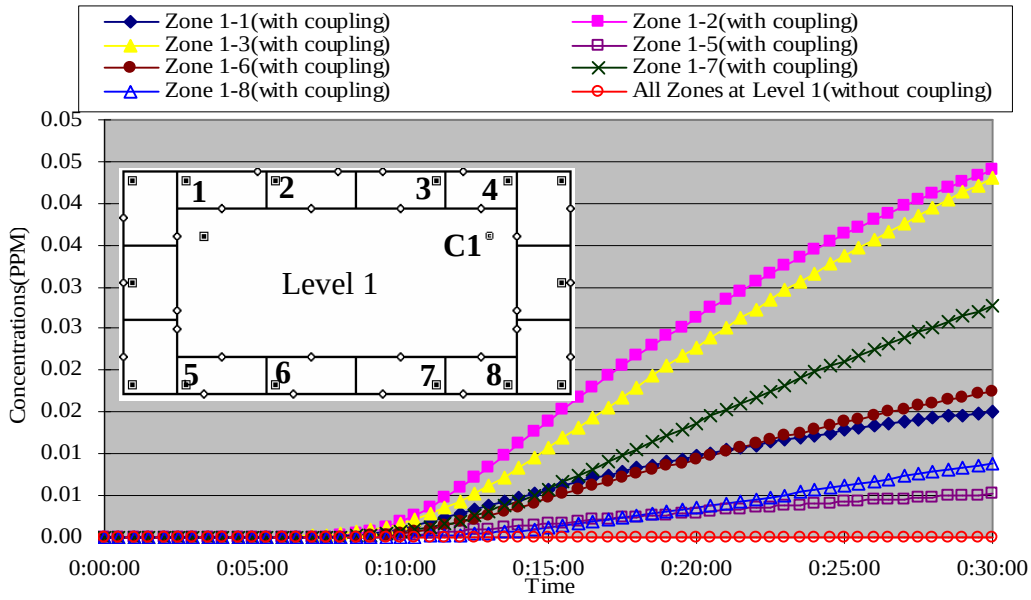

(a)

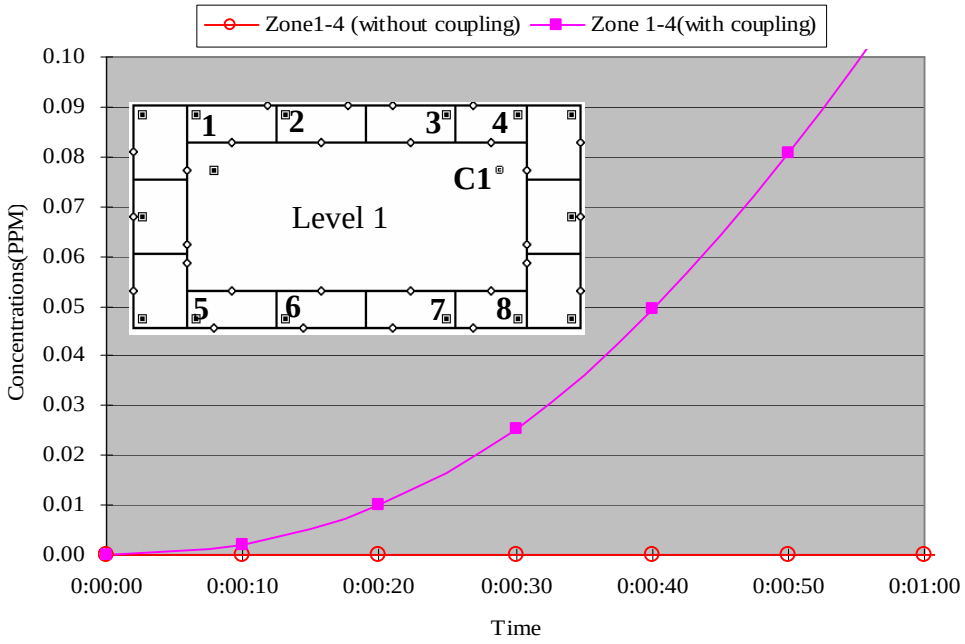

(b)

Fig. 5.12 Comparison of transient C1 concentration with and without coupling for (a) zones 1 through 8 except 4 at Level 1; (b) zone 4 at Level 1.

Fig. 5.12(a) shows that the transport time from the C1 source to most of the neighboring zones at Level 1 was rather long. For example, it takes ten minutes for zone 2 and twenty-five minutes for zone 5 to reach the C1 concentration of 0.01 ppm. On the other hand, Fig. 5.12(b) shows that it only takes twenty seconds for zone 4 to reach 0.01 ppm.

Only selected zones at level 1 are discussed and similar analyses could be applied to the simulation results of Levels 2 and 3. When the assumption related to the instantaneous transport of contaminants along each flow path fails, the coupled simulation of CONTAM and CFD0 could predict the transport time from the source zone to the neighboring zones. Then the transient dispersion of a contaminant in a building could be calculated.

5.2.3. Simulation of Transient Airflow and Transient Contaminant Transport

In real cases, both airflow and contaminant transport can be at transient state, for example, when mechanical emergency ventilation is turned on during building evacuation. The coupled CONTAM-CFD0 program can model this type of transient events and provide important information required for the placement of contaminant sensors and the strategy of occupant evacuations. This study used the same building as the previous sections with the addition of systems of emergency ventilation and control networks to demonstrate the coupled program in the simulation of an emergency ventilation.

As shown in Fig. 5.13, the emergency ventilation system was modeled in CONTAM as a Simple Air Handling System, which included a supply vent for each room and eight ceiling exhaust fans (EF) for the atrium. During emergencies, fresh air will be supplied from the room vent for pollution dilution and room pressurization. At the same time, the ceiling fans will exhaust polluted air from the atrium to create a “Pull-Push” effect. The emergency ventilation system was controlled by the building control network, which was comprised of a contaminant sensor in the atrium, a control link, a control node, and a control actuator. When the contaminant concentration at the sensor reached the set value,

C_{set}, the sensor transferred an "ON" signal through control links to control nodes, which directed the actuators to turn on the room vents and ceiling fans. The emergency ventilation system continues running till all occupants evacuate the building.

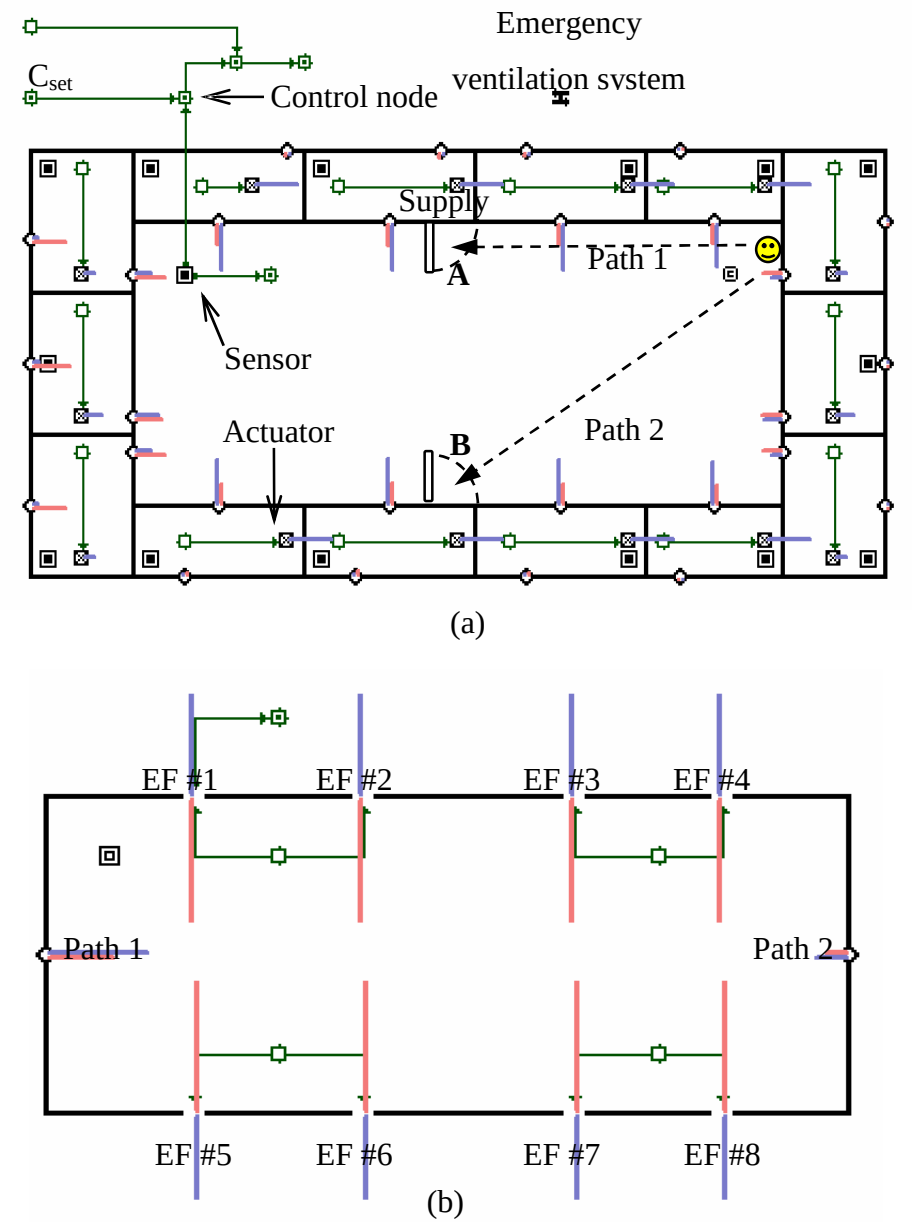

Fig. 5.13 Emergency ventilation, control systems, and airflow distribution when the emergency ventilation is on at (a) the first floor and (b) the top of the 3-story building.

The operating conditions of the emergency ventilation are

- C_{set} = 0.1 ppm;
- Designed airflow rate of room supply is 15 ACH;
- Designed airflow rate of the atrium is 22 ACH.

Three independent coupled simulations with different contaminant sensor locations as shown in Fig. 5.7 were studied. The best scenario was the location of Sensor #1, which was placed near the contaminant source and the worst case is Sensor #3 at the third floor, close to Path 1. The medium scenario was the location of Sensor #2 at the third floor close to Path 2. The transient simulations included a total time of ten minutes with a time step of one second.

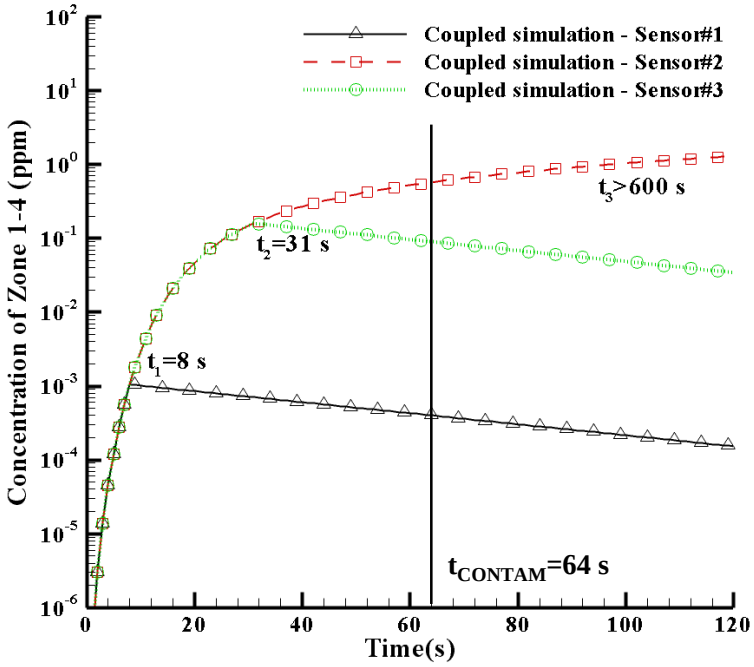

Fig. 5.14 Concentration history of zone 1-4 for three sensor locations before and after the emergency ventilation system is on.

Fig. 5.14 illustrates the history of C1 concentration of Zone 1-4, which is the zone closet to the C1 source, for the three sensor locations. Without coupling, CONTAM predicted the sensor will respond at 64 s after the C1 release no matter where the sensors were placed. The coupled simulation provided more reasonable results than CONTAM. Before the set point was reached, the C1 concentrations of Zone 1-4 were the same for all sensor locations. At 8 s, Sensor #1 is the first to respond so that the C1 concentration started to drop in Zone 1-4. In comparison, it took 31 s for Sensor #2 and more than 10 minutes for Sensor #3 to take action. Since CONTAM calculated the concentration of Zone 1-4 to be zero, as shown in previous sections, it was not shown in Fig. 5.14. Note that the C1 concentration dropped linearly due to the logarithm scale of Y-axis.

Once the sensor responded, the control nodes activated the ceiling exhaust fans to pull the polluted air out of the atrium and the room supply vents to pressurize the rest zones. As shown in Fig. 5.13, fresh air would flow into the atrium through all airflow paths except the exhaust fans so that the ceiling fans exhausted the contaminant from the atrium. Fig. 5.15 shows the importance of the ceiling fans by comparing the distribution of C1 concentration with and without their running. When the sensor was placed at Sensor #3, the ceiling fans were not activated even at the end of 10 mins. Fig. 5.15(a) shows that the contaminant could disperse farther into the atrium from the source, endangering the occupants' safety. However, if the sensor was at the location of Sensor #1, the ceiling fans would be turned on at 8 s after the C1 release. Fig. 5.15(b) illustrates that the C1 concentration at the plane of Y=10.5 m for Sensor #1 was far less than that for Sensor #3 at the end of 10 mins. Thus, the “Push-Pull” effect of the emergency ventilation would effectively remove the contaminant from the atrium when the sensor was placed at Sensor #1.

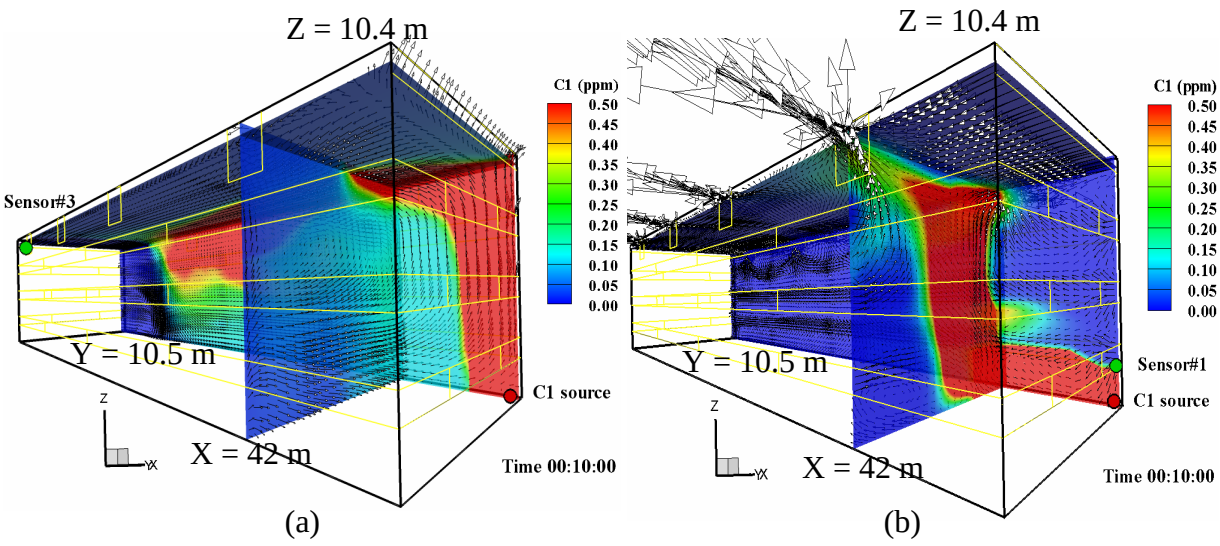

Fig. 5.15 Airflow and C1 concentrations at 10 minutes after the release of C1 for the sensor locations of (a) Sensor #3 and (b) Sensor #1.

Besides the capability to evaluate the performance of the emergency ventilation system, the coupled simulation can also help to determine the occupants' evacuation strategies. Supposing that an occupant would evacuate the building through Door A by Path 1 or Door B by Path 2 at the first floor as shown in Fig. 5.13(a), his best survival scenario is that he starts to run at the time of zero when the sensor was at Sensor #1. Intuitionally, he should choose Door A since Path 1 is shorter than Path 2. In fact, Fig. 5.16 shows that the occupant will have more transient exposure if he follows Path 1 rather than Path 2, especially from 10 sec to 16 sec. Moreover, the accumulated exposure to the contaminant for Path 1 could be about twice higher than for Path 2, which indicates that the evacuation through Door B was the better choice. Although the determination of evacuation strategies in real cases could be more complicated than this example, this study shows that the coupled CONTAM-CFD0 simulation has the potential for the analyses of personal exposures and evacuation strategies.

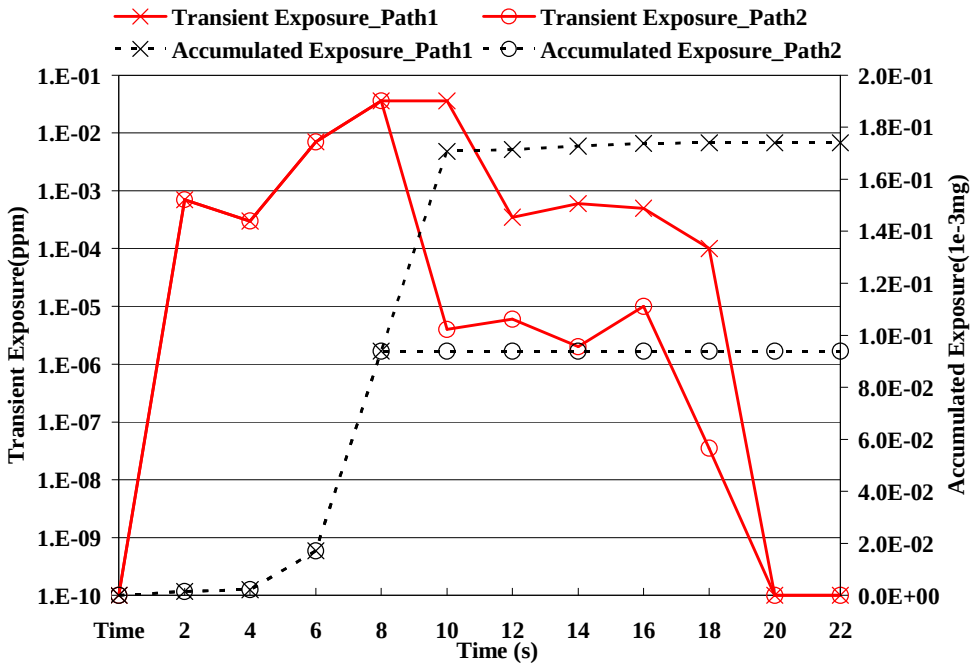

Fig. 5.16 Personal exposures to the C1 concentration and to the incremental C1 magnitude when occupants evacuate through paths 1 and 2.

5.3. Summary

This chapter applies the indirect and the direct coupling of CONTAM and CFD0-C to realistic cases. With the WPC link or the WPP link, the indirect coupling is able to provide a spatial distribution of wind pressures or wind pressure coefficients on a building surface so that the CONTAM obtains more realistic wind data. The direct coupling demonstrates the three coupling algorithms for indoor airflow and contaminant transport simulations. The algorithms are capable of improving CONTAM simulations by predicting non-uniform distributions of momentum, temperature, and contaminant concentration for real designs and analyses. The application studies also present more proof for the uniqueness of the solution. The coupled simulation will have a unique solution at each time step of a transient airflow simulation as long as the simulation is convergent and stable.

CHAPTER 6. CFD ZONE SELECTIONS FOR COUPLED CONTAM-CFD0 SIMULATIONS

A coupled CONTAM-CFD0 simulation applies CFD0-C to the zones, where multizone assumptions fail, and CONTAM to the rest of the zones. In the previous chapters, we selected the CFD zones by either applying the "rule of thumb" or comparing CONTAM results with experimental or CFD0 data to find the problematic zones. When experimental and CFD results are unavailable, it is important to study the underlying principles of multizone assumptions and provide guidelines for the zone selection. By applying non-dimensional analyses among the cases from the previous chapters, this chapter provides suggestions of CFD zone selection for coupled simulations of non-uniform distributions of air momentum, contaminant concentration, and temperature. A selection procedure is also developed for users to use these suggestions.

6.1. CFD Zone Selection for Non-Uniform Momentum Distributions

Multizone models assume quiescent air inside a zone, which could become problematic for zones with strong momentum effect and significant indoor air movement. If the momentum effect cannot be totally dissipated, the airflow distribution downwind can be greatly affected. We have shown this problem in the case of 90-degree planar branch in Chapter 2.1.3, the momentum-driven flows in Chapter 0, and the 4-zone chamber with the strong momentum effect in Chapter 4.2.2. The dissipation of airflow momentum effects depends on many parameters such as airflow pattern, inflow and outflow locations, inflow velocity, the size of the opening and zone, etc.

The dissipation of the momentum effect first depends on the airflow pattern/type. Graça (2002) divided the airflow with strong momentum effects into three types, based on the ratio of inflow opening area to the cross-sectional area of room, $C=A_r/A_{in}$.

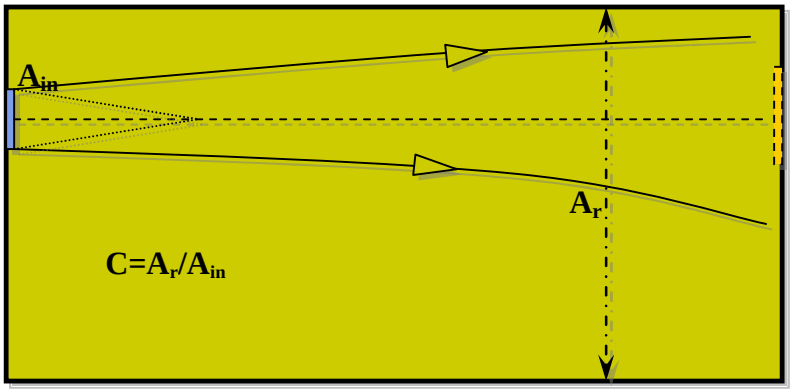

Fig. 6.1 Illustration of airflow patterns/types into a room.

As shown in Fig. 6.1,

$$C = \begin{cases} : \ 1.0 & \text{channel flow} \\ ? \ \ 1.0 & \text{recirculation flow} \\ : \ 2.0 & \text{combination of channel and recirculation flow} \end{cases} \Big\} \text{jet flow}$$

This study combined the second and the third flow types since the flow becomes a jet flow when C is more than a unit. Different guidelines of CFD zone selection for channel and jet flows have been developed, as discussed next.

6.1.1. CFD Zone Selection for Channel Flow with Strong Momentum Effect

A channel flow occurs when the inflow opening area is close to the cross-sectional area of the room so that air will attach to the walls, as shown by the case of a 90-degree planar branch in Chapter 2.1.3. More examples can be found in a cross-ventilation flow through a long corridor or a vertical shaft with a strong chimney effect. The wall attachment of the channel flow causes easy penetration of inflow momentum into the zone and thus the

assumption of quiescent air is invalid. The stronger the inflow momentum effect, the harder the inflow momentum gets dissipated. This study used the Reynolds number of the inflow to characterize the strength of the momentum effect.

$$\mathrm{Re} = \frac{VW}{\upsilon} \tag{6.1}$$

where V is inflow velocity, W is channel width, and υ is air kinematic viscosity.

For the channel flow in a 90-degree planar branch of Chapter 2.1.3, Fig. 6.2 shows the errors caused by neglecting the inflow momentum effects, compared to CFD results from Hayes (1989), Kelka (2000), and Zhai (2004). As expected, a higher Reynolds number caused greater errors, which was more than 20% if Re was greater than 30. Since an error of 20% is normally acceptable for most multizone simulations (Emmerich, 2001), CFD0 is needed for channel flows when

$$\mathrm{Re} > 30 \tag{6.2}$$

If the order of channel width, W, is "1 m", the resultant inflow velocity will be in the order of 10^{-4} m/s for the Reynolds number of 30. Therefore, this conclusion indicates that CFD may be considered for most channel flows.

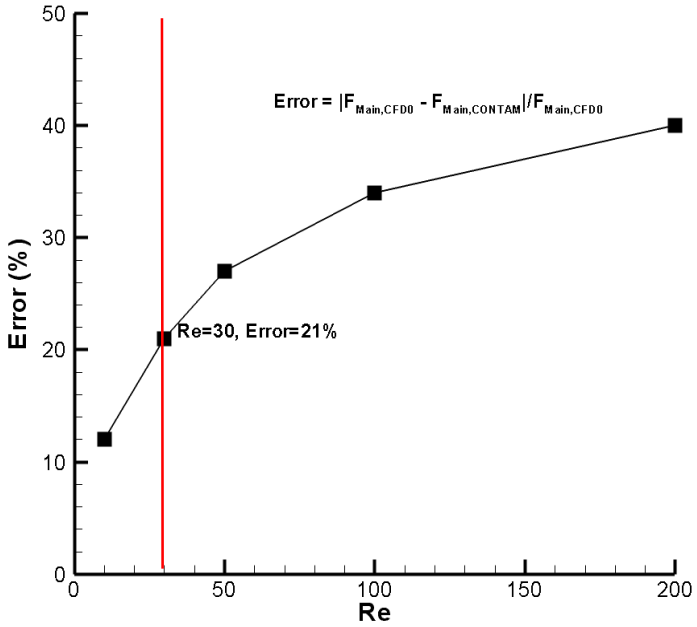

Fig. 6.2 The errors caused by neglecting airflow momentum effects under different Reynolds numbers for channel flows.

6.1.2. CFD Zone Selection for Jet Flow with Strong Momentum Effect

Jet flow occurs more often than channel flow given that the inflow opening area is often less than that of the cross-sectional area of a room. Comprised by a jet expansion area and a recirculation area, as shown in Fig. 6.3, a jet flow is also more complicated than a channel flow. The jet expansion area can be further divided into four zones (ASHRAE, 2005), depending on how much the jet is dissipated.

- Zone 1: initial zone, where the maximum velocity and temperature remain constant
- Zone 2: transition zone, where the initial jet flow is transforming into fully turbulent flow
- Zone 3: fully developed turbulent flow
- Zone 4: degradation/dissipation zone, where maximum air velocity and temperature drop rapidly and the jet is considered almost dissipated.

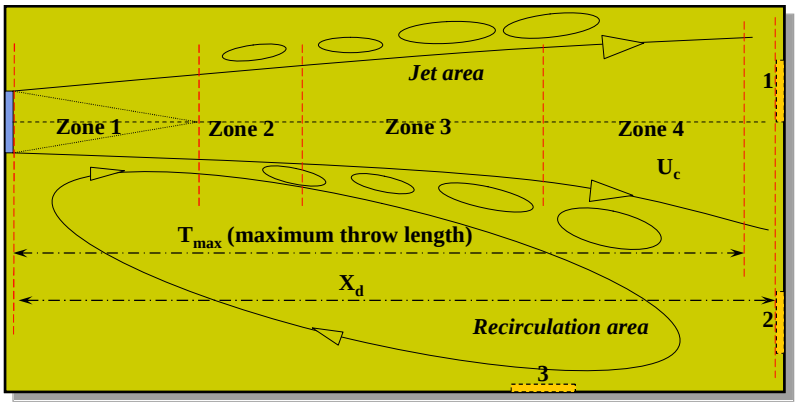

Fig. 6.3 Illustration of airflows inside a room for jet flows.

The 4-zone classification of a jet flow describes how the jet is expanded and dissipated inside a zone. The impact of jet momentum effect on airflow distribution downwind depends on the opening location about the four jet zones. If an opening is located outside the jet expansion zone, such as in openings 2 and 3 in Fig. 6.3, or in Zone 4, such as opening 1, the momentum effect of the jet will have minimal impact on the opening airflow. For the rest of the cases, an opening in Zone 1-3 will be subject to the momentum effect due to incomplete jet dissipation.

Therefore, this study suggests using the distance from the inflow opening to Zone 4, i.e. the maximum jet throw length, to estimate jet dissipation, which was defined by ASHRAE (2005) as

$$T_{max} = 1.13\frac{KQ}{U_c\sqrt{C_d R_{fa} A_c}} \tag{6.3}$$

where T_{max} is the maximum throw length of the jet with the unit of m; K is proportionality constant, which is determined by the opening type and inflow velocity in Table 2, Chapter 33 of ASHRAE Handbook (2005); Q is the volumetric inflow rate, m^3/s; U_c is the characteristic velocity in Zone 4, which is suggested to be 0.25 m/s; C_d is the discharge coefficient of the inflow opening, which is usually between 0.65 and 0.90; R_{fa}

is the ratio of free area to gross area of the inflow opening; A_c is the gross area of the inflow opening, m^2.

As illustrated in Fig. 6.3, CFD is needed when an opening is inside the zone with incomplete jet dissipation.

$$X_d < T_{max} \tag{6.4}$$

where, X_d is the distance from the inflow opening to the opening downwind in the jet direction. Otherwise, the jet flow is considered dissipated so that it can be appropriate to neglect the momentum effect.

Three cases with non-uniform momentum distributions in Chapter 0 were used to verify Inequality (6.4):

- Case 1: pressure gradient flows in an office suite in Fig. 3.8,
- Case 2: cross ventilation in a four-zone building model in Fig. 3.12 and
- Case 3: jet flows in a four-zone chamber in Fig. 4.16.

Table 6.1 Verification of the suggestion for the CFD zone selection for jet flows by Case 1: pressure gradient flows in an office suite and Case 2: cross ventilation in a four-zone building model in Chapter 3.

Cases	T_{max} (m)	X_d (m)	CFD required?
Case 1: an office suite	15.1	10.0	Yes
Case 2: four-zone building model	45.2	2.8	Yes

As shown in Table 6.1, the maximum throw length was 15.1 m for Case 1 and 45.2 m for Case 2. The distance from door 1 to door 2 in Fig. 3.8 and that from door A to door C in Fig. 3.12 was 10.0 m and 2.8 m, respectively, both less than the maximum throw length of the jets. Therefore, the inflow momentum could not be dissipated before exiting the zones, and CFD was required for both cases.

Table 6.2 Verification of the suggestion for the CFD zone selection for jet flows by Case 3: the chamber experiment of non-uniform momentum distributions in Chapter 4.2.2.

Supply (m^3/s)	T_{max} (m)	X_d (m)	Flow ratio	Errors	CFD required?
0.0345	5.2	1.83	1.6	19%	Yes
0.0533	8.1	1.83	2.2	27%	Yes
0.1052	15.9	1.83	2.4	29%	Yes
0.1397	21.1	1.83	2.5	30%	Yes
0.2152	32.5	1.83	2.5	30%	Yes
0.0113	*1.75*	*1.83*	*1.07*	*3%*	*No*

Case 3 is the jet flow experiments in the 4-zone chamber in Chapter 4.2.2. The experiment tested different inflow momentum effects by changing the supply airflow rates from 0.0345 to 0.2152 m^3/s, for which CFD0 was required. We applied Inequality (6.4) to explain why the momentum effects could not be neglected for the supply rates from 0.0345 to 0.2152 m^3/s. Table 6.2 shows that the calculated maximum throw lengths for the supply of 0.0345 to 0.2152 m^3/s were all greater than the distance from the supply to opening 1 in Fig. 4.16 so that air exited zone 1 directly with incomplete dissipation. To provide more proof of Inequality (6.4), we simulated the same case with the supply flow of 0.0113 m^3/s, for which the calculated T_{max} value became less than $X_{d,}$ as shown by the italics in Table 6.2. In this case, the inflow momentum effect was considered dissipated and the error caused by neglecting the inflow momentum effect was only 3%. Therefore, CFD0 was not needed for the supply flow of 0.0113 m^3/s.

Note that these verifications used 0.25 m/s as the characteristic velocity for the jet degradation zone, as suggested by ASHRAE (2005). The characteristic velocity could be different if experimental results are available.

6.2. CFD Zone Selection for Non-uniform Contaminant Concentration Distributions

Multizone models assume that the contaminant is perfectly mixed in a zone, which is often not true. In fact, the mixing of contaminants in a zone is dependent on the locations of the contaminant source, air inflow and outflow, and the local airflow pattern, the air

velocity direction and magnitude, and the strength of turbulence effect. To find the relations of these parameters to contaminant mixing, previous studies tried to apply the mixing theory of mechanical turbines and agitation tanks to indoor contaminant transport. Baughman (1994) and Drescher (1995) successfully studied the mixing of an instantly released point source in a room with natural and forced convections, respectively. They found that the contaminant would be completely mixed after a certain amount of time, i.e. mixing time, in an unventilated space. Mora (2002) extended their studies to the potential mixing improvement by occupant activities, such as moving, breathing, and generating thermal plumes from the body. These findings implied that the CFD method should be used before the mixing time for an unventilated enclosure.

The mixing theory for unventilated rooms, however, could not be applied to spaces with inflows and outflows (or so-called mechanically ventilated space) (Thatcher et al., 2004). Finlayson (2004) and Thatcher (2004) conducted experiments and CFD simulations to study the mixing of a continuously released point source in a mechanically ventilated space. It was found that the contaminant concentration was hardly well-mixed for a mechanically ventilated space, especially ones that had physical obstructions (Gadgil et al., 2003) such as partitions or people, as illustrated in Fig. 6.4. Some exceptions do exist, such as when the contaminant is brought in only by inflow air, which apparently will cause a uniform distribution of the contaminant. Another exception could be that the contaminant source is also a heat source so that the buoyancy effect could be strong enough to improve contaminant mixing in the space. This thesis, therefore, tried to study the condition under which the buoyancy effect can play a significant role for contaminant mixing.

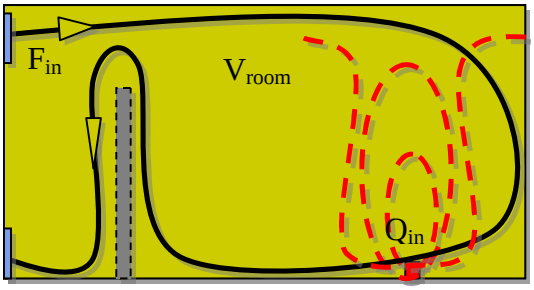

Fig. 6.4 Illustration of airflow and contaminant transport in a room with an internal partition.

For a mechanically ventilated space with an internal heat source, Fig. 6.4, the Archimedes number characterizes the relative strength of the buoyancy force to the inertial force (Incropera and DeWitt, 2007)

$$\mathrm{Ar} = \frac{\mathrm{Gr}}{\mathrm{Re}^{n}} \tag{6.5}$$

where Gr is the Grashof number, Re is the Reynolds number, and n is the exponent of Re, which is normally 2 (ASHRAE, 2005).

For building simulations, it was suggested to weight more on the exponent of Re than "n=2" in Eq. (6.5), which was considered to underestimate the inertial force (Zhang et al., 1993). Xue (1994) studied the airflow characteristics and the temperature stratification in a ventilated tunnel and suggested the exponent could be 2.5 (Xue and Shu, 1999). Reynolds (1986) found that the air motion inside a heated stairwell model could be better represented by a relation of $\mathrm{Gr} \propto \mathrm{Re}^{3}$. Combining these published results with the experimental data in this thesis, this study suggested that the exponent of 3 could be used in Eq. (6.5).

$$\mathrm{Ar} = \frac{\mathrm{Gr}}{\mathrm{Re}^{3}} \tag{6.6}$$

In Fig. 6.4,

$$\mathrm{Gr}=\frac{g b Q_{in} L^3}{r C_p F_{in} u^2} \tag{6.7}$$

and

$$\mathrm{Re}=\frac{F_{in}}{L u} \tag{6.8}$$

where g is the acceleration of gravity, b is the volumetric thermal expansion coefficient, and Q_{in} is the heat input, L is the characteristic length of the room, which is $V_{room}^{1/3}$ (Gadgil et al., 2003), V_{room} is the total volume of the room, r is the air density, C_p is the heat capacity at constant pressure, F_{in} is the volumetric airflow rate into the room, and u is the kinematic viscosity of the air.

An index of non-uniformity of contaminant was defined to evaluate the mixing level of contaminant. The greater the non-uniformity index is, the less uniform the contaminant will be.

$$m=\sqrt{\frac{\sum_{i=1}^{N}(C_i-\overline{C})^2 V_i}{\sum_{i=1}^{N} V_i}} \tag{6.9}$$

and

$$\overline{C}=\frac{\sum_{i=1}^{N} C_i V_i}{\sum_{i=1}^{N} V_i} \tag{6.10}$$

where m is the non-uniformity index, C_i is the contaminant concentration at sample cell/point i, $\overline{C}$ is the volumetric averaged contaminant concentration, V_i is the volume of sample cell i, and N is the total number of the sample cells.

Table 6.3 The parameters required to calculate dimensionless Ar number in order to judge when the CFD is required for the cases of a 4-zone chamber, a 3-story building, displacement ventilation in an office, and mechanical ventilation in a house.

Cases	Ar	Q_{in} (w)	F_{in} (m^3/s)	L (m)	CFD required?
Case 1: indoor airflow with contaminant concentration gradient (Schaelin et al., 1994) in Chapter 2.1.4	70	500	0.07	4.2	Yes
Case 2: displacement ventilation in an office (Srebric et al., 1999) in Chapter 4.1.3	24	173	0.05	3.5	Yes
Case 3: non-uniform contaminant concentration distribution in the 4-zone chamber in Chapter 4.2.3 (cases in italics are the results from numerical simulations)	0	0	0.1	2.22	Yes
	200	*400*	*0.018*	*2.22*	*Yes*
	400	*810*	*0.018*	*2.22*	*No*
	500	*1000*	*0.018*	*2.22*	*No*
Case 4: natural ventilation in the 3-story building with a large atrium in Chapter 5.2.1	0	0	13.6	17.7	Yes

In order to find the correlation of Ar ~ m, this study used the cases from the previous chapters, as shown in Table 6.3, which also illustrates the parameters used to calculate Ar. Note that three new simulations, indicated by italics, were conducted for the case of the 4-zone chamber.

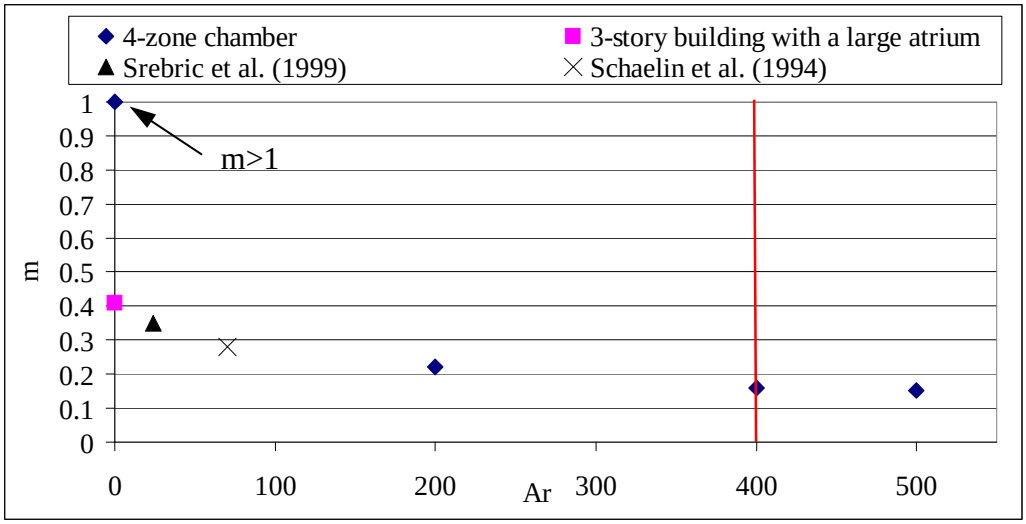

Fig. 6.5 The correlation of Ar ~ m for the cases of a 4-zone chamber, a 3-story building, displacement ventilation in an office, and mechanical ventilation in a house.

Fig. 6.5 shows the calculated Ar and m for the four cases. For the case of the 4-zone chamber, the non-uniformity index is more than the unit, and the contaminant concentration is highly non-uniform when Ar is zero. With the increase of the heat input, the buoyancy effect improved the contaminant mixing so that the value of m was less than 0.2 for Ar = 400.

Compared to the case of the 4-zone chamber, the case of the 3-story building had a smaller value of m, although the building is much bigger than the chamber. This could be explained by the fact that the inflow rate of the building was much higher than the chamber so that the turbulence mixing was dominant. The non-uniformity index of the other two cases fell between the previous two cases, with a value of m about 0.3 and an Ar less than 100.

The definition of the non-uniformity index in Eq. (6.9) is the RMS of the difference of local contaminant concentrations from the average value, which indicates the error caused by the assumption of uniform contaminant concentration. As already known, an error of 20% is normally considered acceptable for multizone simulations (Emmerich,

2001). This study therefore suggests that CONTAM results are acceptable and therefore the CFD0 is not needed when

$$Ar > 400 \tag{6.11}$$

When Ar is less than 400, especially when the Ar is zero, the buoyancy effect is not strong enough to improve contaminant mixing. As a result, the contaminant distribution can highly depend on the local airflow pattern, air velocity, internal partition, and the location of the contaminant source. The studies of Schaelin (1994), Yuan (2003), and Ren (2005) suggested that the CFD method should be used for the zone, which contains the contaminant source and where the contaminant concentration tends to be less uniform than the rest of the zones of a building.

6.3. CFD Zone Selection for Non-uniform Temperature Distributions

Multizone models assume uniform temperature distribution in a zone, which could cause errors when the temperature gradient is significant, as shown by the case of the buoyancy-driven airflows in a stairwell in Chapter 2.1.2. Evidence was also found that the assumption of uniform temperature could become acceptable for a moderate temperature gradient, as in the case of the non-uniform temperature distribution in the 4-zone chamber in Chapter 4.2.4. This chapter studied the conditions when the CFD method is needed, if the assumption of the uniform temperature fails.

For the room in Fig. 6.6, the magnitude of temperature gradient could be defined by

$$\frac{\Delta T}{T_{av}} = \frac{|T_t - T_b|}{T_{av}} \tag{6.12}$$

where ΔT is the temperature gradient, T_{av} is the average zone temperature, T_t is the temperature at the top of the zone, and T_b is the temperature at the bottom of the zone.

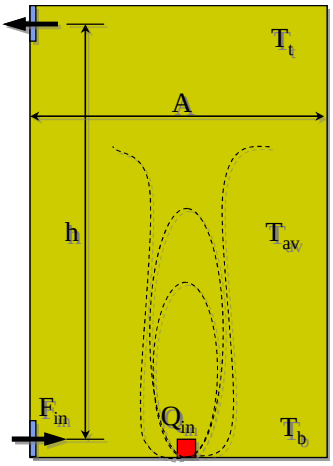

Fig. 6.6 Illustration of the non-uniform distribution of temperatures in a room.

A smaller value of $\Delta T/T_{av}$ indicates a better mixing of temperature in a zone; for example, it is zero for a perfectly mixed zone. Reynolds (1986) found that for buoyancy-driven airflows with internal temperature gradient, $\Delta T/T_{av}$ could be related to the Reynolds number and the Stanton number

$$\frac{\Delta T}{T_{av}} \propto t = \mathrm{Re}^{1/3}\,\mathrm{St}^{2/3} \tag{6.13}$$

where

$$\mathrm{Re} = \frac{F_{in}}{Lu} \tag{6.14}$$

$$\mathrm{St} = \frac{Q_{in}}{r C_p T_{av} A (gh)^{1/2}} \tag{6.15}$$

where t is the dimensionless temperature gradient, F_{in} is the volumetric inflow rate, L is the characteristic length of the room, which is $V_{room}^{1/3}$ (Gadgil et al., 2003), V_{room} is the total volume of the room, u is the kinematic viscosity of the air, Q_{in} is the total heat input, A

is the cross-sectional area of the room, and h is the height from the inflow opening to the outflow opening.

We then defined the error caused by neglecting the temperature gradient as

$$\text{Error} = \left| \frac{F_{CONTAM} - F_{exp}}{F_{exp}} \right| \tag{6.16}$$

where F_{CONTAM} is the volumetric airflow rate predicted by CONTAM and F_{exp} is the volumetric flow rate from the experiment.

Table 6.4 The parameters required to calculate dimensionless temperature in order to judge when CFD is required for the cases of a stairwell model, a 4-zone chamber, and a light well model.

Cases	τ	Q_{in} (w)	F_{in} ($\times 10^2$ m^3/s)	L (m)	A (m^2)	h (m)	T_{av} (K)	CFD required?
Case 1: buoyancy-driven airflows in a stairwell model (Zohrabian et al., 1990) from Chapter 2.1.2	0.015	100	0.24	1.43	0.46	1.22	299	No
	0.035	300	0.37	1.43	0.46	1.22	303	Yes
	0.061	600	0.52	1.43	0.46	1.22	311	Yes
	0.083	900	0.60	1.43	0.46	1.22	313	Yes
Case 2: non-uniform temperature distribution in the 4-zone chamber from Chapter 4.2.4	0.011	300	5.8	2.45	6.01	2.44	296	No
	0.017	600	5.8	2.45	6.01	2.44	298	No
	0.022	900	6.0	2.45	6.01	2.44	300	No
Case 3: natural ventilation through a light well model (Kotani et al., 2003)	0.035	10	0.035	0.2	0.021	0.48	299	Yes
	0.057	20	0.042	0.2	0.021	0.48	307	Yes
	0.077	30	0.048	0.2	0.021	0.48	313	Yes
	0.096	40	0.054	0.2	0.021	0.48	322	Yes

Intuitionally, it was expected that a higher dimensionless gradient leads to more error by CONTAM assumption. To verify this claim, this study tried to find a correlation of "Error ~ τ" from two cases from the previous chapters, as listed in Table 6.4. To have more data, we also used Case 3, an experimental study of natural ventilation through a light well by Kotani (2003).

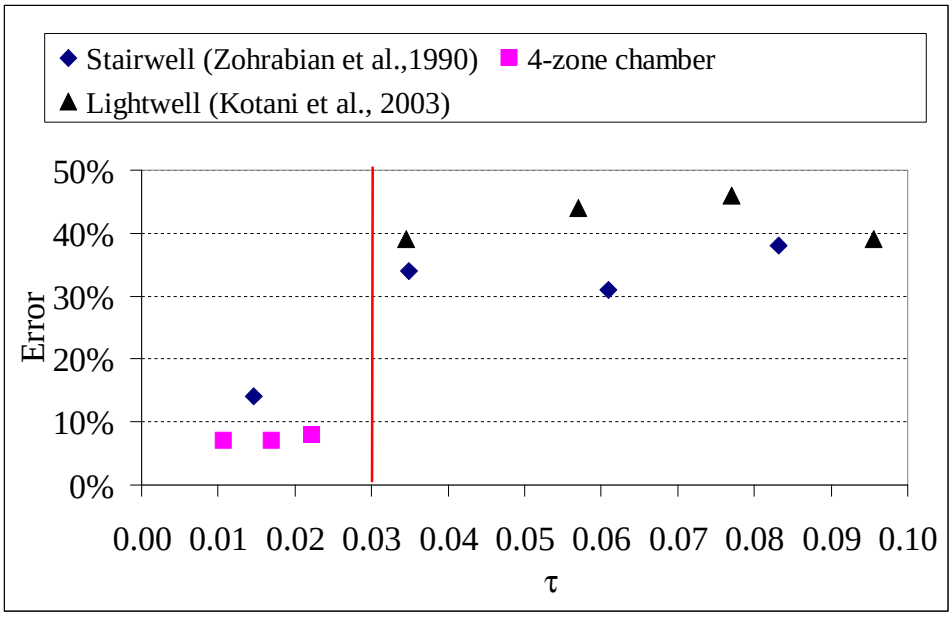

Fig. 6.7 The errors caused by the assumption of uniform temperature for dimensionless temperature gradient for the case of a stairwell model, a 4-zone chamber, and a light well mode.

Fig. 6.7 shows the correlation of "Error ~ τ" for the three cases. When t is less than 0.03, the error is less than 20%, which implies that the CONTAM results are acceptable. For the rest of the cases, the temperature gradient in a room cannot be neglected so that the error can reach 30% ~ 50%. Therefore, this study suggests that it is necessary to use CFD0 when

$$t > 0.03 \qquad (6.17)$$

Note that the above conclusion was based on the experimental data with the average zone temperature ranging from 296 K to 322 K. More verification studies should be needed if the zone temperature is outside this range.

6.4. Summary

This chapter conducted dimensionless analyses for simulations of non-uniform distributions of air momentum effects, air temperatures, and contaminant concentrations. By checking the errors caused by the well-mixing assumption of multizone models, several suggestions were provided about under what conditions the CFD method is required.

- For airflows with non-uniform distribution of air momentum effect, the CFD is needed when
  - Re > 30 for channel flow
  - $X_d < T_{max}$ for jet flow, where X_d is the distance from the jet opening to the opening downwind in the jet flow direction, and T_{max} is the maximum throw length of the jet
- For airflows with non-uniform distribution of contaminant concentration, CFD is needed for the zone containing the contaminant source, except Ar > 400, when the contaminant source is also a heat source.
- For airflows with non-uniform distribution of air temperatures, CFD is needed when the dimensionless temperature gradient, $\tau > 0.03$.

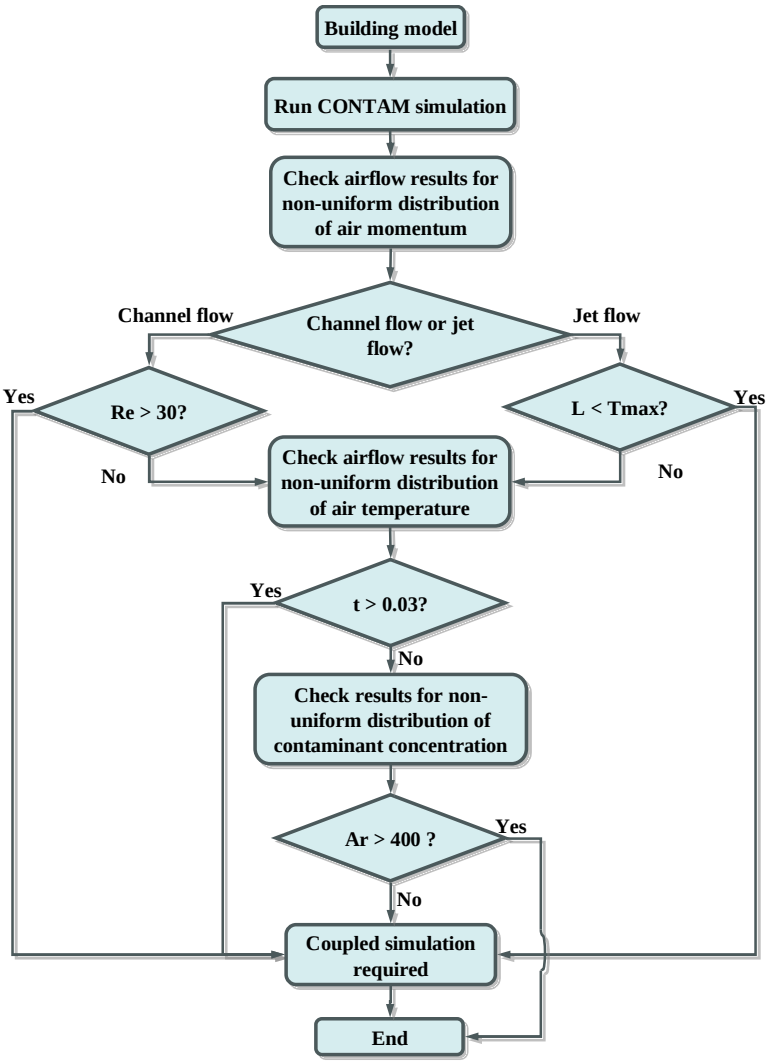

Fig. 6.8 Procedure to judge when CFD is required by the suggestions for non-uniform distribution of air momentum effect, air temperature, and contaminant concentration.

The above suggestions for CFD zone selection can be used by following the procedure in Fig. 6.8, which is simply a combination of ordered criteria. Users should note that

- To calculate the dimensionless numbers, i.e. Ar, Gr, Re, and St, it is necessary to perform a CONTAM simulation first to provide preliminary parameters.
- The order of applying these suggestions could be different from that of the procedure, depending on the type of the simulation in question.

Furthermore, the suggestions in this chapter were obtained through the analyses of limited data, which may only characterize certain airflows, temperature distributions, and contaminant transports. More verification studies and dimensionless investigations are necessary to evaluate multizone assumptions in the future.

CHAPTER 7. CONCLUSIONS AND FUTURE WORK

7.1. Conclusions

Building ventilation designs and indoor air quality analyses are essential to provide a safe, healthy, and comfortable indoor environment for a building's occupants. Current design and analysis tools, as well as multizones, CFDs, and zonal models have their own merits and drawbacks when used individually. Multizone models require the least computational time, but their applications are limited to the simulations, where many of their assumptions are applicable. Inaccuracies in simulated results or sometimes errors may happen when multizone assumptions fail. The literature review shows that the failed cases include airflows with

- non-uniform distribution of wind pressures around buildings,
- non-uniform distribution of momentum effects,
- non-uniform distribution of temperatures, and
- non-uniform distribution of contaminant concentrations

For such cases, CFD programs can be coupled with multizone programs to improve their calculations.

This study has investigated how to improve the accuracy of airflow and contaminant transport calculations in a multizone network model, CONTAM, by coupling it with a CFD program, CFD0-C. For the non-uniform distribution of wind pressures, the present study proposed an indirect/virtual coupling strategy to provide spatial distributions of wind pressures for CONTAM simulations. By using a Wind Pressure and Contaminant concentration (WPC) link or a Wind Pressure Profile (WPP) link in numerical tests, the

proposed method could effectively improve the description of wind pressures around buildings.

For the problems caused by well-mixing assumptions of air pressures, temperatures, and contaminant concentrations for simulations of indoor airflows and contaminant transport, CONTAM and CFD0-C were coupled through the airflow rates or pressure drops at the interfaces. Through theoretical analysis, this study has also proven that the coupled program has a solution and the solution is unique with the three coupling methods.

In this investigation, we have studied three feasible coupling methods between CONTAM and CFD0-C for coupled indoor air simulations:

1. CONTAM gives pressure to CFD0 and CFD0 returns the pressure to CONTAM;
2. CONTAM gives pressure to CFD0 and CFD0 returns the flow rate to CONTAM; and
3. CONTAM gives flow rate to CFD0 and CFD0 returns the pressure to CONTAM.

The Scarborough criterion was used to evaluate the convergence of the numerical solutions and to analyze the stability of the three coupling methods during their iterative coupling processes. Method 1, which exchanges pressure boundary conditions between multizone and CFD programs, is unconditionally stable, while Methods 2 and 3 are conditionally stable. Two numerical experiments were conducted to demonstrate the theory: one was pressure gradient flow in an office suite and the other was cross ventilation in a four-zone building model. Although experimental data is either unavailable or limited for these two cases, numerical results show the theory to be valid.

To validate the numerical simulations, this study first verified the conversion of CFD0-C from CFD0-F, the FORTRAN version of CFD0, by comparing the CFD0-C results with published data for six cases. CFD0-C was shown to provide results with reasonable accuracy. In order to validate the coupled program, this investigation then used a four-zone environmental chamber to measure the airflow rate and the distributions of air

velocity, air temperature, and contaminant concentration simulated by SF_6. The experiment was designed to study non-uniform distributions of momentum, contaminant, and the temperature gradient in a zone. CONTAM, the coupled CONTAM-CFD0, CFD0, and a commercial CFD program (Airpak) were used for the investigation. The results show that CONTAM could not consider the flow in a zone with strong non-uniform distributions of momentum and contaminant concentration. However, the impact of a non-uniform temperature gradient on CONTAM simulation is small, if the zone air temperature can be correctly estimated. In general, the coupled CONTAM-CFD0 program performs better than the CONTAM for all the cases studied, and is as good as the CFD0 for all the zones but with a major reduction in computing time. Both the coupled CONTAM-CFD0 and the CFD0 programs can predict reasonably well the distributions of air velocity, temperature, and SF_6 concentration in the chamber, but there are discrepancies. The discrepancies could be caused by the boundary conditions provided by CONTAM and by the zero-equation model used in CFD0.

The validations also found the limitations of CFD0-C program. For airflows with strong momentum effects, CFD0-C could not predict the airflow distribution as well as the commercial software, such as Airpak, which uses the standard k-ε turbulence model. When used for outdoor airflow simulations, CFD0-C may perform unsatisfactorily for the surfaces with storng turbulence separation and recirculation flows.

This study also proposed three algorithms for coupling CONTAM with CFD0-C for steady airflow and steady contaminant transport, steady airflow and transient contaminant transport, and transient airflow and transient contaminant transport. The three schemes were demonstrated by the simulations of natural ventilation in a three-story building with a large atrium, to which CFD0 was applied. The results show that the coupled program can give more realistic results than CONTAM. The coupled program could also help to evaluate emergency ventilation and control systems, and calculate personal contaminant exposure for the determination of evacuation strategies.

Through dimesional analyses, this study also found correlation of simulation errors, which were caused by the multizone assumptions, to the mixing levels of air properties and contaminant concentrations in a zone. The assumption of uniform air temperatures is critical when a non-dimensional temperature gradient is higher than 0.03. The assumption of uniform air momentum effects could fail when the airflow with a strong momentum effect cannot be totally dissipated in a zone. The assumption of uniform contaminant concentrations can be invalid for the zone containing the contaminant source except that the contaminant source is also a heat source. The well-mixing assumption of contaminant concentration could be used if the new Archimedes number is greater than 400.

7.2. Challenges for Future Studies

In building airflow distribution and contaminant transport simulations, some challenges remain unsolved for coupling multizone and CFD programs. This section briefly outlines these challenges, which could be the bases of future studies.

Atmospheric Contaminant Dispersion under Transient Weather Condition

Airflow and contaminant transport around buildings are always transient due to the unsteady feature of the weather. For transient airflow, this thesis used the Wind Pressure Profile (WPP) link of CONTAM and CFD0 to predict the distribution of wind pressure coefficients for variable wind speed. However, the WPP link was unable to predict atmospheric contaminant dispersion under transient weather, although it could simulate contaminant transport at a steady state for a certain wind direction. It is necessary to develop a method of contaminant dispersion under transient weather conditions, which is more realistic than the simulation at a steady state.

The simulation of airflow and contaminant dispersion under a specific weather at transient state makes it hard to reuse the previously-calculated results. One alternative is to consider airflow at a quasi-steady state within one time step, and the contaminant transport to be always transient throughout all the time steps. This means that transient contaminant transport can be calculated by using pre-calculated steady-state airflow

results at the same time step. When the wind velocity is different from that of the pre-calculated airflow results, a correction of airflow velocity can be applied, which is similar to the correction of wind pressure coefficients in the WPP link. By reusing pre-calculated airflow data, this method will save huge computational costs. Furthermore, since using airflow is relatively easier to reach steady state than using contaminant dispersion, it is reasonable to use airflow at a quasi-steady state within one time step for transient contaminant simulation.

Single Solver for Integrated Multizone and CFD Equations for Airflow, Energy, and Contaminant Simulations

This thesis studied the methods to run multizone and CFD programs separately while exchanging boundary conditions between them. It is desirable that a solver or a single program can be developed to calculate the assembled equations of multizone and CFD programs for airflow, energy, and contaminant transport. The single solver can avoid the convergence and stability problems associated with different coupling methods. The single solver also calculates integrated energy equations so that the zone temperature can be predicted instead of being specified by users.

Chapter 3.2.3 showed an assembled matrix equation of multizone and CFD models for air mass conservation in Eq. (3.12). Similarly, a linearized assembled equation can also be written for momentum, energy, and contaminant/species conservations, which are combined with air mass conservation as:

$$\mathbf{CP} + \mathbf{F} = \mathbf{B} \quad \text{(Air mass conservation)} \tag{7.1}$$

where **C** is the flow coefficient maxtric, **P** is the vector of unkown pressures of multizone and CFD cells, **F** is the vector of unkown flow rates through interface paths and cells, and **B** is the vector of mass source term.

$$\mathbf{C_m U} + \Delta\mathbf{P} = \mathbf{B_m} \quad \text{(Momentum conservation)} \tag{7.2}$$

where $\mathbf{C_m}$ is the coefficient matrix in an assembled momentum conservation equation, **U** is the vector of unknown air velocities through an opening or CFD cell face, D**P** is the vector of pressure difference, $\mathbf{B_m}$ is the vector of source term in an assembled momentum conservation equation.

$$\mathbf{C_e T} + \mathbf{Q} = \mathbf{B_e} \text{ (Energy conservation)} \quad (7.3)$$

where $\mathbf{C_e}$ is the coefficient matrix in an assembled energy conservation equation, **T** is the the vector unknown temperatures, **Q** is the vector of heat inputs, and $\mathbf{B_e}$ is the vector of the source terms in an assembled energy conservation equation.

$$\mathbf{C_c M} + \mathbf{S} = \mathbf{B_c} \text{ (Contaminant/Species conservation)} \quad (7.4)$$

where $\mathbf{C_c}$ is the coefficient matrix in an assembled species conservation equation, **M** is the vector of species concentrations, **S** is the vector of species mass source terms, and $\mathbf{B_c}$ is the vector of source terms in an assembled species conservation equation.

A point-to-point (cell-to-cell) linear solver can be used to solve Eqs. (7.1) – (7.4), such as the Gauss Seidel method, or faster linear Multi-grid solver. Note that the momentum conservation equation becomes airflow path resistance model in multizone methods. Furthermore, the integration of multizone and CFD methods links a spatially one-dimensional model with a three-dimensional method. Therefore, some assumptions must be employed for the physical links/interfaces between the zones of the two methods. For example, it is often assumed that

- tangential air velocity at an interface airflow path are zero, and
- spatial distribution of pressures and velocities along the interface path are uniform.

Under some situations, these assumptions could become critical, which thus cause simulation errors, as discussed next.

Potential Asymmetric Problems Associated with Coupled Multizone and CFD Simulations

An integrated multizone and CFD simulation apply the CFD model to the zones, where multizone assumptions fail, and multizone models are applied to the rest of the zones of a building. The distinctions of multizone and CFD methods may cause asymmetrical results for a symmetrical problem, as illustrated in Fig. 7.1 (Axley, 2006).

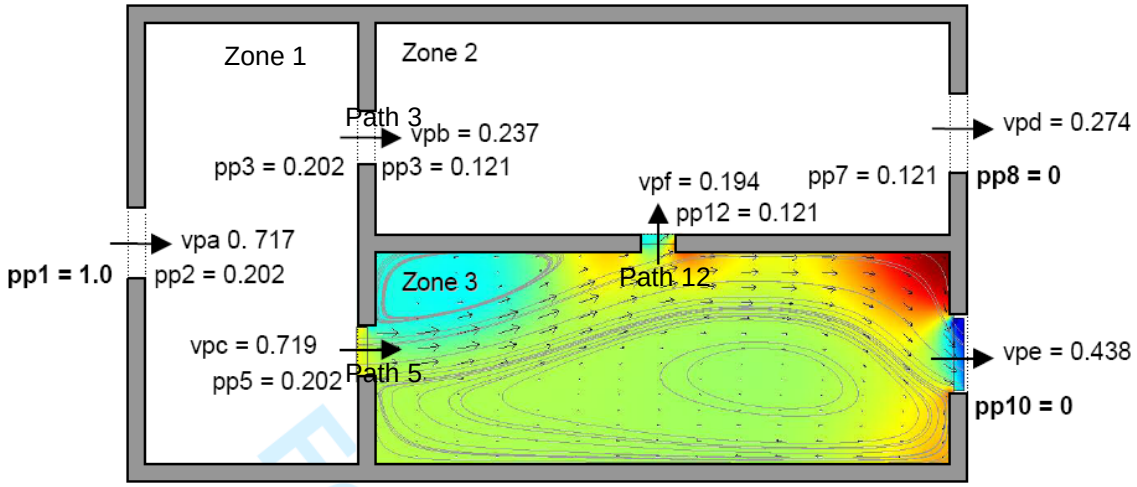

Fig. 7.1 Asymmetric results caused by the difference of multizone and CFD methods and the inappropriate selection of CFD zones (Axley, 2006).

A 4-zone house with symmetrical configuration in Fig. 7.1 was solved asymmetrically when the CFD method was only applied to Zone 3. As a result, the airflow through Path 12 was non-zero, which was apparently incorrect. The asymmetrical solution was caused by the assumption of zero tangential velocities at Path 5, which was otherwise unavailable from the multizone equations. Some researchers claimed that the asymmetrical solution was an intrinsic limitation for integrated macro-micro methods. This thesis, however, suggested two possible solutions for the asymmetrical results. One solution is to apply the CFD method to both Zone 1 and Zone 3 in order to capture the correct airflow directions at Paths 3 and 5. The other is to simulate both Zone 2 and Zone

3 as a CFD zone, which will make the integrated simulation symmetrical. So far, it is not clear if these solutions could improve the results. Therefore, more studies on the asymmetrical problem related to the integrated methods and the impact of neglecting tangential velocities at the interface paths should be done in the future.

Contaminant Mixing Level and Mixing Time

One of the major multizone assumptions is that the contaminant is perfectly mixed in a zone without time delay. As already discussed in this thesis, contaminant mixing depends on many factors such as contaminant source locations, local air velocities and flow patterns, and internal blockages. For contaminant transports at a transient state, it also takes time for contaminants to spread in a room.

More theoretical and experimental studies are necessary for contaminant mixing level and mixing time in a room. This thesis already showed the possibility of applying dimensionless analyses to study the contaminant mixing enhanced by buoyancy effects, although it was limited to the situation, where the contaminant source was also a heat source. Experimental studies are also possible, such as the studies done on mixing time by Baughman (1994), Drescher (1995), Thatcher (2004), and Finlayson (2004).

Applications of Multizone, CFD, or the Coupled Multizone-CFD Programs to Building Evacuations and Real-time Controls

This thesis has demonstrated the coupled CONTAM-CFD0 program for outdoor airflow simulations through the indirect/virtual coupling, and indoor simulations by the direct coupling, as shown in CHAPTER 5. It was shown that the coupled program was able to help evaluate the building evacuation strategies and the design of building control systems before and after building construction. One of the more important applications is simulation and control at real-time, which is especially important for designing safe and immune buildings. For example, with real-time inputs from sensor information, the simulation could predict safe evacuation routes before the contaminant concentration reaches lethal level.

Several barriers exist, however, for real-time analyses and control. The computing time of the coupled multizone-CFD program is still too high for real-time applications. The multizone program itself seems a good alternative in terms of simulation time, but it may provide inaccurate answers due to its assumptions. More future studies should be done to further reduce the computational cost of CFD methods and to understand the applicability of multizone assumptions. Moreover, numerical simulations are often found to be at odds with the measured data. More studies could be conducted on how to use the real-time data from sensors to improve the simulation accuracy.

As a whole, the current study developed a coupled CONTAM-CFD0 program for airflow distribution and contaminant transport simulations outside and inside buildings. Theoretical studies proved that the coupled program has a solution and the solution is unique. The coupled program was then validated by comparing the numerical results with experimental data. The demonstration of the coupled CONTAM-CFD0 program to real design problems illustrated that the coupled program could effectively improve the CONTAM calculations. This study also found that many challenges remain unsolved and pointed out several potential solutions, which could be used as bases for future studies.

LIST OF REFERENCES

LIST OF REFERENCES

Allard, F. and C. Inard (1992). Natural and mixed convection in rooms: prediction of thermal stratification and heat transfer by zonal models. International Symposium of Room Air Convection and Ventilation Effectiveness, University of Tokyo, Tokyo,Japan.

Arvelo, J., A. Brandt, R. P. Roger and A. Saksena (2002). "An enhanced multizone model and its application to optimum placement of CBW sensors." ASHRAE Transactions **108(2)**: 658-666.

ASHRAE (2005). ASHRAE Handbook of Fundamentals, American Society of Heating, Refrigerating and Air-Conditioning Engineers.

Axley, J. (2006). Embedded detail microscopic models of rooms within macroscopic models of whole building systems. Final Report Presentation to National Institute of Standard and Technology, Gaithersburg,MD.

Bartak, M., I. Beausoleil-Morrison, J. A. Clarke, J. Denev, F. Drkal, M. Lain, I. A. Macdonald, A. Melikov, Z. Popiolek and P. Stankov (2002). "Integrating CFD and building simulation." Building and Environment **37**(8-9): 865-871.

Baughman, A. V., A. J. Gadgil and W. W. Nazaroff (1994). "Mixing of a Point-Source Pollutant by Natural-Convection Flow within a Room." Indoor Air-International Journal of Indoor Air Quality and Climate **4**(2): 114-122.

Beausoleil-Morrison, I. (2002). "The adaptive conflation of computational fluid dynamics with whole-building thermal simulation." Energy and Buildings **34**(9): 857-871.

Bouia, H. and P. Dalicieux (1991). Simplified modeling of air movements inside dewelling room. Building Simulation 91 Conference, Nice, France, IBPSA (The international Building Performance Simulation Association).

Buhl, W. F., A. E. Erdem and F. C. Winkelmann (1993). Recent improvement in SPARK: Strong componoent decomposition, multivated objects, and graphical interface. Building Simulation 93 Conference, Adelaide, Australia, IBPSA (The international Building Performance Simulation Association).

Chen, Q. and Z. Jiang (1992). "Significant questions in predicting room air motion." ASHRAE Transactions **98(1)**: 929-939.

Chen, Q. and L. Wang (2005). Development, analysis and validation of approaches for coupling CONTAM and CFD0-C for simulating contaminant transport in buildings, Final Report for NIST SB1341-04-Q-0771. West Lafayette, IN, School of Mechanical Engineering,Purdue University**:** 62.

Chen, Q. and W. Xu (1998). "A zero-equation turbulence model for indoor airflow simulation." Energy and Buildings **28**: 137-144.

Clarke, J. A. (1985). Energy Simulation in Building Design. Bristol, Adam Hilger Ltd.

Clarke, J. A. (2001). "Domain integration in building simulation." Energy and Buildings **33**(4): 303-308.

Clarke, J. A., W. M. Dempster and C. O. R. Negrao (1995a). The implementation of a computational fluid dynamics algorithm within the ESP-r System. Building Simulation 95 Conference, Madison, Wisconsin, USA, IBPSA (The international Building Performance Simulation Association).

Clarke, J. A., J. Hensen and C. O. R. Negrao (1995b). Predicting indoor air flow by combining network approach, CFD and thermal simulation. 16th AIVC Conference, Palm Springs, California,USA.

Clarke, J. A. and T. W. Maver (1991). "Advanced design tools for energy conscious building design - development and dissemination." Building and Environment **26**(1): 25-34.

Cochran, L. (2000). Storms. Chapter 14 Wind engineering as related to tropical cyclones,Routledge hazards and disasters series. R. A. Pielke. London ; New York, Routledge**:** 2 v.

Deardorff, J. W. (1970). "A numerical study of three-dimensional turbulent channel flow at large Reynolds numbers." Journal of Fluid Mechanics **42**: 453-480.

Dorgan, C. B., M. S. Kanarek and A. J. Willman (1998). "Health and productivity benefits of improved indoor air quality." ASHRAE Transactions **104(1)**: 658-666.

Drescher, A. C., C. Lobascio, A. J. Gadgil and W. W. Nazaroff (1995). "Mixing of a Point-Source Indoor Pollutant by Forced-Convection." Indoor Air-International Journal of Indoor Air Quality and Climate **5**(3): 204-214.

Emmerich, S. J. (1997). Use of computational fluid dynamics to analyze indoor air quality issue. Gaithersburg, MD, National Institute of Standards and Technology.

Emmerich, S. J. (2001). "Validation of multizone IAQ modeling of residential-scale buildings: a review." ASHRAE Transactions **107(2)**: 619-628.

Emmerich, S. J. and K. B. McGrattan (1998). "Application of a large eddy simulation model to study room airflow." ASHRAE Transactions **104**: 1128-1140.

Emmerich, S. J., A. K. Persily and S. J. Nabinger (2002). Modeling moisture in residential buildings with a multizone IAQ program. Indoor Air 2002, Monterey, CA.

Etheridge, D. and M. Sandberg (1996). Building ventilation theory and measurement. New York, John Wiley & Sons.

Feustel, H. E. (1999). "COMIS - an international multizone air-flow and contaminant transport model." Energy and Buildings **30**(1): 3-18.

Feustel, H. E. and J. Dieris (1992). "A survey of airflow models for multizone structures." Energy and Buildings **18**(2): 79-100.

Finlayson, E. U., A. J. Gadgil, T. L. Thatcher and R. G. Sextro (2004). "Pollutant dispersion in a large indoor space. Part 2: Computational fluid dynamics predictions and comparison with a scale model experiment for isothermal flow." Indoor Air **14**(4): 272-283.

Fisk, W. (2000). "Health and productivity gains from better indoor environments and their relationship with building energy efficiency." Annual Review of Energy and the Environment **25**: 537-66.

Fluent (2002). Airpak user manual, Fluent Inc. and ICEM-CFD Engineering.

Gadgil, A., C. Lobscheid, M. O. Abadie and E. U. Finlayson (2003). "Indoor pollutant mixing time in an isothermal closed room: an investigation using CFD." Atmospheric Environment **37**(39-40): 5577-5586.

Gao, Y. (2002). Coupling of computational fluid dynamics and a multizone airflow analysis program for indoor environmental design. Cambridge, MA., Massachusetts Institute of Technology.

Gao, Y. and Q. Chen (2003). Coupling of a multi-zone airflow analysis program with a computational fluid dynamics program for indoor air quality studies. The 4th International Symposium on HVAC, Symposium on HVAC, Tsinghua University, Beijing, China.

Graça, G. C. d. and P. F. Linden (2002). "Simplified Modeling Of Cross Ventilation Airflow." ASHRAE Transactions **109**(Part 1): 32.

Grelat, A. (1987). Approche des phenomenes de circulatiion et de stratification de l'air dans les locaux chauffes par le programme de simulation thermique multizone

Griffith, B. T. (2002). Incorporating nodal and zonal room air models into building energy calculation procedures. Cambridge, MA., Massachusetts Institute of Technology.

Haghighat, R., Y. Lin and A. C. Megri (2001). "Development and validation of a zonal model POMA." Building Environment **36**: 1039-1047.

Hayes, R. E., K. Nandakumar and H. Nasr-El-Din (1989). "Steady laminar flow in a 90 degree planar branch." Computers and Fluids **17(4)**: 537-553.

Higginson, N. (2003). Dirty bomb. USA, PBS**:** 60 mins.

Holmes, J. D. (1986). Wind loads on low-rise buildings. The Structural and environmental effects of wind on building and structures, Chapter 12. Melbourne,Australia, Monash University.

Holmes, J. D. (1994). "Wind pressures on tropical housing." Journal of Wind Engineering and Industrial Aerodynamics **53**(1-2): 105-123.

Inard, C. (1988). Contribution a letude du couplage thermique entre un emetteur de chauffage et un local. Etudes experimentales en chambers climatiques. Lyon, France, National Institute of Applied Science (INSA).

Incropera, F. P. and D. P. DeWitt (2007). Fundamentals of heat and mass transfer. Hoboken, NJ, John Wiley.

Jayaraman, B., D. Lorenzetti and A. Gadgil (2004). Coupled model for simulation of indoor airflow and pollutant transport. Berkeley, CA, USA, Lawrence Berkeley National Laboratory.

Jiang, Y. (2002). Study of natural ventilation in buildings with large eddy simulation. Cambridge, MA., Massachusetts Institute of Technology, U.S.A.

Jiang, Y. and Q. Chen (2001). "Study of natural ventilation in buildings by large eddy simulation." Journal of Wind Engineering and Industrial Aerodynamics **89(13)**: 1155-1178.

Kato, S., S. Murakami and C. N. Kong (1998). Zonal climate design of Grand Opera Theatre based on contribution ratio of cooled air from supply openings. Roomvent 98: 6th International Conference on Air Distribution in Rooms, Stockholm, Sweden.

Kelka, K. M. and D. Choudhury (2000). "Numerical method for the prediction of incompressible flow and heat transfer in domains with specified pressure boundary conditions." Numerical Heat Transfer Part B **38**: 5-36.

Kotani, H., R. Satoh and T. Yamanaka (2003). "Natural ventilation of light well in high-rise apartment building." Energy and Buildings **35**(4): 427-434(8).

Ladeinde, F. and M. Nearon (1997). "CFD applications in the HVAC&R industry." ASHRAE Journal **39(1)**: 44-48.

Lebrun, J. (1970). Exigences physicologiques et modalites physiques de la climatisation par source statique concentree. Belgium, University of Liege.

Li, Y., D. A, S. JG and C. L. (1998a). Comparison of zonal and CFD modeling of natural ventilation in a thermally stratified building. The 6th International Conference on Air Distribution in Rooms, Stockholm.

Li, Y., L. Chen, A. Delsante and G. Hesford (2000). CFD and multi-zone modeling of fog formation risk in a naturally ventilated industrial building. Roomvent 2000, Reading, U.K.

Li, Y., A. Delsante, J. G. Symons and L. Chen (1998b). Comparison of zonal and CFD modeling of natural ventilation in thermally stratified building. Air Distribution in Rooms Conference, ROOMVENT 98, Stockholm,Sweden.

Li, Y., S. Duan, I. T. S. Yu and T. W. Wong (2005a). "Multi-zone modeling of probable SARS virus transmission by airflow between flats in Block E, Amoy Gardens." Indoor Air **15**(2): 96-111.

Li, Y., X. Huang, I. T. S. Yu, T. W. Wong and H. Qian (2005b). "Role of air distribution in SARS transmission during the largest nosocomial outbreak in Hong Kong." Indoor Air **15**(2): 83-95.

Linden, P. F. (1999). "The fluid mechanics of natural ventilation." Annual Review of Fluid Mechanics **31**: 201-38.

Lorenzetti, D. M. (2002). "Computational aspects of nodal multizone airflow systems." Building and Environment **37**(11): 1083-1090.

Mendell, M. J. (1993). "Non-specific symptoms in office workers: a review and summary of the epidemiologic literature." Indoor Air **3**: 227-236.

Mokhtarzadeh-Dehghan, M. R., S. Ergin-Ozkan and A. J. Reynolds (1994). "Natural convection between two compartments of a stairwell – numerical prediction and comparison with experiment." Numerical Heat Transfer, Part A **27**: 1-17.

Mora, L. (2003). Thermal and airflow prediction in building by associating models with different levels of details within an object-oriented simulation environment. La Rochelle, France, Université de la Rochelle,France.

Mora, L. and A. J. Gadgil (2002). Theoretical Study of Pollutant Mixing in Rooms Induced by Occupancy. RoomVent 2002, Copenhaguen, Denmark.

Mora, L., A. J. Gadgil and E. Wurtz (2003). "Comparing zonal and CFD model predictions of isothermal indoor airflows to experimental data." Indoor Air **13**(2): 77-85.

Murakami, S., S. Kato and S. Akabayashi (1991). "Wind tunnel test on velocity pressure field of cross-ventilation with open windows." ASHRAE Transactions **97(1)**: 525-538.

Musser, A. (2001). "An analysis of combined CFD and multizone IAQ model assembly issues." ASHRAE Transactions **107(1)**: 371-382.

Musy, M. (1999). Automatic generation of zonal models to perform airflow and thermal simulation in buildings (in French). La Rochelle,France, University of La Rochelle.

Negrao, C. O. R. (1995). Conflation of computational fluid dynamics and building thermal simulation. Glasgow, Scotland, University of Strathclyde.

Negrao, C. O. R. (1998). "Integration of computational fluid dynamics with building thermal and mass flow simulation." Energy and Buildings **27**(2): 155-165.

Nielsen, P. V. (1998). "The selection of turbulence models for prediction of room airflow." ASHRAE Transactions **104 (B)**: 1119-1127.

Nishizawa, S., T. Sawachi, N. Ken-ichi, H. Seto and Y. Nishikawa (2003). Comparison between experimental and CFD analysis in full-scale building model using standard κ-ε model. The First International Workshop on Natural Ventilation, Tokyo, Japan.

Patankar, S. V. (1980). Numerical heat transfer and fluid flow. New York, McGraw-Hill Book Company.

Peng, X. and A. H. C. v. Paassen (1995). A state space model of indoor temperature distributions. the 2nd International Symposium on Heating, Ventilating and Air Conditioning, Tsinghua-HVAC 95, Beijing,China.

Persily, A. K. (1998). Modeling study of ventilation, IAQ and energy impacts of residential mechanical ventilation. Gaithersburg, MD., National Institute of Standards and Technology

Persily, A. K. (2003). Workshop on non-uniform zones in multizone network models. The Workshop on Non-uniform Zones in Multizone Network Models, Gaithersburg, MD., National Institute of Standard and Technology.

Persily, A. K. and E. M. Ivy (2001). Input data for multizone airflow and IAQ analysis. Gaithersburg, MD., National Institute of Standard and Technology.

Raw, G. J., M. S. Roys and A. Leaman (1990). Further findings from the office environment survey: productivity. the 5th International Conference on Indoor Air Quality and Climate, Toronto,Canada.

Ren, Z. (2002). Enhanced modeling of indoor air flows, temperatures, pollutant emission and dispersion by nesting sub-zones within a multizone model. Belfast, Northern Ireland, UK, The Queens University of Belfast.

Ren, Z. and J. Stewart (2005). "Prediction of personal exposure to contaminant sources in industrial buildings using a sub-zonal model." Environmental Modeling & Software **20**(5): 623-638.

Reynolds, A. J. (1986). "The Scaling of Flows of Energy and Mass through Stairwells." Building and Environment **21**(3-4): 149-153.

Salemi, R., F. Alamdari and P. J. Fishwick (1996). Air distribution in a naturally ventilated office. CIBSE/ASHRAE Joint National Conference, Harrogate,U.K.

Sawachi, T., K. Narita, N. Kiyota, H. Seto, S. Nishizawa and Y. Ishikawa (2003). Wind pressure and airflow in a full-scale building model under cross ventilation. the First International Workshop on Natural Ventilation, Tokyo, Japan.

Scarborough, J. B. (1966). Numerical Mathematical Analysis. Baltimore, MD,USA, The Johns Hopkins Press.

Schaelin, A., V. Dorer, J. v. d. Maas and A. Moser (1994). "Improvement of multizone model predictions by detailed flow path values from CFD calculations." ASHRAE Transactions **100**(Part 2): 709-720.

Spengler, J. D. and Q. Chen (2000). "Indoor air quality factors in designing a healthy building." Annual Review of Energy and the Environment **25**: 567-600.

Srebric, J., Q. Chen and L. R. Glicksman (1999). "Validation of a zero-equation turbulence model for complex indoor airflows." ASHRAE Transactions **105(2)**: 414-427.

Srinivas, T. (2001). Evaluation and enhancement of computational techniques in indoor air quality analysis. Biological Engineering. Halifax, Nova Scotia,Canada, Dalhousie University.

Stewart, J. and Z. Ren (2003). "Prediction of indoor gaseous pollutant dispersion by nesting sub-zones within a multizone model." Building and Environment **38**(5): 635-643.

Sundell, J. (2004). "On the history of indoor air quality and health." Indoor Air **14**: 51-58.

Swami, M. V. and S. Chandra (1987). Procedures for calculating natural ventilation airflow rates in buildings. Cape Canaveral, Florida Solar Energy Center.

Swami, M. V. and S. Chandra (1988). "Correlations for pressure distributions on buildings and calculation of natural-ventilation airflow." ASHRAE Transactions **94(1)**: 243-266.

Tannehill, J. C., D. A. Anderson and R. H. Pletcher (1997). Computational fluid mechanics and heat transfer, second edition, Taylor & Francis

Thatcher, T. L., D. J. Wilson, E. E. Wood, M. J. Craig and R. G. Sextro (2004). "Pollutant dispersion in a large indoor space: Part 1 - Scaled experiments using a water-filled model with occupants and furniture." Indoor Air **14**(4): 258-271.

U. S. EPA (1995). The inside story: a guide to indoor air quality, United States Environmental Protection Agency and the United States Consumer Product Safety Commission**:** 32.

U.S. EIA (1995). U.S. Energy Information Administration-State energy data report 1995:Tables 3-7.

Upham, R. (1997). A validation study of the airflow and contaminant migration computer model CONTAM as applied to tall buildings. University Park, Pennsylvania, the Pennsylvania State University.

Versteeg, H. K. and W. Malalasekera (1995). An introduction to Computational Fluid Dynamics, Addison-Wesley Pub Co, UK. .

Walton, G. N. and W. S. Dols (2003). CONTAMW 2.1 user manual. Gaithersburg, MD, USA, National Institute of Standards and Technology.

Wolkoff, P. (1995). "Volatile organic compounds - Sources, measurements, emissions, and the impact on indoor air quality." Indoor Air: 1-73.

Wurtz, E. (1995). Three-dimensional modeling of thermal and airflow transfer in building using an object-oriented simulation environment (in French). Paris,France, Ecole Nationale des Ponts et Chaussees.

Xue, H., E. Hihara and T. Saito (1994). "Temperature Stratification of Heated Air-Flow in a Fire Tunnel." Jsme International Journal Series B-Fluids and Thermal Engineering **37**(1): 187-194.

Xue, H. and C. Shu (1999). "Mixing characteristics in a ventilated room with non-isothermal ceiling air supply." Building and Environment **34**(3): 245-251.

Yuan, J. (2003). Effective prediction of air distribution and contaminant transport in entire buildings by coupling multizone, CFD and energy models. University Park, Pennsylvania, The Pennsylvania State University

Yuan, J. and J. Srebric (2002). Improved prediction of indoor contaminant distribution for entire buildings. The 2002 ASME International Mechanical Engineering Congress and Exposition, New Orleans, Louisiana, USA.

Zhai, Z. (2003). Developing an integrated building design tool by coupling building energy simulation and computational fluid dynamics programs. Department of Architecture. Cambridge, MA., Massachusetts Institute of Technology**:** 276.

Zhai, Z. and Q. Chen (2003). "Solution characters of iterative coupling between energy simulation and CFD programs." Energy and Buildings **35**(5): 493-505.

Zhai, Z., Y. Gao and Q. Chen (2004). Pressure boundary conditions in multi-zone and CFD program coupling. 1st IBPSA-USA Conference – SimBuild, Boulder, CO.

Zhai, Z., J. Srebric and Q. Chen (2003). "Application of CFD to predict and control chemical and biological agent dispersion in buildings." International Journal of Ventilation **2**(3): 251-264.

Zhang, J. S., G. J. Wu and L. L. Christianson (1993). "A new similitude modeling technique for studies of non-isothermal room ventilation flows." ASHRAE Transactions **99**(1): 129-138.

Zohrabian, A. S., M. R. Mokhtarzadehdehghan and A. J. Reynolds (1990). "Buoyancy-driven airflow in a stairwell model with through-flow." Energy and Buildings **14(**2): 133-142.

APPENDICES

Appendix A. Manual for CFD0-C

This appendix is a manual for using CFD0-C, C version of the CFD0. CFD0-C uses Cartesian coordinates, the SIMPLE algorithm, the upwind and power-law differencing schemes, the TDMA solver (Patankar, 1980), and the indoor zero-equation eddy-viscosity turbulence model (Chen and Xu, 1998). A detailed description for the turbulence modeling of CFD0 can be found in ASHRAE RP-927 (Srebric et al., 1999). CFD0-C solves velocity component U in the x-direction, V in the y-direction, and W in the z-direction, air pressure: P, air temperature: T, species concentration (≤ 5): C, and turbulence effective viscosity: μ at steady state or transient state.

Appendix A.1 - A.4 is for general-purpose usage of CFD0-C and Appendix A.5 -A.6 for advanced users with the aim of further development of CFD0-C.

A.1 Installation and Execution of CFD0-C

The executable PC version of CFD0-C include a Graphic User Interface (GUI), which defines a CFD simulation, generates simulation meshes, creates CFD input file, and visualize CFD results, and a Windows Console program, CFD0C.EXE, which is the CFD solver. Fig. A.1 shows the GUI of CFD0-C. The GUI and the solver can be copied and run directly without further installation. Note that to run the GUI of CFD0-C, users need to obtain a "Registration Number" from Professor Qingyan (Yan) Chen by sending an email with a randomly generated "Information Number" to YANCHEN@PURDUE.EDU as shown in Fig. A.2.

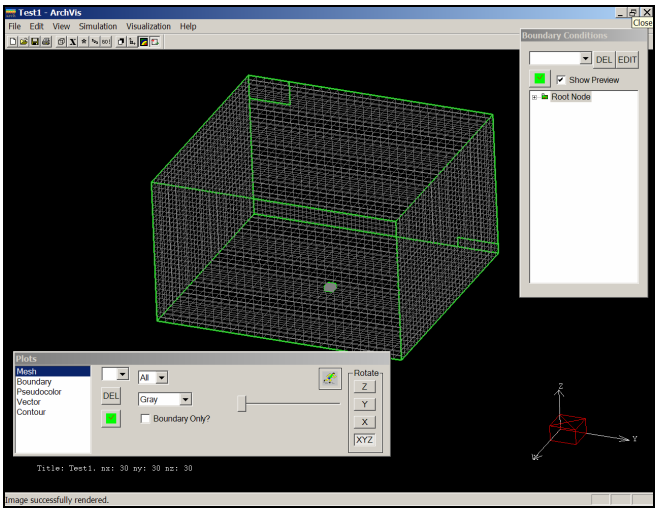

Fig. A.1 The Graphic User Interface (GUI) of CFD0-C.

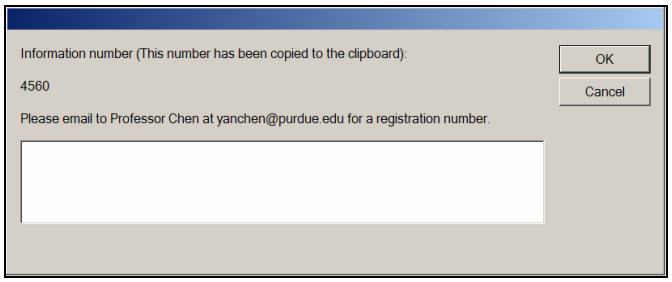

Fig. A.2 The window for registration of CFD0-C.

There are two methods to execute CFD0-C. One method is to run CFD0-C by choosing the CFD0C.EXE inside the CFD0C GUI as illustrated by Fig. A.3.

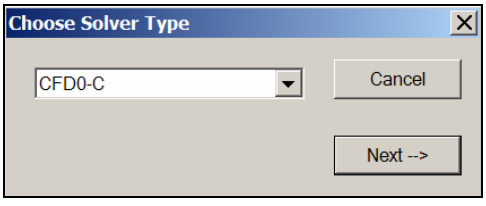

Fig. A.3 Run CFD0-C from the CFD0C GUI.

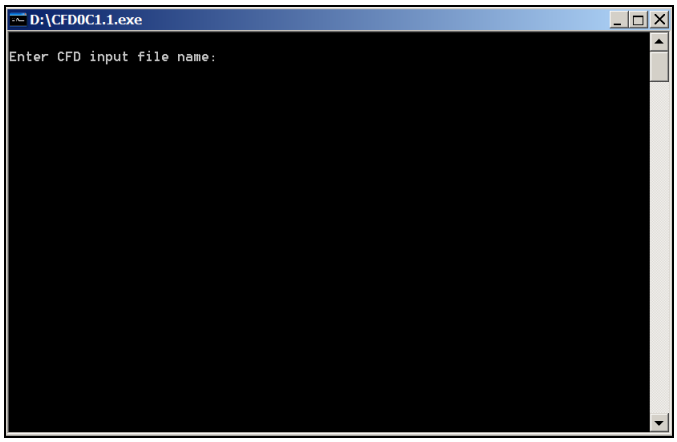

Fig. A.4 Run CFD0-C from WINDOWS Console.

The second method is to run CFD0C.EXE by double clicking the CFD0C.EXE in WINDOWS environment as shown in Fig. A.4. Users must specify the full path location of the CFD input file, "*.CFD".

A.2 Inputs and Outputs

Table A.1 Input and output files of CFD0-C.

Input	
• CFD	the ASCII input file defining geometry, boundary conditions, control parameters etc.;
Outputs	
• RET	the ASCII output of CFD results of flow rates, spatial air velocities, temperatures, pressures, contaminant concentrations at grid points.
• DAT	the data file for post-processing in TECPLOT (compatible with TECPLOT 360)
• BAL	outputs of convergence history, e.g. residues of calculations of velocities and temperatures etc.
• VAR	the binary file with the whole data of air pressures, velocities and temperatures for the calculations of airflow restart and the contaminant dispersion based on existent flow field.
• OUT	the output file for visualization in the CFD0C GUI
Optional Outputs	
• EWC	the binary file of wind pressures for the WPC link of CONTAM (optional)
• CFDLOG	the output of the simulation definition from a CFD input (optional)
• WDB	the binary file of wind pressure coefficients for the WPP link of CONTAM (optional)
• CDB	the binary file of contaminant concentrations from the simulations of atmospheric contaminant dispersion (optional)

A.3 Preparation of an Input File for CFD0-C

The CFD0C input file, *.CFD, can be created either by the CFD0-C GUI or manual preparation by users. When preparing an input file from the GUI, users can use the instant help by resting the mouse arrow over where they want to get help. A green popup box with tips will show up as illustrated by Fig. A.5.

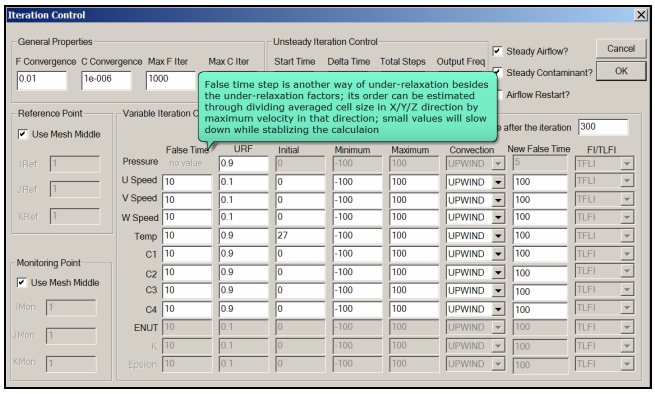

Fig. A.5 Instant help in the CFD0-C GUI.

Since the input file is in ASCII format, which users can prepare or edit manually. All the input information is in SI units. Manual input must follow an exact format requirement as follows. It is suggested prepare a manual input file always by starting with a template input file to avoid format errors. Note that all the input data values in the following format must be separated by comma.

Lines	**Input Data**
The first line:	User specified title of the case to be simulated in quotation marks
The next two lines:	Subtitle information
The next four lines:	Title of problem definition
The next one line:	Title of stead or unsteady control parameters of velocity and contaminant
The next one line:	stead or unsteady control parameters of velocity and contaminant, respectively (1=steady; 0=unsteady), respectively. Calculation for WPP link? (1=Yes; 0=No) (Only if Yes), Reference Height, Reference Wind Velocity, Atmospheric boundary layer thickness at a weather station, Wind profile exponent at a weather station, Atmospheric boundary layer thickness at local site, Wind profile exponent at local site, The first

	calculated wind angle, The last calculated wind angle, The step of calculated wind angle.
The next two lines:	Title of Time step, maximum time, residual of contaminant and maximum iterations of contaminant computation
The next one line:	Time step, maximum time for unsteady contaminant computations, residual and maximum iterations for contaminant computations
The next two lines:	Title of the control parameter for energy computation
The next one line:	The control parameter for energy computation (1=solve energy equation; 0=not solve energy equation)
The next two lines:	Title of the control parameters for contaminant computation, number of contaminants computed and whether the computation starts from an existent file of flow field
The next one line:	The control parameter for contaminant computation (1=compute contaminants; 0=not compute contaminant), total number of contaminants involved in the computation (<=5), the control parameter for whether the contaminant computation starts from an existent *.VAR file of flow field (1=based on a flow field file; 0=not based on a flow field file)
The next two lines:	Title of the residual and maximum iterations of velocity computation
The next one line:	The residual of velocity computation, the maximum iterations of velocity computation
The next two lines:	Title of the control parameter for flow regime
The next one line:	The control parameter for flow regime (F=turbulence flow; T=laminar flow)
The next two lines:	Title of turbulence models (if the flow regime is laminar, these two lines should be non-existent)
The next one line:	Variable of turbulence models (0=zero equation model; 1=κ-ε model (not available in current version). if the flow regime is laminar, this line should be non-existent)

The next four lines:	Title of the geometry data
The next three lines:	Explanation of the flow domain
The next line:	The flow domain size (m) in the x, y, and z direction (XX, YY, ZZ), respectively
The next three lines:	Grid size information
The next line:	The total number of control volumes (grid numbers) in the in x, y and z direction (NNX, NNY, NNZ), respectively
The next two lines:	Information of the control volume
The next line:	Title for the x-direction
The next line(s):	The size of the control volumes in the x-direction (DELX). The sum of these values must be equal to XX.
The next line:	Title for the y-direction
The next line(s):	The size of the control volumes in the y-direction (DELY). The sum of these values must be equal to YY.
The next line:	Title for the z-direction
The next line(s):	The size of the control volumes in the z-direction (DELZ). The sum of these values must be equal to ZZ.
The next two lines:	Title for the openings
The next line:	The number of inlet and outlet openings (NBIN, NBOUT)
The next block:	Exists only when NBIN > 0

The next two lines:	Title information for inlet opening(s)
The next line:	Title for the x-direction
The next line:	The first and last grid number of the opening in the x-direction
The next line:	Title for the y-direction
The next line:	The first and last grid number of the opening in the y-direction
The next line:	Title for the z-direction
The next line:	The first and last grid number of the opening in the z-direction

The next line: types of openings[(1)] (1=small opening; 2=large openings), types of boundary conditions (1=velocity, 2=pressure),

- (if =1, velocity boundary conditions) velocity in the x-direction (m/s), velocity in the y-direction (m/s), velocity in the z-direction (m/s), mass inflow (kg/s, set the mass inflow to a non-zero value, only when the momentum method is used for the inlet), temperature (^{o}C) and total number of contaminants (must be <=5; if no contaminant computation, put '0' or leave it blank), respectively.
  - (if total number of contaminants≠0) the next line: index of the contaminant (1-5), mass fraction of this contaminant.
    Repeat for all the contaminants
- (if =2, pressure boundary conditions) pressure (Pa), mass flow coefficient (kg/s·Pa^{n} , if opening type is '2', the flow coefficient and exponent specified here will not be used), flow exponent, temperature (^{o}C) and total number of contaminants (must be <=5; if no contaminant computation, put '0' or leave it blank), respectively.
  - (if total number of contaminants≠0) the next line: index of the contaminant (1-5), mass fraction of this contaminant.
    Repeat for all the contaminants

Repeat for all the inlet openings

The next block: Exists only when NBOUT>0

The next two lines:	Title information for outlet opening(s)
The next line:	Title for the x-direction
The next line:	The first and last grid number of the opening in the x-direction
The next line:	Title for the y-direction
The next line:	The first and last grid number of the opening in the y-direction
The next line:	Title for the z-direction
The next line:	The first and last grid number of the opening in the z-direction
The next line:	types of openings [1] (1=small opening; 2=large openings), types of boundary conditions (1=velocity, 2=pressure),

- (if =1, velocity boundary conditions) velocity normal to the outlet (m/s), mass outflow (kg/s, from which CFD0 compute the outlet velocity internally), temperature (^{o}C) and total number of contaminants (must be <=5; if no contaminant computation, put '0' or leave it blank), respectively.
  - (if total number of contaminants≠0) the next line: index of the contaminant (1-5), mass fraction of this contaminant.
    Repeat for all the contaminants
- (if =2, pressure boundary conditions) pressure (Pa), mass flow coefficient (kg/s·Pa^{n} , if opening type is '2', the user-specified flow coefficient and exponent will not be used), flow exponent, temperature (^{o}C) and total number of contaminants (must be <=5; if no contaminant computation,

put ‘0’ or leave it blank), respectively.

- (if total number of contaminants≠0) the next line: index of the contaminant (1-5), mass fraction of this contaminant.
  Repeat for all the contaminants

Repeat for all the outlet openings

The next two lines: Title for the blockage number

The next line: The total number of the blockages

The next block: Exists only when the total number of the blockages is greater than zero

The next two lines: Title for the first blockage

The next line: Title for the x-direction

The next line: The first and last grid number of the blockage in the x-direction

The next line: Title for the y-direction

The next line: The first and last grid number of the blockage in the y-direction

The next line: Title for the z-direction

The next line: The first and last grid number of the blockage in the z-direction

The next line: Title for blockage types, the heat flux and number of contaminant (if any)

The next line: The blockage type (1=solid blockage; 2=fluid blockage), The heat generation rate from the blockage, HSOU (W) and the total number of contaminants (if ≠0, must <=5; if =0, just leave it to blank)

- (if total number of contaminants≠0) the next line: index of the

contaminant (1-5), mass generation rate of this contaminant[2] (kg/s).
Repeat for all the contaminants

Repeat for all the blockages.

The next two lines: Title for non-adiabatic surfaces given by a constant temperature

The next line: The total number of non-adiabatic surfaces with a constant temperature (NAWT)

The next block: Exists only when NAWT>0

- The next two lines: Title for the first surface
- The next line: Title for the x-direction
- The next line: The first and last grid number of the surface in the x-direction
- The next line: Title for the y-direction
- The next line: The first and last grid number of the surface in the y-direction
- The next line: Title for the z-direction
- The next line: The first and last grid number of the surface in the z-direction
- The next line: Title for the temperature
- The next line: The surface temperature, TNAW (^{o}C)

Repeat for all the surfaces.

The next two lines: Title for surface sources of heat (given by a constant heat generation rate) and of contaminant (given by a constant mass generation rate)

The next line: The total number of surface sources with a constant heat rate or contaminant mass rate (NAWQ)

The next block: Exists only when NAWQ>0

- The next two lines: Title for the first surface
- The next line: Title for the x-direction
- The next line: The first and last grid number of the surface in the x-direction

The next line:	Title for the y-direction
The next line:	The first and last grid number of the surface in the y-direction
The next line:	Title for the z-direction
The next line:	The first and last grid number of the surface in the z-direction
The next line:	Title for the heat rate and mass rate
The next line:	The heat generation rate (QNAW (W), if no heat, just put '0'), the total number of contaminants (if ≠0, must <=5; if =0, just leave it to blank)

- (if total number of contaminants≠0) the next line: index of the contaminant (1-5), mass generation rate of this contaminant[2] (kg/s). Repeat for all the contaminants

Repeat for all the surfaces.

The next four lines:	Title for numerical and control parameters
The next two lines:	Title for differential schemes of U,V,W,T and C
The next line:	The differential schemes of U, V, W, T, C [3] (1=Upwind; 2=Power Law)
The next two lines:	Title for initial and reference temperature
The next line:	Initial temperature (^{o}C) (TINIT) and reference temperature (^{o}C) (TM)
The next two lines:	Title for buoyancy model
The next line:	Buoyancy model [4] (1=Bousinesq; 0=non-Bousinesq, density variable with temperature)
The next two lines:	Title for minimum and maximum values
The next line:	The minimum and maximum values for U velocity (m/s), V velocity (m/s), W velocity (m/s), and temperature (^{o}C) (UMIN, UMAX, VMIN, VMAX, WMIN, WMAX, TMIN, TMAX), respectively

The next two lines:	Title for under-relaxation
The next line:	The linear under-relaxation values [3] for U velocity, V velocity, W velocity, pressure, temperature, kinetic energy, dissipation rate and contaminant (URFU, URFV, URFW, URFP, URFT, URFEK, URFED, URFC)
The next two lines:	Title for false-time-steps
The next line:	The false-time steps [3] for U velocity, V velocity, W velocity, pressure, temperature, kinetic energy, dissipation rate and contaminant (DTU, DTV, DTW, DTT, DTKE, DTED, DTC)
The next two lines:	Title for change of false time step
The next line:	Set T if the change for the false time step is needed
The next two lines:	Exists only when 'T', Title for new false time step
The next line:	The iteration number when the new false time step is to be used (ISTEP) and the new false time steps [3] for U velocity, V velocity, W velocity, temperature, kinetic energy, dissipation rate and contaminant (CDTU, CDTV, CDTW, CDTT, CDTKE, CDTED, CDTC)
The next two lines:	Title for printing frequency
The next line:	Printing frequency for the residuals during the calculation to the PC monitor (PINTV)
The next two lines:	Title for monitoring point
The next line:	The grid number for the monitoring point in the x-, y-, and z-direction (IMON, JMON, KMON), respectively
The next two lines:	Title for reference point
The next line:	The grid number for the reference point in the x-, y-, and z-direction (IREF, JREF, KREF), respectively
The next two lines:	Title for printing frequency to the *.RET (text results) file
The next line:	The number of the first control volume, last control volume and interval for printing results in the x-direction (IP1, IP2, IPSTP) and

	the number of the first control volume, last control volume and interval for printing results in the y-direction (JP1, JP2, JPSTP)
The next two lines:	Title for restarting the computation based on the results of the previous computation and output control parameter of EWC file and output control parameter for *.CFDLOG file
The next line:	Set to 0 if not starting from the previous results and set to 1 if starting from the previous results (ICOMPU), EWC output control parameter (EWCYN) (0=do not create EWC file; 1=create EWC file), output control parameter for *.CFDLOG file (DUMPLOG) (0=do not create *.CFDLOG file; 1=dump input data only; 2=dump residuals of pressure correction equation only; 3=dump both input data and residuals of pressure correction equation for code checking)
The next four lines:	Title for ambient conditions and material properties
The next two lines:	Title for ambient pressure
The next line:	Ambient pressure (PAMB, (Pa))
The next line:	Title for fluid reference density
The next line:	Reference density (REFDENS,(kg/m^3), usually=1.2kg/m^3 for air)
The next line:	Title for fluid operating density
The next line:	Operating density (OPERDENS, (kg/m^3), usually= the ambient density)
The next line:	Title for kinematic viscosity
The next line:	Fluid kinematic viscosity (m^2/s) (ANU)
The next line:	Title for thermal conductivity
The next line:	Fluid thermal conductivity (W/m K) (AK)
The next line:	Title for specific heat at constant pressure
The next line:	Fluid specific heat at constant pressure (J/kg K) (ACP)
The next line:	Title for Prandtl number
The next line:	Fluid Prandtl number (PRL)

NOTE

[1] Explanation of types of openings. If it is a small opening, the user-specified flow coefficients and exponents will be used for the pressure boundary conditions to characterize the opening resistance. If it is a large opening, these parameters will not be used. Instead, the conventional CFD method of handling the flow resistance of openings is used. For details refer to the section 2.1.2 of Chen and Wang (2005).

[2] If the mass generation rate of a contaminant source is at the scale of 10^{-6} kg/s, for example 2.0×10^{-6} kg/s, 2.0 kg/s is suggested be used instead of 2.0×10^{-6} kg/s so that the computed mass fraction will be in the unit of PPM. Usually, a value of 2.0 kg/s also helps to avoid possible round-off errors, which may be caused by a value of 2.0×10^{-6} kg/s.

[3] The setting of the input information requires experience and expertise in CFD simulations and it is recommended that the default values specified in the template input file of CFD should be used.

[4] CFD0-C uses the Bousinesq buoyancy model, in which only the density in the W momentum equation is variable with temperature.

[5] For the WPP link, CFD0-C will first check if there is an existent VAR file for a certain wind angle. If yes, CFD0-C will skip the calculation for this wind angle and continue to calculate the next wind angle. For example, for a simulation of "Case1.CFD" of the wind angle from 0° ~ 360° with a step of 30°, a WPP calculation will skip the calculation for the wind of 90° if there is already a file with the name of "Case1-wind-90.VAR". The file name of "Case1-wind-90.VAR" is created automatically for each wind angle during a WPP calculation.

[6] If a WPP simulation for a certain wind angle is not convergent (for example, more than 2000 iterations), CFD0-C will not create a VAR file for that wind angle. To get

convergence, users can adjust control parameters and restart the whole calculation. For previously-convergent wind angles, which already have their VAR file created, the restart will not calculate them again. CFD0-C will only calculate those which are not convergent at the previous run before user's adjustment of the control parameters.

A.4 Result Analyses from Outputs

The results of CFD0-C simulations can be screen outputs, which are for convergence monitoring, and file outputs, which are for visualization and further analyses.

Monitoring Screen Outputs during CFD Calculation

During the calculation, several important parameters are displayed on the PC monitor, which monitors the calculation progress. These parameters are:

- NITER: the index of iteration,
- RESOU, RESOV, RESOW, RESOT, and RESOM: the relative residuals for the air velocity component of U, V, W, air temperature, and air mass continuity respectively, and
- the location of the monitored grid point and the values of U, V, W and T at the monitored grid point.

The output frequency of the screen monitoring can be specified in the CFD input file.

CFD Result Analyses through Output Files

After CFD0-C simulations, several output files are created, i.e. *.BAL, *.RET, *VAR, *.DAT, *. OUT, and optional outputs, *.CFDLOG, *.EWC, *.WDB, and *.CDB.

The BAL file contains residual values of air mass, T, U, V and W momentum equations at each iteration during the calculation, which is the same as the screen monitoring outputs during the calculation. It can help users to check the convergence after the completion of the calculation.

The RET file contains the results of the air velocity component of U, V, W, the mean scalar velocity, temperature, contaminant concentration, and effective turbulence viscosity. The output frequency in the X-direction (or I-direction) and the Y-direction (or J-direction) can be controlled in the CFD input file.

The VAR file stores the whole airflow results in binary format after the completion of a CFD simulation. The results can be used to restart the airflow calculation, or calculate steady/transient contaminant dispersion. A format description of the binary VAR file can be found in Appendix A.7.

The DAT file is in TECPLOT data file. TECPLOT is a post-processing program for visualization and analysis of the numerical data. The CFD0-C DAT file includes the following data:

- the positions of the cell center (X, Y and Z)
- the values of the velocity components at the cell center (UC, VC and WC)
- averaged air velocity (VTT), pressure (P), temperature (T), contaminant concentration (C1, C2, …, C5), total pressure (TP), wind pressure coefficient (CP), and effective turbulence viscosity (VIS)
- control parameter for "Value Blanking" in TECPLOT of blockages (BLANK). To use "Value Blanking" in TECPLOT, users can choose "Blank entire cell" to be "when all corners are blanked", "Constraint" to be "Blank When BLANK is less than or equal to 0". This will make only solid blockages visible in TECPLOT visualization, e.g. building blocks, so that the calculated contour values on building surfaces can be shown.
- name of CFD objects for "Object Labeling" in TECPLOT (OBJECTS). The "Object Labeling" will help users to identify the names of different objects in TECPLOT, which is very helpful for simulations with many inlets, outlets, or blockages. To use the "Object Labeling" in TECPLOT, users need to go to "Label Points and Cells" in TECPLOT's PLOT Menu, Choose "Show Node Labels" and Select OBJECTS for "Show Variable Value", then select "Number Format" to be

"Custom".

The OUT file is an ASCII file, which is required by the CFD0-C GUI for visualization purposes. It is a counterpart in the CFD0-C GUI as the DAT file in TECPLOT. The current version of the CFD0-C GUI can only visualize results of steady-state simulations. Users should use the DAT file in TECPLOT for transient simulations.

The CFDLOG is an optional log file for the purpose of checking the input data of CFD0-C and the residuals of pressure correction equation of each iteration for advanced users.

The EWC file is an optional wind pressure data file in binary format for pressure information around a building to be used by CONTAM. A format description of the binary EWC file can be found in Appendix A.7.

The WDB file is an optional file containing wind pressure coefficients in binary format for the WPP link of CFD0-C and CONTAM. A format description of the binary WDB file can be found in Appendix A.7.

The CDB file is an optional file containing atmospheric contaminant concentrations in binary format for CONTAM. A format description of the binary CDB file can be found in Appendix A.7.

A.5 Program Structure of CFD0-C

The source codes comprise of three C source files and six C header files as show in Table A.2. CFD0-C borrowed many valuable functions and ideas from CONTAM so that some new features were added since the FORTRAN version of CFD0, e.g. dynamic allocation of memory, which was developed by Mr. George Walton of NIST, USA.

CFD0-C source codes can be compiled in two modes: a stand-alone CFD0-C program and a coupled program with CONTAMX source code. A macro with the name of 'FLOWC' in the first line of flow.c defines the mode. For the default value of '1', CFD0-

C works as a stand-alone CFD program and the value of ‘0’ means that CFD0-C works in the mode of coupling with CONTAM. The most recent version to be coupled with CFD0-C is CONTAM2.4b dated at August 2006. Fig. A.6 is the program structure of CFD0-C and Table A.3 describes each of CFD0-C functions.

Table A.2 The source code files of CFD0-C.

C Source Files	
flow.c:	a CFD0 core file, containing all CFD functions;
HeapCFD.c:	a utility file and a counterpart of Heap.c in CONTAM, containing functions of dynamic allocation and deallocation of memories;
UtilsCFD.c:	a utility file and a counterpart of Utils.c in CONTAM, containing functions of management of input and output file names;
C Header Files	
comflo.h:	a header file, declaring all global variables in flow.c;
fprtype.h:	a header file, declaring all functions in flow.c;
prtypCFD.h:	a header file and a counterpart of prtyp.h in CONTAM, declaring functions in HeapCFD.c and UtilsCFD.c;
sglobCFD.h:	a header file and a counterpart of sglob.h in CONTAM, declaring variables about paths and names of input and output files;
sxtrnCFD.h:	a header file and a counterpart of sxtrn.h in CONTAM, declaring some temporary variables;
typesCFD.h:	a header file and a counterpart of types.h in CONTAM, defining types of variables.

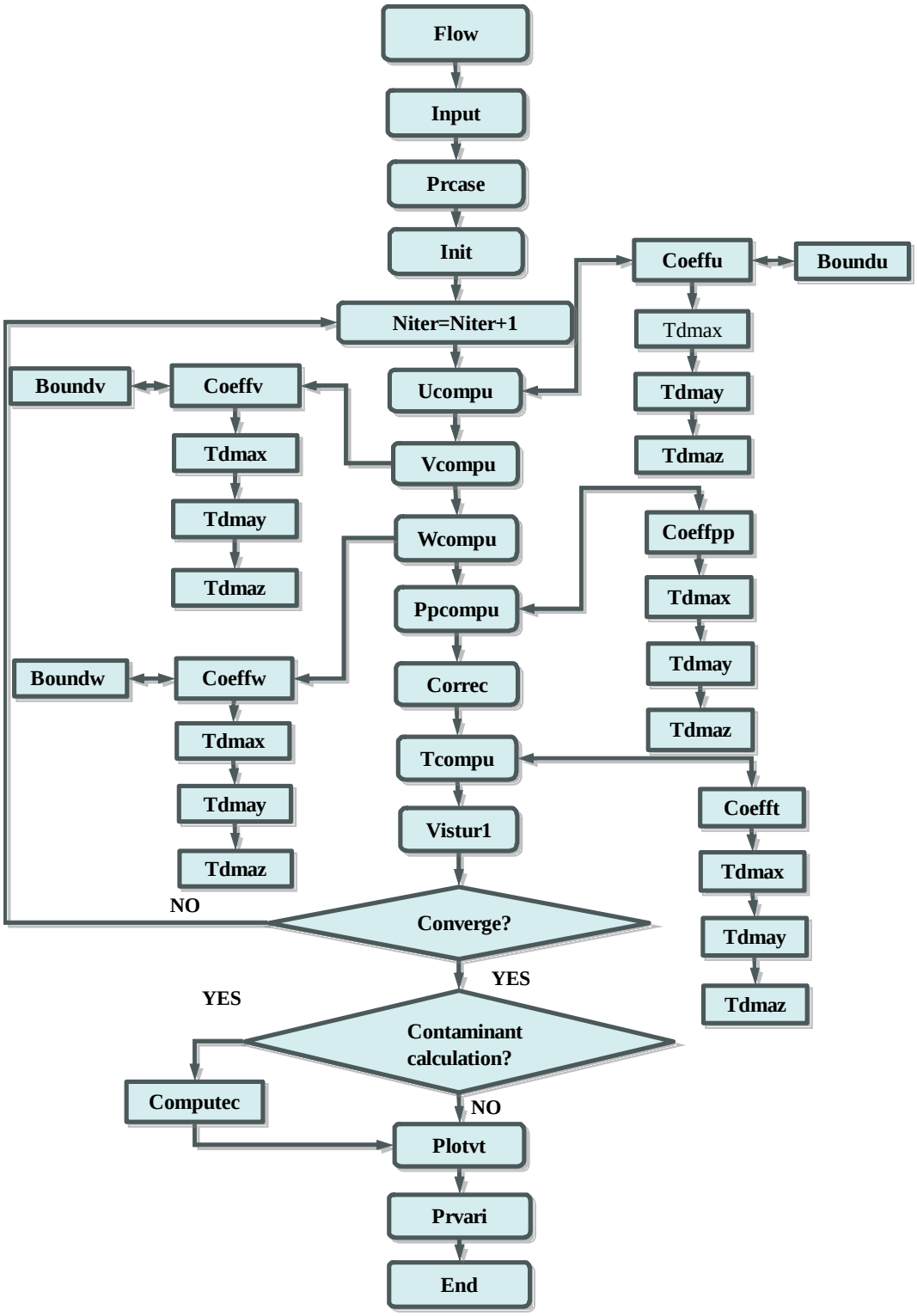

Fig. A.6 Program structure of SIMPLE algorithm in CFD0-C.

Table A.3 The description of CFD0-C functions.

Flow	Main program;
Input	Read CFD0-C input files;
Prcase	Create the RET file;
Init	Initialize CFD0-C simulations;
Coeffu, Coeffv, Coeffw, Coefft, Coeffpp	Calculate coefficients of X , Y , Z momentum equations, energy equation and pressure correction equation, respectively;
Boundu, Boundv and Boundw	Implement boundary conditions for X , Y and Z momentum conservation equations, respectively;
Ucompu, Vcompu and Wcompu	Solve U , V and W velocities through momentum conservation equations, respectively;
Ppcompu	Solve pressure correction equation;
Correc	Correct air velocities based on the results of pressure corrections;
Tcompu	Solve energy equation;
Computec	Solve species conservation equation;
Vistur1	Update effective turbulence viscosities;
Tdmax, Tdmay and Tdmaz	Solve linear equations by TDMA algorithm in X, Y and Z directions, respectively;
Plotvt	Create TECPLOT data files;
Prvari	Output CFD results to the RET files.

Note: Niter is the current number of iterations.

A.6 Description of Variables Used in the CFD0-C Code

This section describes the global variables used in the source code of CFD0-C.

- TITLE - a character variable, (dimension defined by LINELEN, default, up to 144 characters), for the title of the simulated case.
- XX, YY, ZZ - real variables for the flow domain in the X, Y, and Z direction, respectively. Note that the gravitational force is always in the negative z-direction. For a two-dimensional case, use 0.0 m for the third dimension, but the program will adjust it to 1.0 m automatically.
- NNX, NNY, NNZ - the number of control volumes (grids) in the x-, y-, and z-direction, respectively.
- DELX, DELY, DELZ - the arrays that store the dimension for each control

volume (grid size) in the X, Y, and Z direction, respectively. The sum of all the control volumes in the x-direction must be equal to XX. The same rule applies to YY and ZZ.

- X, Y, Z - the arrays that contain the coordinates for the grid nodes (control volume centers).
- AREX, AREY, AREZ - the arrays that store the surface area for each control volume normal to the x-, y-, and z-axis, respectively.
- VOL - a three-dimensional array with volume size for each control volume.
- NBIN - the total number of the inlet openings. This number should be equal or less than ten.
- LBIN - an array to define the location of an inlet opening by the first and last control volume occupied by the inlet in the x-direction, the first and last control volume occupied by the inlet in the y-direction, and the first and last control volume occupied by the inlet in the z-direction, respectively. For a two-dimensional inlet, the third direction is represented by the two same numbers. If the inlet opening is on the x=0 wall, use 1, 1 for instance. The inlet must be on a wall not in the flow domain.
- UBIN, VBIN, WBIN - the arrays that store inlet velocities in the x, y and z direction, respectively.
- AMASSIN - an array for the mass flows through the inlet.
- TBIN - an array for the inlet temperature.
- NBOUT - the total number of the outlet openings. This number should be equal or less than ten.
- LBOUT - an array that defines location of the outlet openings in the same way as that for LBIN. Outlet openings are treated as two-dimensional objects that can be placed on the enclosure walls. Hence, rules explained for the definition of location for inlet openings also apply for the outlet opening.
- VBOUT - an array for the outlet velocity. The values should be set in accordance with mass continuity.
- TBOUT - an array for the outlet temperature. These values should be set as close

as possible to the real value. The outlet temperature and velocity have an impact on the convergence speed.

- NBL - the total number of the blockages used in the flow field. The blockages are usually used for furniture, lights, occupants, partition walls, etc. This number should be equal or less than fifty.
- IBL - an array that defines positions for each blockage in the same way as LBIN. The blockages are always three-dimensional and must be in the flow domain.
- HSOU - an array that stores the heat generated by each blockage.
- NAWT - the total number of the enclosure surfaces with a constant temperature. The maximum number of the non-adiabatic surfaces is fifty.
- LNAW - an array that defines the positions for the surfaces in the same way as that for LBIN. The definition of the location has the same restrictions as for the inlets.
- TNAW - an array for the temperature of the non-adiabatic walls.
- NAWQ - the total number of enclosure surfaces with constant heat flux. The maximum number of the non-adiabatic surfaces is fifty.
- LNAWQ - an array that defines the positions of the enclosure areas with heat flux. The definition of the location has the same restrictions as for inlet openings.
- QNAW - an array for the heat from the non-adiabatic walls
- NITMAX - the maximum iteration number for the run.
- CRITE - a convergence criterion. The computation ends when the total residual is smaller than CRITE or when the maximum iteration number is reached.
- LAMIN - a logical variable to identify if the flow is laminar (true) or turbulent (false)
- ITUR - a parameter to select turbulence model. When ITUR=0, the zero-equation model is used. When ITUR=1, the standard k- model (Launder and Spalding 1974) is used. However, the standard k- model may not work properly at present.
- TINIT - an initial value for the temperature field. The initial velocities are internally set to zero.

- TM - the reference temperature
- UMIN, UMAX, VMIN, VMAX, WMIN, WMAX, TMIN, TMAX - the minimum and maximum values for U, V, W, and T, respectively, during the solving procedure. This will help the solution because the values will not run out of control during the iteration. Those ranges, however, should be wide enough.
- URFP, URFU, URFV, URFW, URFT - the linear under-relaxation factors for P, U, V, W, and T, respectively. The value of these factors should be between 0 and 1. A value of 1 implies no relaxation. A lower value will slow the convergence but will stabilize the calculation.
- DTU, DTV, DTW, DTT - the false time steps for U, V, W, and T, respectively. The false time steps work in a similar way as the linear under-relaxation factors. However, the range of the false time steps can be from 10-30 to 1030. A large value means no relaxation and a small value implies heavy relaxation. The false time steps can be increased one order higher or lower in the calculation to achieve a converged solution.
- ISTEP - the iteration number when the new false time step to be used. In some cases, it is possible to speed up the convergence by changing values of the false time steps during the calculation.
- CDTU, CDTV, CDTW, CDTT - new false-time-step values for U, V, W, and T, respectively. As a rule of thumb they can be used one order higher than those set for DTU, DTV, DTW, DTT.
- PINTV - a real variable setting the printing frequency for the residuals during the calculation
- IMON, JMON, KMON - the grid number in the x-, y-, and z-direction, respectively, for the monitoring point. When the values of the variables at the monitoring grid do not change significantly, a converged solution is reached.
- IREF, JREF, KREF - the grid number for the reference point. It should not be inside a blockage.
- IP1, IP2, IPSTP - The number of the first control volume, last control volume and interval for printing results in the x-direction.

- JP1, JP2, JPSTP - The number of the first control volume, last control volume and interval for printing results in the y-direction
- ICOMPU - Set to 0 if not starting from the previous results and set to 1 if starting from the previous results
- DENS - Fluid density (kg/m3)
- ANU - Fluid kinematic viscosity (m2/s)
- AK - Fluid thermal conductivity (W/m K)
- ACP - Fluid specific heat at constant pressure (J/kg K)
- PRL - Fluid Prandtl number

A.7 Description of Formats of Binary Output Files

The following rules are used to describe the formats of the binary files.

- There are no separations between any pair of data values, such as Space, Comma, and Period etc.
- The description of data formats and other explanations are bracketed and are not output information of the binary file.

The Format of the VAR File

(From the first grid in X direction, I1, to the last grid in X direction, IMAX, repeats the following)

(From the first grid in Y direction, J1, to the last grid in Y direction, JMAX, repeats the following)

(From the first grid in Z direction, Z1, to the last grid in Z direction, ZMAX, repeats the following)

U (velocity in X direction at i, j, k; double)

V (velocity in Y direction at i, j, k; double)

W (velocity in Z direction at i, j, k; double)

P (pressure at i, j, k; double)

T (temperature at i, j, k; double)

VIS (effective turbulence viscosity at i, j, k; double)

The Format of the EWC File

Fig. A.7 shows the output domain, for which CFD0-C creates the EWC, WDB, and CDB files. For a detailed explanation of the data format, please refer to the function in FLOW.C, **void makeewc()** .

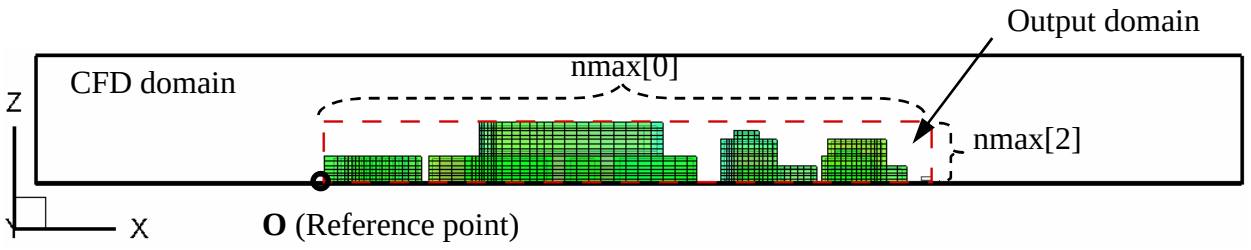

Fig. A.7 The flow domain inside the dashed box is output to create the EWC, WDB, and CDB files (note that Point O is the origin of the output domain, at which xref, yref, zref is the ordinates relative to the whole CFD domain).

The Format of the WDB File

(The WDB file is created by the same function as that for the EWC file in FLOW.C, **void makeewc()**, except that "**COUPLEWPP=1**". Please refer to the FLOW.C source code for the data and binary file format.)

The Format of the CDB File

(The CDB file is created by the function in FLOW.C, **void makecdb()**, which uses very similar data and file formats to that of the WDB file. Please refer to the FLOW.C source code for details.)

Appendix B. Manual for the Coupled CONTAM-CFD0C Program

The coupled CONTAM-CFD0C program will embed CFD simulations of selected zones in the multizone calculations of airflow network. The two programs can iteratively exchange airflow rates or pressure boundary conditions with each other. A resistance model can also be specified for the paths connecting multizone and CFD zones. A coupling definition file, *.CPL, is needed to provide required control parameters for a coupled simulation. The coupled program will also create an output file, *.CMO, which contains intermediate convergence information and final calculation results. Users can check the results also from CONTAMW or the output files of CFD0-C.

B.1 Preparation of an Definition File for a Coupled Simulation

An ASCII coupling definition file, *.CPL, is required to specify which zone is the CFD zone, what methods should be used for airflow paths connecting multizone and CFD zones, and coupling control parameters. It can be prepared and edited manually by following the file format as the next. Users may want to edit the provided sample/template file for their own simulations. Note that all the input data values must be separated by comma. Some more explanations can be found in the notes at end of this section.

Lines	**Input Data**
The first three lines:	Notation lines
The next one line[NOTE1]:	Total number of CFD zones, Running mode of the coupled simulation (0=Quasi coupling; 1=Dynamic coupling; 2=Post-processing; 3=CFD only; 4=CONTAM only), Coupled contaminant transport simulation (0=No; 1=Steady state; 2=Transient state), Contaminant index number in CFD simulation (only needed for coupled contaminant transport simulation), Calculate Contaminant

transport from a previously-calculated CFD airflow data file? (0=No; 1=Yes)

Repeat the following section for each CFD zone

{

The next two lines: Notation lines

The next one line: Zone index number in CONTAM, Total number of coupled airflow paths for this zone (all airflow paths of the CFD zone should be included)

Repeat the following section for each coupled airflow path of this zone [NOTE2]

{

The next two lines: Notation lines

The next one line: Airflow index number in CONTAM, large or small opening (1=Small; 2= Large), Type of boundary condition for CFD0 run provided by CONTAM (0=Constant mass airflow rate; 1=Mass airflow rate, which is variable during the coupling iteration; 2=Constant pressure condition; 3=Pressure condition, which is variable during the coupling iteration), Type of boundary condition for CONTAM run provided by CFD0 (0=Change the flow coefficient in CONTAM, based on algorithm of Gao (2002; 2003); 1=Pressure condition, which is local value near airflow path in the CFD zone; 2=Mass airflow rate, which is variable during the coupling iteration; 3=No feed back from CFD0 for CONTAM)

}

}

The next two lines: Notation lines

The next one line[NOTE3]: Reference zone (0=the ambient; index number if it is a zone other than the ambient zone)

The next two lines:	Notation lines
The next one line[NOTE4]:	Maximum coupling iterations (for dynamic/direct coupling only); Output intermediate coupling results to the CMO file? (0=No; 1=Yes; 2=dump intermediate results of coupled transient contaminant dispersion simulations), Clear allocated internal memory for CFD0 simulation? (1=Yes; 0=No), Step for output the CMO file

NOTE

[1] The current version of the coupled program is only tested for the coupled simulation with only one CFD zone. Further tests are needed for more than one CFD zones.
Quasi coupling means the coupled program running in a mode of "CONTAM-CFD0-CONTAM", which involves no further coupling iterations between the two programs.
Dynamic coupling is the direct coupling of CONTAM and CFD0, for which the running mode is "CONTAM-CFD0-CONTAM" with iterations until the coupling convergence criterion is met, i.e. the exchanged boundary conditions stabilize.

The mode of Post-processing means "CONTAM-CFD0", in which CFD0 simply obtains boundary conditions from CONTAM without feeding back information or further coupling iterations.

In the CFD-only running mode, CFD0 will be run as a stand-alone program. That is to say, CFD0 will read the boundary conditions from the CFD input file, *CFD, instead obtaining them from CONTAM. There are no actual coupling between CONTAM and CFD0.

In the CONTAM-only running mode, CONTAM will be run as a stand-alone program without calling CFD0. The modes of CFD-only and CONTAM-only are for advanced purposes such as debugging the codes etc.

Contaminant index number refers to the contaminant species simulated by the coupled simulation. Since the current version of the coupled program can simulate only one contaminant species at one time, users must specify which contaminant species needs to be calculated if multiple species (≤5) are defined in CFD0.

Users can calculate contaminant transport from a previously-calculated CFD0 airflow data file, i.e. the VAR file. This is useful for coupled simulations of steady-state airflow and steady-state contaminant transport, or steady-state airflow and transient contaminant transport. For transient airflow and transient contaminant transport, this option means that the VAR file is used as an initial airflow conditions.

[2] The coupled airflow paths must be defined in the CPL file in the same order as they are defined in the CFD input file, the CFD file.

Large or small opening refers to how to consider the flow resistance in CFD0. For details, refer to the manual of CFD0-C. It is considered that for large openings, conventional CFD methods of implementing pressure boundary conditions should be used. That is to say, pressure boundary condition is looked at as stagnation pressure for inflow opening and as static pressure for outflow opening (Kelka and Choudhury, 2000). For small openings, a power-law resistance model can be specified for CFD0 simulation by flow coefficient and exponent, if it is considered necessary and appropriate.

For CFD0 run, CONTAM can provide several different boundary conditions. Constant mass airflow rate is for fans or other devices with fixed mass flow rates. For the cases, where mass flow rates are calculated, variable mass flow rate condition should be used. If an airflow path of the CFD zone is connected to the ambient or a zone with known pressure, constant pressure condition should be used. For the rest cases with pressure boundary conditions, pressures are calculated so that variable pressure condition should be used.

For CONTAM run, CFD0 can feed back several boundary conditions too. The method of "change the flow coefficient" is suggested by Gao (Gao, 2002; 2003), which needs to be further validated. The rest two methods, "pressure condition" and "mass airflow rate", are the methods suggested by this study, which should be used for common users. For example, the method of "**Pressure-Pressure**" coupling for a **large** opening with an index number **12** should use the following definition: 12,2,3,1 if it is not connected to the ambient, or 12,2,2,1 if it is connected to ambient or a zone with known pressure. One more example, for a fan with **constant mass flow rate** and index number **5** in CONTAM, users should use 5,1,1,3 or 5,2,1,3. Here, it is not important if the fan is considered large opening or small opening since there are no resistance model needed for a fan.

[3] The specification of reference zone is needed to obtain reference temperature, reference density values for CFD simulations. It is suggested to use the ambient zone as the reference zone.

[4] The maximum coupling iteration is used to end the coupled simulation if the coupling convergence criterion is not met after a long run. The output of intermediate results to the CMO file and The function of clearing allocated internal memory are for debugging purposes. It is suggested use No for both options. A frequent output to the CMO file will result in a big file size. Therefore, it is suggested to use a big value of the output step, for example, 50 or 100.

B.2 The Output File of a Coupled Simulation

A output file, the CMO file, will be created to provide intermediate results for debugging purposes, and final results of convergence of a coupled simulation.

Format Description of Intermediate Output in a CMO File (Optional Output)

- In a CMO file: **Path, Outlet?, Flow1, Flow2, Pbc1, Pbc2, Coe, Exp**

Explanation:

Path: coupled airflow path index number;

Outlet?: is it an outlet or inlet? 1=outlet; 0=inlet, as related to the CFD zone;

Flow1: CONTAM-calculated mass airflow rate at the previous coupling iteration;

Flow2: CONTAM-calculated mass airflow rate at the current coupling iteration;

Pbc1: CONTAM-calculated pressure boundary conditions at the previous coupling iteration;

Pbc2: CONTAM-calculated pressure boundary conditions at the current coupling iteration;

Coe: linearized flow coefficient of the airflow path

Exp: exponent of the resistance model of the airflow path

- In a CMO file: **FlowBC, Pbc, Coe, Exp, udrl**

Explanation:

FlowBC: boundary condition of mass flow rate, which is provided by CONTAM for CFD0

Pbc: pressure boundary condition, which is provided by CONTAM for CFD0

Coe: linear flow coefficient used in CFD0 simulation

Exp: flow exponent of the resistance model used in CFD0 simulation

udrl: under-relaxation factor used in exchanging boundary conditions

- In a CMO file: **Path, Outlet?, Cmass1, Cmass2, Pcfd1, Pcfd2, Coe, Exp, Mult, Crate1, Crate2**

Explanation:

Path: airflow path index number

Outlet?: is it an outlet or inlet? 1=outlet; 0=inlet, as related to the CFD zone;

Cmass1: CFD0-calculated mass flow rate at the previous coupling iteration;

Cmass2: CFD0-calculated mass flow rate at the current coupling iteration;

Pcfd1: CFD0-calculated local pressure near the airflow path at the previous coupling iteration;

Pcfd2: CFD0-calculated local pressure near the airflow path at the current coupling iteration;

Coe: linear flow coefficient used in CFD0 simulation

Exp: flow exponent of the resistance model used in CFD0 simulation

Mult: correction of the multiplier for implementation of local pressures in CONTAM

Crate1: CFD0-calculated contaminant mass flow rate through the airflow path at the previous coupling iteration;

Crate2: CFD0-calculated contaminant mass flow rate through the airflow path at the current coupling iteration;

- In a CMO file: **CONTAM Time: XXX, CFD0 TIME: XXX**
  path XXX
  : XXXXXX**[kg/s]** XXXXXX**[kg/kg]**

Explanation:

CONTAM Time: current simulation time in CONTAM for debugging purposes;

CFD0 Time: current simulation time in CFD0 for debugging purposes;

path: airflow path index number involved in coupled contaminant dispersion simulation followed by CFD0-calculated contaminant mass flow rate [kg/s] transferred to CONTAM as contaminant source through the coupled airflow paths and CFD0-calculated local contaminant concentration [kg/kg] transferred to CONTAM.

Format Description of Final Output in a CMO File (Normal Output)

- In a CMO file: **Path CPL CFD0_NITER Coe_CONTAM Exp_CONTAM PressureB_CONTAM PressureB_CFD0 Mass_CONTAM Mass_CFD0 PressureL_CFD0 Pressure_ext_CFD0**

Explanation:

Path: index number of coupled airflow path;

CPL: Coupling iteration number

CFD0_NITER: total internal iterations of CFD0 to achieve CFD convergence at current coupling iteration

Coe_CONTAM: corrected flow coefficient at current coupling iteration in CONTAM for this path

Exp_CONTAM: flow exponent of this path at current coupling iteration in CONTAM

PressureB_CONTAM: pressure boundary condition calculated by CONTAMCFD0 for CFD0 at current coupling iteration

PressureB_CFD0: actual pressure boundary condition used in CFD0 simulation, which could be different from PressureB_CONTAM due to possible under-relaxation. By default, they are the same.

Mass_CONTAM: mass flow rate calculated by CONTAM;

Mass_CFD0: mass flow rate calculated by CFD0

PressureL_CFD0: local pressure, i.e. pressure boundary condition, calculated by CFD0

Pressure_ext_CFD0: flow coefficient should be corrected for the next CONTAM run in order to achieve the goal of Mass_CONTAM=Mass_CFD0.

B.3 Modifications in CONTAMX and CFD0-C for the Coupled Program

Advanced users can compile the coupled source codes if needed. First, users need to change the first line of FLOW.C from "#define FLOWC 1" to "#define FLOWC 0". Then, they can copy flow.c, comflo.h, fprtype.h and other two files, couple.c and interface.h, into the directory of the source codes of CONTAMX and recompiled all source files to get the executable of the coupled CONTAM-CFD0 program. Note that the version of coupled source codes works with the CONTAM version of CONTAM2.4b dated at August 2006 or prior ones.

This appendix shows the changes (in italic fonts) made to the CONTAMX source code for the coupling with CFD0-C. The purposes for these changes are explained in the brackets after the line number. Advanced users can always search "//coupling" through all the source code files to find where the modifications are needed in CONTAMX.

- WndProc.c (for the WPC link in order to create the WPC file in the same directory with the EWC file, the following codes in 'WndProc.c' were changed in the CONTAM source codes)

  - Line 29

    I1 _wpcdrive[_MAX_DRIVE]; / drive letter for WPC file */*

    I1 _wpcdir[_MAX_DIR]; / directory path for WPC file */*
  - Line 1562

    if(streql(_PLDdat.WPCfile, "null"))

    {

    pathsplit(_PLDdat.EWCfile, _wpcdrive,_wpcdir,_string,_stringx);

    pathmerge(_PLDdat.WPCfile, _wpcdrive, _wpcdir, _prjname, ".WPC");

    }

- contamx.c

  - Line 45: (the following line added to call function cplloop(), a function in coupling data interface, within CONTAMX)

    extern IX cplloop();
  - Line 371: (the following line added a label in CONTAMX to form a coupling loop within CONTAMX together with the next changes in Line 482)

    L200:
  - Line 482: (the following line and the previous Line 371 form a loop within CONTAMX for the coupling)

    if(COUPLE)

{
if(cplloop()) goto L200;
}

- heap.c (some new functions added for 3D arrays allocation in CFD0, they are: alc_ac, chk_ac and fre_ac)

  - Functions of dynamic allocation of 3D arrays for CFD0

- simulate.c

  - Line 35: (the following line added to call incontam_loc() in CONTAMX, a function to change the local pressure of the paths in the pressure-pressure coupling. Pressure-pressure coupling was tried but not stable so there are no too many discussions in this thesis.)
    extern void incontam_loc();
  - Line 36: (the following line added to introduce a variable '_cpl', which used to control whether to do coupling in CONTAMX)
    extern _cpl;
  - Line 728: (the following line added to run the function 'incontam_loc()' in CONTAMX for the pressure-pressure coupling)
    if(_cpl) incontam_loc();
  - Line 748: (the following line added to run the function 'incontam_loc()' in CONTAMX for the pressure-pressure coupling, the difference between it and the last one is that this is for another case in CONTAMX, that is when the height difference of the path is less than 0.001)
    if(_cpl) incontam_loc();

- prtyp.h

  - Line 85- Line 87: (the following lines added to declare the functions added in the heap.c, which are for 3D array allocations)
    *void *alc_ac(IX, IX, IX, IX, IX, IX, IX, I1 *);*
    *void chk_ac(void *, IX, IX, IX, IX, IX, IX, IX, I1 *);*
    *void *fre_ac(void *, IX, IX, IX, IX, IX, IX, IX, I1 *);*

- sglob.h

  - Line 278: (the following lines added to declare another control variable about whether to do coupling or not in CONTAMX. It is a global variable.)
    #define COUPLE 1 //couple or not?

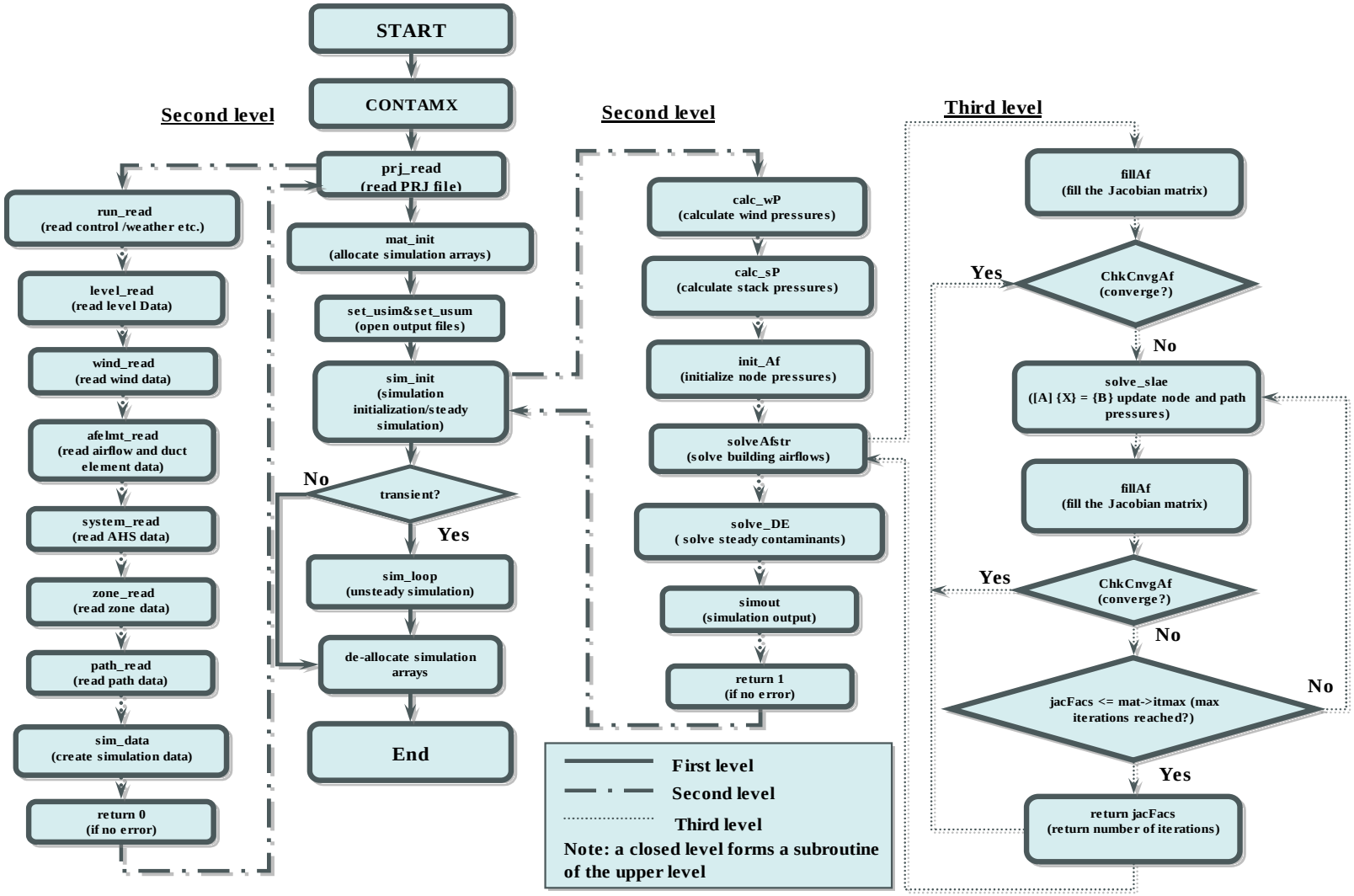

Fig. B.1 Program structure of CONTAMX 2.

Appendix C. Examples of Input Files

CFD0-C Input File for Flow in the 90-degree Planar Branch with Re=400 in Chapter 4.1.1

'2D-RE-400'

Problem Definition

Velocity steady? (1=YES,0=NO),Contaminant steady?(1=YES,0=NO)

1, 1

Time step, Max time, Residue of concentration computation, Maximum iterations

1, 5, 0.000001, 2000

Energy (compute energy equation?)

0

Contaminant (compute contaminant?); number of contaminants; start from a velocity file?

0, 0, 0

Convergence criterion for flow, The maximum iteration number

0.00001,10000

Is the flow laminar?

T

GEOMETRY, MESH AND BOUNDARY CONDITIONS

Size of the enclosure

X(L) Y(W) Z(H)

0.05, 0.093, 0.

Number of control volumes in three directions

x y z

30, 58, 0

Size of control volumes

x direction

.001 .001 .001 .001 .001 .001 .001 .001 .001 .001

.002 .002 .002 .002 .002 .002 .002 .002 .002 .002

.002 .002 .002 .002 .002 .002 .002 .002 .002 .002

y direction

.002 .002 .002 .004 .004 .004 .002 .002 .002 .002

.002 .002 .002 .002 .002 .002 .002 .002 .002

.001 .001 .001 .001 .001 .001 .001 .001 .001 .001

.001 .001 .001 .001 .001 .001 .001 .001 .001

.001 .001 .001 .001 .001 .001 .001 .001 .001 .001

.002 .002 .002 .002 .002 .002 .002 .002 .002 .002

z direction

0.0

Total number of openings

1, 2

THe control volumes covered by inlet opening

in x direction

1, 10

in y direction

1, 1

in z direction

1, 1

Inlet velocity and temperature

1,1,0, 0.6, 0, 0.0, 20

The control volumes covered by outlet opening

in x direction

1, 10

in y direction

58, 58

in z direction

1, 1

outlet velocity and temperature

2,2,0.0,0.0,0.0,20.

The control volumes covered by outlet opening

in x direction

30, 30

in y direction

21, 30

in z direction

1, 1

outlet velocity and temperature

2,2,0.0,0.0,0.0,20.

Total number of blockages

2

Block 1

in x direction

11, 30

in y direction

1, 20

in z direction

1, 1

heat flux

1,0

Block 2

in x direction

11, 30

in y direction

31, 58

in z direction

1, 1

heat flux

1,0

TOtal number of non-adiabatic walls given by T=const.

0

Total number of non-adiabatic walls given by Q=const

0

CONTROL PARAMETERS

Differential schems for u,v,w,t,c(1=Upwind,2=Power law)

1,1,1,1,1

Inital value for T, reference value for T

20.0, 20.0

Buoyancy?(use Bousinesq?)

1

Limits UMIN,UMAX, VMIN,VMAX, WMIN,WMAX, TMIN,TMAX

-10.0,10.0, -10.0,10.0, -10.0,10.0, 0.0,80.0

Linear relaxations URFU,URFV,URFW,URFP,URFT,URFEK,URFED,URFC

0.1, 0.1, 0.1, 0.9, 0.6, 1.0, 1.0,0.6

False-time step DTU DTV DTW DTT DTEK DTED DTC

.125, .125, .125, 30, 1E+30, 1E+30,30

Is there step chance for the false-time step relaxation?

T

Step change: Iter., DTU, DTV, DTW, DTT, DTEK, DTED DTC

300, 2.0E00, 1.0E00, 2.0E00, 3.0E+2, 1.0E30, 1.0E30,300

Printing frequency for the residuals during the calculation

5.0

Monitoring point during the calculation

2,5,2

Reference point

21,5,5

Printing Ifirst,Ilast,Istep, Jfirst,Jlast,Jstep

1, 20, 2 1, 18, 5

Do you want to restart the calculation? (0-no, 1-yes), creat EWC file? create CFDLOG file?

0,0,1

MATERIAL PROPERTIES FOR AIR

---

pressure ambient

101325.0

reference density

1.2

operating density

1.2

kinematic-visc.

1.513E-5

conductivity

0.0262

speficit heat at constant pressure

1005.6

laminar Prandtl number

0.71

CFD0-C Input File for Displacement Ventilation in Chapter 4.1.3

'DISPLACEMENT VENTILATION'

Problem Definition

Velocity steady? (1=YES,0=NO),Contaminant steady?(1=YES,0=NO)

1,1

Time step, Max time, Residue of concentration computation, Maximum iterations

1,100,0.000001,2000

Engergy(compute energy equation?)

1

Contaminant (compute contaminant?); number of contaminants; start from a velocity file?

1,1,0

Convergence criterion for flow, The maximum iteration number

0.001, 3000

Is the flow laminar?

F

Turbulence model: simple (0) or k-e model (1)

0

GEOMETRY, MESH AND BOUNDARY CONDITIONS

Size of the enclosure

X (L) Y(W) Z(H)

5.16, 3.65, 2.43

Number of control volume in three directions

x y z

25, 18, 16

Size of control volumes

in x direction

0.12 0.23 0.23 0.23 0.22 0.20 0.25 0.25 0.25

0.20 0.20 0.20 0.20 0.15 0.20 0.20 0.20 0.20

0.24 0.24 0.25 0.25 0.20 0.15 0.10

in y direction

0.10 0.15 0.20 0.13 0.17 0.20 0.35 0.20 0.11

0.21 0.22 0.31 0.35 0.20 0.30 0.20 0.15 0.10

in z direction

0.10 0.25 0.25 0.10 0.05 0.09 0.10 0.16 0.14

0.10 0.20 0.28 0.28 0.13 0.10 0.10

Total number of openings

1, 1

The control volumes covered by inlet opening

in x direction

1, 1

in y direction

9, 11

in z direction

1, 8

Inlet velocity and temperature

2,1,0.086, 0.0, 0.0, 0.0, 17.0

The control volumes covered by outlet opening

in x direction

12, 13

in y direction

10, 11

in z direction

16, 16

Outlet velocity and temperature

2,2,0.0,0.0,0.0,26.7

Total number of blockages

16

Table 1

in x direction

3, 12

in y direction

1, 5

in z direction

5, 5

heat flux

1,0.0

Table 2

in x direction

15, 25

in y direction

15, 18

in z direction

5, 5

heat flux

1,0.0

Cabinet 1

in x direction

1, 2

in y direction

1, 4

in z direction

1, 10

heat flux

1,0.0

Cabinet 2

in x direction

21, 25

in y direction

1, 4

in z direction

1, 9

heat flux

1,0.0

Computer 1

in x direction

10, 11

in y direction

2, 3

in z direction

6, 8

heat flux

1,108.5

Computer 2

in x direction

16, 17

in y direction

16, 17

in z direction

6, 8

heat flux

1,173.4

Person 1

in x direction

10, 11

in y direction

7, 7

in z direction

1, 8

heat flux

1,75

Person 2

in x direction

16, 17

in y direction

13, 13

in z direction

1, 8

heat flux

1,75

Lamp 1

in x direction

6, 6

in y direction

2, 7

in z direction

15, 15

heat flux

1,34.0

Lamp 2

in x direction

12, 12

in y direction

2, 7

in z direction

15, 15

heat flux

1,34.0

Lamp 3

in x direction

18, 18

in y direction

2, 7

in z direction

15, 15

heat flux

1,34.0

Lamp 4

in x direction

6, 6

in y direction

13, 17

in z direction

15, 15

heat flux

1,34.0

Lamp 5

in x direction

12, 12

in y direction

13, 17

in z direction

15, 15

heat flux

1,34.0

Lamp 6

in x direction

18, 18

in y direction

13, 17

in z direction

15, 15

heat flux

1,34.0

Tracer gas1

in x direction

11, 11

in y direction

6, 6

in z direction

9, 9

heat flux

2,0.0,1

1,0.013

Tracer gas2

in x direction

17, 17

in y direction

16, 16

in z direction

9, 9
heat flux
2,0.0,1
1,0.013

Total number of non-adiabatic walls given by T=const.
12

Ceiling - first part
in x direction
1, 12
in y direction
1, 18
in z direction
16, 16
temperature
25.3

Ceiling - second part
in x direction
13, 25
in y direction
1, 18
in z direction
16, 16
temperature
26.0

Floor - first part
in x direction

1, 12

in y direction

1, 18

in z direction

1, 1

temperature

22.4

Floor - second part

in x direction

13, 25

in y direction

1, 18

in z direction

1, 1

temperature

24.5

East wall - parapet

in x direction

25, 25

in y direction

1, 18

in z direction

1, 7

temperature

24.4

East wall - window

in x direction

25, 25

in y direction

1, 18

in z direction

8, 13

temperature

27.7

East wall - above the window

in x direction

25, 25

in y direction

1, 18

in z direction

14, 16

temperature

26.6

West wall - above the inlet

in x direction

1, 1

in y direction

1, 18

in z direction

9, 16

temperature

25.4

North wall - lower part

in x direction

1, 25
in y direction
18, 18
in z direction
1, 7
temperature
23.9

North wall - upper part
in x direction
1, 25
in y direction
18, 18
in z direction
8, 16
temperature
26.0

South wall - lower part
in x direction
1, 25
in y direction
1, 1
in z direction
1, 7
temperature
23.9

South wall - upper part
in x direction

1, 25

in y direction

1, 1

in z direction

8, 16

temperature

26.0

Total number of non-adiabatic walls given by Q=const.

0

CONTROL PARAMETERS

Differential schems for u,v,w,t,c(1=Upwind,2=Power law)

1,1,1,1,1

Initial value for T, reference value for T

22.0, 22.0

Buoyancy?(use Bousinesq?)

1

Limits UMIN,UMAX, VMIN,VMAX, WMIN,WMAX, TMIN,TMAX

-4.0, 4.0, -4.0, 4.0, -4.0, 4.0, 0.0, 80.0

Linear relaxations URFU,URFV,URFW,URFP,URFT,URFEK,URFED,urfc

0.1, 0.1, 0.1, 0.9, 0.6, 1.0, 1.0,0.6

False-time step DTU, DTV, DTW, DTT, DTEK, DTED
2.0E-1, 1.0E-1, 2.0E-1, 3.0E+1, 1.0E30, 1.0E30,30

Is there step change for the false-time step relaxation?
T

Step change: Iter., DTU, DTV, DTW, DTT, DTEK, DTED
300, 2.0E00, 1.0E00, 2.0E00, 3.0E+2, 1.0E30, 1.0E30,300

Printing frequency for the residuals during the calculation
5.0

Monitoring point during the calculation
10,2,10

Reference point
10,12,10

Printing Ifirst,Ilast,Istep, Jfirst,Jlast,Jstep
1, 25, 1 1, 18, 1

Do you want to restart the calculation? (0-no, 1-yes), creat EWC file? create CFDLOG file?
0,0,3

MATERIAL PROPERTIES FOR AIR
---

pressure ambient

101325.0
reference density
1.2
operating density
1.2
kinematic-visc.
1.513E-5
conductivity
0.0262
speficit heat at constant pressure
1005.6
laminar Prandtl number
0.71

CFD0-C Input File for Cross Ventilation in a 4-Zone Building Model in Chapter 4.1.4

'Momentum driven air flow in 4Zone with cross ventilation 0Degree'

Problem Definition

Velocity steady? (1=YES,0=NO),Contaminant steady?(1=YES,0=NO)
1,1

Time step, Max time, Residue of concentration computation, Maximum iterations
1, 5, 0.000001, 2000

Energy (compute energy equation?)

0

Contaminant (compute contaminant?); number of contaminants; start from a velocity file?

0, 0, 0

Convergence criterion for flow, The maximum iteration number

0.001, 7000

Laminar Flow?

F

Turbulence model: simple (0) or k-e (1)

0

GEOMETRY, MESH, AND BOUNDARY CONDITIONS

Size of the enclosure

X(L) Y(W) Z(H)

16.1, 15.5, 9.0

Number of control volumes in three directions

x y z

50, 54, 32

Size of control volumes

x direction

0.42 .45 .84 .84

0.84 0.84 0.42 0.3 0.1 0.05 0.05

0.05 0.13 0.3

0.42 0.42 0.42 0.42

0.3 0.18

0.1 0.025

0.025 0.1

0.18 0.3

0.42 0.42 0.42 0.42

0.3 0.13 0.05

0.05 0.05 0.1 0.3 0.21 .21 .42 .42 .42 .42

.42 .42 .42 .42 .42 .42 .3

y direction

.285 .42 .42 .42 .42 .42

.615 .225 .42 .42 .21 .21 .3 .1 .05 .05

0.05 0.13 0.3

0.42 0.42 0.42 0.42

0.3 0.18

0.1 0.025

0.025 0.1

0.18 0.3

0.42 0.42 0.42 0.42

0.3 0.13 0.05

0.05 0.05 0.1 0.3 0.21 .21 .42 .42 .225 .615

.42 .42 .42 .42 .42 .285

z direction

0.25 0.25

0.35 0.3 0.3 0.3 0.3

0.19 0.14 0.2 0.21 0.16 0.05

0.05 0.05 0.1 0.3 0.21 0.21 0.42 0.66 0.18 0.42

0.42 0.42 0.42 0.42 0.42 0.42 0.42 .23 .23

Total number of openings

1, 1

west-inlet

in x direction

1, 1

in y direction

8, 47

in z direction

1, 21

Inlet velocity and temperature

2,1,3.0, 0.0, 0.0,0.0,21.8,0

east-outlet

in x direction

50, 50

in y direction

1, 54

in z direction

1, 32

Inlet velocity and temperature

2,1,1.022, 0.0,21.8,0

Total number of blockages

22

west1

in x direction

12, 12

in y direction

17, 19

in z direction

3, 13

heat flux

1,0

west2

in x direction

12, 12

in y direction

20, 21

in z direction

9, 13

heat flux

1,0

west3

in x direction

12, 12

in y direction

22, 27

in z direction

3, 13

heat flux

1,0

west4

in x direction

12, 12

in y direction

28, 38

in z direction

3, 13

heat flux

1,0

east1

in x direction

33, 33

in y direction

17, 27

in z direction

3, 13

heat flux

1,0

east2

in x direction

33, 33

in y direction

28, 33

in z direction

3, 13

heat flux

1,0

east3

in x direction

33, 33

in y direction

34, 35

in z direction

9, 13

heat flux

1,0

east4

in x direction

33, 33

in y direction

36, 38

in z direction

3, 13

heat flux

1,0

south1

in x direction

12, 22

in y direction

17, 17

in z direction

3, 13

heat flux

1,0

south2

in x direction

23, 33

in y direction

17, 17

in z direction

3, 13

heat flux

1,0

north1

in x direction

12, 22

in y direction

38, 38

in z direction

3, 13

heat flux

1,0

north2

in x direction

23, 33

in y direction

38, 38

in z direction

3, 13

heat flux

1,0

roof

in x direction

12, 33

in y direction

17, 38

in z direction

13, 13

heat flux

1,0

x1

in x direction

12, 14

in y direction

27, 28

in z direction

3, 12

heat flux

1,0

x2

in x direction

31, 33

in y direction

27, 28

in z direction

3, 12

heat flux

1,0

y1

in x direction

22, 23

in y direction

17, 19

in z direction

3, 12

heat flux

1,0

y2

in x direction

22, 23

in y direction

36, 38

in z direction

3, 12

heat flux

1,0

c1

in x direction

19, 22

in y direction

27, 28

in z direction

3, 12

heat flux

1,0

c2

in x direction

23, 26

in y direction

27, 28

in z direction

3, 12

heat flux

1,0

c3

in x direction

22, 23

in y direction

24, 27

in z direction

3, 12

heat flux

1,0

c4

in x direction

22, 23

in y direction

28, 31

in z direction

3, 12

heat flux

1,0

floor

in x direction

12, 33

in y direction

17, 38

in z direction

1, 2

heat flux

1,0

Total number of non-adiabatic walls given by T=const

0

Number of adiabatic walls given by Q-const.

0

CONTROL PARAMETERS

Differential schems for u,v,w,t,c(1=Upwind,2=Power law)

1,1,1,1,1

Inital value for T, reference value for T

21.8, 21.8

Buoyancy?

1

Limits UMIN,UMAX, VMIN,VMAX, WMIN,WMAX, TMIN,TMAX

-5.0,5.0, -5.0,5.0, -5.0,5.0, 0.0,80.0

Linear relaxations URFU,URFV,URFW,URFP,URFT,URFEK,URFED,URFC

0.1, 0.1, 0.1, 0.9, 0.6, 1.0, 1.0,0.6

False-time step DTU DTV DTW DTT DTEK DTED DTC

15, 15, 1, 30, 1E+30, 1E+30,30

Is there step chance for the false-time step relaxation?

t

Step change: Iter., DTU, DTV, DTW, DTT, DTEK, DTED, DTC

2000, 2.0E00, 2.0E00, 2.0E00, 3.0E+2, 1.0E30, 1.0E30,300

Printing frequency for the residuals during the calculation

5.0

Monitoring point during he calculation

10,2,1

Reference point

10,12,1

Printing Ifirst,Ilast,Istep, Jfirst,Jlast,Jstep

1, 20, 2 1, 18, 5

Do you want to restart the calculation? (0-no, 1-yes)

0,0,3

MATERIAL PROPERTIES FOR AIR

---

pressure ambient

101325.0
ref density
1.198
oper den
1.198
kinematic-visc.
1.513E-5
conductivity
0.0262
speficit heat at constant pressure
1005.6
laminar Prandtl number
0.71

An Example of The CPL File

This appendix demonstrates an example of the CPL file, coupling definition file. The selected case is the natural ventilation in a 3-story building with a large atrium with steady-state airflow and transient contaminant transport as discussed in Chapter 5.2.2.

Couple CFD0C and CONTAM

Coupled zones and types
1,1,2,1,1

Zone names to be coupled; number paths
35,44

Definition of coupled airflow path

1,1,3,1

Definition of coupled airflow path
13,1,3,1
Definition of coupled airflow path
17,1,3,1

Definition of coupled airflow path
19,1,3,1

Definition of coupled airflow path
41,1,3,1

Definition of coupled airflow path
45,1,3,1

Definition of coupled airflow path
47,1,3,1

Definition of coupled airflow path
69,1,3,1

Definition of coupled airflow path
73,1,3,1

Definition of coupled airflow path
75,1,3,1

Definition of coupled airflow path
63,1,3,1

Definition of coupled airflow path
64,1,3,1

Definition of coupled airflow path
65,1,3,1

Definition of coupled airflow path
66,1,3,1

Definition of coupled airflow path
70,1,3,1

Definition of coupled airflow path
74,1,3,1

Definition of coupled airflow path
76,1,3,1

Definition of coupled airflow path
78,1,3,1

Definition of coupled airflow path
79,1,3,1

Definition of coupled airflow path
80,1,3,1

Definition of coupled airflow path
81,1,3,1

Definition of coupled airflow path
2,1,3,1

Definition of coupled airflow path
7,1,3,1

Definition of coupled airflow path
8,1,3,1

Definition of coupled airflow path
9,1,3,1

Definition of coupled airflow path
10,1,3,1

Definition of coupled airflow path
14,1,3,1

Definition of coupled airflow path
18,1,3,1

Definition of coupled airflow path
20,1,3,1

Definition of coupled airflow path
22,1,3,1

Definition of coupled airflow path
23,1,3,1

Definition of coupled airflow path
24,1,3,1

Definition of coupled airflow path
25,1,3,1

Definition of coupled airflow path
35,1,3,1

Definition of coupled airflow path
36,1,3,1

Definition of coupled airflow path
37,1,3,1

Definition of coupled airflow path
38,1,3,1

Definition of coupled airflow path
42,1,3,1

Definition of coupled airflow path
46,1,3,1

Definition of coupled airflow path
48,1,3,1

Definition of coupled airflow path
50,1,3,1

Definition of coupled airflow path
51,1,3,1

Definition of coupled airflow path
52,1,3,1

Definition of coupled airflow path
53,1,3,1

Reference Zone (0 if it is ambient,index number if it is a specifed zone)
0

Maximum couple iterations (for dynamic only); Output intermediate results?(1=Yes,0=No)
300,0,0,1

VITA

VITA

Liangzhu Wang was born in Handan, China on January 15, 1977. He obtained his B.S. in Thermal Engineering from Tianjin Institute of Urban Construction in 1999. With the highest total grade in the graduate entrance exams for Tianjin University, he joined the school of Civil Engineering and conducted researches on Heating, Ventilating, and Air Conditioning with the emphasis of building simulations of indoor environment and energy consumption. In 2002, he was awarded his M.S. at Tianjin University, where he also met his classmate and wife, Jinxia Liu.

In August 2002, Liangzhu Wang joined the doctoral program of the school of Mechanical Engineering at Purdue University and worked as a research and teaching assistant under the guidance of Dr. Qingyan (Yan) Chen. He conducted research on integrated building simulations of airflow and contaminant transport by using multizone and CFD models. After completing his Ph.D., he will work at National Institute of Standard and Technology (NIST) as a guest post-doctoral researcher beginning March 2007.